Università degli Studi di Palermo

AREA RICERCA E TRASFERIMENTO TECNOLOGICO
SETTORE DOTTORATI E CONTRATTI PER LA RICERCA
U. O. DOTTORATI DI RICERCA

University of Copenaghen

Technologies and Science for Human Health
Department of Biological, Chemical and Pharmaceutical Sciences and Technologies (STEBICEF)
SSD BIOS-07/A

Developing 3D In Vitro Tumor Models: Extracellular Matrix Remodeling by Collagenases to Increase Drug Efficacy

PhD Thesis by:
Gabriele Lo Buglio

Director of PhD
Prof. Valeria Vetri

Supervisor
Prof. Giulio Ghersi

Co-supervisor
Simona Campora, PhD

Supervisor
Prof. Vito Foderà

Cycle XXXVIII
2026

Finanziato dall'Unione europea NextGenerationEU
Ministero dell'Università e della Ricerca
Italiadomani
PIANO NAZIONALE DI RIPRESA E RESILIENZA

UNIVERSITY OF COPENHAGEN
FACULTY OF HEALTH AND MEDICAL SCIENCES
DEPARTMENT OF PHARMACY

PhD Thesis

Gabriele Lo Buglio

Developing 3D In Vitro Tumor Models: Extracellular Matrix Remodeling by Collagenases to Increase Drug Efficacy

Principal supervisor: Vito Foderà

Co-supervisor: Giulio Ghersi

This Thesis has been submitted to the Graduate School of Health and Medical Sciences (University of Copenhagen, 13th February 2026)

PhD Student

Gabriele Lo Buglio

Thesis "*Developing 3D In Vitro Tumor Models: Extracellular Matrix Remodeling by Collagenases to Increase Drug Efficacy.*"

PhD Course "Technologies and Sciences for Human Health" - XXXVIII Cycle

Double PhD Program:

- University of Palermo
- University of Copenhagen

Principal Supervisor (University of Palermo)

Giulio Ghersi, Professor

Department of Biological, Chemical, and Pharmaceutical Sciences and Technologies (STEBICEF)

University of Palermo, Italy

Principal Supervisor (University of Copenhagen)

Vito Foderà, Professor

Department of Pharmacy,

Faculty of Health and Medical Sciences

University of Copenhagen, Denmark

Co-Supervisor (University of Palermo)

Simona Campora, PhD

Department of Biological, Chemical, and Pharmaceutical Sciences and Technologies (STEBICEF)

University of Palermo, Italy

PREFACE

The PhD thesis entitled "*Developing 3D In Vitro Tumor Models: Extracellular Matrix Remodeling by Collagenases to Increase Drug Efficacy*" was submitted to the University of Palermo and to the University of Copenhagen. The research was carried out within a dual PhD program established in 2022 under a collaborative agreement between the University of Palermo (Italy), the home institution, and the University of Copenhagen (Denmark), the host institution. At the University of Palermo, the PhD training was carried out within the *Technologies and Science for Human Health* PhD program, while at the University of Copenhagen, the research activities were conducted under the *Graduate School of Health and Medical Sciences*. The PhD project was performed from November 1, 2022, to October 31, 2025, and involved research activities performed across multiple institutions. The first year of the PhD (November 1, 2022–October 31, 2023), together with specific periods of the second year (November 1, 2023–February 5, 2024, and August 1, 2024–October 31, 2024) and the third year (November 1, 2024–October 31, 2025), were conducted at the *Department of Biological, Chemical, and Pharmaceutical Sciences and Technologies (STEBICEF)* of the University of Palermo, under the supervision of Professor Giulio Ghersi and the co-supervision of Dr. Simona Campora. From February 5, 2024, to July 27, 2024, research activities were carried out at the University of Copenhagen within the *Drug Delivery and Biophysics of Biopharmaceuticals (DDBB)* Group at the Department of Pharmacy, under the supervision of Professor Vito Foderà. The PhD fellowship at the University of Palermo was funded by the National Recovery and Resilience Plan (PNRR).

The following articles were produced during the PhD program:

I. Lo Buglio G, Lo Cicero A, Campora S, Ghersi G. The Multifaced Role of Collagen in Cancer Development and Progression. Int J Mol Sci. 2024 Dec 17;25(24):13523. doi: 10.3390/ijms252413523. PMID: 39769286; PMCID: PMC11678882.

II. Lo Cicero A, Campora S, Lo Buglio G, Cinà P, Lo Pinto M, Scilabra SD, Ghersi G. Enhancing therapeutic efficacy through degradation of endogenous extracellular matrix in primary breast tumor spheroids. FEBS J. 2025 Jul;292(13):3494-3507. doi: 10.1111/febs.70069. Epub 2025 Mar 17. PMID: 40098313; PMCID: PMC12220849.

III. Lo Cicero A, La Monica F, Lo Buglio G, Campora S, Gangemi F, Cinà P, Salamone M, Lo Pinto M, Scilabra SD, Ghersi G. A vascularized three-dimensional model integrating primary breast tumor cells and microvascular fragments: mimicking the tumor microenvironment involved in chemoresistance. Cancer Cell Int. 2026 Jan 8. doi: 10.1186/s12935-025-04154-6. Epub ahead of print. PMID: 41507925.

Thesis Outline

This PhD thesis is structured into four main chapters, each addressing a specific aspect of tumor microenvironment modulation and nanomedicine-based therapeutic strategies:

- Improving Therapeutic Efficacy Through Endogenous Extracellular Matrix Remodeling in Primary Breast Tumor Spheroids: The first study focused on the generation of three-dimensional tumor spheroids from primary tumor cells (PTCs) isolated from chemically induced mammary tumors in Wistar rats. The resulting spheroids, capable of producing a collagen-rich endogenous extracellular matrix, were treated with a combination of ultrapure recombinant collagenases to enhance doxorubicin penetration and cytotoxicity. This approach demonstrated the effectiveness of a two-step synergistic therapeutic strategy for the treatment of solid tumors. The results presented in this chapter have been published in *The FEBS Journal* in 2025 in the manuscript *"Enhancing therapeutic efficacy through degradation of endogenous extracellular matrix in primary breast tumor spheroids"* by Lo Cicero et al. [1]

- Synergistic Effect of Collagenase and PVP-AEDP-Doxorubicin Nanoparticles in Primary Tumor Cell Spheroids: The second study concentrated on the application of PVP-AEDP nanoparticles loaded with doxorubicin in combination with enzymatic treatment in PTC spheroids. The aim was to increase therapeutic specificity and to validate in vitro the efficacy of nanostructured systems responsive to tumor microenvironmental cues, resulting in an improved pharmacological response. The manuscript is in preparation.

- Enhancing Drug Penetration and Cytotoxicity in 3D Primary Breast Cancer Cultures via BSA-Nanoparticles: The third study addressed the synthesis and biophysical characterization of pH-sensitive bovine serum albumin (BSA) nanoparticles loaded with doxorubicin, obtained through chemical crosslinking. The combined application of these nanoparticles with collagenases in PTC spheroids led to a significant increase in cytotoxicity. In parallel, BSA nanoparticles conjugated with collagenases were synthesized and characterized using a thermal crosslinking approach to preserve the catalytic activity of the conjugated enzyme while simultaneously improving its immunocompatibility and biological performance. The manuscript is in preparation.

- Development and Characterization of 3D Vascularized Tumor Model Integrating Rat Adipose-Derived Microvascular Fragments and Breast Cancer Cells: Evaluation of ABCB1 Expression and Drug Response: The fourth study focused on the generation of an advanced three-dimensional model based on co-cultures of PTCs and microvascular

fragments, to more faithfully recapitulate the tumor microenvironment and mimic neoangiogenic processes in vitro. In these vascularized tumor models, characterized by the overexpression of molecules associated with drug resistance, the response to pharmacological treatments was evaluated using doxorubicin, thereby enhancing the biological and translational relevance of the model. The data discussed in this chapter have been published in *Cancer Cell International* (2026) by Lo Cicero et al. in the manuscript "*A vascularized three-dimensional model integrating primary breast tumor cells and microvascular fragments: mimicking the tumor microenvironment involved in chemoresistance*" [2]

ABSTRACT

Background:

Solid tumors display a highly complex biological microenvironment, named Tumor Microenvironment (TME), characterized by a dense Extracellular Matrix (ECM), abnormal vasculature, and dynamic tumor–stroma interactions that collectively limit drug penetration and therapeutic efficacy. Traditional two-dimensional (2D) culture systems fail to adequately reproduce these features, underscoring the need for advanced three-dimensional (3D) models that better reflect tumor architecture and resistance mechanisms.

Hypothesis and Aim of the Study

The research project aims 1) to develop a two-step, synergistic strategy based on the controlled remodeling of the collagen-rich tumor ECM using ultrapure recombinant collagenases, which enhances drug penetration and antitumor efficacy of the anticancer drug Doxorubicin (DOX) in solid tumors and 2) to conjugate collagenases and DOX to biocompatible and stimuli-responsive nanoparticles to improve intratumoral drug bioavailability while reducing off-target effects. To test these hypotheses, the project has been focused on the 1) evaluation and comparation of the therapeutic performance of DOX-loaded bovine serum albumin (BSA) nanoparticles and glutathione-responsive poly(vinyl pyrrolidone) (PVP) nanoparticles (NPs) in advanced 3D tumor models and 2) validation of a vascularized tumor model incorporating microvascular fragments to better recapitulate the tumor microenvironment and improve the predictive value of *in vitro* drug testing.

Methods:

Primary tumor cells (PTCs) were isolated from a breast tumor chemically induced in Wistar rats, using ultrapure recombinant collagenases. PTCs were used to generate 3D tumor spheroids capable of producing an endogenous type I collagen–rich matrix, as confirmed by immunofluorescence staining. ECM remodeling was achieved using ultrapure recombinant collagenases (class I and II). Doxorubicin (DOX) was administered in PTC spheroids as a free drug, conjugated to pH-sensitive BSA NPs, or incorporated into glutathione-responsive PVP NPs, and their efficacy was evaluated through a cell viability assay. BSA–DOX NPs were synthesized using the desolvation method and crosslinked with glutaraldehyde, whereas enzyme-loaded BSA nanoparticles were thermally crosslinked. The resulting constructs were characterized by Dynamic Light Scattering (DLS), Transmission Electron Microscopy (TEM), Nanoparticle Tracking Analysis (NTA),

and spectrophotometry. In addition, Microvascular Fragments (MVFs) isolated from rat adipose tissue were co-cultured with PTCs to generate so-called *"Angiotumoroids"* that recapitulate the tumor–endothelial cell crosstalk. Co-cultures were characterized by Scanning Electron Microscopy (SEM) and immunofluorescence, while protein expression was evaluated by proteomic analysis. Across all 3D models investigated in this study, drug uptake was assessed by confocal microscopy image analysis, and cell viability was assessed using an ATP-based luminescent assay.

Results and discussion:

Tumor spheroids developed a dense, collagen-rich ECM that markedly limited doxorubicin penetration. Pre-treatment with recombinant collagenases reduced ECM density and synergistically enhanced intratumoral DOX accumulation and antitumor efficacy, both for free DOX and nanoparticle-based formulations (PVP NPs and BSA NPs). It is well known that tumor cells present higher levels of intracellular glutathione compared to normal ones. Therefore, DOX was conjugated to OPVP NPs through a redox-responsive linker to obtain a controlled drug release mechanism. On the other hand, tumor cells and microenvironment present low pH, and, therefore, BSA–DOX nanoparticles were formulated to exhibit pH-dependent aggregation behavior, suggesting a potential acidity-mediated retention within the tumor microenvironment *in vivo*. To improve the immunocompatibility of collagenases, the enzymes were conjugated to BSA nanoparticles via thermal crosslinking, a strategy that preserved their catalytic activity more effectively than conventional chemical crosslinking approaches. Finally, advanced three-dimensional tumor models were generated by co-culturing Microvascular Fragments (MVFs) with PTCs, giving rise to structures termed *Angiotumoroids*. These models displayed a homogeneous endothelial organization throughout the spheroid architecture and demonstrated pronounced neoangiogenic potential, mediated both by direct tumor–endothelial cell interactions and by soluble pro-angiogenic factors. Moreover, Angiotumoroids exhibited marked overexpression of efflux transporters, such as ATP Binding Cassette Subfamily B Member 1 (ABCB1), which conferred a drug-resistant phenotype, as confirmed by cytotoxicity assays. Taken together, these characteristics support the use of angiotumoroids as robust and physiologically relevant in vitro platforms for studying mechanisms of tumor drug resistance and assessing treatment efficacy.

Conclusions:

The combined targeting of the tumor ECM and the use of responsive nanoparticles significantly improve chemotherapeutic delivery in solid tumor models. Advanced 3D and

vascularized tumor systems represent powerful and predictive platforms for investigating tumor resistance mechanisms and optimizing innovative drug-delivery strategies.

RESUMÉ

Baggrund:

Solide tumorer udviser et yderst komplekst biologisk mikromiljø, betegnet tumorens mikromiljø (Tumor Microenvironment, TME), som er karakteriseret ved en tæt ekstracellulær matrix (Extracellular Matrix, ECM), abnorm vaskularisering og dynamiske tumor–stroma-interaktioner, der tilsammen begrænser lægemiddelpenetration og terapeutisk effektivitet. Traditionelle todimensionelle (2D) cellekultursystemer formår ikke i tilstrækkelig grad at reproducere disse egenskaber, hvilket understreger behovet for avancerede tredimensionelle (3D) modeller, der bedre afspejler tumorarkitektur og resistensmekanismer.

Hypotese og formål med studiet:

Dette forskningsprojekt har til formål 1) at udvikle en totrins, synergistisk strategi baseret på kontrolleret remodellering af den kollagenrige tumor-ekstracellulære matrix ved anvendelse af ultrapure rekombinante kollagenaser med henblik på at forbedre lægemiddelpenetration og antitumoral effekt af det anticancerogene lægemiddel doxorubicin (DOX) i solide tumorer, samt 2) at konjugere kollagenaser og DOX til biokompatible og stimulus-responsive nanopartikler for at øge den intratumorale lægemiddeltilgængelighed og samtidig reducere off-target-effekter. For at teste disse hypoteser har projektet fokuseret på 1) evaluering og sammenligning af den terapeutiske ydeevne af DOX-indlæste bovint serumalbumin (BSA) nanopartikler og glutathion-responsive poly(vinylpyrrolidon) (PVP) nanopartikler (NP'er) i avancerede 3D-tumormodeller samt 2) validering af en vaskulariseret tumormodel, der inkorporerer mikrovaskulære fragmenter, for bedre at genskabe tumorens mikromiljø og øge den prædiktive værdi af in vitro-lægemiddeltestning.

Metoder:

Primære tumorceller (Primary Tumor Cells, PTC'er) blev isoleret fra en kemisk induceret brysttumor i Wistar-rotter ved anvendelse af ultrapure rekombinante kollagenaser. PTC'er blev anvendt til at generere 3D-tumorsfæroider, som var i stand til at producere en endogen type I kollagenrig matrix, hvilket blev bekræftet ved immunofluorescensfarvning. ECM-remodellering blev opnået ved brug af ultrapure rekombinante kollagenaser (klasse I og II). Doxorubicin (DOX) blev administreret til PTC-sfæroider enten som frit lægemiddel,

konjugeret til pH-sensitive BSA-nanopartikler eller inkorporeret i glutathion-responsive PVP-nanopartikler, og effekten blev evalueret ved celleviabilitetsassays. BSA–DOX-nanopartikler blev syntetiseret ved desolvatationsmetoden og krydsbundet med glutaraldehyd, mens enzymindlæste BSA-nanopartikler blev termisk krydsbundet. De resulterende konstruktioner blev karakteriseret ved dynamisk lysspredning (Dynamic Light Scattering, DLS), transmissionselektronmikroskopi (Transmission Electron Microscopy, TEM), nanoparticle tracking analysis (NTA) og spektrofotometri. Endvidere blev mikrovaskulære fragmenter (Microvascular Fragments, MVF'er) isoleret fra rottefedtvæv og co-kultiveret med primære tumorceller for at generere såkaldte "angiotumoroider", der genskaber tumor–endotelcelle-interaktioner. Co-kulturer blev karakteriseret ved scanning elektronmikroskopi (Scanning Electron Microscopy, SEM) og immunofluorescens, mens proteinudtryk blev analyseret ved proteomisk analyse. På tværs af alle 3D-modeller undersøgt i dette studie blev lægemiddeloptag vurderet ved konfokal mikroskopisk billedanalyse, og celleviabilitet blev evalueret ved et ATP-baseret luminescensassay.

Resultater og diskussion:

Tumorsfæroider udviklede en tæt, kollagenrig ekstracellulær matrix, som markant begrænsede doxorubicinpenetration. Forbehandling med rekombinante kollagenaser reducerede ECM-tætheden og øgede synergistisk den intratumorale akkumulering af DOX samt den antitumorale effekt, både for frit DOX og nanopartikelbaserede formuleringer (PVP- og BSA-nanopartikler). Det er velkendt, at tumorceller udviser højere intracellulære niveauer af glutathion sammenlignet med normale celler. Derfor blev DOX konjugeret til PVP-nanopartikler via en redox-responsiv linker for at opnå en kontrolleret lægemiddelfrigivelsesmekanisme. Omvendt er tumorceller og deres mikromiljø karakteriseret ved lav pH, og BSA–DOX-nanopartikler blev derfor designet til at udvise pH-afhængig aggregering, hvilket indikerer potentiel surhedsmedieret retention i tumorens mikromiljø in vivo. For at forbedre kollagenasernes immunokompatibilitet blev enzymerne konjugeret til BSA-nanopartikler via termisk krydsbinding, en strategi der bedre bevarede deres katalytiske aktivitet sammenlignet med konventionelle kemiske krydsbindingsmetoder. Endelig blev avancerede tredimensionelle tumormodeller genereret ved co-kultur af mikrovaskulære fragmenter (MVF'er) og primære tumorceller (PTC'er), hvilket gav anledning til strukturer betegnet angiotumoroider. Disse modeller udviste en homogen endotelial organisering gennem hele sfæroidarkitekturen og demonstrerede udtalt neoangiogent potentiale, medieret både af direkte tumor–endotelcelle-interaktioner og af

opløselige proangiogene faktorer. Desuden viste angiotumoroider en markant overekspression af efflux-transportører, såsom ATP-binding cassette subfamily B member 1 (ABCB1), hvilket gav en lægemiddelresistent fænotype, som blev bekræftet ved cytotoksicitetsassays. Samlet set etablerer disse karakteristika angiotumoroider som pålidelige og fysiologisk relevante in vitro-modeller til undersøgelse af tumorlægemiddelresistens og terapeutisk respons.

Konklusioner:

Den kombinerede målretning af tumorens ekstracellulære matrix og anvendelsen af stimulus-responsive nanopartikler forbedrer markant kemoterapeutisk levering i solide tumormodeller. Avancerede 3D- og vaskulariserede tumorsystemer repræsenterer kraftfulde og prædiktive platforme til undersøgelse af tumorresistensmekanismer og optimering af innovative lægemiddelleveringsstrategier.

CONTENTS

ABBREVIATION LIST

ADAMTs	a disintegrin and metalloproteinase with thrombospondin motifs
BBB	blood brain barrier
BSA	bovine serum albumin
CAFs	cancer-associated fibroblast
CAR	chimeric antigen receptor
CM	conditioned medium
COLG	collagenase g
COLH	collagenase h
DALYs	disability-adjusted life years
DDR1	discoidin domain receptor 1
DDS	drug delivery system
DLS	dynamic light scattering
DMBA	7,12-dimethylbenz(a)anthracene
DMEM	dulbecco modified
DMSO	dimethyl sulfoxide
DOX	doxorubicin
E-beam	electron-beam
ECM	extracellular matrix
EGF	epidermal growth factor
EMT	epithelial-to-mesenchymal transition
EPR	enhanced permeability and retention
FA	formic acid
FAK	focal adhesion kinase
FAP	fibroblast activation protein
FBS	dulbecco's modified eagle medium
HG	high glucose
HGF	hepatocyte growth factor
HIF	hypoxia-inducible factors
HMDS	hexamethyldisilazane
HUVECs	human umbilical vein endothelial cells
IFP	interstitial fluid pressure
IL	interleukin
LFQ	label-free quantification

LNPs	lipid-based nanoparticles
MDR	multidrug resistance (MDR)
MMPs	matrix metalloproteases
MVF	microvascular fragment
NETs	neutrophil extracellular traps
NPs	nanoparticles
NTA	nanoparticles tracking analysis
P4HA	prolyl 4-hydroxylases
PBS	phosphate-buffered saline
P-GP	p-glycoprotein
PDAC	pancreatic ductal adenocarcinoma
PDGF	platelet-derived growth factor
PDI	polydispersity index
PD-L1	programmed death-ligand 1
PNP	polymer-based nanoparticles
POSTN	periostin
PTC	primary tumor cell
PVP	polyvinylpyrrolidone
SAXS	small-angle x-ray scattering
SEM	scanning electron microscopy
Shh	sonic hedgehog
SVF	stromal vascular fraction
TAMs	tumor-associated macrophages
TEM	transmission electron microscopy
TGF-β	transforming growth factor beta-1
TILs	tumor-infiltrating lymphocytes
TIMP-1	tissue inhibitor of metalloproteinase 1
TME	tumor microenvironment
TNBC	triple-negative breast cancer
TNC	tenascin
VEGF	vascular endothelial growth factors
VTM	vascularized tumor model
α-SMA	α-smooth muscular actin

Chapter 1

INTRODUCTION

1.1 Solid Tumors: Epidemiology and Biological Features

Cancer represents one of the most pressing global public-health challenges, not only because of its high incidence and mortality, but also due to its profound and long-lasting impact on quality of life. Recent global health analyses estimate that, in 2023, the worldwide cancer burden achieved 18.5 million new cases and over 10 million deaths, contributing to more than 270 million (DALYs) [3]. These numbers highlight the devastating nature of the disease, but they also conceal marked disparities. Most cancer diagnoses and deaths occur in low- and middle-income countries, where access to prevention, early detection, and treatment remains limited [4]. Projections for the coming decades indicate an even more dramatic trend, with estimates suggesting that global incidence could exceed 30 million new cases by 2050, accompanied by a substantial rise in mortality, with regions with limited resources still being the most affected. This is probably related to modifiable risk factors. Behavioral, environmental, and metabolic determinants, such as tobacco use, unhealthy diet, obesity, and exposure to pollutants, are collectively responsible for more than 40% of all cancer-related deaths [5]. Historically, a relatively small number of modifiable risks has accounted for nearly half of global cancer DALYs, underscoring the central role of prevention strategies in fighting cancer [6].

Solid tumors constitute the largest and most clinically heterogeneous group of malignancies. This category includes carcinomas, sarcomas, and various other non-hematologic tumors arising from epithelial or mesenchymal tissues [7]. Their global impact is particularly evident in high-incidence and high-mortality cancers such as breast, lung, and colorectal tumors, which together account for a substantial proportion of worldwide cases and deaths and are often associated with unhealthy lifestyles. For instance, some solid tumors, such as pancreatic and liver cancer, are increasingly shaped by metabolic risk factors, including rising rates of high body mass index and elevated fasting glucose levels, which have been associated with projected increases in mortality in the coming years [8,9]. From a clinical perspective, managing solid tumors represents a significant challenge. Effective treatment often requires complex, multimodal approaches, including surgery, systemic therapies, and radiotherapy. These interventions not only demand extensive healthcare infrastructure and economic resources but are also associated with considerable long-term morbidity, as many patients live for extended periods with side effect treatments, recurrence, or metastatic disease. The persistent inequities in healthcare access further exacerbate such challenges. In fact, in many countries, diagnostic delays and limited availability of essential cancer services result in patients presenting at

more advanced stages, reducing the possibility of successful outcomes. Beyond individual suffering, the growing incidence of solid tumors places mounting pressure on global health systems. Without decisive action, the rising global cancer cases will continue to weigh down on increasing and potentially unsustainable pressure on healthcare systems. This scenario not only threatens to undermine the ability of institutions to provide timely and effective care but also significantly affects the psychological and social well-being of the population, further widening inequalities and diminishing the quality of life of patients and their families.

1.1.2 Limitations of Conventional Therapies in Solid Tumors

Conventional therapies for solid tumors, such as chemotherapy and radiotherapy, compromising their clinical efficacy. The limitation of canonical chemotherapeutic agents is their low specificity, which often leads to significant side effects due to systemic toxicity, adversely affecting patients' quality of life [10]. However, one of the major challenges is the poor penetration of drugs within tumor tissue. The dense and complex structure of the stroma, coupled with elevated interstitial pressure and irregular vascularization, reduces the uniform distribution of therapeutic agents, exposing several cells to subtherapeutic doses [11]. This insufficient exposure can promote the development of resistance mechanisms and hinder complete tumor eradication. The combination of limited efficacy and systemic toxicity represents a critical challenge in the clinical management of solid tumors, particularly in those with highly fibrotic or dense microenvironments.

1.1.3 Biology of Solid Tumors

Solid tumors represent a heterogeneous class of neoplasms characterized by the uncontrolled clonal proliferation of malignant cells that generate a compact three-dimensional mass within the tissues. They mainly include carcinomas of epithelial origin, such as those of the breast, lung, colorectal, and pancreatic origins, each displaying distinct genetic, epigenetic, and phenotypic profiles [7].

Tumor cells exhibit pronounced intratumoral heterogeneity, encompassing differentiated subpopulations and subclones with variable metastatic potential, adaptive metabolic profiles, and resistance to therapeutic strategies [12]. This heterogeneity is further amplified by the dynamic interactions between tumor cells and the surrounding components of the tumor mass, which influence important signaling pathways involved in proliferation, apoptosis, invasion, and angiogenesis [13]. They actively produce and

remodel the extracellular matrix (ECM), thereby influencing tissue stiffness, interstitial fluid pressure, and drug diffusion [14,15]. Moreover, the gradients of oxygen, pH, metabolites, and growth factors determine specific micro niches that selectively enhance aggressive cellular phenotypes and contribute to drug resistance [16,17].

This results in a tumor microenvironment (TME) that constitutes a critical component of the solid tumor, where bidirectional interactions with tumor cells and other tumor elements regulate key processes that enhance tumor progression.

1.2 The Tumor Microenvironment as an Anti-Therapeutic Barrier

The global increase in solid tumor cases, together with the limitations of conventional therapies, highlights the urgent need for more effective treatment strategies grounded in a deeper understanding of the tumor microenvironment (TME). Despite considerable advances, many solid tumors remain difficult to eliminate due to their inherent biological heterogeneity and the complex network of interactions established among malignant, stromal, immune, and acellular components. Standard treatments, while capable of reducing tumor mass, often fail to disrupt the mechanisms that enable tumor cells to adapt, persist, and eventually relapse or metastasize [18].

The TME constitutes a major barrier to therapeutic success. Key features, such as hypoxia, acidosis, ECM remodeling, immunosuppressive signaling, and aberrant vasculature, limit drug penetration and antitumor immune responses. Consequently, tumors must be viewed as dynamic ecosystems in which malignant progression results from continuous microenvironment-driven support [19].

These results underscore the need for therapeutic strategies that address not only cancer cells but also the microenvironmental factors supporting their survival.

1.2.1 Structure and Composition of Tumor Microenvironment

Tumor Microenvironment (TME) is defined as the ensemble of structures and cell populations that surround neoplastic cells and profoundly modulate their biological and metabolic behavior. It includes several cellular components, such as cancer-associated fibroblasts (CAFs), endothelial cells (ECs), immunocytes, adipocytes, blood vessels, and the ECM, the most representative acellular component [20]. These components strongly affect the abnormal proliferation of tumor cells, initiating and sustaining mechanisms of invasiveness, migration, and both physical and biochemical resistance to anticancer therapies [21]. The tumor microenvironment supports cancer progression by disrupting normal regulatory signals that control cell proliferation and growth. This enables tumor

cells to avoid programmed cell death, sustain unchecked growth, invasion of tissues, reprogram metabolic pathways, induce new blood vessel formation, and evade immune responses [22]. The TME is not merely a collection of cells and structural components, but also a chemically and physically altered context compared to healthy tissues. TME is characterized by a reduced pH resulting from the elevated glucose consumption and lactate production of tumor cells, further exacerbated by poor oxygenation. This acidic milieu promotes invasiveness, weakens the immune response, and diminishes the effectiveness of many therapeutic approaches [23]. Another key hallmark is hypoxia, which arises from the disorganized and inefficient vascular network that fails to deliver oxygen uniformly. Tumor cells respond by activating adaptive programs, which enhance their aggressiveness and survival under adverse conditions [24]. Within this complex chemical and physical scenario, a continuous crosstalk develops among tumor cells, stromal cells, immune cells, and the ECM. This bidirectional communication, mediated by soluble factors, metabolites, and physical interactions, actively reshapes the microenvironment and promotes tumor growth, while compromising the integrity and function of neighboring tissues. The main elements of the ECM and the tumor microenvironment are shown in Figure 1 [25].

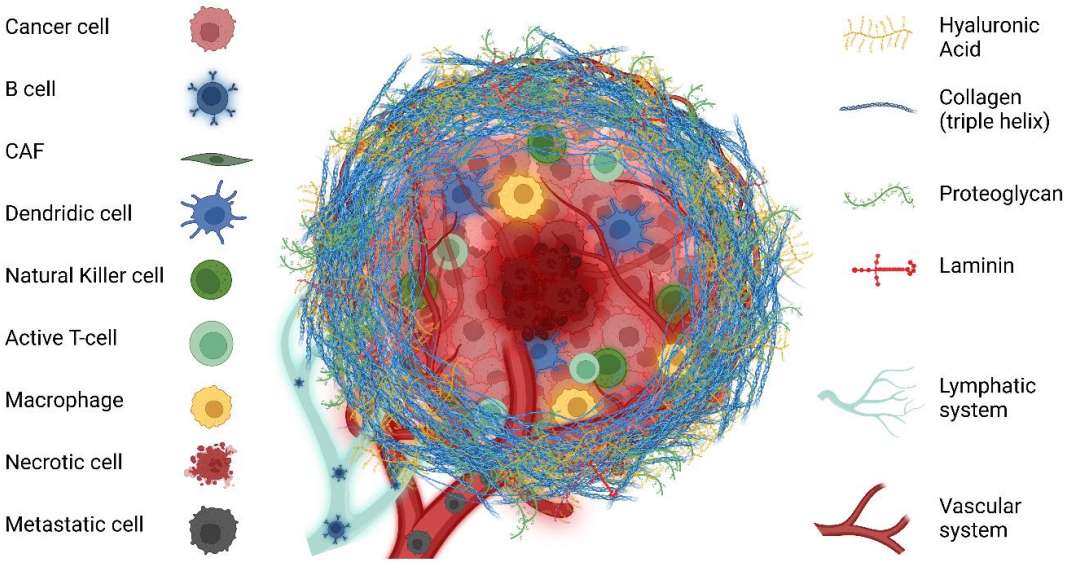

Figure 1: Schematic representation of the key components within the tumor microenvironment of solid tumors. The tumor microenvironment is a complex and dynamic structure that consists of tumor cells, immune cells, stromal cells, and the extracellular matrix. One of the major factors influencing the stiffness of the ECM is the excessive deposition of collagen fibers, which significantly alters the biomechanical properties of the tumor.

Image from Lo Buglio et al., *'The Multifaceted Role of Collagen in Cancer Development and Progression*,' IJMS, 2024, doi: 10.3390/ijms252413523 [25]. Copyright via CC BY-NC-ND 4.0 - https://creativecommons.org/licenses/by/4.0/

1.2.2 Cellular Components of the Tumor Microenvironment: Stromal, Immune, and Endothelial Cells

The tumor microenvironment is shaped not only by its chemical, physical, and signaling features but also by its cellular constituents, which actively govern tumor behavior. Among these, stromal cells, immune cells, and endothelial cells play central roles in driving tumor growth, invasion, and therapeutic response. -

1.2.2.1 Stromal cells: Cancer-Associated Fibroblasts (CAFs)

The most abundant and functionally active stromal cells within the TME are the Cancer-Associated Fibroblasts (CAFs). They are pivotal components of the tumor microenvironment that possess enhanced functional properties, such as proliferation, migration, and secretion of ECM amorphous compounds, including collagen. Although they were previously identified as homogeneous cell populations, recent studies have shown that they can exhibit high variability [26,27]. In fact, compared to normal

fibroblasts, CAFs are characterized by larger sizes and more distinct shapes. They originate from various sources, including epithelial cells, peri-tumoral adipocytes, hematopoietic stem cells, endothelial cells, or mesenchymal cells such as fibroblasts [28,29]. Moreover, CAFs' heterogeneous subpopulations can coexist within the same tumor mass, and they interact in different ways with tumor ECM and TME cells. Immunohistochemical studies have shown that CAFs generally express proteins such as the cell surface protein Thy1 (CD90), smooth muscle alpha-actin (α-SMA), fibroblast activation protein (FAP), and S100A4 protein [30]. CAFs' subpopulations can modify their phenotypes during tumor progression, highlighting the dynamic nature of the tumorigenic process [31]. They have an important relationship with the tumor microenvironment. These cells maintain a hyperactivated state and display heightened metabolic activity. These conditions increase production of ECM factors, such as tenascin (TNC), periostin (POSTN), and secreted protein acidic and rich in cysteine (SPARC) [32]. Their activity contributes to shaping the tumor mass in a thick tumoral ECM. This contribution occurs through the synthesis and altered deposition of laminin, HA, fibronectin, and collagens type I, III, IV, and V, above all, collagen type I [33]. CAFs, stimulated by cancer cells, hyperexpress the hyaluronic and proteoglycan binding protein 1 (HAPLN1), compared to normal fibroblasts [34]. Through HAPLN1, CAFs promote the invasion of cancer cells by remodeling the extracellular tumor matrix, due to an upregulation of the HA/CD168/ERK pathway [35]. Moreover, CAFs are involved in the initiation, growth, and invasion of cancer cells through the secretion of several tumor-promoting factors, such as stromal-derived factor 1 (SDF-1), interleukin 1β (IL-1β), PDGF, phosphatase and tensin homolog (Pten), and Sonic hedgehog (Shh) (Fig.2) [36–38]. In addition, through the secretion of hepatocyte growth factor (HGF), CAFs enhance the stem cell-like characteristics of tumor cells, which is essential for tumor progression. A brief overview of the main protumorigenic roles of CAFs is shown in Figure 2 [39].

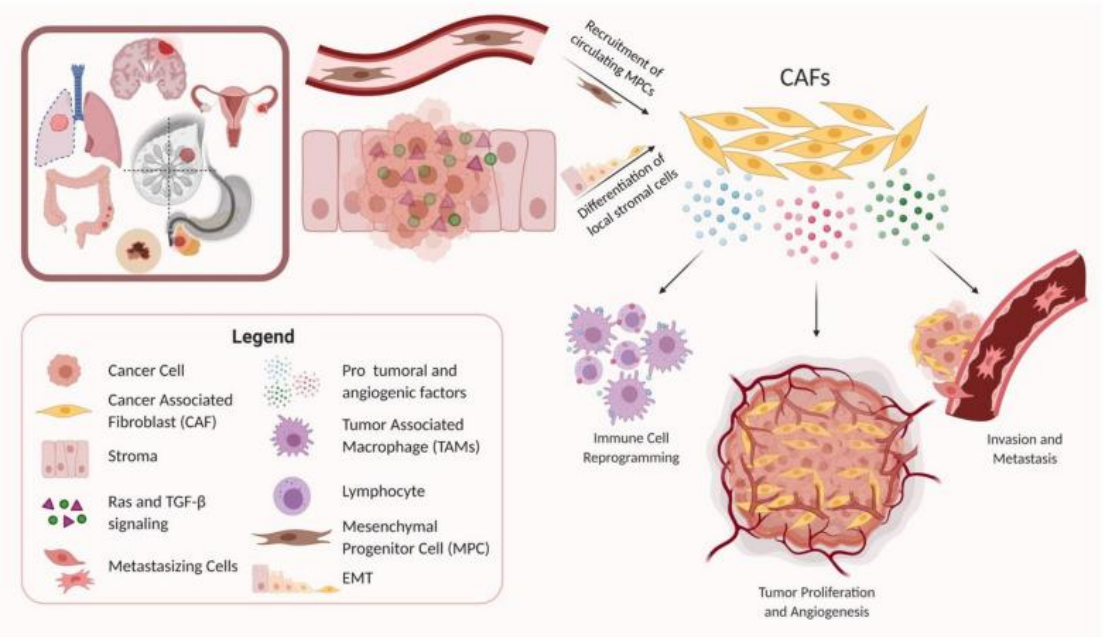

Figure 2: The role of cancer-associated fibroblasts (CAFs) in cancer. Illustration of the diverse mechanisms involving cancer-associated fibroblasts (CAFs) within the tumor microenvironment (TME). CAFs contribute to tumor progression by orchestrating multiple protumorigenic processes, including remodeling of the immune cells, secretion of extracellular matrix components and cytokines, stimulation of tumor cell proliferation and angiogenesis, and facilitation of cancer cell invasion and metastatic dissemination. Collectively, these activities promote tumor growth, therapeutic resistance, and disease progression.

Image from Karan Kohli et al. 'Key chemokines direct migration of immune cells in solid tumors', Cancer Gene Therapy, 2022, doi: 10.1038/s41417-021-00303-x [39]. Copyright via CC BY-NC-ND 4.0 - https://creativecommons.org/licenses/by/4.0/

1.2.2.2 Tumor-Associated Immune Cells

Together with CAFs, immune cells constitute key components of the tumor microenvironment, actively interacting with tumor and stromal cells to influence cancer progression. On one hand, the tumor microenvironment limits the function of tumor-infiltrating lymphocytes (TILs) through entrapment within the dense collagen matrix and engagement of inhibitory signals, including Programmed Death-Ligand 1 (PD-L1) and Leukocyte-Associated Immunoglobulin-like Receptor 1 (LAIR-1) [40–42]. However, additional immune and stromal elements actively contribute to immunosuppression, thereby facilitating tumor growth, invasion, and drug resistance. For example, the secretion of cytokines, such as interleukins (IL-4, IL-6, IL-10, IL-13) and Transforming Growth Factor Beta-1 (TGF-β) by Tumor-associated macrophages (TAMs), including M2-polarized macrophages, contributes to TME remodeling and immune suppression [43–45]. TAM2s can promote tumor progression by producing collagen I and activating signaling pathways like α2β1 integrin/PI3K/Akt, and regulate immune cell activity, often

suppressing cytotoxic T lymphocyte function [46,47]. Moreover, the collagen I interacted with Discoidin Domain Receptor 1 (DDR1) has been shown to upregulate chemokine CXCL5. The resulting increase in CXCL5 promotes the formation of neutrophil extracellular traps (NETs) by tumor-associated neutrophils (TANs), a key driver of metastatic dissemination [48]. Based on the above facts, the complex interaction between immune cells and the TME becomes evident, as several immune populations contribute to tumor progression. Therefore, the immune compartment does not exclusively exhibit antitumor functions but also includes cellular populations that actively support tumor growth and progression, as illustrated in Figure 3 [49].

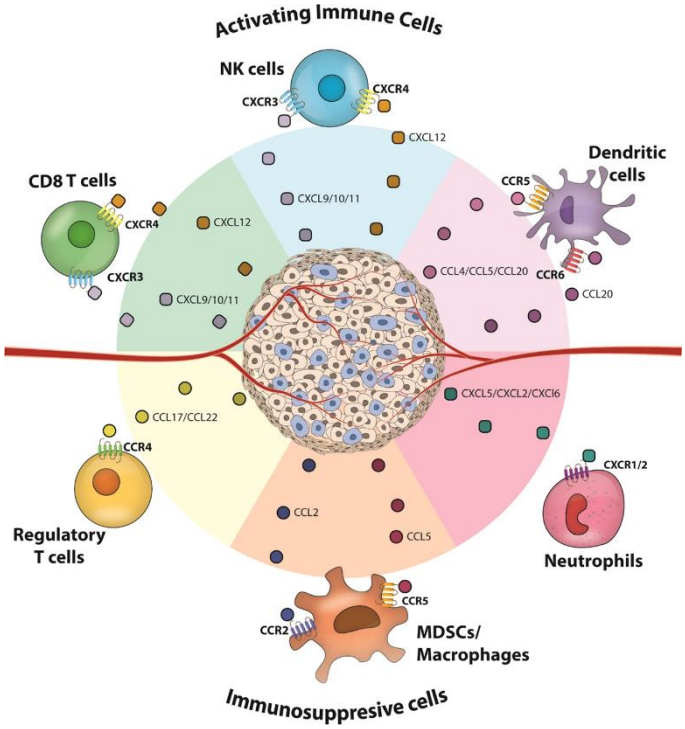

Figure 3: Dual Role of Immune Cells in the Tumor Microenvironment. Schematic representation of the dual role of immune cells within the tumor microenvironment. While some immune cell populations contribute to antitumor immunity, others promote tumor growth and progression by fostering immunosuppression, through the release of cytokines, chemokines, and growth factors.

Image from Cameron Walker et al. '*Role of Extracellular Matrix in Development and Cancer Progression*', *IJMS,* 2018, doi: 10.3390/ijms19103028 [49]. Copyright via CC BY-NC-ND 4.0 - https://creativecommons.org/licenses/by/4.0/

1.2.2.3 Endothelial Cells and Tumor Vascular Network

Endothelial cells form the inner lining of blood vessels and constitute the fundamental structural and functional unit of the vascular system. In healthy tissues, they maintain

vessel quiescence, regulate permeability, ensure oxygen and nutrient exchange, and remain tightly anchored to a continuous basement membrane [50–52]. Their behavior is tightly controlled by mechanical cues, growth factors, and interactions with pericytes and the ECM [53].

Within tumors, endothelial cells undergo profound phenotypic and functional alterations, giving rise to aberrant angiogenesis with irregular vessel organization, excessive branching, incomplete pericyte coverage, discontinuous basement membranes, and enlarged fenestrations up to ~780 nm [54,55]. This structural disarray promotes uncontrolled passage of large solutes into the tumor interstitium, inducing the Enhanced Permeability and Retention (EPR) effect [56,57]. Combined with rapid proliferation of tumor and stromal cells and insufficient lymphatic drainage, this leads to increased osmotic pressure and elevated interstitial fluid pressure (IFP) [58,59]. Unlike healthy tissues, where IFP is maintained within 3 mmHg of atmospheric pressure, tumors may reach values up to 100 mmHg [60], generating a steep pressure gradient that drives interstitial fluid outward, restricting drug diffusion and complicating dosing strategies, thus enhancing therapeutic resistance (Drug Resistence) [61,62].

From a biochemical perspective, angiogenesis is driven by the vascular endothelial growth factor (VEGF) family, including VEGFA, VEGFB, VEGFC, and VEGFD [63]. VEGFs are synthesized and released into the TME by stromal cells, endothelial cells, and tumor cells, promoting new vessel formation (Neoangiogenesis) [64]. Pro-angiogenic signaling is further enhanced by hypoxia, resulting from uncontrolled TME expansion and vascular dysfunction, as well as delivering of oxygen and nutrients, and dissemination of metastasis (Fig.4) [65,66]. Tumor adaptation relies primarily on hypoxia-inducible factors (HIF1, HIF2), with HIF-1 inducing transcription of VEGF and other pro-angiogenic genes to restore oxygen supply[67,68].

Therefore, the tumor vascular system plays a pivotal role in cancer progression. Its abnormal, leaky architecture contributes to hypoxia, high interstitial fluid pressure, and impaired drug delivery, directly impacting therapeutic efficacy.

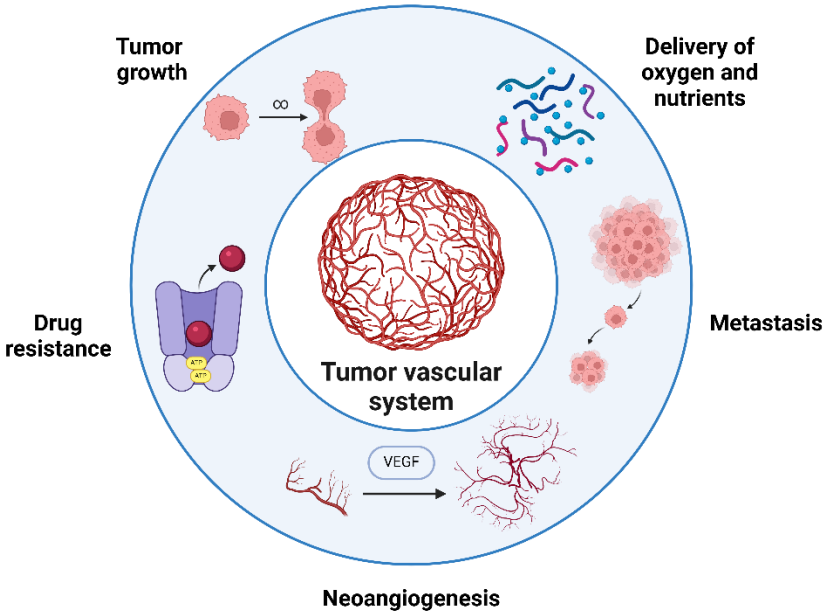

Figure 4: Schematic representation of the tumor vasculature and its roles in cancer progression. The tumor vasculature supports growth by facilitating nutrient and oxygen delivery, while also contributing to chemoresistance by limiting drug penetration. Additionally, it promotes metastasis by enabling tumor cells to enter the bloodstream, allowing for the spread of cancer to distant organs.

1.2.3 Non-Cellular Components of the Tumor Microenvironment

In addition to stromal, immune, and endothelial cells, the tumor microenvironment is defined by a complex network of non-cellular components that play a biochemical and mechanical role in tumor cell behavior. For instance, cytokines, secreted by both tumor and infiltrating immune cells, modulate inflammation, immune cell recruitment, and polarization, thereby shaping antitumor responses [69]. Key pro-inflammatory cytokines, including IL-6 and IL-8, directly enhance tumor proliferation and survival, whereas immunosuppressive molecules such as IL-10 and TGF-β attenuate cytotoxic T lymphocyte activity and promote epithelial-to-mesenchymal transition (EMT), favoring invasion and metastasis [70–72]. Soluble growth factors, including VEGF, platelet-derived growth factor (PDGF), and epidermal growth factor (EGF), drive proliferation, survival, and angiogenesis, stimulating new vessel formation that ensures oxygen and nutrient delivery to rapidly expanding tumor areas [73]. These factors interact with their respective receptors on stromal, endothelial, and tumor cells, generating positive feedback loops that further amplify neoplastic progression [74]. In this contest, extracellular vesicles (EVs), including exosomes and microvesicles, function as nanoscale shuttles of proteins, lipids, and nucleic acids, facilitating distal modulation of angiogenesis, immune suppression, and metastatic competence [75].

Within solid tumors, all these factors are partially sequestered, organized, and dynamically exchanged within the ECM, which acts as a biochemical and biophysical scaffold integrating their signals [76]. Among non-cellular TME components, the ECM holds a central role, acting not merely as a structural scaffold, but as a dynamic integrator of chemical, mechanical, and metabolic cues that regulate tumor growth, invasion, and therapeutic response. Its composition, alignment, and continuous remodeling influence cell proliferation, migration, immune evasion, and drug diffusion, establishing the ECM as a critical determinant of tumor progression.

1.2.4 The Tumor Extracellular Matrix

The ECM is a dynamic component of all tissues that provides both a structural scaffold and instructive biochemical cues. It is composed of water, minerals, and a three-dimensional network of macromolecules, such as, fibronectin, laminins, elastin, proteoglycans (heparan sulfate and versican), and adhesive glycoproteins, including tenascin-C and thrombospondin. Among the more than 300 proteins that compose the ECM and regulate its functions, typically classified within the so-called matrisome, collagen is the most abundant, since it plays a key role in tissue biomechanics [25,77]. The functions performed by the ECM vary within tissues and strongly depend on the different composition of proteins. In general, the ECM is involved in pH maintenance, regulation of cell proliferation and differentiation, and support and anchoring for cells [78,79]. Based on different needs, each tissue develops a bio-physical and bio-chemical dynamism where the ECM represents the component that changes the most [80]. A synergistic relationship is established, wherein cells modulate the ECM's compactness, which in turn induces the activation of various mechanotransduction pathways [47]. However, the ECM plays a key role in the formation and progression of solid tumors.

From a structural point of view, the ECM of solid tumors is an envelope that surrounds, protects, and interacts with tumor cells that compose the tumor mass [81]. Tumor ECM has components that share similarities with the ECM of healthy tissues, such as collagens, hyaluronic acid, elastin, proteoglycans, glycoproteins, such as tenascin-C, laminins, fibronectins, and other proteins [82]. However, changes in the percentage composition of these elements compared to healthy tissues lead to structural and functional alterations that trigger and promote tumor development [83].

Thanks to the macromolecules that compose it, a strong rigidity is generated, which is abnormal when compared to healthy tissues' ECM. As an example, the stiffness of ECM in

some districts, such as breast, brain, liver, lung, and pancreas, is generally around 1 kPa, while it can reach values between 4-10 kPa in tumors located at the same sites [82,84].

1.2.5 Role of Tumor Extracellular Matrix in Cancer Progression

During tumor growth, the fibrotic extracellular environment is continuously modified by multiple factors, such as matrix metalloproteinases (MMPs). In normal tissue, the constant remodeling of ECM depends on proteases, particularly MMPs, "a disintegrin and metalloproteinase with thrombospondin motifs" (ADAMTs), and Tissue Inhibitor of Metalloproteinase 1 (TIMP-1), secreted by resident cells [85,86]. By modifying various constituents of the ECM, these enzymes alter microenvironmental density, producing mechanical signals that influence cellular behavior. However, MMPs actively participate in tumor progression through extracellular matrix remodeling [87].

Moreover, CAFs play a significant role in ECM architecture. Their heightened secretion of growth factors and deposition of extracellular components, including collagen, cause stiffness of the ECM, which impedes the accessibility of drugs and immune cells, reducing therapeutic efficacy. The ECM turnover by CAFs is a complex process, in which a heterogeneous structure is created with high-density regions of collagen [88]. In this way, the invasive capacity and the drug resistance of cancer cells are amplified [89]. Hypoxia also drives ECM remodeling: HIF-1 regulates genes involved in collagen synthesis and MMP activity [90], inducing rigid, aligned collagen fibrils through P4HA1, P4HA2, PLOD1, and PLOD2 [91]. This ECM reorganization in sarcomas and breast cancer lines enhances tumor cell invasion and migration [92–95].

Therefore, a dynamic balance is established between the deposition of collagen and other ECM components, which increases matrix stiffness, and the remodeling mediated by MMP, shaping the ECM architecture to support both the protective and invasive needs of the tumor. This remodeling alters the biochemical composition and mechanical properties of the ECM, ultimately influencing tumor cell behavior and invasion (Fig. 5).

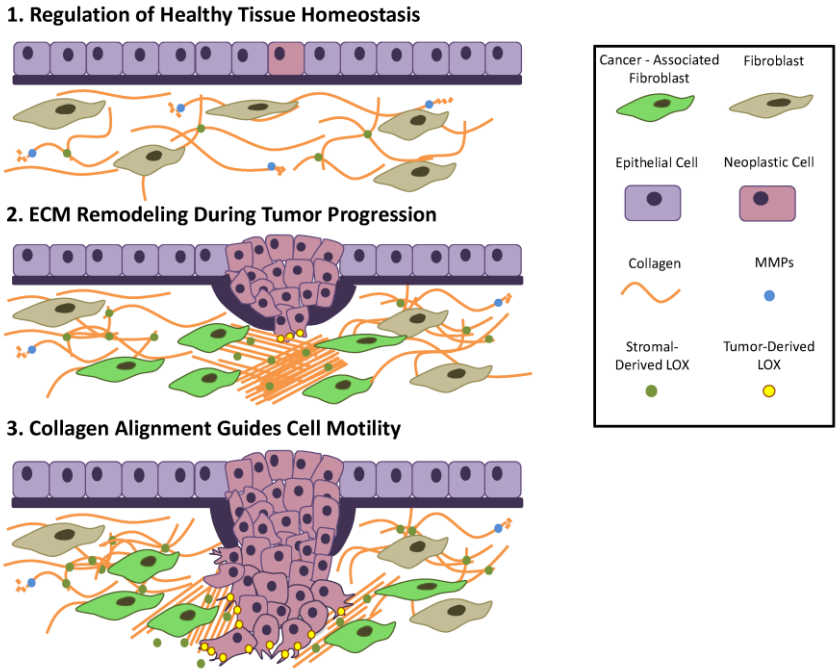

Figure 5: Extracellular Matrix Remodeling as a Driver of Tumor Initiation and Invasion. Rapid proliferation of neoplastic cells induces mechanical stress on the basement membrane, leading to its deformation. Cancer-associated fibroblasts promote collagen deposition and alignment through stromal enzymes, such as MMPs and LOX, facilitating basement membrane disruption and directional cancer cell invasion along remodeled collagen fibers.

Image from Cameron Walker et al. *'Role of Extracellular Matrix in Development and Cancer Progression'*, *IJMS*, 2018, doi: 10.3390/ijms19103028 [49]. Copyright via CC BY-NC-ND 4.0 - https://creativecommons.org/licenses/by/4.0/

1.2.6 Biochemical Signaling, Mechanical Properties, and Implications for Drug Resistance of Tumor Extracellular Matrix

In addition to serving as a physical scaffold, the ECM acts as a reservoir of bioactive molecules, including growth factors, cytokines, chemokines (TGF-β, VEGF, PDGF, and tenascin-C) [96,97]. These factors can be sequestered within the matrix and released upon proteolytic cleavage, thereby modulating tumor cell proliferation, survival, and invasion [98–100].

Among the various functions that the ECM performs within the tumor microenvironment, it also plays a key role in regulating tumor cell metabolism, including the Warburg effect [101]. Increased ECM stiffness hinders lactate diffusion, promoting its local accumulation and acidification of the TME [102].

Moreover, the ECM modulates paracrine signaling by retaining or presenting soluble factors to neighboring cells, thereby orchestrating the cross-talk among tumor, stromal,

endothelial, and immune cells [103]. Vesicular trafficking, mediated by exosomes and microvesicles, further amplifies this communication by transporting bioactive molecules that influence angiogenesis, immune evasion, and the metastatic potential of the tumor [50,75,104].

The tumor ECM stiffness progressively increases, forming a dense and rigid shell that supports their uncontrolled expansion, amplifying pro-tumorigenic signaling, enhancing cell survival, migration, and invasive behavior through the activation of several protumoral pathways [105,106]. Its extreme rigidity, resulting from the accumulation of collagen and other proteins, creates a compact network that hinders drug penetration, reducing both diffusion and convective transport [82]. This elevated stiffness can increase interstitial pressure and alter the morphology of tumor blood vessels, thereby compromising the transfer of therapeutic molecules from the bloodstream to the tumor tissue [107,108].

In addition, the ECM further promotes chemoresistance by activating mechanotransduction pathways. For instance, the increased ECM stiffness promotes drug resistance in gastric cancer and in hepatocellular carcinoma [109,110].

Therefore, the tumor ECM plays a pivotal role in shaping the biochemical and mechanical properties of the tumor microenvironment, influencing cell behavior, signaling, and drug resistance. However, among its different components, collagen represents a key structural and functional element, critically contributing to matrix stiffness, cell–matrix interactions, and cell metabolism.

1.2.7 Collagens in the Tumor Extracellular Matrix: Multifaceted Roles in Mechanotransduction, Chemoresistance, and Immune Evasion

Collagens are a fundamental and multifaceted constituent of the tumor ECM, serving as both a physical scaffold and an active regulator of tumor cell function. In solid tumors, its deposition becomes dysregulated, with a pronounced accumulation of fibrillar collagens such as type I and IV, which strongly contribute to increased matrix stiffness and altered biomechanical properties Figure 6 illustrates the different collagen types, highlighting their structural characteristics and their roles in tumor progression. (Fig. 6) [25].

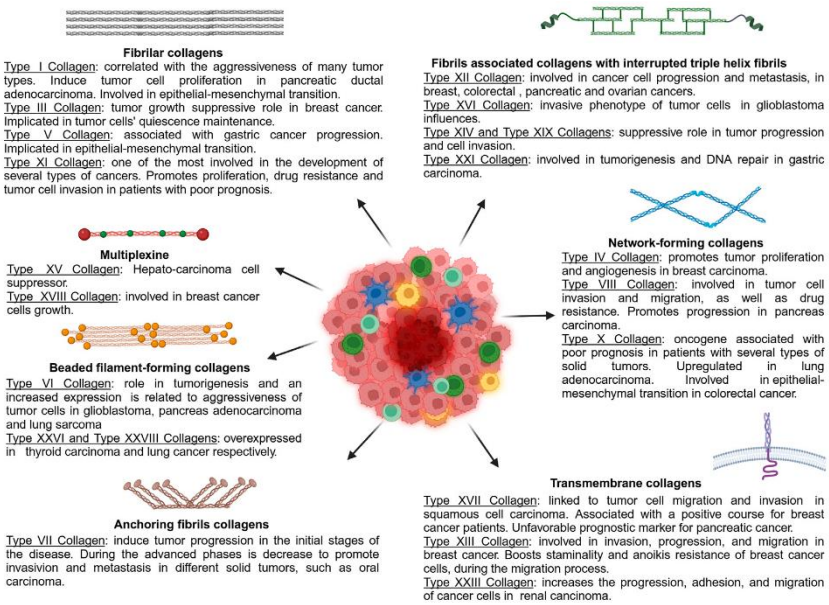

Figure 6: Overview of Collagens in Tumor Progression. *Collagens classification* by *their* supramolecular organization, highlighting their distinct contributions to tumor development. Each collagen type plays specific roles in modulating the extracellular matrix, influencing cancer cell behavior, invasion, and metastasis.

Image from Gabriele Lo Buglio et al. '*The Multifaced Role of Collagen in Cancer Development and Progression*, *IJMS,* 2024, doi: 10.3390/ijms252413523 [25]. Copyright via CC BY-NC-ND 4.0 - https://creativecommons.org/licenses/by/4.0/

This stiffening arises from excessive collagens synthesis and enzymatic cross-linking, mediated mainly by LOX and LOX-like enzymes, whose upregulation in the tumor stroma and malignant cells reinforces a mechanically rigid ECM [111,112]. The collagen interaction with the cell adhesion receptors, such as integrins, establishes a crosstalk between these matrix components and the cells of the tumor microenvironment, transducing extracellular signals into intracellular pathways such as FAK (focal adhesion kinase), PI3K/AKT, and Rho-GTPases [113–115]. For instance, integrin-mediated signaling regulates key tumor cell behaviors, including proliferation, chemoresistance, and migration [116,117]. Integrins are transmembrane glycoproteins that act as mechanosensors, receiving physical stimuli from the extracellular environment, primarily through interactions with collagens, and triggering appropriate cellular responses, such as polarity, migration, differentiation, and survival [118]. Specifically, some of these glycoproteins are known to be involved in the metastatic process, mediating the interactions between tumor cells and the site predisposed to metastasis. For example, integrin αvβ3 is over-expressed in breast or prostate cancer patients with propensity to develop bone metastases [119–122].

Beyond structural tension, collagen influences tumor cell metabolism. High collagen density has been shown to stimulate the Warburg-like metabolic reprogramming in cancer cells, activating integrin-dependent PI3K/AKT signaling, which upregulates glycolytic effectors such as GLUT1 and PKM2, thus facilitating adaptation to a stiff microenvironment [123]. Concomitantly, collagen remodeling via MMPs and LOX facilitates dynamic ECM networking, enabling invasive processes. The interaction between collagens and integrin triggers persistent signaling such as YAP/TAZ, invadopodia formation, and epithelial–mesenchymal transition [124,125]. The interplay between collagen and cell death pathways also underscores its regulatory versatility. Collagen-integrin engagement can enhance anti-apoptotic signaling, for instance via β-catenin and Bcl-2, while interactions with DDRs modulate apoptotic sensitivity, depending on the specific collagen isoforms interaction [126,127]. This duality is well aligned with the concept of collagen as a "double-edged sword" in cancer progression: while it may restrain early neoplastic proliferation, it actively supports disease advancement in established tumors. In metastatic and invasive contexts, the organization of collagen fibers becomes highly strategic. CAFs not only produce collagen but remodel it into aligned fibrillar networks that guide invasive fronts.

Collagen also supports chemoresistance through both physical and biochemical mechanisms. Dense collagen matrices not only restrain drug diffusion but also transduce survival signals: integrin α2β1–collagen interactions can upregulate ABC transporters and DNA methyltransferases (e.g., DNMT1), thereby contributing to enhanced drug efflux and epigenetic alterations that favor resistance [128–130]. Finally, collagen modulates immune cell behavior within the tumor microenvironment: its dense and aligned fibers can form physical barriers to immune infiltration, while its interaction with receptors such as LAIR-1 on T lymphocytes suppresses anti-tumor immune responses, thereby facilitating immune evasion [131–133]. Taken together, these insights reveal collagens as dynamic and central regulators of tumor biology, a molecule whose abundance and functional plasticity enable it to orchestrate mechanotransduction, metabolism, survival signaling, migration, chemoresistance, and immune crosstalk (Fig. 6).

In conclusion, this evidence indicates that the tumor ECM is a key factor in the progression of solid tumors, for example, by triggering mechanisms of resistance to chemotherapeutic agents and to immune-cell activity. Indeed, the excessive ECM density and stiffness form a physical barrier that impairs drug penetration and promotes the activation of survival signaling pathways. Since collagen is the main component, its controlled degradation may

represent a promising strategy to reduce stromal rigidity, enhance the diffusion of drugs and immune cells, and potentiate their efficacy.

1.3 Tumor Priming Strategies to Enhance Drug Penetration and Overcome Chemoresistance

In solid tumors, multiple structural and pathophysiological features, such as a dense collagen-rich ECM, elevated interstitial fluid pressure, and aberrant vasculature, impede immune-cell infiltration, intratumoral drug diffusion, and efficacy [134–136]. For instance, these features thereby compromise the efficacy of cytotoxic agents, which is often hindered by irregular access to tumor tissue [137]. Moreover, suboptimal penetration of chemotherapeutics into solid tumors may lead to insufficient therapeutic efficacy and can promote chemoresistance. In fact, sublethal intracellular drug concentrations induce tumor and stromal cells to chemoresistance, for example, with an increased membrane exposure of efflux pumps, such as P-glycoprotein (ABCB1 or P-gp) [138]. This mechanism results in a condition known as Multidrug Resistance (MDR), in which cancer cells exhibit reduced drug uptake and sensitivity to chemotherapeutic agents [139]. Consequently, these insufficient drug levels fail to eradicate the tumor and increase the risk of recurrence, as resistant cell populations persist within the microenvironment [140]. For this reason, tumor priming could represent a therapeutic strategy aimed at temporarily modifying the tumor microenvironment to enhance the penetration, distribution, and efficacy of antitumor agents and/or immune cells, as well as reduce chemoresistance. Tumor priming aims to overcome these barriers in a controlled and transient manner, leading to an increased permeability so that therapeutic molecules or cells can more effectively reach cancerous tissues [141].

A critical aspect of this approach is the precise temporal coordination between the priming intervention and the administration of the therapies, as improvements in intratumoral perfusion may be limited in time [142]. Beyond enhancing drug diffusion and efficacy, pretreatment can also make tumor cells more sensitive to subsequent therapeutic interventions. Several strategies can be employed to achieve effective tumor priming. For instance, hyperthermia and ultrasound promote vascular dilation and drug diffusion, while protease treatment, such as collagenases, can modulate the ECM, increasing therapy administration [143–146]. These approaches create a transient manner to improve enhanced permeability.

1.3.1 Synergistic Strategies Combining ECM Degradation and Chemotherapy in Solid Tumors

The synergistic approach that combines ECM degradation with the administration of antitumor therapies represents a promising strategy to overcome the physical and biochemical barriers typical of solid tumors.
Several studies, including an *in vivo* investigation in rats with colorectal peritoneal carcinomatosis, have demonstrated that collagenase reduced extracellular fibrosis and enhanced drug accessibility [147]. On the other hand, collagenases can also be conjugated to liposomes, generating so-called collagozomes, as demonstrated by Wang and colleagues. In particular, in mouse models of pancreatic ductal adenocarcinoma (PDAC) collagozomes reduced stromal fibrosis and increased intratumoral accumulation of the subsequently administered chemotherapeutic agent Paclitaxel, improving therapeutic efficacy without increasing systemic [147]. Moreover, collagenases have improved the precision, safety, and accessibility of Chimeric Antigen Receptor (CAR) T cells, reinforcing their potential as adjunctive therapies in solid tumors, such as pancreatic cancer [148].
Taken together, these data demonstrate the effectiveness of "two-step" strategies in the treatment of fibrotic solid tumors, based on pretreatment with collagenase followed by administration of the chemotherapeutic agent. However, in addition to the sequential approaches, co-delivery formulations have also been explored.

For example, thermosensitive hydrogels with antivascular effects containing both collagenase and the trastuzumab antibody enable controlled ECM degradation, improved penetration of the therapeutic antibody, as well as an increase in drug retention by one additional week compared to controls [149]. A further approach was described in a recent study on pancreatic carcinoma, in which copper-based mesoporous nanoparticles decorated with collagenase enabled significant ECM remodeling *in vitro* and *in vivo*, improving the efficacy of the therapeutic agent [150]. Similarly, Li *et al*. developed collagenase-functionalized liposomal nanozymes, showing improved drug diffusion and enhanced antitumor responses in breast cancer models [151].

Finally, it is also well reported that the combination of ECM degradation with conventional chemotherapy. For instance, Wang *et al.* developed pH-sensitive nanocarriers carrying collagenases, capable of selectively degrading collagen and promoting intratumoral accumulation of liposomes loaded with the anticancer drug Doxorubicin (DOX-Lip), showing an increase of up to nearly three-fold in drug accumulation compared with controls [152]. Additional strategies include gold nanoparticles decorated with

collagenases and conjugated with doxorubicin, resulting in a more intensive synergistic effect [153].

1.4 Collagen as a Therapeutic Target

Collagen represents a structural and functional determinant of the tumor ECM, making it an attractive therapeutic target for stromal normalization. Several strategies, for instance, using antifibrotic drugs, have been developed to modulate collagen abundance, biosynthesis, organization, and signaling within solid tumors [102,154,155]. One major therapeutic approach involves inhibiting collagen cross-linking, primarily mediated by LOX and LOX-like enzymes, which drive ECM stiffening and promote drug resistance [156]. Pharmacological or antibody-based LOX/LOX-L inhibitors, for example, in triple-negative breast cancer (TNBC), can reduce matrix rigidity, enhance intratumoral perfusion, and increase tumor permeability, sensitivity to chemo and immunotherapies [157]. A second strategy focuses on suppressing collagen synthesis by targeting enzymes essential for collagen maturation, such as prolyl 4-hydroxylases (P4HA) type 1 and 2 [158]. Inhibiting these enzymes decreases stromal collagen deposition, attenuates desmoplasia, and enhances drug diffusion in preclinical models. Upstream regulators, such as TGF-β, can also be blocked to limit fibroblast activation and collagen production [159]. Interfering with collagen uptake and metabolism represents an additional therapeutic avenue. Targeting collagen–cell interactions is another promising direction. For instance, inhibitors of integrins such as TC-I-15 or DDRs can disrupt collagen-driven mechanotransduction pathways that promote tumor survival and invasion [160,161]. Collagen-derived fragments, including tumstatin and tetrastatin, also exhibit anti-angiogenic activity, offering therapeutic opportunities to exploit collagen [162,163]. Additionally, circulating collagen fragments have emerged as biomarkers of stromal remodeling and predictors of therapeutic responsiveness, supporting patient stratification for ECM-targeting treatments [164].

There is also a therapeutic approach that involves the use of oncolytic viruses conjugated to collagen-targeting proteases, as well as bacteria, such as *Salmonella typhimurium*, capable of recognizing and degrading type I collagen within the tumor ECM, to enhance the accessibility of drugs or immune cells [165,166].

The use of specific proteases, either recombinant or extractive, such as collagenases, has enabled the targeted degradation of tumor-associated collagen, thereby enhancing therapeutic efficacy. Collagenase-based approaches aim to directly digest the pathological

collagen network, reducing stiffness and enhancing the penetration of both chemotherapeutics and immune cells [167]. However, the use of collagenases involves both promising advantages and notable challenges. A balanced assessment of these potential benefits is therefore necessary to understand their role within emerging tumor-targeting strategies.

1.4.1 Collagenases Treatment: Advantages and Limitations

Collagenases are extracellular proteases capable of selectively degrading collagen, the main structural component of the tumor ECM. By enzymatically cleaving collagen fibers, collagenases reduce matrix rigidity, thereby enhancing the penetration and distribution of chemotherapeutic agents within the tumor mass [136].

This effect has been demonstrated in multiple preclinical models, where collagenase treatment improved intratumoral perfusion and increased drug efficacy. In addition to facilitating drug delivery, collagenase-mediated ECM remodeling can enhance immune responses [168]. Collagenases can better access cytotoxic T lymphocytes and other effector immune cells to tumor cells, potentially augmenting the efficacy of immunotherapies [147,148]. Collagenase therapy can be made highly versatile, as this enzyme can be combined with different delivery systems to target various tumor types and their corresponding microenvironmental conditions. For instance, when co-administered with micro- or nanoparticles or hydrogels, it becomes possible to achieve a more controlled and targeted release of the drugs (Fig. 7) [169].

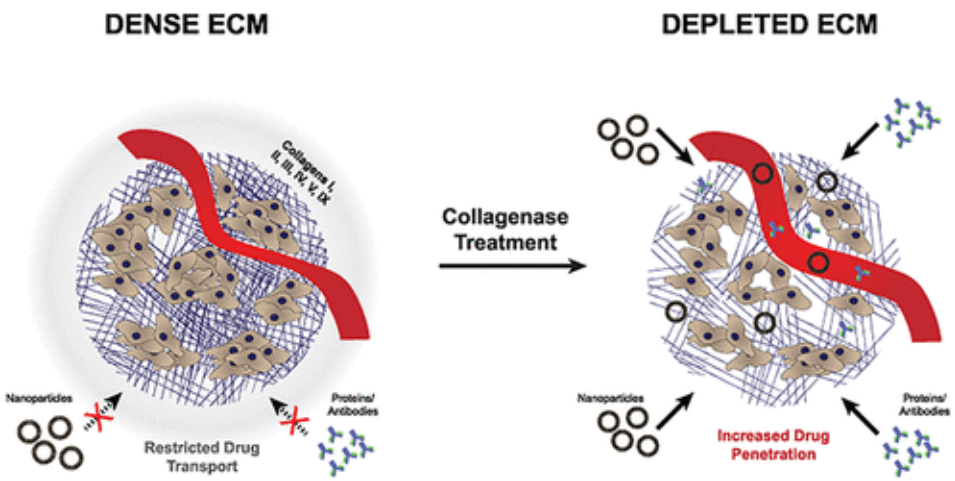

Figure 7: Collagen of tumor ECM and the role of collagenase treatment to improve drug delivery. The collagen overexpression in tumors is associated with enhanced tumor growth and metastasis. These ECM components contribute to a protective tumor microenvironment by increasing interstitial fluid pressure and creating physical barriers that limit the effective convection and diffusion of chemotherapeutic agents, antibodies, and nanoparticles. This figure illustrates how collagenase treatment, which depletes extracellular collagen, has been shown to normalize the tumor microenvironment, improving drug uptake and diffusion.

Reproduced with permission (license number 6206611089440, 12 Feb 2026) from Dolor, A.; et al. *'Digesting a Path Forward: The Utility of Collagenase Tumor Treatment for Improved Drug Delivery' ACS,* 2018, 15, 6, 2069-2083 doi: 10.1021/acs.molpharmaceut.8b00319. Copyright 2018 American Chemical Society [169].

Thus, the use of collagenases to digest the solid tumor ECM provides significant benefits, as the enzyme selectively cleaves collagen fibers, reducing stromal stiffness and interstitial fluid pressure that impedes drug diffusion. In this way, a deeper and more spatially uniform penetration of chemotherapeutic agents is achieved. Moreover, the localized degradation of collagen could interfere with pro-survival signaling pathways mediated by integrin-collagen interactions, further sensitizing tumor cells to treatment. In conclusion, the transient increase in stromal accessibility creates a therapeutic window that promotes enhanced drug uptake by tumor cells, thereby improving overall treatment efficacy and reducing the risk of recurrence. However, despite its therapeutic potential, collagenase therapy presents several risks, including possible off-target matrix degradation, inflammatory responses, and immunogenicity.

Collagenases, particularly when derived from exogenous sources such as bacteria (e. g., *Clostridium histolyticum*), cause several immunological risks that must be carefully considered in clinical applications [170]. One significant concern is immunogenicity through the production of specific antibodies against the enzymes, leading to

hypersensitivity reactions, inflammation, short half-life, and other adverse effects [171,172]. Moreover, extractive collagenases can carry residual endotoxins that pose safety concerns for *in vivo* applications. The presence of these endotoxins may trigger inflammatory responses and limit the therapeutic use of bacterial collagenases, highlighting the need for rigorous purification and quality control [173]. Collagenases can cause a range of allergic reactions, from mild symptoms like swelling and redness to more severe reactions, including anaphylaxis. Furthermore, the use of collagenases can trigger osteoarthritis *in vivo* [174]. Collagenases can exhibit off-target proteolytic activity, degrading ECM components not only within the tumor, but also in surrounding healthy tissues [175,176]. This off-target effect may lead to structural damage, inflammation, and compromise organ integrity. Consequently, the low specificity represents a significant challenge that must be carefully controlled in therapeutic applications, for example, via intravenous administration.

1.5 In Vitro Models for Studying the Tumor Microenvironment

The use of *in vitro* models is a vital tool in cancer research since it allows investigation of the cellular and molecular processes that underlie tumor progression and therapeutic responses. It provides reproducible and cost-effective analyses, while avoiding the ethical and physiological issues of animal models. However, the simplification *in vitro* can also become a significant limitation when compared with *in vivo* conditions.

Traditional two-dimensional (2D) models, commonly employed in cancer research, exhibit structural and functional constraints that compromise their ability to faithfully reproduce the tumor microenvironment complexity. In a 2D system, cancer cells grow on uniform surfaces that do not recapitulate the tridimensional depth, biochemical composition, and biomechanical dynamics of the TME *in vivo* [177]. Consequently, cell polarity and the spatial distribution of membrane receptors are lost. This leads to biochemical alterations across various signaling pathways, including those mediated by integrins, Focal Adhesion Kinase (FAK), Rho GTPases, and YAP/TAZ, which regulate adhesion, proliferation, metabolism, and drug response [178]. Moreover, 2D models fail to reproduce oxygen, pH, and metabolic gradients, including paracrine gradients, that characterize the TME. *In vivo*, this distribution generates regions of hypoxia, necrosis, or active proliferation, shaping functional heterogeneity [179].

Consequently, 2D models are often inadequate in predicting tumor behavior, drug resistance, and invasive mechanisms. To overcome these limitations, research has

progressively shifted toward three-dimensional (3D) cultures, which are capable of reliably recreating the biochemical, mechanical, and structural properties of the TME.

1.5.1 Spheroids as *In Vitro* Three-Dimensional (3D) Tumor Models.

3D models represent a fundamental advancement in the study of tumor biology and in preclinical drug evaluation, as they reproduce *in vitro* many of the structural, biochemical, and biomechanical properties characteristic of native tissues. Unlike bidimensional cultures, which constrain cells within a static and flattened environment, 3D systems promote radial growth, enabling the formation of tissue-like architectures, the establishment of cell–cell and cell–matrix interactions, and the spontaneous generation of oxygen and metabolite gradients [180]. These features recapitulate key aspects of tumor pathophysiology, including hypoxia, metabolic and cellular heterogeneity, pH variations, and functional compartmentalization, phenomena that shape proliferation, survival, and therapeutic response [181].

Among 3D approaches, spheroids represent the most versatile and widely adopted model. Spheroid cultures allow reproducing interactions among diverse cellular components, the activation of paracrine signaling pathways, and the genetic and biochemical modulation of the tumor phenotype. Their customizable cellular composition provides a powerful system to investigate processes such as immune evasion, ECM remodeling, and angiogenesis (Fig. 8) [182][183].

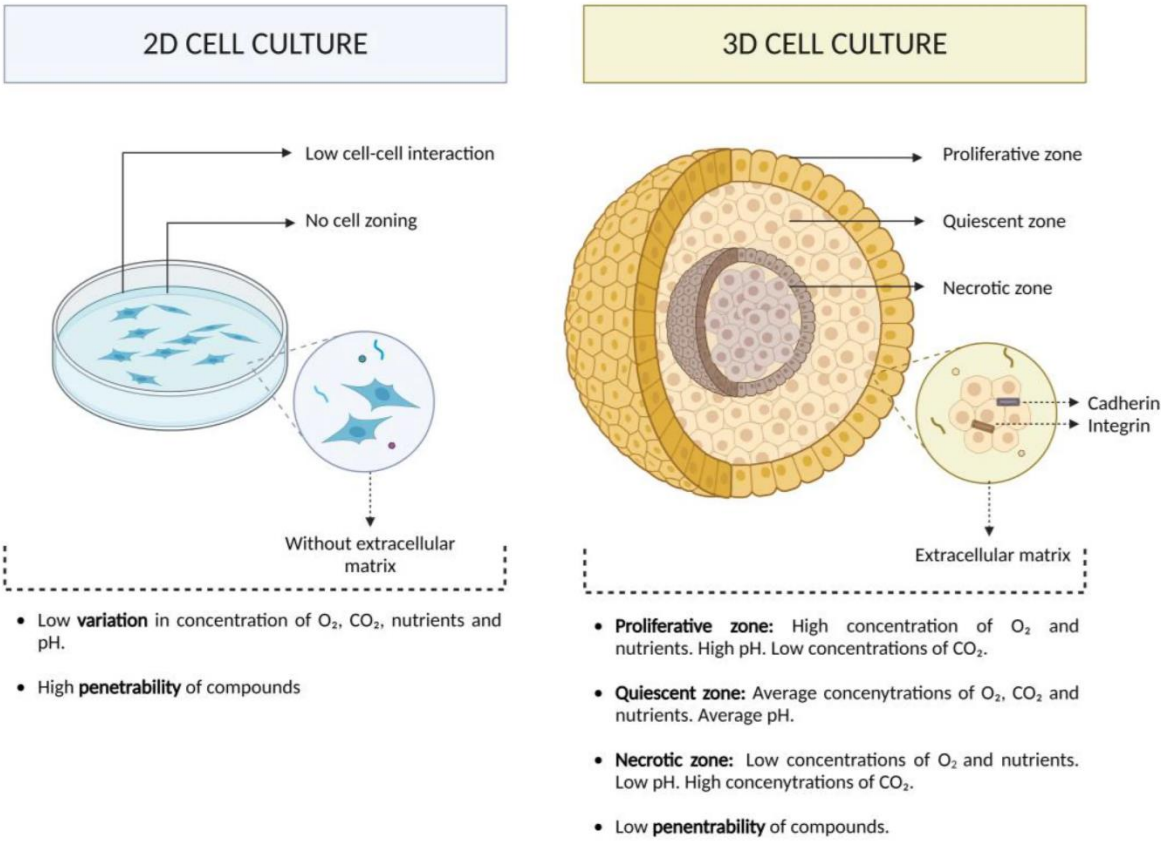

Figure 8: Schematic comparison between monolayer cell culture systems and three-dimensional spheroid models. Characteristics of conventional 2D monolayer cultures and 3D spheroids, emphasizing their structural, biological, and functional differences. While monolayer cultures provide a simplified and highly environment, 3D spheroids better recapitulate key aspects of tissue architecture, cell–cell and cell–matrix interactions, and the formation of biochemical gradients, representing a more physiologically accurate model for exploring tumor biology and drug response.

Image from Anali del Milagro Bernabe Garnique et al. *'Two-Dimensional and Spheroid-Based Three-Dimensional Cell Culture Systems: Implications for Drug Discovery in Cancer'*, *Drug and Drug Candidates*, 2024, doi: 10.3390/ddc3020024 [183]. Copyright via CC BY-NC-ND 4.0 - https://creativecommons.org/licenses/by/4.0/

The 3D tumor spheroids are classified into homotypic spheroids, composed of a single cell population, and heterotypic spheroids, which include multiple cell types and allow the investigation of interactions between tumor cells and stromal or vascular components. While homotypic spheroids provide a simpler and more reproducible system to study fundamental tumor-related mechanisms, heterotypic spheroids offer a more complex and physiologically relevant representation of the tumor microenvironment [184]. An additional level of biological relevance is achieved with spheroids generated from primary tumor cells (PTCs) isolated directly from patients, which retain the genetic and phenotypic heterogeneity of the original tumor [185]. Compared to established cell lines, these models more accurately reflect therapeutic responses and resistance mechanisms [186].

Spheroids retain several unique strengths. They are cost-effective, highly reproducible, require minimal specialized equipment, and naturally develop physiological intratissue gradients that closely mimic those of primary solid tumors. Their flexibility in cellular composition and potential for standardization make them ideal for comparative studies, drug screening, and chemoresistance analyses. For these reasons, spheroids represent the most efficient compromise among biological complexity, cost, scalability, and experimental control within the landscape of available 3D models.

1.5.2 Endothelial–Tumor Cell Co-Cultures: Advanced Spheroid Models

Among heterotypic spheroids, co-cultures of tumor spheroids with endothelial cells represent an advanced model for the study of angiogenesis processes [184]. In these systems, endothelial cells are integrated within or around the spheroid, promoting the spontaneous formation of vascular structures and the deposition of ECM. The presence of the endothelial cells allows the analysis of pro-angiogenic factor secretion (such as VEGF and PDGF) in a TME model, directional migration, vessel assembly, and matrix remodeling in relation to the angiogenic process [187–189]. Moreover, these spheroids recapitulate the dynamic cooperation between tumor and vasculature, providing a highly reliable 3D model for investigating tumor vascular permeability, drug resistance, or the efficacy of antiangiogenetic therapies.

Beyond the effects on vascular structures, these co-cultures can highlight how the vascular microenvironment can modulate tumor cell proliferation, survival, and invasiveness. Recent studies have shown that the integration of human umbilical vein endothelial cells (HUVECs) into patient-derived head and neck cancer spheroids allows a more accurate evaluation of the response to anti-angiogenic drugs, such as 5-fluorouracil or sunitinib, compared to 2D models or homotypic spheroids. Furthermore, the ability to combine stromal cells, fibroblasts, and immune components with endothelial cells in heterotypic spheroids enables monitoring of increased stemness marker expression and simulating conditions increasingly closer to the *in vivo* tumor complexity [190]. Among heterotypic spheroids, i.e., spheroids composed of multiple cell types, co-cultures of tumor spheroids with endothelial cells represent an advanced model for the study of angiogenesis processes.

However, models that use endothelial cells exclusively lack some key components, such as pericytes and the stromal vascular fraction (SVF), which *in vivo* contribute to vessel stability and maturation. The absence of these cellular populations can also limit the model’s ability to fully recapitulate the complexity of the tumor vascular

microenvironment and the associated paracrine signaling. Integrating pericytes or the SVF through co-cultures with isolated microvessels would make heterotypic models more predictive for the study of angiogenesis and therapeutic response.

1.6 Nanotechnology-Based Drug Delivery Systems in Cancer Therapy: Design, Mechanisms, and Applications

Drug Delivery System (DDS) represents one of the most important applications of nanotechnology in the cancer therapeutic area, enabling the transport of therapeutic molecules to specific tissues while minimizing systemic toxicity [191]. Nanoparticles (NPs) overcome these limitations by acting as multifunctional carriers able to protect drugs from degradation, improving their biodistribution, and enabling controlled release in response to microenvironmental cues such as pH, redox state, or temperature [192,193].

The physicochemical properties of NPs, size, shape, composition, and surface functionalization, critically determine their behavior. Size-dependent biodistribution regulates circulation time, extravasation, and clearance, with particles small enough to evade the mononuclear phagocyte system yet large enough to avoid renal filtration [194]. Similarly, surface chemical modifications, including PEGylation, can prolong blood half-life, modulate immune interactions, and enhance accumulation in target tissues [195]. Functional groups on their surface facilitate conjugation with targeting ligands, antibodies, or nucleic acids, enabling site-specific delivery and combination therapies (Fig 9).

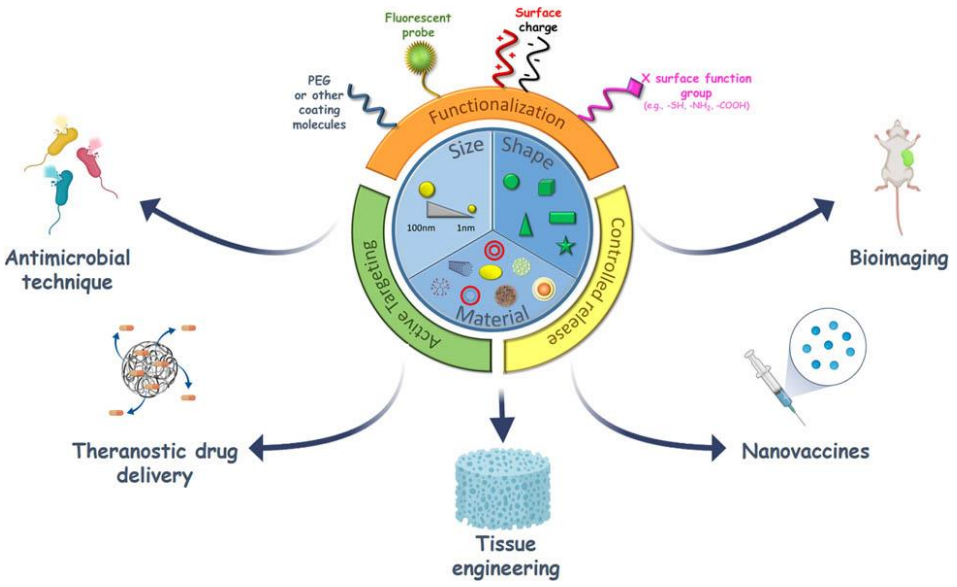

Figure 9: Overview of Nanoparticle Characteristics and Applications. Schematic representation of nanoparticles highlighting their key physicochemical properties and functional features. The figure illustrates typical size and shape variations (spherical, cuboidal, rod-like), diverse core materials (e.g., gold, silver, polymeric), and common surface functionalizations such as PEGylation or fluorescent probes. Major biomedical applications are also shown, including bioimaging, vaccine delivery, theranostics, and antimicrobial therapies, emphasizing the versatility of nanoparticles in translational research.

Image from Simona Campora and Giulio Ghersi: '*Recent developments and applications of smart nanoparticles in biomedicine*', *Nanotechnology Review*, 2022 Vol 11, Issues 1, doi: 10.1515/ntrev-2022-0148 [191]. Copyright via CC BY-NC-ND 4.0 - https://creativecommons.org/licenses/by/4.0/

A broad spectrum of nanomaterials has been engineered as smart DDS. Mesoporous silica nanoparticles (MSNs), with their tunable pore architecture and high surface area, can encapsulate large drugs and achieve controlled release through pH-responsive coatings or polymer grafting, significantly enhancing anticancer efficacy compared with free drugs [196]. Lipid-based nanoparticles (LNPs), including liposomes and solid lipid nanoparticles, offer biocompatibility and the ability to encapsulate both hydrophilic and hydrophobic molecules [197]. Polymer-based nanoparticles (PNPs) constitute another major class of DDS. Their versatility in composition and synthesis allows fine control of drug loading, degradation rate, and release kinetics [198]. Several studies demonstrate their ability to cross biological barriers, including the blood–brain barrier (BBB), or to deliver drugs selectively to cancer cells, achieving enhanced therapeutic indices while limiting cytotoxicity to non-target tissues [199]. Amphiphilic copolymers can self-assemble into micellar structures that encapsulate hydrophobic drugs and accumulate preferentially in tumor tissues, due to the EPR effect that enhances passive targeting of these platforms, as well as the other types [200] (Fig. 10).

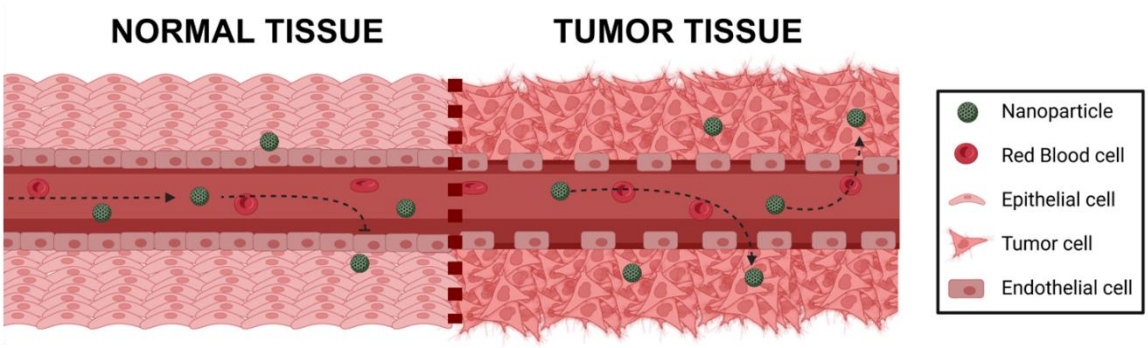

Figure 10: Schematic illustration of Enhanced Permeability and Retention (EPR) Effect. On the right, nanoparticles struggle to permeate the endothelial cells due to tight junctions between them, decreasing drug delivery. On the left, enhanced nanoparticle uptake is observed due to the presence of vascular fenestrations, which increase vascular permeability and allow nanoparticles to accumulate more efficiently in the tumor tissue.

Besides passive targeting, nanoparticles can also exploit active targeting, which relies on the conjugation of specific molecules, such as antibodies, peptides, aptamers, or small ligands, to their surface. These targeting molecules selectively recognize and bind receptors overexpressed on diseased cells, such as tumor cells, thereby enhancing cellular uptake and improving the precision of drug delivery.

Altogether, these advances indicate how nanotechnology enables a therapeutic revolution compared to conventional drugs. By integrating protection, targeting, controlled release, and diagnostic capabilities within a single nanosystem, NP-based DDS offer opportunities to improve therapeutic efficacy and reduce adverse effects across a wide range of diseases, like cancer. Within this broader category are included albumin-based nanoparticles, such as bovine serum albumin (BSA) NPs, as well as polyvinylpyrrolidone (PVP) nanoparticles.

1.6.1 Albumin-Based Nanoparticles for Drug Delivery: Mechanisms, Synthesis, and Therapeutic Applications

Albumin is a highly versatile protein employed in drug delivery due to its intrinsic biocompatibility, non-immunogenicity, and natural role as a transporter of endogenous ligands. A key advantage of albumin-based systems is their long circulatory half-life, mediated by the interaction with the neonatal Fc receptor (FcRn), which protects albumin from degradation and prolongs systemic exposure [201].

Furthermore, albumin interacts with specific proteins such as gp60 and SPARC: the gp60 receptor, found on vascular endothelial cells, promotes the transendothelial transport of albumin, while SPARC is highly upregulated in many tumor cell types and exhibits only low basal expression in normal tissues [202]. This combination of passive and active

targeting mechanisms makes albumin-based nanoparticles particularly advantageous for anticancer therapy.

Within this class, BSA NPs are among the most widely studied. They are typically synthesized via desolvation or coacervation, followed by crosslinking, either chemical, using agents like glutaraldehyde, or physical, through heat or UV treatment, to stabilize the protein platform [203,204]. These methods allow fine control over particle size, surface properties, and drug encapsulation efficiency. In the albumin-based NPs, like BSA NPs, the chemotherapeutic agents can either be encapsulated within the protein matrix of BSA nanoparticles or covalently attached to their outer surface. Encapsulation provides protected, sustained drug release, while surface conjugation allows controlled exposure of the active molecule and facilitates targeted interactions [205]. These complementary strategies enable flexible optimization of therapeutic delivery.

Compared with polymeric or lipid-based nanosystems, BSA nanoparticles are simple to prepare, cost-effective, and highly stable, offering excellent drug-loading capacity and broad compatibility with both hydrophilic and hydrophobic agents. Their tunability and safety profile make them an attractive platform for engineered next-generation drug delivery strategies.

1.6.2 PVP-Based Nanoparticles for Drug Delivery: Properties, Synthesis, and Controlled Release Strategies

Polyvinylpyrrolidone is a synthetic, highly biocompatible polymer widely employed in nanomedicine due to its excellent solubility, chemical stability, and low immunogenicity, which make it a good candidate for drug-delivery nanosystem formulation. The PVP nanoparticles are produced through the polymerization of the monomer vinylpyrrolidone [206].

A key advantage of them is their ability to form stable hydrophilic shells that prevent protein adsorption, reduce opsonization, and extend circulation time, thereby improving pharmacokinetics and systemic persistence. In addition to passive accumulation through the EPR effect, PVP nanoparticles can be engineered for controlled release of conjugated drugs or active targeting, by introducing bonds responsive to physical stimuli or surface ligands capable of binding overexpressed receptors on tumor cells [207]. PVP nanoparticles can be produced via various methodologies, including nanoprecipitation, solvent evaporation, and self-assembly processes, followed by stabilization through crosslinking [208,209]. Physical crosslinking techniques are particularly attractive for biomedical applications, as they eliminate the need for chemical agents: electron-beam (E-

beam) irradiation, for instance, induces controlled polymer network formation while maintaining low cytotoxicity and high structural integrity [209]. These approaches allow fine modulation of nanoparticle size, rigidity, and drug-loading capacity, facilitating the nanocarriers design optimized for specific therapeutic needs. In PVP-based nanoparticles, chemotherapeutic agents can be incorporated following two complementary strategies. Even in this case, drugs can be encapsulated within the polymeric network, where the hydrophilic and hydrogen-bonding environment of PVP promotes stable retention and sustained release profiles. Alternatively, therapeutic molecules can be covalently conjugated to functional groups on the nanoparticle surface, allowing greater control over exposure, targeted interactions, and release kinetics under specific physiological conditions [210].

Chapter 2

AIM AND OBJECTIVES

2.1 Aim

Our strategy relies on the use of ultrapure recombinant collagenases (Abiel srl), free of proteolytic contaminants and endotoxins, allowing controlled remodeling of the tumor matrix without undesired off-target degradation or systemic effects [211,212]. Pre-treatment with these enzymes enhances doxorubicin penetration and potentiates the therapeutic response, overcoming the limitations imposed by the dense fibrillar stroma typical of solid tumors. Doxorubicin, an antitumor antibiotic of the anthracycline class, acts mainly on proliferating cells by interfering with topoisomerase II and inducing cell-cycle arrest through DNA double-strand breaks, increased production of reactive oxygen species, and apoptosis [213]. Its intrinsic fluorescence enables monitoring of its distribution and release *in vitro* and *in vivo*, making it an ideal model drug for evaluating advanced delivery systems. Moreover, its well-established pharmacokinetics and the extensive knowledge of its side effects, such as cardiotoxicity, make doxorubicin a reliable reference for testing innovative drug-delivery strategies [214].

Therefore, based on the complexity of the TME and its central role in tumorigenesis, our working hypothesis is that a combined two-step and synergistic approach administering *in vitro* and *in vivo* ultrapure recombinant collagenases to digest the collagen-rich tumor ECM can enhance doxorubicin penetration and cytotoxicity, ultimately interfering with tumor progression. Furthermore, the conjugation of these enzymes to BSA nanoparticles and the conjugation of DOX to biocompatible BSA are expected to increase the therapeutic efficacy of the drug *in vitro* and *in vivo*, while simultaneously reducing systemic side effects and improving intratumoral bioavailability.

The *in vitro* efficacy of doxorubicin-loaded BSA nanoparticles will be compared with that of doxorubicin-conjugated PVP nanoparticles. We hypothesize that nano systems conjugated with doxorubicin and responsive to altered microenvironmental cues (pH sensitivity for BSA NPs, and glutathione sensitivity for PVP NPs) will enable more targeted release, increase treatment specificity, while reduce off-target toxicity.

Finally, the integration of species-specific microvascular fragments (MVFs) from rat abdominal adipose tissue into co-culture with primary rat tumor cells would enable the development of even more advanced and complex 3D models. These Vascularized tumor models (VTMs) models can replicate the vascularization and structural organization of the TME, thereby improving the predictive reliability of *in vitro* systems for evaluating therapeutic responses.

2.2 Objectives

The specific objectives of this research are outlined as follows:

a) Analyze the effect of collagenases on the tumor matrix and doxorubicin penetration

The primary objective was to determine the extent to which pre-treatment with ultrapure collagenases, both class I (COLH) and class II (COLH), modifies the density of the ECM and enhances DOX penetration in tumor spheroids. For this reason, a breast tumor was chemically induced in an immunocompetent Wistar rat to isolate PTCs and generate 3D cultures. This approach allows investigation of the enzymes' capacity to reduce the physical barrier *in vitro* and potentially increase chemosensitivity.

b) Evaluate the efficacy of PVP-DOX NPs and BSA-DOX NPs

Compare BSA nanoparticles with PVP-based nanoparticles conjugated to DOX via a glutathione-sensitive linker, leveraging the altered glutathione levels characteristic of tumor cells. By comparing *in vitro* results on primary-cell–derived spheroids, this aims to assess both pH-responsive and redox-responsive controlled-release systems, identifying potential advantages of protein-based albumin carriers over synthetic polymers in terms of therapeutic efficacy and reproducibility.

c) Develop Bovin Serum Albumin nanoparticles (BSA NPs) as drug-delivery systems

Synthesize BSA nanoparticles loaded with DOX as well as BSA nanoparticles as carriers of COLG and COLH. These nano systems are designed to improve therapeutic efficacy and enhance, respectively, drug specificity and bioavailability. In the case of BSA-COL NPs, enzyme encapsulation is expected to protect them from immune recognition, thereby improving immunocompatibility and protein half-life. BSA NPs conjugated with doxorubicin are synthesized to obtain a pH-sensitive release platform, to obtain controlled drug release with stromal remodeling.

d) Validate a vascularized 3D tumor model to investigate resistance mechanisms mediated by tumor–vessel crosstalk

The final objective was to integrate PTCs with MVFs to generate vascularized 3D tumor co-cultures. This advanced model allows the study of interactions among ECM, vasculature, efflux transporters (such as ABCB1), and response to DOX, simulating more physiologically relevant conditions and increasing the predictive reliability of *in vitro* results.

In summary, the rationale of this research integrates selective degradation of the tumor ECM via ultrapure collagenases, either free or encapsulated in albumin matrices,

controlled release of DOX (free or delivered through BSA nanoparticles), comparison with redox-sensitive PVP-DOX nanoparticles, and the use of advanced 3D tumor models. This combined approach enables a systematic investigation of the physical and biological barriers of the TME, providing a significant contribution to the development of advanced 3D models, innovative drug-delivery systems for solid tumors, and the understanding of mechanical and biochemical mechanisms of therapeutic resistance.

Chapter 3

MATERIALS AND METHODS

3. Materials and Methods

The following Materials and Methods section is organized into four main research areas, each describing the specific experimental methodologies applied. These include:

- Improving Therapeutic Efficacy Through Endogenous Extracellular Matrix Remodeling in Primary Breast Tumor Spheroids
- Synergistic Effect of Collagenase and PVP-AEDP-Doxorubicin Nanoparticles in Primary Tumor Cell Spheroids
- Enhancing Drug Penetration and Cytotoxicity in 3D Primary Breast Cancer Cultures via BSA-Nanoparticles
- Development and Characterization of 3D Vascularized Tumor Model Integrating Rat Adipose-Derived Microvascular Fragments and Breast Cancer Cells: Evaluation of ABCB1 Expression and Drug Response

3.1 Improving Therapeutic Efficacy Through Endogenous Extracellular Matrix Remodeling in Primary Breast Tumor Spheroids

3.1.1 Animal model and ethical statement

The experimental protocols involving animals were conducted under the approval of the University of Palermo (authorization n° 523/2022-PR), in strict adherence to the Italian Legislative Decree 26/2014 (Article 31) from the Istituto Superiore di Sanità. Female Wistar rats, sourced from ENVIGO RMS SRL, were housed in pairs within cages equipped with EPA filters. Environmental conditions were regulated at a temperature of 23°C ± 0.5°C and 50% ± 5% of humidity level. Lighting followed a 12-hour cycle, active from 7:00 a.m. to 7:00 p.m., with food available ad libitum. At 55 days of age, mammary tumorigenesis was induced via a single intraperitoneal administration of 7,12-dimethylbenz(a)anthracene (DMBA, 50 mg/kg) dissolved in corn oil [215]. Following a six-month observation period, rats displaying detectable tumor masses were euthanized using 2% isoflurane sedation, followed by tumor excision for downstream cellular analysis.

3.1.2 Primary Tumor Cell (PTC) isolation and culture

PTCs were isolated from the DMBA-induced mammary tumor in the Wistar rat. After excision, tumor biopsies were disinfected in 70% ethanol and transferred into HG-DMEM (Sigma-Aldrich, Milan, Italy) containing high-dose antibiotics (300 U/mL penicillin, 300 mg/mL streptomycin, Euroclone). The tissue was mechanically dissected and subjected to enzymatic digestion at 30°C for 120 minutes under constant agitation. The digestion

cocktail consisted of ultrapure recombinant collagenases (Abiel) Class I (Col G, 106.4 U/g) and Class II (Col H, 453.2 U/g), supplemented with Thermolysin (Promega) at 266.4 µg/g. The reaction was terminated by adding HG-DMEM with 10% FBS. Isolated cells were recovered via centrifugation (500 g for 5 minutes), washed thrice, and resuspended in DMEM/F12 medium (10% FBS, 2 mM L-glutamine, 300 U/mL penicillin G, and 300 mg/mL streptomycin). For initial culture, cells were seeded onto an acetic acid-treated collagen-coated plate (50 µg·mL−1 in 0.02 N acetic acid). PTC cultures were maintained under sterile conditions at 37°C within a humidified incubator supplemented with 5% CO_2. The growth medium, consisting of HG-DMEM with 10% FBS, 1% L-glutamine, and 1% penicillin/streptomycin, was systematically refreshed every 72 hours to ensure optimal nutrient availability.

3.1.3 3D spheroid generation and culture

To produce 3D tumor models, $1x10^4$ PTCs at passages 15-19 were seeded per well into 96-well low-attachment plates. In specific experimental setups, wells were pre-coated with 40 µL of agarose (1,5% in DMEM-HG). The spheroids were maintained in complete DMEM at 37°C and 5% CO2, allowing 6 days for mature spheroid formation.

3.1.4 Proteomic analysis

Cells from both 2D and 3D cultures were lysed in STET buffer (10 mM Tris/HCl, 1 mM EDTA, 100 mM NaCl, and 5% Triton X-100 [v/v]) supplemented with a protease inhibitor cocktail (Roche, Basel, Switzerland). The lysates were centrifuged at 14,000 × g for 5 minutes to remove cell membranes. Using a colorimetric 660 nm micro BCA assay, the extracted proteins were quantified. 30 µg of proteins per sample was processed to filter-aided sample preparation (FASP) using 10 kDa Vivacon 500 spin filter columns (Sartorius, Göttingen, Germany), as previously described [216].

Each sample was first treated with dithiothreitol (DTT, Sigma-Aldrich) in 200 µL of UA buffer (8 M urea in 0.1 M Tris/HCl, pH 8.5) to induce reduction and denaturation. Alkylation was then performed using 50 mM iodoacetamide (IAA, Sigma-Aldrich). Following these steps, samples were rinsed three times with UB buffer (8 M urea in 0.1 M Tris/HCl, pH 8.0) to remove excess reagents. Proteolytic digestion was carried out sequentially, first with LysC at an enzyme-to-protein ratio of 1:50, and then with trypsin at 1:100.

Peptides were collected from the filter columns by centrifugation at 14,000 × g for 60 min and then acidified with 20 µL of 8% formic acid (FA). Desalting was performed using stop-

and-go extraction (STAGE) tips packed with reverse-phase C18 material, and the peptides were subsequently eluted in 40 µL of 60% acetonitrile containing 0.1% formic acid [217]. The sample volume was concentrated using a SpeedVac (Thermo Fisher Scientific, Waltham, MA, USA), and the peptides were subsequently resuspended in 20 µL of 0.1% formic acid. Peptide concentration was determined by a NanoDrop 2000 spectrophotometer (Thermo Scientific).

3.1.5 uHPLC–MS/MS and data analysis

As previously described [218]For each sample, 1 µg of peptides was loaded onto a nanoLC system (Vanquish Neo UHPLC, Thermo Scientific) fitted with an Acclaim PEPMap C18 column (25 cm × 75 µm ID, Thermo Scientific). Peptide separation was achieved over a 130-minute gradient using water and acetonitrile, both containing 0.1% formic acid. The eluted peptides were analyzed by tandem mass spectrometry (MS/MS) on an Exploris 480 mass spectrometer (Thermo Fisher Scientific). Protein identification and quantification were performed using label-free quantification (LFQ) in combination with data-independent acquisition (DIA). DIA consisted of a full MS1 scan from 400 to 1200 m/z, followed by 60 sequential isolation windows with 1 m/z overlap and optimized window placement. Full scans were obtained at a resolution of 120,000, using an automatic gain control (AGC) target of 3×10^6 and a maximum injection time of 50 ms. The 60 DIA windows were subsequently scanned at 30,000 resolutions, with an AGC target of 8×10^5, and the maximum injection time was set to automatic to optimize cycle time. Peptide fragmentation was achieved using higher-energy collisional dissociation (HCD) at 30% normalized collision energy. MS data were processed using DIA-NN software (version 1.8.1) with a predicted spectral library generated from an *in silico* digestion of the Rattus norvegicus UniProt reference proteome (ID UP000002494). Cleavage at lysine and arginine residues (K* and R*) was allowed, with up to two missed cleavages and a minimum peptide length of six amino acids. Peptide and protein identifications were filtered at a 0.01% false discovery rate (FDR). Protein quantification was performed using LFQ, and values were log2-transformed. Statistical analysis comparing protein expression between two-dimensional and three-dimensional cultures (n = 5) was carried out using a two-sided Student's t-test. The resulting proteomics data have been deposited to the ProteomeXchange Consortium via the PRIDE repository under dataset ID PXD061082.

3.1.6 Immunofluorescence and confocal imaging

Spheroids and 2D cells were fixed in 3.7% formaldehyde (1 hour for 3D; 15 minutes for 2D) and permeabilized with 0.1% Triton X-100 in PBS. To prevent non-specific binding,

samples were incubated for 1 hour with 1% BSA in PBS. Primary antibody incubation was conducted overnight at 4°C with Rabbit anti-collagen type I (1:20, Millipore). Subsequent detection utilized fluorophore-conjugated secondary antibodies (Invitrogen), phalloidin-FITC (1:500) for actin, and DAPI (1:20,000) for nuclei. Coverslips were mounted with a mounting solution, and 2D cultures were analyzed with an epifluorescence microscope (Leica, Wetzlar, Germany), while 3D cultures were analyzed with a confocal microscope (Olympus FV10i and Stellaris 5, Leica, Wetzlar, Germany). Data were processed using ImageJ.

3.1.7 Cell viability assays

6-day spheroids were washed and incubated with recombinant collagenases (20 U/mL COLG and 80 U/mL COLH, Abiel) in serum-free DMEM for 75 minutes at 37°C. FBS-containing media was then used to stop enzymatic activity.

Spheroids (control or collagenase-treated) were exposed to 20 μM Doxorubicin for intervals of 2, 4, 8, or 24 hours. Post-incubation, area measurements (including necrotic regions) and drug uptake were assessed through confocal imaging and ImageJ software.

Spheroids, either untreated or pretreated with collagenases, were incubated with 20 μM doxorubicin for 8, 16, and 24 h at 37 °C.

3.1.8 Statistical analysis

Experimental data are expressed as Mean ± SD. Comparative analysis was performed via one-way or two-way ANOVA using GraphPad Prism software, with statistical significance defined by a *p-value <0.05.

3.2. Synergistic Effect of Collagenase and PVP-AEDP-Doxorubicin Nanoparticles in Primary Tumor Cell Spheroids

3.2.1 Quantification of doxorubicin conjugation to PVP-AEDP Nanoparticles

UV-vis spectrophotometer (SinergyHT, BioTek, Winooski, VT, USA) was used to calculate the doxorubicin conjugated to PVP-AEDP nanoparticles. For this purpose, 100 μL of solution containing nanoparticles was measured using a UV-vis spectrophotometer at 480 nm to confirm the concentration of the drug. The amount of doxorubicin was calculated using a standard curve.

3.2.2 Generation of tumor spheroids from primary tumor cells

PTCs from rat tumor mass were cultured using DMEM high glucose supplemented with 1% penicillin/streptomycin, 1% L-glutamine, and 10% fetal bovine serum (FBS) for 15

passages. Cells were propagated at 37°C in a humid atmosphere with 5% CO2. To generate spheroids, primary cancer cells were seeded into a 96-well under low-attachment conditions at a density of 1×10^4 cells per well in complete DMEM. The cells were incubated at 37°C and 5% CO2 and allowed to grow for 6 days.

3.2.3 Cell viability assay

For the 2D cell viability assay, PTCs were treated with free doxorubicin (DOX) or PVP-AEDP-DOX nanoparticles at concentrations ranging from 0.125 to 20 µM for 24 h. Cell viability was subsequently assessed using the Alamar Blue assay (Thermo Fisher). For the 3D model, 6-day spheroids were washed and incubated with recombinant collagenases (20 U/mL COLG and 80 U/mL COLH, Abiel) in serum-free DMEM for 75 minutes at 37°C. FBS-containing media were then used to stop enzymatic activity. After 2 washes, spheroids were incubated with 20 µm doxorubicin conjugated with polyvinylpyrrolidone (PVP)-AEDP nanoparticles for 24 h at 37 °C. Following treatment, spheroids were washed with PBS three times, resuspended in 100 µL of DMEM, and mixed with an equal volume of CellTiter-Glo® 3D Reagent (Promega) according to the datasheet. The plates were agitated for 5 min at 240 g, followed by a 25 min incubation at room temperature, after which luminescence was measured using a luminometer (SinergyHT, BioTek, Winooski, VT, USA).

3.2.4 Immunofluorescence staining and imaging

Cells (2D and 3D) were fixed in 3.7% formaldehyde (1 hour, 15 minutes for 2D cells, at room temperature), and, after washing three times in PBS, nuclei were stained with DAPI (1:20,000 in PBS) for 15 minutes, while 2D cultures were stained also with phalloidin-FITC (1:500) for actin. After washing, coverslips were mounted with a mounting medium and examined by an epifluorescence microscope (Leica, Wetzlar, Germany). Data were processed using ImageJ.

3.2.5 Statistical analysis

Experimental data are expressed as Mean ± SD. Comparative analysis was performed via one-way ANOVA using GraphPad Prism software, with statistical significance defined by a *p-value <0.05.

3.3 Enhancing Drug Penetration and Cytotoxicity in 3D Primary Breast Cancer Cultures via BSA-Nanoparticles

3.3.1 Synthesis of albumin-based nanoparticles with chemical cross-linking method

BSA nanoparticles (BSA NPs) were prepared using the classical desolvation method according to a previously described protocol [203], which was partially modified to optimize nanoparticle stability. Briefly, 20 mg of bovine serum albumin (Sigma-Aldrich) were resuspended in 100 µL of dimethyl sulfoxide (DMSO, Sigma-Aldrich) and incubated for 5 min, a step essential for obtaining polydisperse nanoparticles. Subsequently, 1 mL of distilled water was added, and the mixture was stirred at 300 rpm for 20 min at room temperature. Desolvation was then induced by adding 3.5 mL of absolute ethanol using a syringe pump at a flow rate of 5 mL/min, followed by 1 h and 30 min of continuous stirring. Crosslinking was achieved by adding 100 µL of 2% glutaraldehyde, and the suspension was incubated overnight. The resulting nanoparticles were purified by three centrifugation cycles at 14,000 rpm and 4°C to remove residual solvent and unconjugated proteins. Finally resuspended in distilled water. For the preparation of drug-loaded nanoparticles (BSA-DOX NPs), BSA was first resuspended in DMSO and then incubated with doxorubicin (350 µL of 2 mg/ml, in water); the subsequent steps were identical to those described above, and the entire procedure was performed in the dark to prevent drug photodegradation.

3.3.2 Drug loading quantification

A UV-vis spectrophotometer (SinergyHT, BioTek, Winooski, VT, USA) was used to confirm the drug loading content (LC) and encapsulated efficiency (EE) of BSA-DOX NPs. Briefly, an aliquot of 100 µL of supernatant from each wash following centrifugation was analyzed using a UV–Vis spectrophotometer at 480 nm to determine the doxorubicin (DOX) concentration. The amount of unencapsulated DOX was then calculated based on a standard calibration curve. The LC was calculated as the mass ratio between the initial DOX amount to that measured in each supernatant. The EE was defined as the percentage of encapsulated DOX.

3.3.3 Transmission Electron Microscopy (TEM) analysis of NPs

A classical protocol for staining was used. 3.5 µL aliquot of the sample was placed onto a Copper 400-mesh grid coated with Formvar/Carbon film (Electron Microscopy Sciences). After 60 s, 10 µL of Milli-Q water was added, and excess liquid was gently removed with filter paper. For negative staining, 10 µL of the BSA nanoparticle solution was placed on the grid and incubated for 30 s. The grid was then aspirated and allowed to air-dry for a

few minutes before imaging. Samples were imaged at the University of Copenhagen's Core Facility for Integrated Microscopy using a Philips CM100 TWIN TEM with a Veleta Camera (Olympus) and processed in iTEM (Olympus). The size distribution of NPs was evaluated by ImageJ.

3.3.4 Evaluation of nanoparticle stability under physiological and acidic conditions

To study the behavior and stability of nanoparticles in solution under varying pH conditions, BSA-NPs and BSA-DOX NPs were resuspended in PBS (100 µM) at pH 7.4, 6.5, and 5.5. The samples were incubated for 24 hours under agitation on a wheel.

The degree of aggregation of the nanoparticles was evaluated by spectrophotometric absorbance analysis (500 nm) at each pH value, both for the control BSA-NPs and for the BSA-DOX NPs. For each experimental condition, 100 µL of the sample was analyzed with a spectrophotometer. The obtained values were normalized relative to the control absorbance at pH 7.4 and converted to a percentage.

3.3.5 Nanoparticle analysis by Dynamic Light Scattering (DLS)

The size and polydispersity index (PDI) of the nanoparticles were determined using the dynamic light scattering (DLS) technique. Measurements were performed with a Zetasizer Nano ZS (Malvern) at room temperature (25°C). The BSA-NP solution was diluted in a 1:10 ratio in PBS pH 7.4 and subsequently placed in cuvettes for DLS analysis. Each sample was analyzed in triplicate, with a minimum of 10 measurements per sample. The results regarding size and polydispersity index (PDI) were analyzed using the dedicated software (Zetasizer).

3.3.6 Zeta Potential measurement (ζ)

The zeta potential (ζ) of the nanoparticles was determined by laser Doppler electrophoresis using a Malvern Zetasizer Nano ZS. The particles were diluted 1:10 in PBS 100 µM (pH 7.4, 6.5, and 5.5). For each sample, measurements were performed at room temperature (25°C) in electrophoretic cells, recording at least three readings per sample from 100 zeta runs. The reported values correspond to the mean ± standard deviation of the triplicate measurements. The zeta potential values were expressed in millivolts (mV).

3.3.7 3D spheroid generation and culture

To produce 3D tumor models, PTCs at passages 15-18 were seeded at a concentration of 5000 cells per well into 96-well low-attachment plates. The 3D cultures were maintained in complete DMEM at 37°C and 5% CO2, allowing 6 days for mature spheroid formation.

3.3.8 Experimental treatments and cell viability assays

6-day spheroids were washed and incubated with recombinant collagenases (20 U/mL COLG and 80 U/mL COLH, Abiel) in serum-free DMEM for 75 minutes at 37°C. FBS-containing media was then used to stop enzymatic activity. Spheroids, untreated or treated with collagenases, were incubated with 10 μm doxorubicin (free or conjugated with BSA NPs) for 24 h at 37 °C. Following treatment, spheroids were washed with PBS three times, resuspended in 100 μL of DMEM, and mixed with an equal volume of CellTiter-Glo® 3D Reagent (Promega), according to the datasheet. The plates were agitated for 5 min at 240 g, followed by a 25 min incubation at room temperature, after which luminescence was measured using a luminometer (SinergyHT, BioTek, Winooski, VT, USA).

3.3.9 Data collection and processing of Small-Angle X-ray Scattering (SAXS) analysis

SAXS experiments were performed at the P12 EMBL BioSAXS beamline at PETRA III, operated at a fixed energy of 10 keV (lambda =0.124 nm), running in SEC-SAXS mode. Briefly, 4 mg/mL of ColH in XX Buffer was injected onto a Superdex S200 column (24 mL volume) using an Agilent1260 HPLC system at a flow rate of 0.5 mL/min. The eluent from the column was routed through a quartz capillary, and SAXS data were continuously collected (1-second frames for the whole run-time of the column). This resulted in roughly 2880 individual SAXS spectra from the whole column run. The collected SAXS data were further processed using the CHROMIXS program from the ATSAS package. Briefly, the CHROMIXS software integrates the intensity in the q-range 0.01-0.08 $Å^{-1}$ for each sequential frame and plots the integrated intensity against the frame number (Fig 1a), allowing for identification of the major protein elution peak. Frames from the identified elution peak were then averaged, and a suitable buffer region containing a similar number of frames was similarly identified, averaged, and subtracted from the averaged elution peak spectra, resulting in the protein SAXS curve (Figure 1b). The resulting SAXS curve is displayed in the Normalised Kratky plot format (Figure 1c), and is indicative of a globular protein. Determination of the radius of gyration by linear fitting of the Guinier equation in the low-q regime (q*Rg =<1.3) indicates a radius of gyration of 4.52 nm (Figure 1d).

For EOM analyses, a model was built consisting of three main sub-units of the protein, namely, MBP (PDB ID: 1MPD), which was linked via flexible glycine linkers to the catalytic domain of ColH determined from the alphafold structure (UniprotID: Q46085). The three C-terminal domains (also taken from the alphafold structure) were linked to the catalytic domain of COLH via flexible linker regions.

EOM was used to construct a library of 10.000 conformations where the COLH catalytic domain was in a fixed position, and the other structured domains were allowed to sample conformational space via the disordered linker regions. For each conformer, a theoretical SAXS curve was generated using the program Crysol. As a subset, or sub-ensemble, of these conformers is then fitted to the experimental scattering curve, this was achieved using the program GAJOE, which employs a genetic algorithm to select the best-fitting ensemble.

3.3.10 Synthesis of albumin-based nanoparticles with thermal cross-linking method

Thermal crosslinked BSA NPs were prepared following the same initial desolvation steps used for the preparation of chemically crosslinked BSA nanoparticles. However, after incubation with ethanol, the nanoparticles were thermal crosslinked in an oven at 65 °C for 25 min. At the end of the incubation, the reaction was stopped by placing the samples on ice. The nanoparticles were then washed three times by centrifugation at 14,000 rpm at 4 °C to remove residual solvent and unconjugated proteins, and finally resuspended in 1 mL of distilled water.

To evaluate the thermal stability of the enzymes, collagenases were incubated at different temperatures (55–65 °C) for varying time intervals (10–40 min). Enzymatic activity was subsequently assessed by gelatin zymography to determine whether heat exposure affected their proteolytic function. The results showed that collagenases retained high enzymatic activity after incubation at temperatures up to 65 °C for 20 min, with no appreciable loss of function. Based on these findings, 65 °C for 20 min was selected as the optimal condition for the thermal crosslinking step during the synthesis of BSA nanoparticles. For the synthesis of collagenase-loaded BSA nanoparticles, 2 mg of collagenase (ColH or COLG) and 18 mg of BSA were used. Subsequent preparation steps were identical to those described for the synthesis of thermally crosslinked BSA NPs control at 65°C for 20 min. After this step, the reaction was stopped by placing the nanoparticle suspension in an ice bath, followed by three washing steps performed at 14,000 rpm for 30 minutes.

3.3.11 Qualitative analysis of enzymatic activity by spotting zymography

The qualitative enzymatic activity was evaluated using a modified version of canonical zymography, which we named spotting zymography. This approach was adopted because the large size of the nanoparticles prevented their migration during conventional electrophoretic separation. Briefly, a 7.5% zymography gel was prepared by mixing acrylamide solution (1,250 µL), 1.5 M Tris-HCl buffer (pH 8.8; 1,250 µL), 10% (w/v) sodium dodecyl sulfate (SDS; 50 µL), distilled water (3 mL), gelatin solution (6 mg/mL;

875 µL), ammonium persulfate (APS; 25 µL), and TEMED (3 µL). The mixture was allowed to polymerize and subsequently incubated at 37 °C for 25 min.

After incubation, the gel was carefully detached from the glass plates and washed for 15 min in washing buffer (2.5% Triton X-100 and 0.02% sodium azide in distilled water). The washing buffer was removed, and the gel was then air-dried for 1 hour. After this step, 2 µL of each sample, supplemented with 2 mM calcium chloride, were spotted onto the gel surface.

The gel was incubated overnight at 37 °C to allow enzymatic digestion of the gelatin substrate. Subsequently, the gel was stained with Coomassie Brilliant Blue R-250 and destained with distilled water. Gel images were finally acquired to visualize white halos related to proteolytic activity.

3.3.12 Statistical analysis

Experimental data are expressed as Mean ± SD. Comparative analysis was performed via one-way or two-way ANOVA using GraphPad Prism software or Microsoft Excel (Microsoft Corporation), with statistical significance defined by *p-value <0.05.

3.4 Development and Characterization of 3D Vascularized Tumor Model Integrating Rat Adipose-Derived Microvascular Fragments and Breast Cancer Cells: Evaluation of ABCB1 Expression and Drug Response

3.4.1 Rat model

All procedures involving animals received formal approval from the University of Palermo. The study was conducted under authorization n° 523/2022-PR, granted in compliance with art. 31 of D.lgs. 26/2014 by the Istituto Superiore di Sanità, Italy. Female Wistar rats, utilized as the biological source for the experiments, were provided by ENVIGO RMS SRL.

3.4.2 Microvascular fragments Isolation

The isolation of microvascular fragments (MVFs) was performed using visceral adipose tissue isolated from female Wistar rats, following previously established protocols [219]. Animals were anesthetized using 2% Isoflurane before sacrifice, after which the abdominal adipose tissue was surgically removed. The explanted adipose tissue was placed in high-glucose Dulbecco's Modified Eagle's Medium (HG-DMEM, Sigma-Aldrich, Milan, Italy) supplemented with 15,000 U/ml penicillin, 300 µg/ml streptomycin, and 0.75 µg/ml amphotericin B (Sigma-Aldrich, USA). After three washes in PBS without $CaCl_2$ and $Mg^{2+,}$ the tissue was finely fragmented with scissors. The adipose fragments were then

incubated in a digestion buffer with ultrapure recombinant collagenase (Col H 300 U/gr, Abiel srl) and 100 µL/gr of Thermolysin (10 mg/ml, Promega). The digestion phase was conducted for 30 minutes at 30°C under constant agitation, followed by an additional 20-minute digestion period after further mixing. The enzymatic reaction was terminated by adding HG-DMEM containing 10% (v/v) FBS (Euroclone, Celbar, Pero (MI, Italy). The suspension was washed three times in HG-DMEM and centrifuged at 700 rcf for 10 minutes to separate the MVFs. The resulting pellet was resuspended in HG-DMEM supplemented with 10% (v/v) FBS, 2 mM L-Glutamine, and 3% of antibiotic-antimycotic, then passed through a 300 µm mesh. Quantification of the MVFs was performed using a Burker's chamber.

3.4.3 Primary Tumor Cells (PTCs) and MVFs 3D co-culture

PTCs, originally isolated from a breast tumor mass in an immunocompetent female Wistar rat, were maintained in complete HG-DMEM (10% FBS, 1% penicillin/streptomycin, and 1% L-Glutamine) at 37°C in a 5% CO_2. The vascularized tumor models were generated by co-culturing PTCs (P15–19) and isolated MVFs in 96-well low-attachment plates for a 5-day period. Three distinct experimental conditions were established by seeding a constant number of PTCs (3000 cells) with either 60, 125, or 250 MVFs. Control groups consisted of spheroids formed by MVFs alone (500 MVFs) or PTCs alone (3000 cells). The size and structure of co-cultures were analyzed through optical microscopy, using ImageJ software.

3.4.4 Spheroids fixation and preparation for scanning electron microscopy (SEM) imaging

Spheroids were washed in complete PBS three times before being fixed in 4% glutaraldehyde in PBS for one hour at 4°C. After two subsequent PBS washes, the samples were dehydrated through a graded ethanol series (30%, 70%, 90% in PBS, and 100%) for 5 minutes each step. To achieve critical point drying, the dehydrated 3D cultures were incubated in hexamethyldisilazane (HMDS, Sigma-Aldrich) for 10 minutes. The 3D cultures were then mounted on stubs using carbon tape, dried at room temperature, and coated with platinum for 15 seconds using a Quorum SC7620 sputter coater. High-vacuum imaging was conducted in Secondary Emission (SE) mode with a SEM EVO 10, and data analysis was performed using SmartSEM Touch software.

3.4.5 Immunofluorescence staining and imaging

The 3D structures were fixed in 3.7% formaldehyde (one hour at room temperature) and permeabilized overnight at 4°C in PBS with 0.1% Triton X-100. Following a one-hour blocking step in PBS with 1% BSA, samples were incubated overnight at 4°C with primary

antibodies: Rabbit anti-CD31 (1:50, Abcam), Rabbit anti-Collagen Type I (1:20, Millipore), Rabbit anti-Collagen Type IV (1:100, Abcam), or Mouse anti-ABCB1 (1:100, Invitrogen). Visualization was achieved using species-specific secondary antibodies (Invitrogen) during a 2-hour incubation. The actin filaments were stained with phalloidin-FITC (1:500, Sigma-Aldrich) for 30 minutes, and nuclei were marked via DAPI staining (1:20,000, Sigma-Aldrich). Coverslips were mounted with a mounting solution, and samples were examined using an Olympus FV10i confocal microscope. Z-stacks were acquired at 20x magnification with a 10 µm step size, maintaining uniform intensity settings across all groups for subsequent ImageJ analysis.

3.4.6 Western Blot analysis

Protein extraction from 3D cultures was performed using RIPA buffer (20 mM Tris, 150 mM NaCl, 0.1% Triton X-100, 1 mM EDTA, pH 7.2) containing protease inhibitors. Proteins were incubated in reducing sample buffer, separated via 10% SDS-PAGE, and transferred to Amersham nitrocellulose membranes. After blocking in PBS/Tween 0.1% (PBS/T) with 5% non-fat milk, membranes were incubated with primary antibodies against CD31 (1:1000, Abcam) or ABCB1 (1:500, Antibodies) diluted in PBS/T. Following four washes in blocking buffer, membranes were incubated with HRP-conjugated secondary antibodies (Sigma) and developed using Super Signal West Femto substrate. Protein bands were captured and analyzed using a ChemiDoc XRS system.

3.4.7 Zymography assay

To evaluate proteolytic activity, 15 µg of proteins from 3D cell models were resolved on 10% acrylamide gels containing 0.09% gelatin. The gels were washed in 2.5% Triton X-100 for 10 minutes and then incubated overnight at 37°C in an activation buffer (50 mM Tris-HCl, 2 mM $CaCl_2$, 0.02% NaN_3, 1.5% Triton X-100). The gel was stained with Coomassie Brilliant Blue R-250 for one hour, followed by aqueous destaining. The quantification of resulting proteolytic bands was assessed by using ImageJ software.

3.4.8 Collagen gel for embedding of MVFs and angiotumorids, and sprouting analysis

MVFs and 3D models were included within a collagen matrix made of 35.3% of buffer solution (2X PBS, 100 mM HEPES, pH 7.4), 35.3% type I collagen extracted from rat tail (3 mg/ml), and 29.4% complete HG-DMEM. While isolated MVFs were maintained in the gel for one week, angiotumoroids and controls were embedded for 48 hours. The degree of sprouting was analyzed through optical microscopy and quantified using ImageJ.

3.4.9 Conditioned media treatments from PTCs and analysis of sprouts

MVF-only spheroids embedded in collagen gels were exposed to conditioned medium collected from PTCs grown in 2D monolayers. Controls were maintained in standard complete HG-DMEM. Sprouting quantification was conducted during the first and second days of treatment through optical microscopy, quantifying them using ImageJ software analysis.

3.4.10 Proteomic analysis

Angiotumoroids and control spheroids (PTC and MVF) were incubated in STET lysis buffer (10 mM Tris-HCl, 1 mM EDTA, 100 mM NaCl, 5% Triton X-100) with protease inhibitors. After centrifugation (14,000 rpm, 5 min), protein concentrations were determined using a microBCA assay. 30 µg of protein per sample were processed via Filter-Aided Sample Preparation (FASP) with 10 kDa spin filters. Samples were reduced with DTT in 8M Urea buffer, alkylated with 50 mM iodoacetamide, and digested sequentially with LysC and trypsin. Peptides were eluted, acidified with 8% formic acid, and desalted using C18 STAGE tips. Final peptide concentrations were measured using Nanodrop 2000.

3.4.11 uHPLC-MS/MS and data analysis

Peptide samples (1 µg) were separated via a Vanquish Neo UHPLC system using an Acclaim PEPMap C18 column over a 110-minute gradient. Mass spectrometry was performed on an Exploris 480 using data-independent acquisition (DIA). Full MS1 scans (380–980 m/z) at 120,000 resolution were followed by 49 DIA windows at 30,000 resolution. Data were analyzed with DIA-NN (v2.0.2) against the *Rattus norvegicus* Uniprot database. A 0.01% FDR was applied for identification. Log2-transformed LFQ values were compared using a two-sided Student's t-test (n=4), and data were deposited in the PRIDE repository.

3.4.12 Doxorubicin uptake analysis by confocal microscopy

To evaluate drug internalization, 125-MVF angiotumoroids and PTC spheroids were treated with 10 µM Doxorubicin for 30, 60, 120, or 240 minutes. Following incubation, samples were processed for immunocytochemistry and visualized using an Olympus FV10i confocal microscope, with subsequent image analysis performed in ImageJ.

3.4.13 Cell viability assay

The metabolic activity of 125-MVF angiotumoroids and PTC spheroids was assessed following a 24-hour exposure to 10 µM Doxorubicin. Post-treatment, samples were washed in PBS and analyzed using the CellTiter-Glo® 3D Reagent (Promega). The plates

were agitated for 5 min at 240 g, followed by a 25 min incubation at room temperature, after which luminescence was measured using a luminometer (SinergyHT, BioTek, Winooski, VT, USA).

3.4.14 Statistical analysis

Experimental results are expressed as mean ± standard deviation (SD). Data were evaluated using one-way or two-way ANOVA via GraphPad Prism software. Statistical significance was defined as a *$p < 0.05$.

Chapter 4

RESULTS AND DISCUSSION

4.1 Improving Therapeutic Efficacy Through Endogenous Extracellular Matrix Remodeling in Primary Breast Tumor Spheroids

4.1.1 Breast Tumor Induction, Primary Tumor Cells Isolation and Characterization

To investigate the extracellular matrix (ECM) dynamics in primary breast tumor spheroids, breast tumor was chemically induced in immunocompetent female Wistar rats by intraperitoneal injection of 7-12 dimethylbenz[a]anthracene (DMBA), according to protocols reported in the literature [220] (Fig.11A). Tumors became detectable approximately 24 weeks after induction and were localized in the abdominal sub-mammary region, displaying a notably large size (Fig.11B). To preserve the intrinsic heterogeneity of the tumor, tissue samples were collected from the external portion of the mass, excluding the inner necrotic core (Fig.11C-D). This strategy enabled the recovery of a mixed cell population consisting of not only tumor cells but also stromal and microenvironment-associated cell types, which are known to play a crucial role in ECM remodeling.

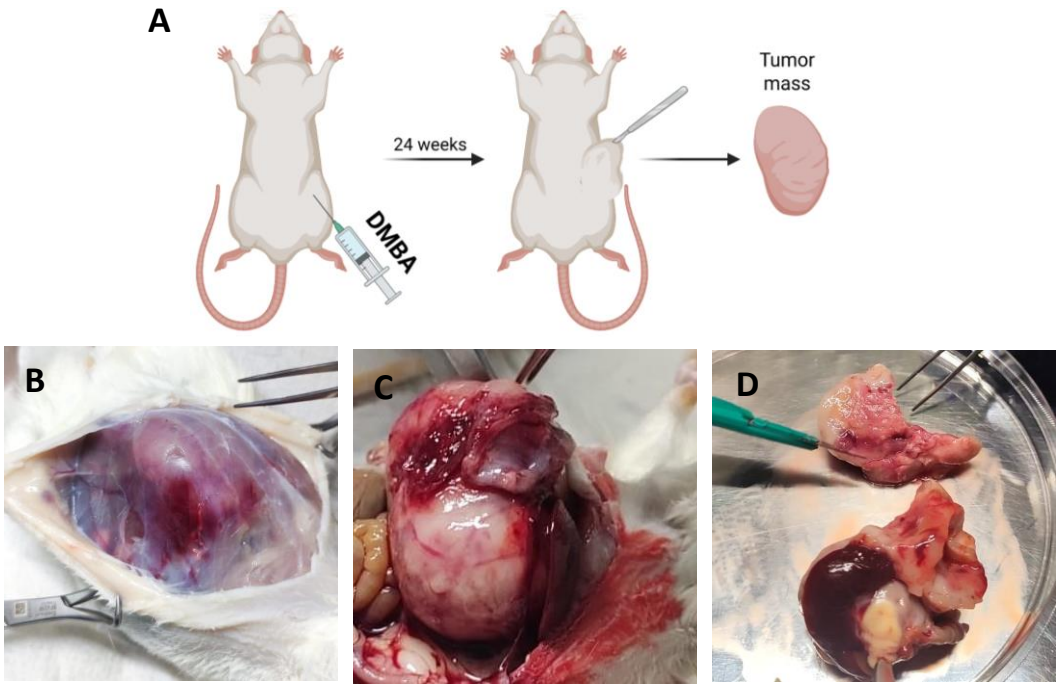

Figure 11:Chemical induction of Breast tumor in immunocompetent Wistar rat by intraperitoneal DMBA injection. (A) Schematic representation of the tumor induction; (B) representative photograph showing the abdominal localization of the tumor mass; (C) morphology of the excised tumor mass; (D) detail of the outer region of the tumor mass, from which PTCs were isolated.

Image (B) adapted from Lo Cicero et al: '*Enhancing therapeutic efficacy through degradation of endogenous extracellular matrix in primary breast tumor spheroids*' *FEBS J.* 2025, doi: 10.1111/febs.70069 [1]. Copyright via CC BY-NC-ND 4.0 - https://creativecommons.org/licenses/by/4.0/

Following tissue dissociation, different enzymatic digestion conditions were evaluated to optimize the isolation of Primary Tumor Cells (PCTs). Specifically, several concentrations of COLH, COLG, and thermolysin and different incubation times were tested to identify the best condition to obtain the highest number of primary cells.

The PTCs displayed morphological heterogeneity, as shown in Figure 12A, reflecting the complex cellular composition typical of the tumor microenvironment. Therefore, it is evident that the presence of cells with different morphologies, sizes, and shapes. Immunostaining for collagen type I (green) confirmed the presence of some cells (probably fibroblasts) able to synthesize collagen, while no signal was detected in the other cells, indicating the presence of distinct cell (Fig.12B). Furthermore, the quantitative analysis of collagen type I–positive cells within the PTC population revealed cellular heterogeneity: only 50% of the total number of cells are positive for collagen and therefore produce collagen. These cells are probably fibroblast compounds, since the principal role of fibroblasts is the production of extracellular molecules like collagen (Fig.12C). Given the intense cellular heterogeneity of the tumor microenvironment, a heterotypic 3D model markedly increases their experimental reliability, conferring a physiological relevance that more accurately reflects the complexity of *in vivo* tumor architecture [221].

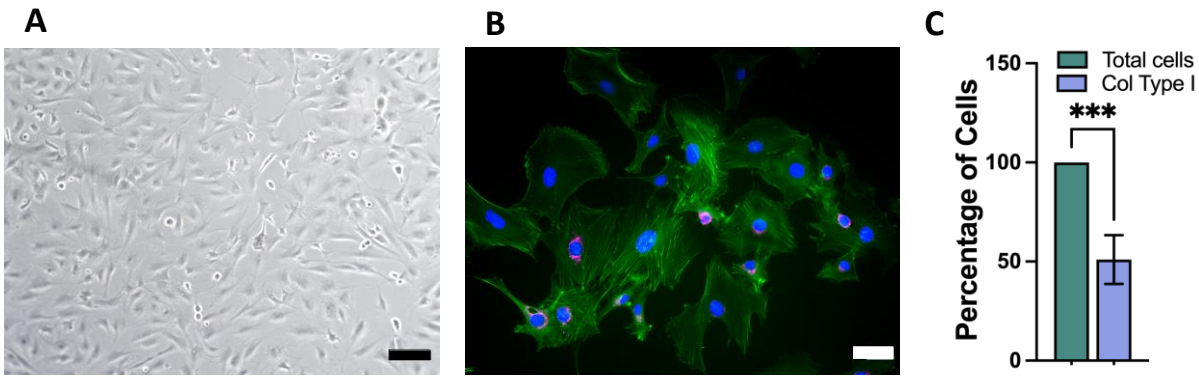

Figure 12: Morphological and immunophenotypic characterization of primary tumor cells. (A) PTCs isolated from the excised tumor mass (PTCs). (B) Fluorescence microscopy analysis of PTCs showing collagen type I immunostaining (magenta) and nuclei stained with DAPI (blue). (C) Quantitative representation of collagen type I–positive cells within the PTC population. Scale bar: 15 µm. Data are mean ± SD. T-test was performed (n = 3) (***P < 0.001).

Image adapted from Lo Cicero et al: '*Enhancing therapeutic efficacy through degradation of endogenous extracellular matrix in primary breast tumor spheroids*' *FEBS J.* 2025, doi: 10.1111/febs.70069 [1]. Copyright via CC BY-NC-ND 4.0 - https://creativecommons.org/licenses/by/4.0/

4.1.2 Generation of Primary Tumor Spheroids

To better recapitulate the structural organization and functional properties of solid tumors in vitro, PTCs were maintained under low-adhesion culture conditions that inhibit cell–substrate interactions. This environment promotes cell-driven aggregation through enhanced cell–cell adhesion, leading to the generation of three-dimensional (3D) tumor spheroids that more closely replicate in vitro the in vivo TME. [182] (Fig.13A). After six days of culture, the spheroids displayed pronounced structural compaction and a smooth, uniform surface, as shown by the optical (Fig.13B) and confocal microscopy (Fig. 3C) images, with diameters consistently ranging between 400 and 450 µm.

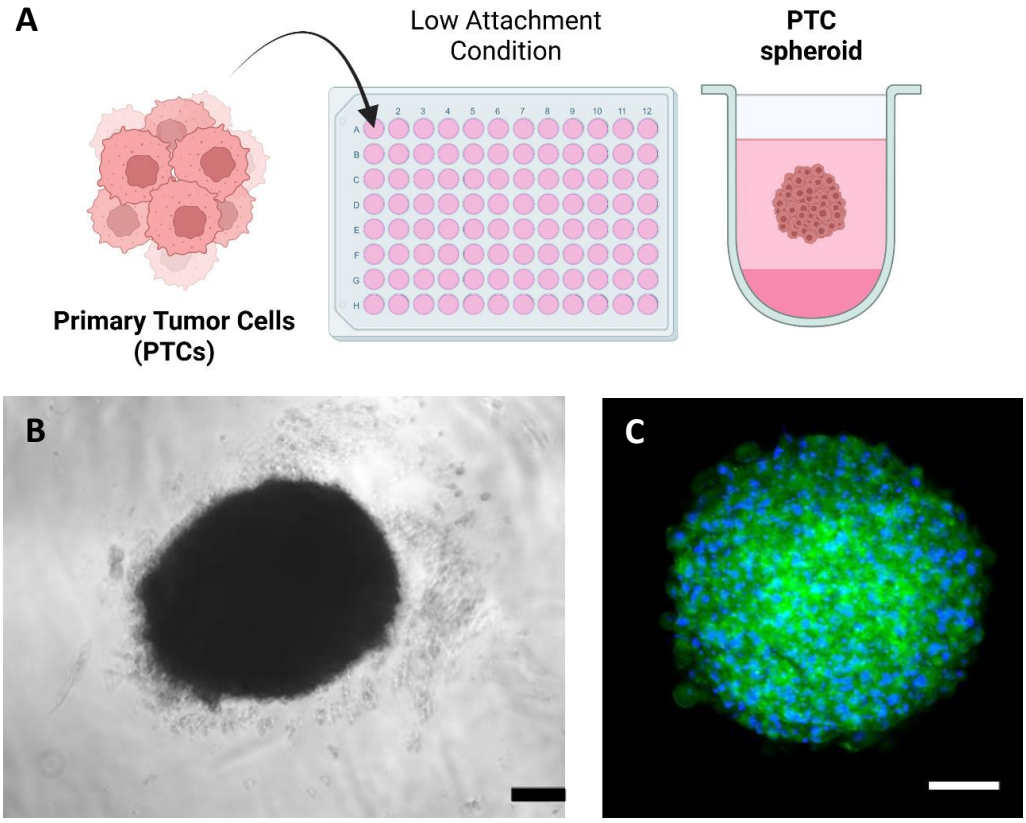

Figure 13: Formation and charachterization of 3D tumor spheroids. (A) Schematic representation of the spheroids formation under low-attachment conditions. (B) Optical microscopy images showing the spheroids with a well-defined, spherical morphology. (C) Confocal microscopy analysis of the spheroids, with F-actin labeled by phalloidin-FITC (green) and nuclei stained with DAPI (blue). Scale bar: 100 µm.

Image adapted from Lo Cicero et al: '*Enhancing therapeutic efficacy through degradation of endogenous extracellular matrix in primary breast tumor spheroids*' *FEBS J.* 2025, doi: 10.1111/febs.70069 [1]. Copyright via CC BY-NC-ND 4.0 - https://creativecommons.org/licenses/by/4.0/

In collaboration with Dr. Simone Dario Scilabra and Dr. Margot Lo Pinto of Ri.MED Foundation, high-resolution proteomic analysis was performed to compare the molecular landscape of PTC cells grown in conventional 2D monolayers *versus* 3D spheroids. 6,572 proteins were detected in spheroids and 6,573 in 2D cultures, with 6,486 shared between the two systems (Fig.14A). Among the common proteins, 1,128 were upregulated in spheroids, whereas 816 were more abundant in 2D cultures, indicating an important proteome reprogramming under 3D conditions.

Focusing specifically on ECM-associated proteins defined by the Gene Ontology term GO:0031012, 128 ECM-related proteins were identified. Of these, 12 were significantly downregulated in spheroids, while 45 exhibited a marked increase (Fig.14B).

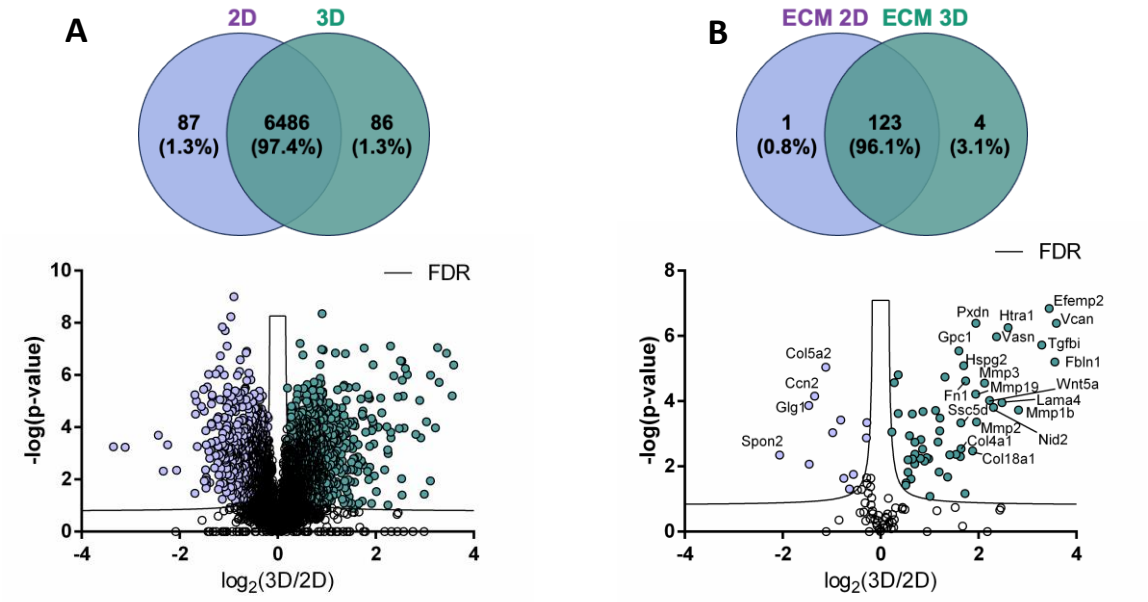

Figure 14: Proteomic comparison of 2D cultures and 3D primary breast tumor spheroids. (A) Venn diagram and volcano plot showing the distribution of all proteins identified in five biological replicates of 2D cell cultures (magenta) and 3D spheroids (green). The volcano plot represents −log10 P-values versus log2 protein ratios, with proteins enriched in 3D spheroids shown in blue and those enriched in 2D cultures in red (n = 5). (B) Venn diagram and volcano plot focusing on extracellular matrix (ECM) proteins, comparing 2D cell cultures and 3D spheroids. The volcano plot illustrates −log10 P-values versus log2 protein ratios for ECM proteins, with 3D spheroid–enriched proteins in blue and 2D culture–enriched proteins in red (n = 5).

Image adapted from Lo Cicero et al: '*Enhancing therapeutic efficacy through degradation of endogenous extracellular matrix in primary breast tumor spheroids*' *FEBS J.* 2025, doi: 10.1111/febs.70069 [1]. Copyright via CC BY-NC-ND 4.0 - https://creativecommons.org/licenses/by/4.0/

Furthermore, several matrix MMPs, including MMP1b, MMP2, MMP3, MMP14, and MMP19, were overexpressed in spheroids (Fig.15A), and MMP9, together with MMP13,

was uniquely detected in the 3D condition, suggesting that 3D spheroids were characterized by intense matrix remodeling processes. MMPs play key roles in tumorigenesis by remodeling the ECM and modulating signaling pathways within the tumor microenvironment. Similarly, collagen isoforms such as Col5a2, Col4a1, Col18a1, Col5a1, Col8a1, Col4a2, and Col16a1 were present in both systems but consistently expressed in 3D cultures compared to 2D cultures (Fig.15B, indicating a more structured and abundant ECM.

These proteomic findings indicated that tumor spheroids recapitulate key ECM features of solid tumors, including enhanced deposition of fibrillar collagens and matrix remodeling enzymes, such as MMPs. MMP9 and MMP13 promote ECM regulation, cell proliferation, and extravasation [222,223], while increased expression of different collagen isoforms can modulate cell behavior, intracellular signaling, and drug sensitivity [224].

In summary, these results suggest that spheroids developed a more complex and physiologically relevant matrix, better mimicking *in vitro* the solid tumor microenvironment.

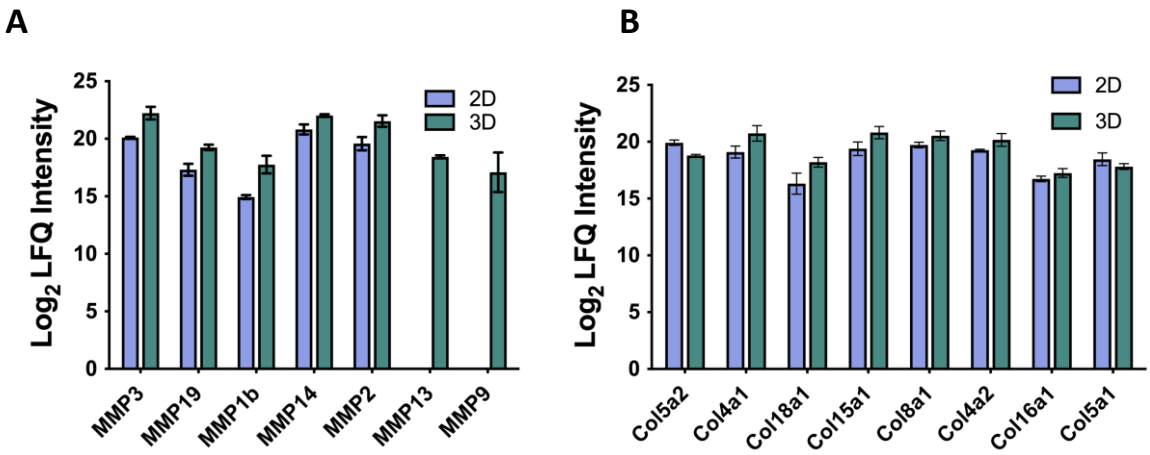

Figure 15: Differential expression of MMPs and collagens in 2D and 3D cultures. (A) Label-free quantification (LFQ) of the most significantly expressed matrix metalloproteinases between 2D and 3D cell cultures (n = 5) reveals that 3D spheroids display a distinct proteolytic profile compared with conventional 2D cultures, reflecting the *in vivo* ECM remodeling of tumor microenvironment. (B) LFQ analysis of the predominant collagen types demonstrates differences in collagen expression between 2D and 3D models, suggesting that the 3D culture environment promotes a more structured ECM. Data are presented as mean ± SD.

Image adapted from Lo Cicero et al: '*Enhancing therapeutic efficacy through degradation of endogenous extracellular matrix in primary breast tumor spheroids*' *FEBS J.* 2025, doi: 10.1111/febs.70069 [1]. Copyright via CC BY-NC-ND 4.0 - https://creativecommons.org/licenses/by/4.0/

4.1.3 Spatial Distribution and Enzymatic Collagen Type I Degradation in Primary Breast Tumor Spheroids

The proteomic evidence of enhanced collagen deposition in spheroids led to an investigation of the spatial organization of collagen type I, the predominant fibrillar collagen in many solid tumors. The image obtained by confocal microscopy showed that spheroids produced a robust endogenous matrix characterized by collagen type I (magenta), primarily distributed in a dense peripheral shell surrounding the spheroid, closely mimicking *in vitro* the *in vivo* tumor ECM architecture (Fig.16).

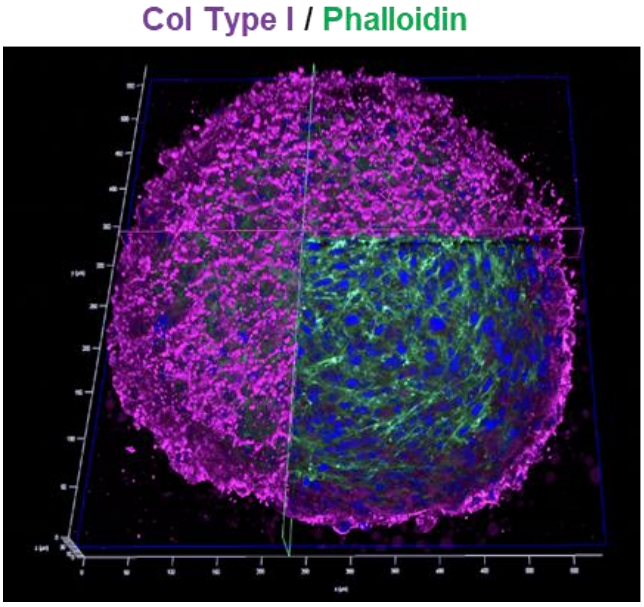

Figure 16: Confocal imaging of primary tumor spheroids. Representative confocal microscopy stacks of primary tumor spheroids, acquired from top to bottom, showing cytoskeletal F-actin labeled with phalloidin-FITC (green), collagen type I (magenta), and cell nuclei stained with DAPI (blue). Scale bar: 100 μm. Experiments were repeated three times (n = 3).

Image adapted from Lo Cicero et al: '*Enhancing therapeutic efficacy through degradation of endogenous extracellular matrix in primary breast tumor spheroids*' *FEBS J.* 2025, doi: 10.1111/febs.70069 [1]. Copyright via CC BY-NC-ND 4.0 - https://creativecommons.org/licenses/by/4.0/

To investigate the role of collagen matrix, the spheroids were treated with the ultrapure recombinant collagenase COLH (class II, active on linear regions of collagen) either alone or in combination with COLG (class I, targeting triple-helical collagen regions. Several concentrations of each enzyme were tested to determine the most effective conditions for

collagen degradation. Treatment with COLH alone resulted in a measurable, but incomplete, reduction of extracellular collagen, as observed by confocal microscopy (Figure 7, center). In contrast, complete degradation of collagen type I was achieved only when COLH and COLG were used in combination (Fig.17). These results highlight that a combination of the two enzymes efficiently digests the collagen-rich ECM in the spheroids and suggest that a specific combination of collagenases could represent a powerful approach to overcoming the ECM-mediated barrier in tumors. Furthermore, these enzymes were able to digest collagen, maintaining the structural integrity of the spheroids.

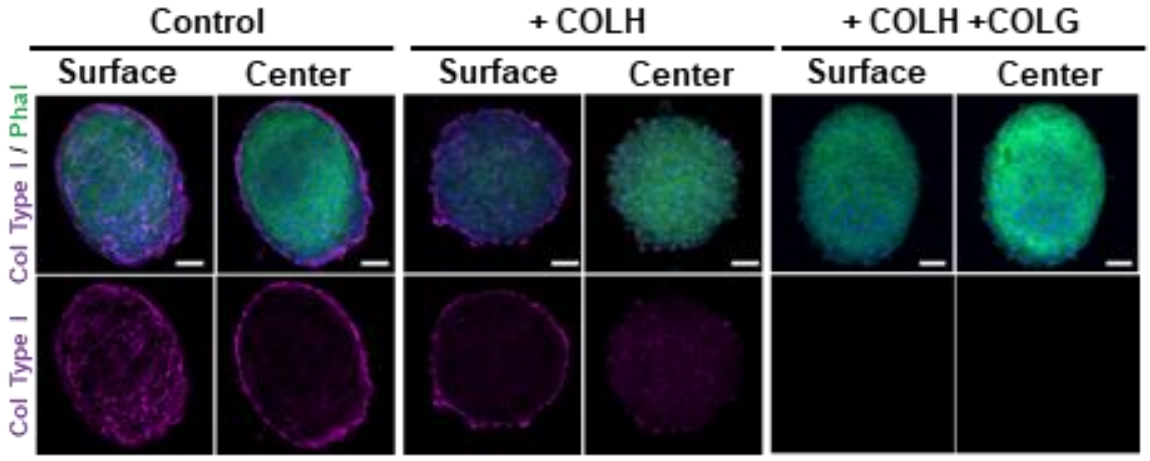

Figure 17: Confocal imaging of primary tumor spheroids after collagenase treatment. Primary tumor spheroids untreated (Control), treated with recombinant collagenase COLH (+COLH) for 1 h 15 min, or in combination with COLG (+COLH/COLG) for 1 h 15 min. Following enzymatic treatment, spheroids were stained with phalloidin-FITC (Phal, green), an anti–collagen type I antibody (magenta), and DAPI (blue) for nuclei, and analyzed by confocal microscopy. Images show both the surface (left) and central region (right) of the spheroids. Scale bar: 100 µm. Experiments were repeated three times (n = 3).

Image adapted from Lo Cicero et al: '*Enhancing therapeutic efficacy through degradation of endogenous extracellular matrix in primary breast tumor spheroids*' *FEBS J.* 2025, doi: 10.1111/febs.70069 [1]. Copyright via CC BY-NC-ND 4.0 - https://creativecommons.org/licenses/by/4.0/

4.1.4 Enhanced Uptake of Doxorubicin Following Collagenase-Based Matrix Degradation

To investigate the impact of ECM degradation due to collagen digestion on drug accessibility, Doxorubicin (DOX) uptake in PTCs spheroid was evaluated using DOX intrinsic autofluorescence. Confocal microscopy images revealed a progressive accumulation of DOX within the spheroids over 24 hours, with the highest fluorescence intensity, indicating significant drug uptake (Fig.18A). Importantly, spheroids pretreated with the combination of collagenases COLG and COLH exhibited 38% increase in total

fluorescence intensity in all spheroid structures (Fig.18B), compared to control (untreated spheroids). These findings suggest that collagen degradation within the ECM increases deeper drug penetration and distribution within the spheroids. This highlights the potential of ECM remodeling as a strategy to enhance intratumoral drug uptake.

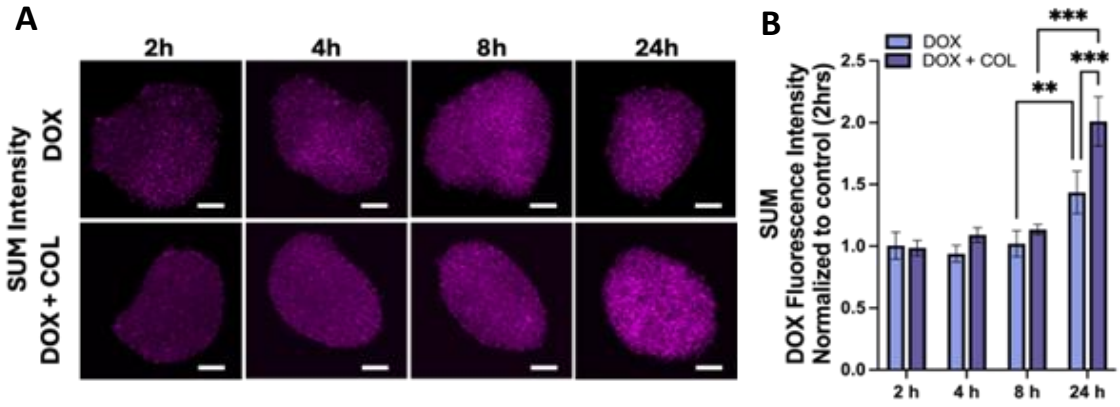

Figure 18: Collagenase treatment enhances doxorubicin uptake in primary breast tumor spheroids. (A) Confocal microscopy analysis (sum intensity of z-stacks, 20 µm) showing doxorubicin uptake (magenta) in control spheroids (DOX) and spheroids pretreated with collagenases (DOX + COL) at different time points (2, 4, 8, 24 h). (B) Fluorescence sum intensities were quantified and normalized to the control. (C) Confocal analysis of the central z-stack (20 µm) highlighting doxorubicin accumulation in the spheroid core for control and collagenase pretreated spheroids over time. (D) Central stack fluorescence intensities were quantified and normalized to control. Doxorubicin autofluorescence is shown in magenta. Scale bar: 100 µm. Data are presented as mean ± SD, and statistical significance was determined by two-way ANOVA ($n = 3$, $^{**}p < 0.01$, $^{***}p < 0.001$).

Image adapted from Lo Cicero et al: '*Enhancing therapeutic efficacy through degradation of endogenous extracellular matrix in primary breast tumor spheroids*' *FEBS J.* 2025, doi: 10.1111/febs.70069 [1]. Copyright via CC BY-NC-ND 4.0 - https://creativecommons.org/licenses/by/4.0/

4.1.5 Collagenase Pretreatment Improves Chemotherapeutic Response

To investigate whether improved drug penetration results in enhanced therapeutic efficacy, spheroids were first treated with collagenases and then incubated with DOX for 24 hours, and the spheroid area, including dead cells, was analyzed (Fig.19A). Collagenases treatment removes the protective effect of collagen type I without altering spheroid architecture, likely due to the presence of other ECM components. DOX alone increased the total spheroid area by 75%, reflecting cell death and structural laxity. Interestingly, collagenase pretreatment potentiated DOX efficacy, resulting in a 34% additional increase in spheroid area compared to those incubated with DOX alone (Fig.19B).

Time-course cell viability analyses further supported these results (Fig.19C). More specifically, after 8 hours of incubation, no significant cytotoxicity was observed in the spheroids treated with collagenases and the drug compared to controls, while partial responses emerged at 16 hours. However, after 24 hours, spheroids pre-treated with collagenases and then with DOX exhibited a 50% reduction in viability compared to those treated only with DOX.

This finding highlights the critical role of ECM as a biomechanical barrier, where collagen degradation facilitates the chemotherapeutic agents penetration. Although collagenases are clinically applied for wound and ulcer debridement, their potential use in tumor treatment remains unvalidated. [224]. These data also suggest that collagenase-mediated ECM remodeling can probably improve immune cell infiltration, since the dense and stiff ECM produced by tumors can physically impede T cell migration [148].

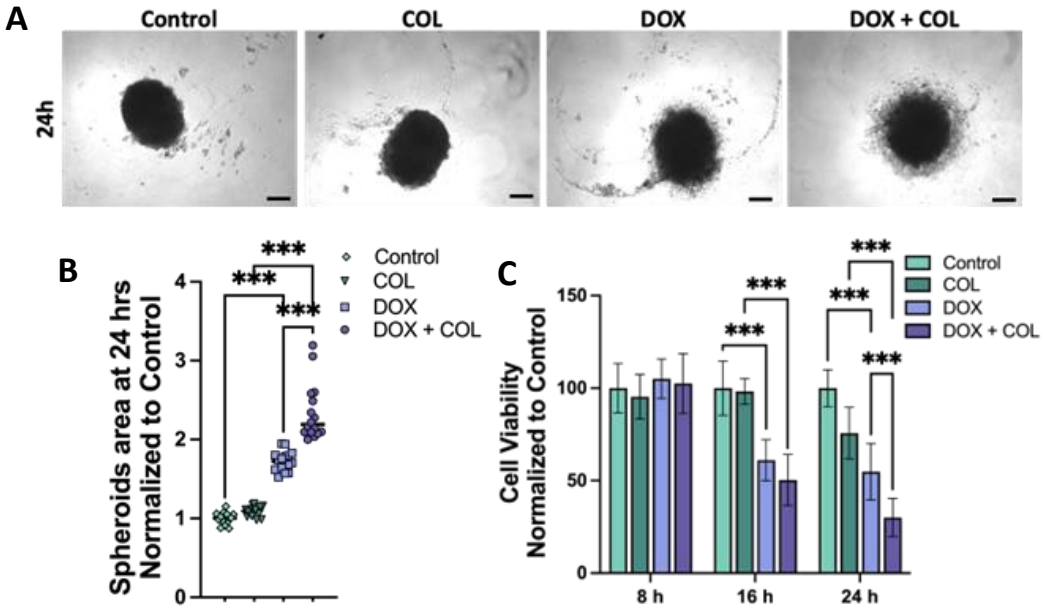

Figure 19: ECM digestion enhances doxorubicin-induced cytotoxicity in primary tumor spheroids. (A) Optical images of primary tumor spheroids under different conditions: untreated control (Control), treated with collagenases alone (COL), treated with doxorubicin 20 µM (DOX), and treated with the combination of collagenases and doxorubicin 20 µM (DOX + COL), at 24 h. (B) Spheroid area quantification at 24 h was normalized to the T0 area. Statistical analysis was performed using one-way ANOVA (n = 3). (C) Cell viability of primary tumor spheroids over time (8, 16, 24 h) under the same treatment conditions. Scale bar: 100 µm. Data are presented as mean ± SD, and statistical significance was determined by two-way ANOVA (n = 3, **p < 0.01, ***p < 0.001).

Image adapted from Lo Cicero et al: '*Enhancing therapeutic efficacy through degradation of endogenous extracellular matrix in primary breast tumor spheroids*' *FEBS J.* 2025, doi: 10.1111/febs.70069 [1]. Copyright via CC BY-NC-ND 4.0 - https://creativecommons.org/licenses/by/4.0/

4.2 Synergistic Effect of Collagenase and PVP-AEDP-Doxorubicin Nanoparticles in Primary Tumor Cell Spheroids

4.2.1 Characterization of PVP-AEDP-DOX NPs

The role of collagen matrix around and inside tumor masses, in limiting drug accessibility, was further investigated by using nanoparticles (NPs) as a vehicle for uptake into the tumor. For this purpose, Polyvinylpyrrolidone (PVP) nanoparticles were synthesized by high-energy electron beam irradiation, in collaboration with Professor Clelia Dispenza's research group (Department of Ingegneria Chimica, Gestionale, Informatica, Meccanica (DICGIM) of the University of Palermo). This technique permitted obtaining sterile and functionalized NPs with a controlled size.

PVP NPs were conjugated to DOX through (3-[(2 aminoethyl)dithio] propionic acid) AEDP linker. The disulfide bond in AEDP is sensitive to the altered intracellular glutathione levels typically found in tumor cells, enabling controlled and selective release of doxorubicin within the tumor microenvironment (Fig.20A). Conjugation of DOX to PVP via the AEDP linker can improve biodistribution, reduce systemic toxicity, and allow for a stimulus-responsive release mechanism that exploits the biochemical differences between tumor and healthy cells [225]. The amount of conjugated drug (62,3 μM) was evaluated by spectrophotometric analysis using a doxorubicin calibration curve. Dynamic Light Scattering (DLS) analysis showed an NPs average size of 113 nm, a PdI value of 0.195, and a Z-potential of -24.6 ± 5.89. The effect of PVP-AEDP-DOX NPs was evaluated both in 2D and 3D systems of PTC cells (Fig. 20B).

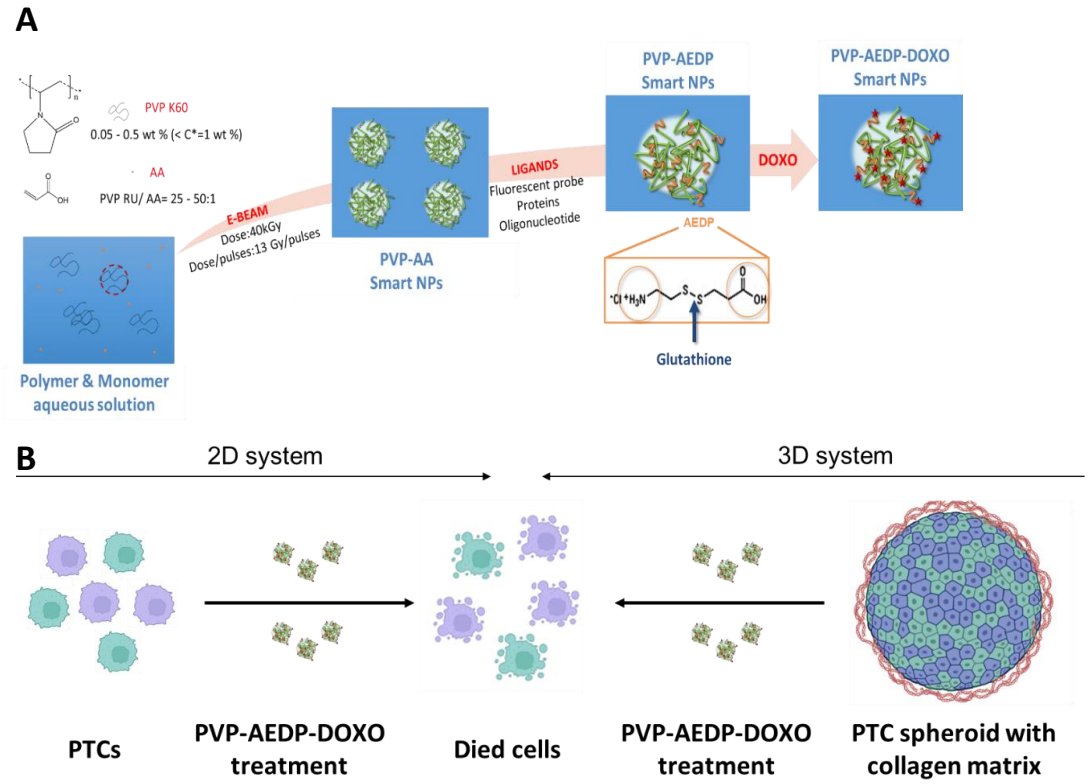

Figure 20: Synthesis of PVP-AEDP–DOX nanoparticles and their application in vitro. (A) Representative schematic illustration of polyvinylpyrrolidone (PVP) nanoparticle synthesis by high-energy electron beam irradiation and subsequent functionalization with doxorubicin via the redox-cleavable AEDP linker. The disulfide bond within the AEDP linker is reduced in the presence of elevated intracellular glutathione levels characteristic of tumor cells, thereby triggering intracellular DOX release within the tumor microenvironment. (B) Representative schematic illustrating the in vitro applications of PVP-AEDP–DOX nanoparticles in PTCs cultured under two-dimensional (2D) and three-dimensional (3D) conditions.

4.2.2 Antitumor Efficacy of PVP-AEDP-DOX NPs in 2D PTC Culture

The effect of PVP-AEDP-DOX on PTC was evaluated both by cytotoxic assay and fluorescence uptake. Cell viability quantification, normalized to untreated controls, revealed that PTCs treated with free DOX exhibited a dose-dependent cytotoxicity, reaching an IC_{50} of approximately 5 µM. In contrast, DOX conjugated to PVP nanoparticles displayed a markedly reduced dose-dependent effect, with the IC_{50} not reached even at the highest tested concentration of 20 µM. Overall, the cytotoxic efficacy of nanoparticle-conjugated DOX was lower compared to free DOX under these experimental conditions (Fig.21).

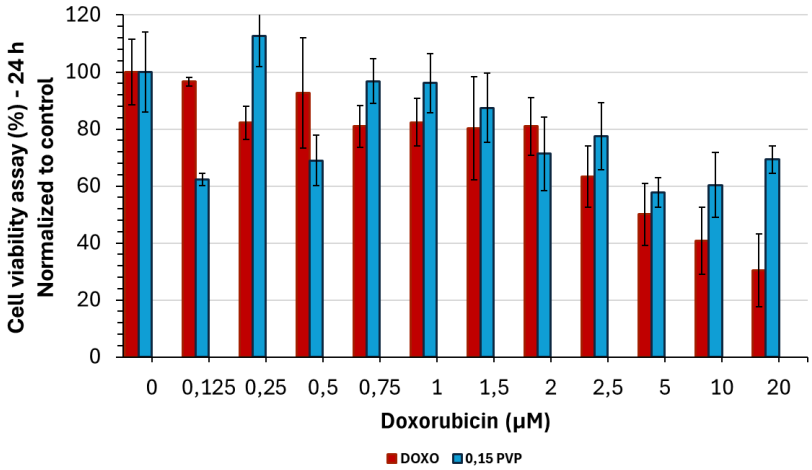

Figure 21: Cytotoxic effect of PVP-AEDP-DOX NPs. Cell viability showed that free DOX (red) induced dose-dependent cytotoxicity, whereas PVP-conjugated DOX (blue) exhibited reduced efficacy compared to the free drug.

On the other hand, fluorescence uptake studies (Fig.22) revealed that the nanoparticles were internalized by cells within 30 minutes. At this time point, the red fluorescence corresponding to doxorubicin was diffusely distributed throughout the cytoplasm and partially colocalized with the nuclei (blue), indicating that the drug remained largely associated with the nanoparticles. After 1 hour, doxorubicin released from the nanoparticles produced an increasingly strong signal, which continued to rise over time. By 8 hours, a reduction in cell density was evident, with the highest doxorubicin accumulation within the nuclei.

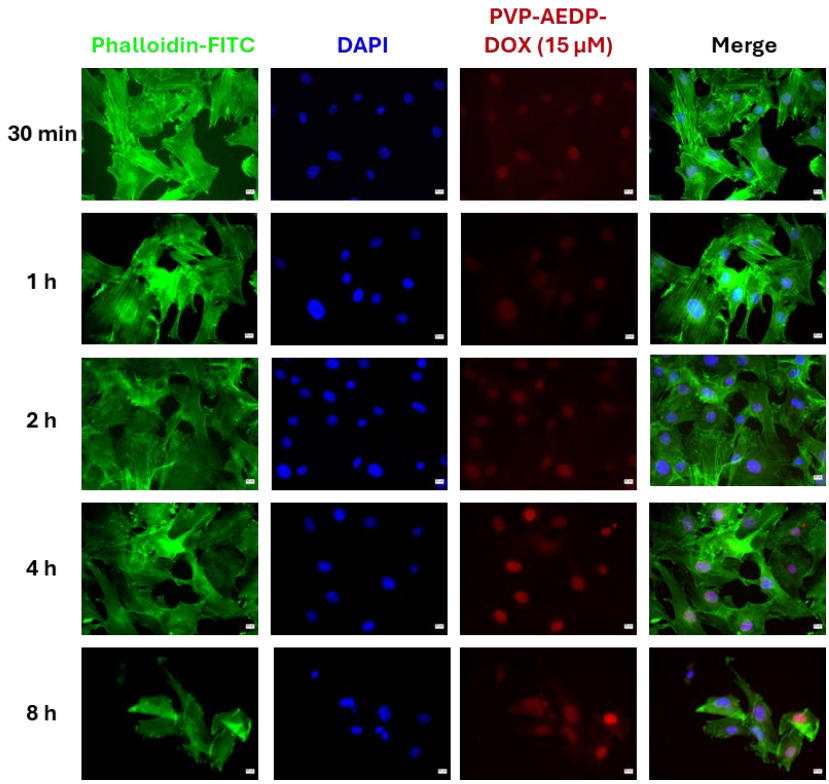

Figure 22: Cellular uptake and nuclear accumulation of PVP–DOX nanoparticles. Time-dependent fluorescence imaging of PTCs treated with PVP–DOX nanoparticles. Within 30 min, DOX (red) was mainly cytoplasmic and partially colocalized with nuclei (blue). Nuclear DOX signal increased over time, reaching maximum accumulation at 8 h, accompanied by reduced cell density.

4.2.3 Cytotoxic Effect of PVP-AEDP-DOX Evaluated in 3D system

While 2D cell cultures are widely used for preliminary cytotoxicity assays, they fail to capture key features of the tumor microenvironment, such as nutrient and oxygen gradients, cell–cell and cell–matrix interactions, and the complex architecture of the ECM [226]. These features, which are characteristic of solid tumors, can lead to elevated intracellular glutathione levels and create physical barriers that limit drug penetration and efficacy, conditions not replicated in flat 2D systems [16,227,228]. To better reflect these in vivo-like conditions, subsequent experiments were conducted using three-dimensional tumor spheroids. In this context, collagenase pre-treatment was employed to partially degrade the dense ECM, thereby facilitating nanoparticle infiltration and enhancing drug-mediated cytotoxicity.

Thus, to investigate whether ECM remodeling further enhances the efficacy of these nanoparticles, PTCs spheroids were incubated for 24 hours with 20 µM PVP-AEDP-DOX NPs, corresponding to the doxorubicin concentration, either with or without collagenase pre-treatment (Fig.23A). Optical microscopy images revealed dead cells surrounding the

spheroids after incubation with NPs, similar to samples treated with free doxorubicin, along with a modest reduction in spheroid size, relative to controls, in both collagenase-un-treated and pre-treated conditions. Cell viability analysis at 24 hours confirmed these findings (Fig.23B). More specifically, spheroids pre-treated with collagenases followed by PVP-AEDP-DOX NPs incubation exhibited approximately 50% lower viability compared to spheroids treated with PVP NPs alone, indicating that ECM digestion enhances the therapeutic impact of the redox-sensitive nanoparticles. Importantly, collagenase treatment alone in control spheroids did not induce significant cytotoxicity, confirming even in this case that enzymatic activity selectively targets the ECM while maintaining spheroid integrity.

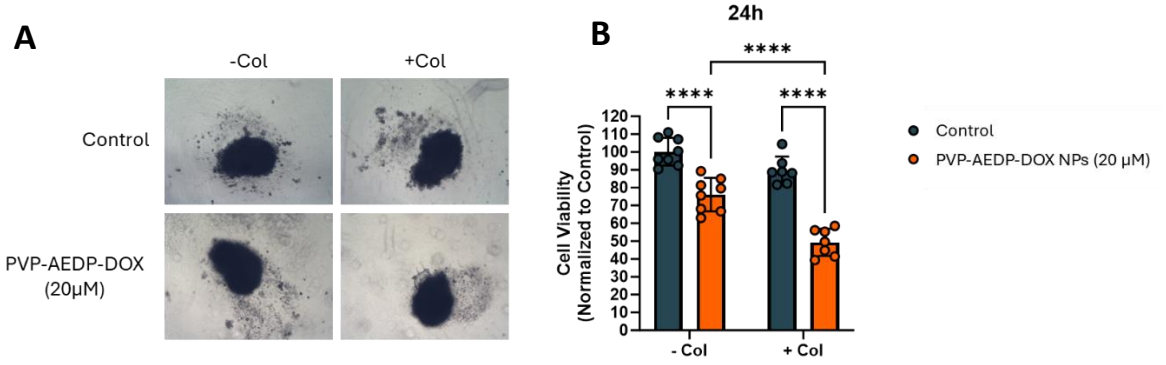

Figure 23: Evaluation of the Therapeutic Efficacy of PVP-AEDP-DOX Nanoparticles. (A) Optical images (10× magnification) of control spheroids and spheroids treated with PVP-AEDP-DOX nanoparticles, with (+ COL) or without (-COL) collagenases pre-treatment. (B) Corresponding cell viability analysis graph after 24 hours of treatment showed a sensible reduction in cell viability. Data are presented as mean ± SD (n = 7-8, ****p < 0.0001).

Uptake analysis using immunofluorescence at 1- and 2-hour post-incubation was conducted to investigate if ECM degradation could increase nanoparticle penetration. As shown in Figure 24A, no significant differences in DOX autofluorescence were detected after 1 hour. However, at 2 hours, spheroids pre-treated with collagenases showed significantly higher DOX content from nanoparticle accumulation compared to those treated with PVP NPs alone (Fig.24B).

These results confirm that ECM remodeling improves the delivery and cytotoxicity of both free drug and glutathione-sensitive PVP-AEDP-DOX nanoparticles in 3D PTCs spheroids.

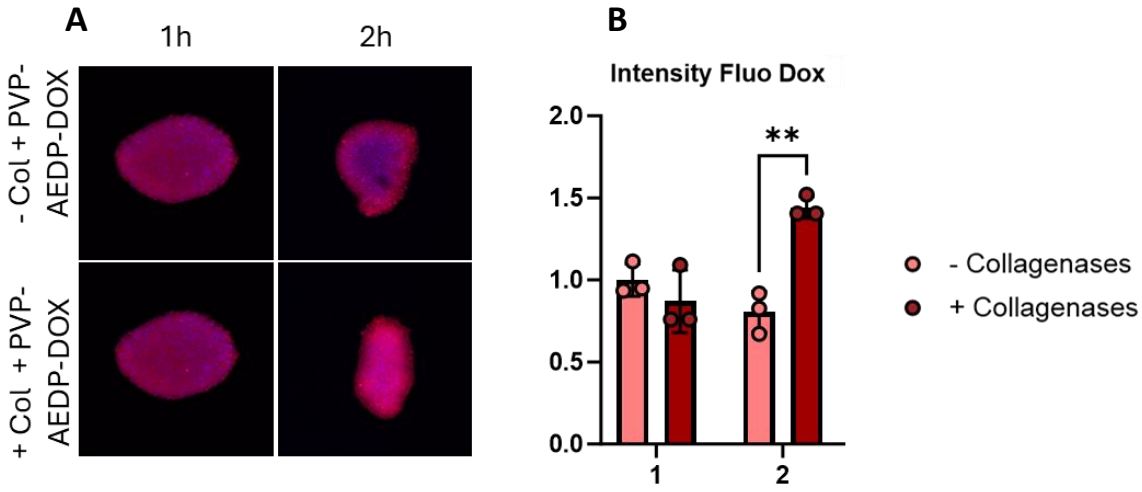

Figure 24: Analysis of Nanoparticle Uptake in PTC Spheroids. (A) merged images showing doxorubicin autofluorescence (red) and DAPI-stained nuclei (blue) in spheroids (10× magnification). (B) Quantification of fluorescence intensity at 1 h and 2 h post-incubation, showing a statistically significant increase in doxorubicin uptake after 2 h in spheroids pre-treated with collagenase compared to those without collagenases. Data are presented as mean ± SD (n = 3, **P < 0.01).

4.3 Enhancing Drug Penetration and Cytotoxicity in 3D Primary Breast Cancer Cultures via BSA-Nanoparticles

4.3.1 Synthesis and Physicochemical Characterization of BSA Nanoparticles

Previous experiments demonstrated that PVP-AEDP-DOX nanoparticles, designed for redox-sensitive drug release, exhibit significant cytotoxic effects in 3D PTC spheroids. However, pH-sensitive BSA–DOX nanoparticles represent a more advantageous therapeutic strategy than glutathione-responsive PVP–DOX systems, primarily due to their enhanced selectivity in drug release within the tumor microenvironment. This is because acidic pH is a consistent and well-conserved feature of the tumor microenvironment, enabling controlled and predictable release of doxorubicin upon nanoparticle internalization by tumor cells [16]. This mechanism ensures high therapeutic efficacy while minimizing premature drug release under physiological conditions. In contrast, glutathione-responsive systems rely on intracellular GSH gradients that can be highly heterogeneous across different tumor types, disease stages, and cellular populations, thereby reducing the reproducibility and uniformity of the therapeutic response [229]. Moreover, elevated glutathione levels are also present in healthy cells as one of the main antioxidant molecules, increasing the risk of non-selective drug release and potential side effects due to off-target toxicity [230]. From a biological point of view, albumin provides additional advantages, including biocompatibility, biodegradability, and the ability to

exploit albumin-mediated uptake mechanisms, thereby promoting tumor accumulation and improving penetration within neoplastic tissues [231]. Building on these considerations, it was evaluated whether similar synergistic effects could be achieved with pH-sensitive nanoparticles based on Bovin Serum Albumin (BSA) conjugated with Doxorubicin (DOX), which can exhibit a retention-based mechanism triggered by the acidic tumor microenvironment. The rationale behind this experiment is to determine if the combination of ECM remodeling via collagenase pre-treatment and the pH-triggered retention of BSA-DOX nanoparticles can replicate or even improve the therapeutic efficacy observed with redox-sensitive PVP-AEDP-DOX.

The first part of the study was dedicated to the synthesis and characterization of Bovine Serum Albumin nanoparticles (BSA NPs) as a control for the optimization and validation of the synthesis protocol of BSA nanoparticles conjugated to doxorubicin (BSA-DOX NPs). The BSA NPs were obtained through a desolvation method, followed by crosslinking with glutaraldehyde, chosen to confer structural stability to the nanoparticles over time (Fig.25A). Glutaraldehyde mainly reacts with free amine groups ($–NH_2$) of lysine side chains present in proteins. Through the formation of Schiff base bond (–C=N–), glutaraldehyde creates inter- and intramolecular link between different albumin molecules [232]. The morphology of the BSA NPs was initially examined by Transmission Electron Microscopy (TEM) in order to observe structural details and confirm the homogeneity of particle size distribution. TEM images showed that the nanoparticles were almost spherical and exhibited a low level of aggregation, with an average diameter of approximately 96 nm (Fig.25B).

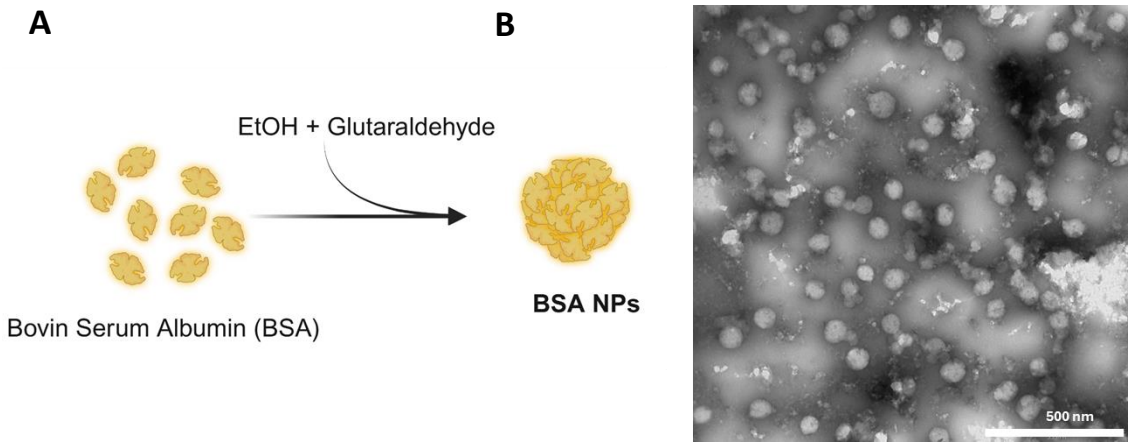

Figure 25: Synthesis and Characterization of BSA Nanoparticles. (A) Schematic representation of the synthesis process. (B) TEM image showing the compact structure and spherical morphology of the nanoparticles.

Subsequently, the size distribution profile and the polydispersity index (PDI), which reflect the uniformity of particle distribution in solution, were obtained using Dynamic Light Scattering (DLS). DLS analyses revealed that the obtained nanoparticles have well-defined nanometric sizes of approximately 110,7 nm, a value determined by the data normalized by the particle volume. The size measured by DLS was higher than that recorded by TEM, likely due to the hydration layer of the particles, which is intrinsically estimated by DLS approaches. The size distribution was highly homogeneous, as indicated by the low PDI values (0.123), reflecting a uniform distribution of nanoparticles.

To further investigate the characteristics of the nanoparticles, additional measurements were performed using Nanoparticle Tracking Analysis (NTA). NTA provided additional information on particle size and concentration, revealing a diameter of 102 nm, determined as the mode of the size distribution. Moreover, the concentration of nanoparticles was $7{,}99 \times 10^{11} \pm 1{,}49 \times 10^{10}$ particles/mL.

Overall, these results indicate that the BSA NPs synthesis protocol was successfully optimized, producing well-characterized nanoparticles with good control over size and low polydispersity, ensuring their homogeneity and stability over time.

4.3.2 pH-Responsive Behavior of BSA Nanoparticles in Acidic Conditions

The response of the nanoparticles to acidic pH, typical of the tumor microenvironment, was studied by exposing the nanoparticles to solutions with pH 6.5 and 5.5. After 24 hours of incubation, nanoparticle aggregation was detected as an increase in solution turbidity both at pH 6.5 and, more markedly, at pH 5.5, where clear sedimentation also occurred (Fig.26).

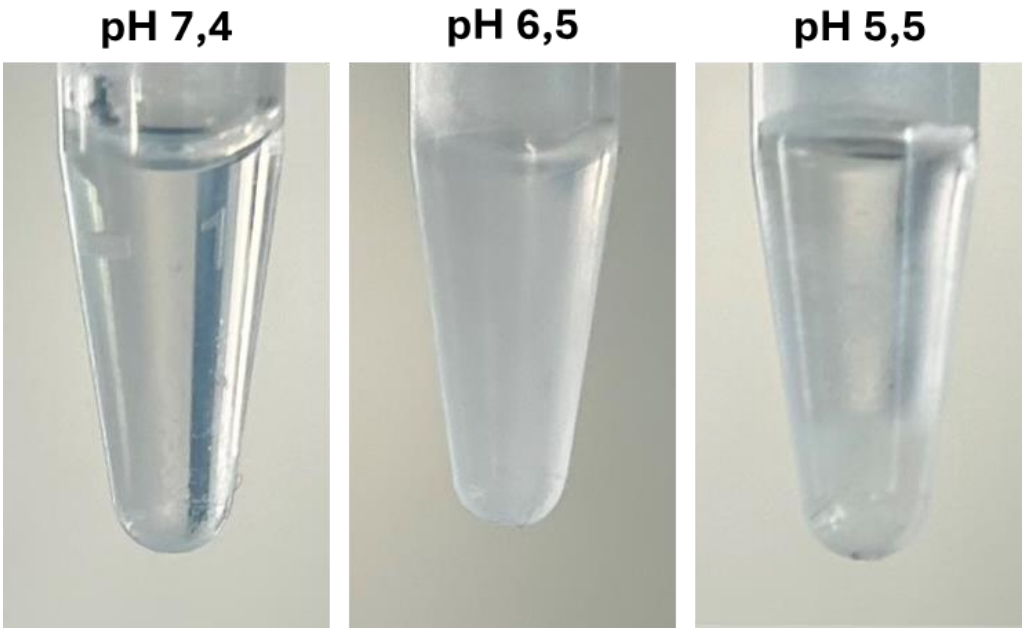

Figure 26: Acid pH–Responsive Behavior of the Nanoparticles. (A) Images of the nanoparticle suspensions at acidic pH, showing evident higher tubidity of solution at pH 6,5, and sediment formation at pH 5.5.

Through zeta potential (ZP) measurement, we analyzed changes in the surface charge of the nanoparticles at different pH values. At pH 7.4, the nanoparticles exhibited a net charge of -18 mV, whereas at pH 6.5 and 5.5 the charge decreased to -1,9 mV and -1,7 mV, respectively, indicating a change in particle stability in response to acidic pH. To analyze the size of nanoparticles in response to acidic pH conditions, we employed the DLS technique. In particular, we focused on the average size of the aggregates.

The results showed that, at neutral pH (7.4), after 24 hours of incubation, the nanoparticles had an average size of 130 nm. At pH 6.5, the nanoparticles exhibited an average size of 143,4 d.nm, a moderate increase compared to neutral pH, suggesting minimal response to acidic pH without drastic aggregation. However, at pH 5.5, we observed a remarkable increase in the average size of the nanoparticles, with a diameter reaching the size of 777 nm with a PDI of 1, indicative of strong size heterogeneity. This significant increase was in agreement with Figure 13 and suggests that under acidic pH, the nanoparticles tend to aggregate more markedly, likely due to a change in particle surface charge that promotes interactions between them.

These results have fundamental importance for the design of drug-loaded nanoparticles. In particular, the observation of control BSA nanoparticles at pH 6.5 and 5.5, compared to physiological pH 7.4, suggests that the nanoparticles can respond dynamically to acidic conditions. This phenomenon could be useful in therapeutic contexts where localized

particle accumulation at the tumor site is desired, exploiting acidic pH conditions to facilitate their retention.

4.3.3 Development and Characterization of BSA Nanoparticles Conjugated with Doxorubicin

Once the synthesis protocol was optimized and the drug-free BSA nanoparticles were characterized, the next step was dedicated to the synthesis of BSA nanoparticles conjugated with doxorubicin (BSA-DOX NPs). The synthesis process was carried out following the same methodology used for the drug-free nanoparticles, with the only difference being the inclusion of doxorubicin during the synthesis process (Fig.27A). To determine the amount of drug incorporated into the nanoparticles, the supernatant from the post-synthesis washes was analyzed through spectrophotometric measurements. These readings allowed the quantification of the unbound drug fraction removed during the washing process, revealing that approximately 50% of the initially added doxorubicin was effectively incorporated within the nanoparticles. This result confirms the efficiency of the conjugation process, ensuring that a significant amount of drug remains stably associated with the system.

The morphology of the BSA-DOX NPs was initially determined by TEM, in order to observe the shape and size distribution of the nanoparticles. TEM images revealed that the BSA-DOX NPs exhibited a perfectly spherical and well-defined shape, with an average diameter of approximately 87 nm (Fig.27B).

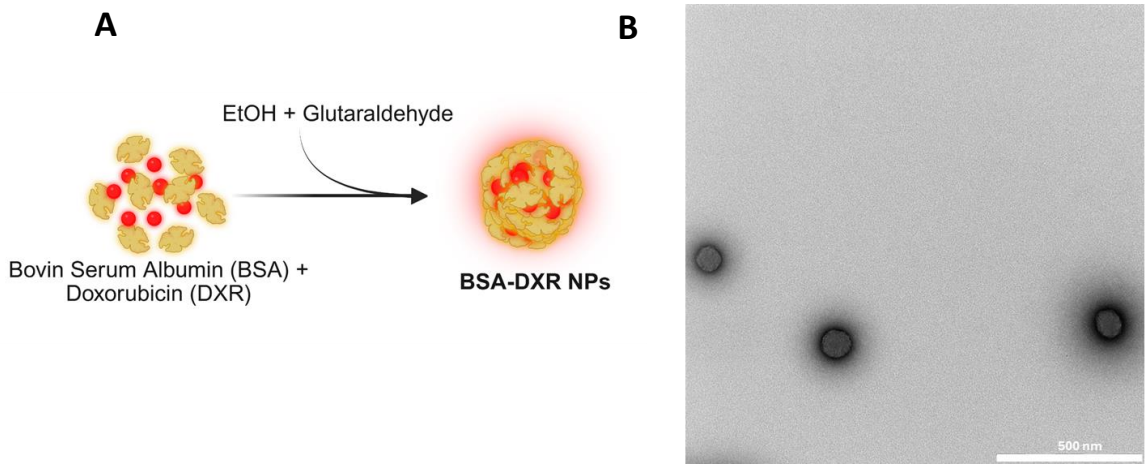

Figure 27: Synthesis and Characterization of BSA-DOX Nanoparticles. (A) Schematic representation of the synthesis process. (B) TEM image showing a NPs compact structure and highly spherical morphology of the nanoparticles conjugated to the drug.

Subsequently, DLS analyses were performed to obtain information on the size profile and

polydispersity index. DLS data, obtained by volume normalization, showed that the BSA-DOX NPs had an average size of 115,6 nm with an even more homogeneous distribution compared to the control NPs (PDI = 0,06). To complete the characterization, Nanoparticle Tracking Analysis (NTA) was performed, revealing a characteristic size of 78.4 d.nm (determined as the mode of size distribution) with a concentration of $9{,}50 \times 10^7 \pm 1 \times 10^7$ particles/mL.

Overall, these results, together with the quantification of the DOX unbound fraction, indicate that the synthesis of BSA-DOX NPs was successful, preserving the reproducibility of the conjugated drug while maintaining the nanoparticle characteristics.

4.3.4 pH-Responsive Behavior of BSA-DOX Nanoparticles in Acidic Conditions

Analogously to the control nanoparticles, the physicochemical dynamics of the drug-conjugated nanoparticles in response to pH variations were studied by exposing the particles to solutions with pH 6.5 and 5.5. After 24 hours of incubation, the BSA-DOX NPs in solution exhibited similar behavior, although with the formation of a sediment already at pH 6.5, as evidenced in the acquired images (Fig.28).

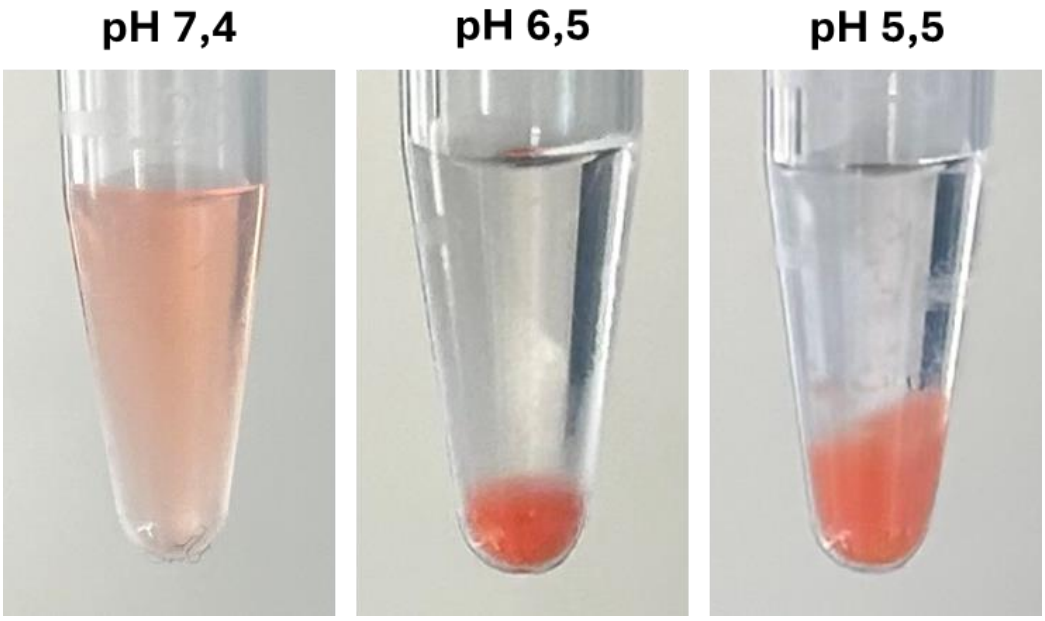

Figure 28: Acid pH–Responsive Behavior of the Nanoparticles. (A) Images of the nanoparticle suspensions at acidic pH, showing clearly visible sediment formation already at pH 6.5, which is further confirmed at pH 5.5.

These results suggest that the drug-conjugated nanoparticles are also sensitive to pH variations, behaving similarly to the BSA NPs. Moreover, in the supernatants, doxorubicin was not detected, indicating that the construct does not display a controlled drug-release

profile under the experimental conditions analyzed. However, this behavior suggests that BSA-DOX NPs could be used as a system for localized drug retention at the tumor site rather than as a release platform.

In parallel, a zeta potential (PZ) analysis of the BSA-DOX NPs was performed at different pH values to examine changes in the surface charge of the particles in response to acidic conditions. Interestingly, despite the clear evidence of sedimentation and aggregation of the nanoparticles at pH 6.5 and 5.5, the zeta potential was close to zero at all tested pH values, with a slight reversal of the charge from physiological pH (+1,68 mV) to acidic pH ($\lesssim$0 mV).

This behavior suggests that, despite the physical changes observed in the nanoparticles, such as sedimentation at acidic pH, the surface charge of the BSA-DOX NPs did not undergo substantial modifications in response to acidic pH. Furthermore, the total difference in surface charge compared to the PZ of control NPs at pH 7,4 (-18 mV) suggests that the conjugation of doxorubicin influenced the net charge of the nanoparticles. This is because doxorubicin is a positively charged molecule. In fact, its positive charge is due to the presence of an amino group (NH2) that, at physiological pH (~7.4), is protonated and therefore contributes to the positive charge of the particle [233]. This phenomenon could thus be a further indication that doxorubicin was indeed conjugated to the surface of the nanoparticles, without severely compromising their ability to maintain a stable form in solution.

To further investigate the size in response to pH variations, the BSA-DOX NPs were analyzed using DLS. As also observed for the BSA NPs, at pH 7.4, the nanoparticles had an average size of 120 nm after 24 hours of incubation, again referring to the recorded intensity. At pH 6.5, the average size of the BSA-DOX NPs doubled, reaching 246,9 nm, suggesting a greater response to pH variation compared to the BSA NPs control. At pH 5.5, a significant increase in size was observed, with the nanoparticles reaching an average size of 933,6 nm, indicating greater aggregation compared to neutral and slightly acidic pH. A significant increase in PDI was also detected, indicating the formation of potential aggregates.

In summary, the data obtained from the BSA-DOX NPs are consistent with those observed for the BSA NPs in response to acidic pH. Although the surface charge of the BSA-DOX NPs did not show drastic variations at pH 6.5 and 5.5, the indication of a slight change in zeta potential suggests that doxorubicin was indeed conjugated to the nanoparticle. This is

because DOX loading shifted the nanoparticle surface potential toward positive values [234–236]. Moreover, the aggregation observed at acidic pH confirms that the BSA-DOX NPs are sensitive to pH variations, with potential for localized retention of the particles in the tumor microenvironment, which is more acidic than healthy tissues.

4.3.5 Combined Effect of Collagenases and BSA-DOX Nanoparticles in PTC Spheroids

After the synthesis and characterization of pH-sensitive BSA-DOX nanoparticles, their cytotoxic activity was evaluated in rat PTCs spheroids. Analogously to what was previously performed with free doxorubicin, the spheroids were pretreated with collagenases, aimed at partial digestion of the endogenous ECM of the spheroids, in order to improve drug permeability and efficacy. Preliminary observations using optical microscopy after 24 hours (Fig.29) of incubation showed that pretreatment with collagenases alone, as well as the combination of collagenase with control nanoparticles devoid of drug, did not induce the formation of a noticeable halo of dead cells around the spheroid. This indicates that enzymatic digestion of the matrix, in the absence of a cytotoxic agent, is not sufficient to cause significant damage to cell viability, and that control NPs do not lead to evident mortality. In contrast, when spheroids were treated with free doxorubicin or with DOX conjugated to BSA NPs, a peripheral halo of dead cells was observed, which was particularly pronounced when the pharmacological treatment was combined with collagenases pretreatment.

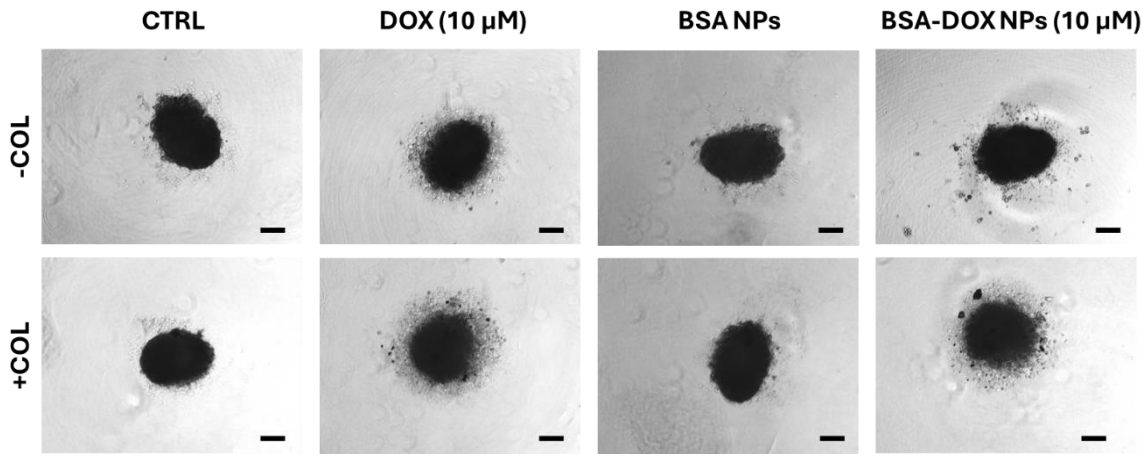

Figure 29: Cytotoxic activity of BSA-DOX nanoparticles in PTC spheroids. Representative optical microscopy images after 24 h showing that collagenase alone (-COL) or in combination with control BSA NPs does not induce evident cell death, whereas treatment with free doxorubicin or BSA-DOX NPs leads to the formation of a peripheral halo of dead cells, particularly enhanced upon collagenases (+COL) pretreatment. Scale bar: 100 µm.

These qualitative observations were supported by quantitative data on cell viability at 24 hours (Fig.30). For this purpose, the results obtained with free drug were normalized to untreated control spheroids, while the results from the conjugated drug treatment were normalized to spheroids treated with control BSA NPs under all experimental conditions. Analysis of the results shown in the graph indicates that treatment with collagenase alone (C + COL) did not cause a significant reduction in cell viability compared to control, confirming that the enzyme is not highly cytotoxic under the experimental conditions used. In contrast, the combination of collagenase with either free DOX or DOX conjugated to BSA NPs led to a significant increase in cell mortality compared to the respective controls. In particular, the combination of collagenase with BSA-DOX was the most effective, reducing cell viability to values close to the IC_{50}, whereas free DOX + collagenases, although showing a noticeable increase in cytotoxicity, remained significantly less effective.

This result represents the most relevant aspect of the study, as cell mortality is significantly higher when DOX is delivered via BSA nanoparticles compared to free DOX in the presence of collagenases, demonstrating the superior therapeutic efficacy of the nanoparticles. Furthermore, these results confirm that collagenases pretreatment improves drug accessibility to the inner cellular layers of the spheroid and that conjugation of doxorubicin to pH-sensitive BSA NPs further enhances this effect. Therefore, the combined approach of collagenases + BSA-DOX emerges as a more effective strategy compared to free doxorubicin in the three-dimensional PTC spheroid model.

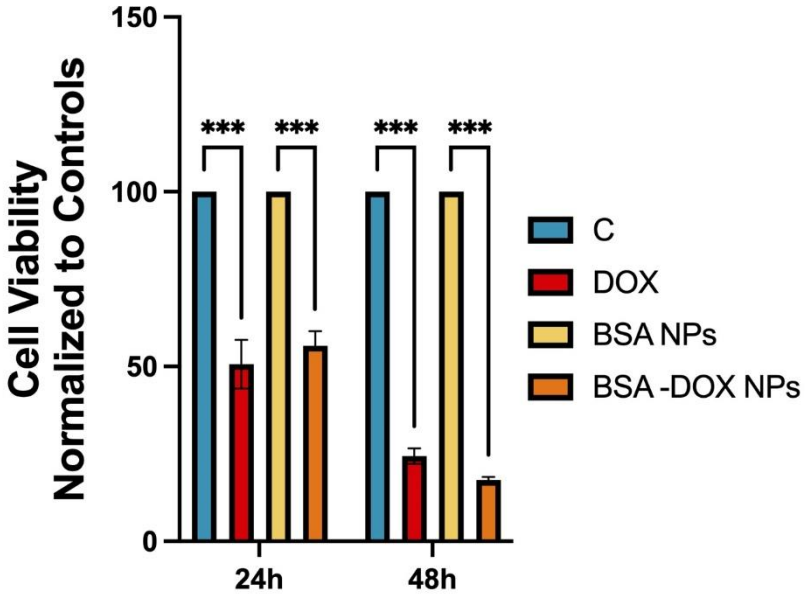

Figure 30: Quantitative analysis of cytotoxicity in PTC spheroids. Graph showing cell viability at 24 h: untreated control (C, orange) and collagenase alone (C + COL, green) do not significantly reduce viability. Treatment with free DOX (red) or BSA-DOX NPs (blue) induces a marked decrease in viability, which is further enhanced when combined with collagenases. The combination of collagenases + BSA-DOX NPs shows the greatest cytotoxic effect, approaching IC_{50} values, highlighting the superior therapeutic efficacy of the nanoparticle-based delivery system. Data are presented as mean ± SD ($n = 3$, $*p < 0.05$, $**p < 0.01$, $***p < 0.001$).

4.3.6 BSA Conjugated with Recombinant Ultrapure Collagenases: SAXS Reveals Compact Conformation of COLH in Solution

The recombinant collagenases Abiel, COLG (Class I), and COLH (Class II) are produced from two distinct genes of *C. histolyticum*, which were cloned to obtain two chimeric forms in *E. coli*. COLG exhibits high collagenolytic activity, specifically hydrolyzing the three-dimensional triple-helix regions of native collagen, whereas COLH shows a more moderate activity toward the collagen triple helix, acting predominantly on linear regions of the molecule.

The advantage of using ultrapure collagenases lies in the possibility of achieving greater experimental reproducibility, as the catalytic activity of the enzymes is precisely known for each batch. Furthermore, the absence of contaminating proteases ensures higher enzymatic specificity and better cell viability. However, a potential limitation of collagenases *in vivo* is due to their bacterial origin, which may induce an important immune response, rapid inactivation, poor biodistribution, and lack of selectivity for tumor tissue [237]. In this context, the use of nanoparticle systems represents a promising strategy to overcome these issues [238]. To improve the immunocompatibility, specificity, and the half-life of the

enzyme, we focused on the synthesis and characterization of BSA-based nanoparticles in which to incorporate the collagenases, starting with BSA-COLH NPs as a model system.

First of all, to gain insight into the solution structure of the recombinant collagenase COLH and to understand its suitability for incorporation into BSA nanoparticles, small-angle X-ray scattering (SAXS) analysis was performed and combined with computational modeling. The Ensemble Optimization Method (EOM) was applied to the set of generated models in order to select sub-ensembles capable of reproducing the experimental SAXS profile as accurately as possible. Through 50 cycles of the genetic algorithm, a sub-ensemble was identified with a χ^2 value of 2,29, indicative of a good fit to the experimental SAXS data (Fig.31A). The radius of gyration (Rg) distribution of the random pool is shown in Figure 31B as black points, while the distribution of the selected pool is represented by the red line. Analysis of the selected sub-ensemble revealed a theoretical radius of gyration of 4,60 nm, in excellent agreement with the Rg value determined by Guinier analysis (4,52 nm).

Comparison of the two distributions highlights that the selected pool exhibits a more compact conformation than expected based on the random pool, suggesting that the protein in solution tends to adopt a globally more compact structure. Consistent with this observation, the most representative structural model shows that the three additional C-terminal domains are spatially close to the main catalytic region of COLH, further contributing to the overall compactness of the protein in solution (Fig.31C).

SAXS and EOM results indicate that COLH adopts a compact conformation in solution, with the C-terminal domains positioned near the catalytic region, making it particularly suitable for integration into BSA protein nanoparticles. Overall, these findings support the structural and physicochemical rationale of the approach adopted for collagenase delivery.

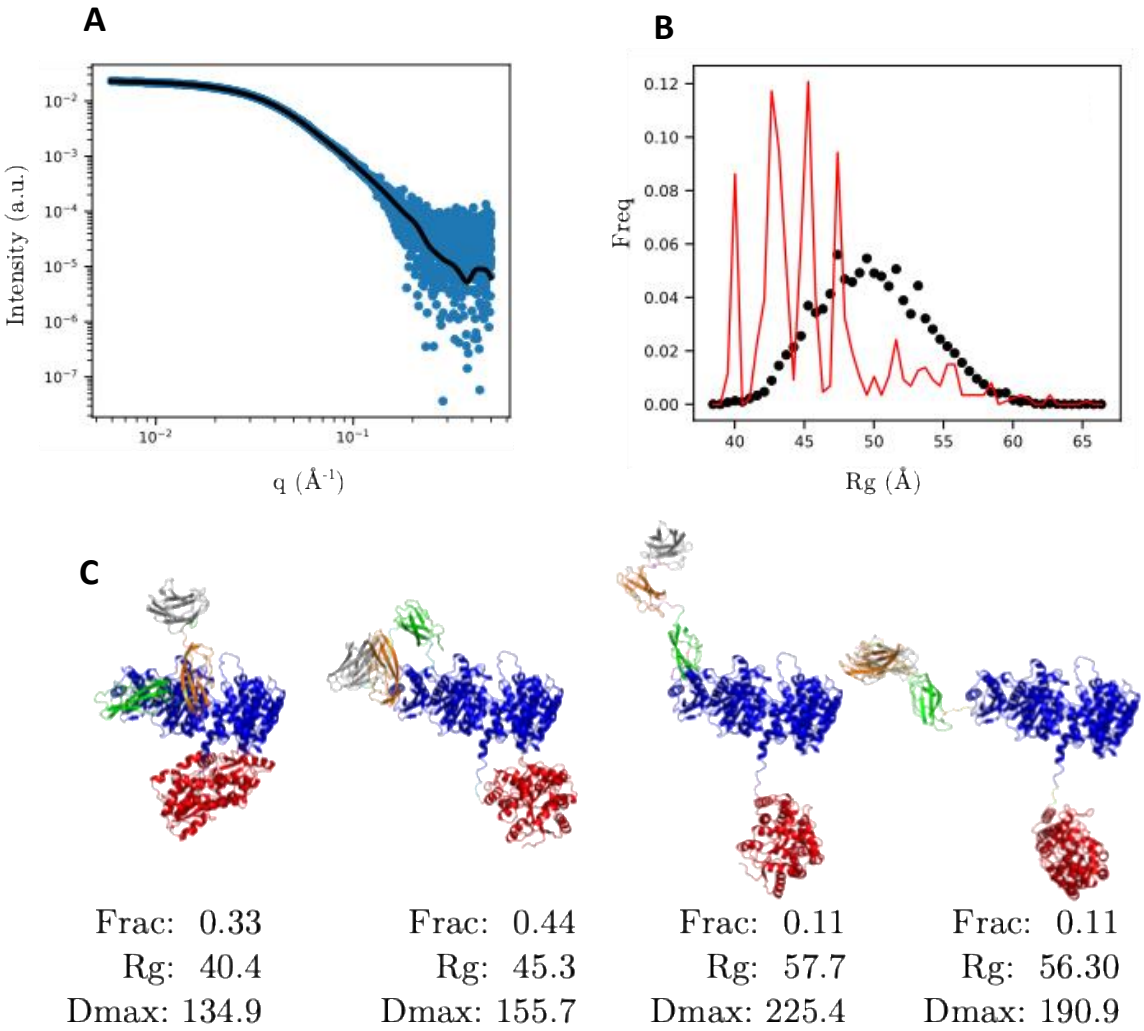

Figure 31: EOM analysis of the ColH form factor. (A) Fit of the sub-ensemble selected by EOM to the SEC-SAXS data. (B) Representation of the selected pool (red dots) compared to the random pool (black dots). (C) Representative conformations selected by EOM and their corresponding sizes as radius of gyration and dmax (both in angstrom).

4.3.7 Glutaraldehyde-Mediated Crosslinking of BSA Nanoparticles Conjugated with Collagenases

The next part of the work was dedicated to the development of BSA nanoparticles conjugated with ultrapure recombinant collagenases designed to promote the digestion of the tumor ECM. The BSA-COL NPs were synthesized using the same desolvation and chemical crosslinking protocol with glutaraldehyde, with a BSA: enzyme ratio of 9:1 (Fig.32A).

The morphology of the BSA-COLH NPs was initially analyzed by TEM to evaluate the shape and size distribution of the nanoparticles. TEM images showed spherical, well-defined, and uniformly distributed nanoparticles with an average diameter of approximately 106.3 nm (Fig.32B).

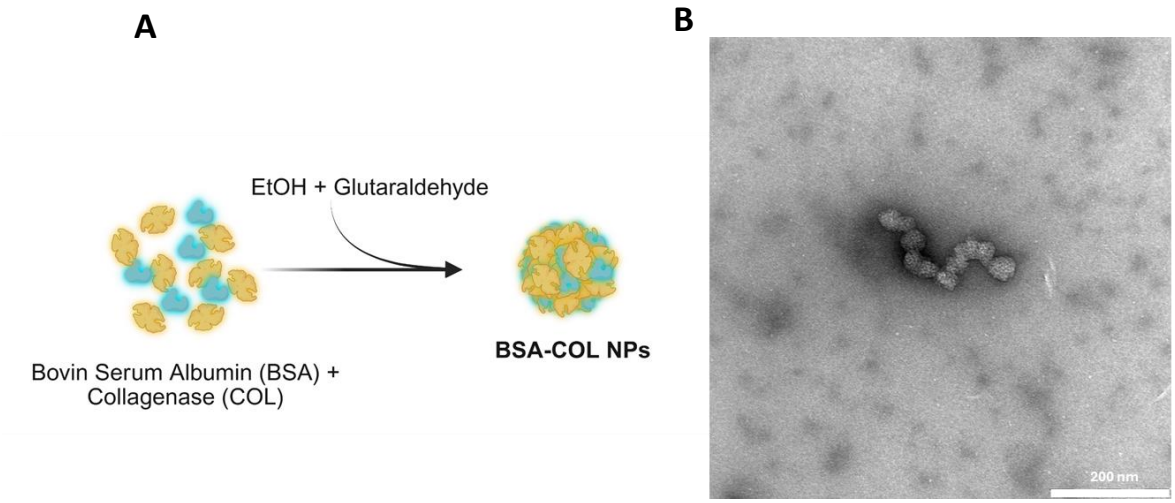

Figure 32: Synthesis and Characterization of BSA-COLH Nanoparticles through glutaraldehyde crosslinking. (A) Schematic representation of the synthesis process. (B) TEM image showing the spherical NPs morphology.

Subsequently, the nanoparticles were characterized by DLS to obtain information on the size profile in solution and the polydispersity index. DLS data, normalized for volume, revealed an average hydrodynamic size of 115 d.nm, with a particularly homogeneous distribution (PDI = 0,16), indicating that collagenase conjugation does not compromise the colloidal stability of the system. Next, it was evaluated whether the nanoparticle synthesis process had altered the catalytic activity of the enzyme. For this purpose, the solution containing the nanoparticles was spotted directly onto zymography gels, and the ability of the conjugated enzyme to digest gelatin was qualitatively analyzed, compared to the positive control given by free collagenase. BSA NPs not conjugated with the enzyme were used as a negative control. As observed, the enzyme-conjugated nanoparticles did not show any catalytic activity. In contrast, the free enzyme clearly exhibited its function (Fig.33).

These results suggest that the conjugation process, carried out via glutaraldehyde, compromises enzymatic activity. Likely, the formation of the rigid chemical bond introduced by the crosslinker interferes with the enzyme's active site, preventing proper function. Consequently, the nanoparticles are unable to replicate the activity observed with the free enzyme, indicating an inhibitory effect of the conjugation.

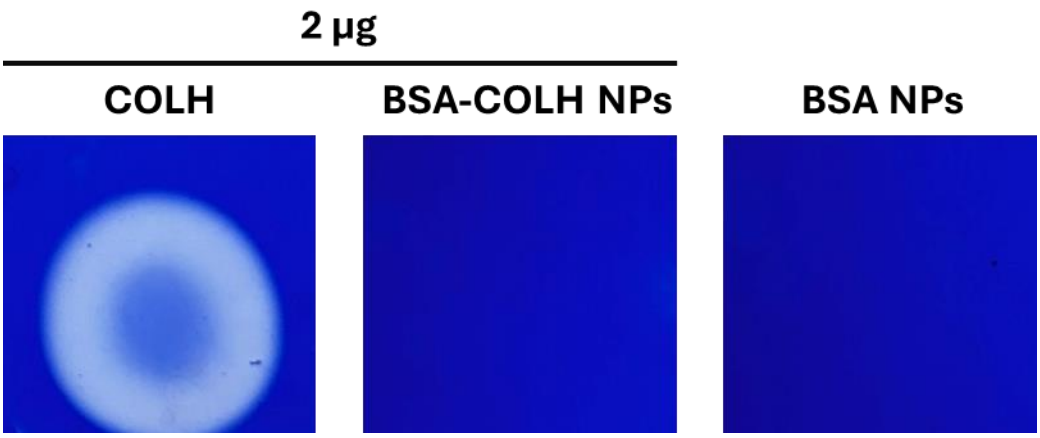

Figure 33: Qualitative analysis of enzymatic activity by spotting zymography. No activity was observed for BSA-COLH NPs compared to free COLH, indicating that the enzyme was likely inactivated during the nanoparticle synthesis process.

4.3.8 Thermal Crosslinking as an Alternative Strategy to Preserve Collagenase Activity in BSA Nanoparticles

The previous result highlighted the need to develop an alternative approach capable of stabilizing the nanoparticles without compromising collagenases' activity. In the literature, several studies report that BSA NPs can be effectively stabilized through high-temperature thermal crosslinking, avoiding the use of potentially denaturing chemical agents such as glutaraldehyde [239].

Following this principle, the synthesis protocol was modified by introducing a thermal treatment. Specifically, the nanoparticles were prepared using the traditional desolvation and resolvation steps, followed by incubation at 65°C, promoting the formation of stable intermolecular bonds within the protein system without the need for chemical solvents (Fig. 34A).

The process was initially tested on control BSA NPs, without the enzyme, to evaluate the effectiveness of thermal stabilization and to determine potential morphological and dimensional changes. The resulting BSA NPs were characterized by TEM, which confirmed their spherical morphology and uniform size distribution, with an average diameter of approximately 101 d.nm (Fig. 34B).

Subsequently, DLS analysis showed an average volume-based size of 129,8 nm, indicating a slight difference compared to the TEM measurements, likely due to the hydrated nature of the particles in solution. NTA further confirmed these characteristics, reporting an average size of 88.9 nm and a concentration of $5{,}14 \times 10^{7} \pm 5{,}75 \times 10^{6}$ particles/mL.

These results demonstrate that thermal crosslinking allows the production of stable, spherical, and uniform nanoparticles with controlled sizes, providing a solid platform for collagenase incorporation. At this point, the nanoparticles are ready for the subsequent enzymatic conjugation step, with the prospect of preserving at least partial catalytic activity of the enzyme, thus overcoming the limitations observed with the previous protocol.

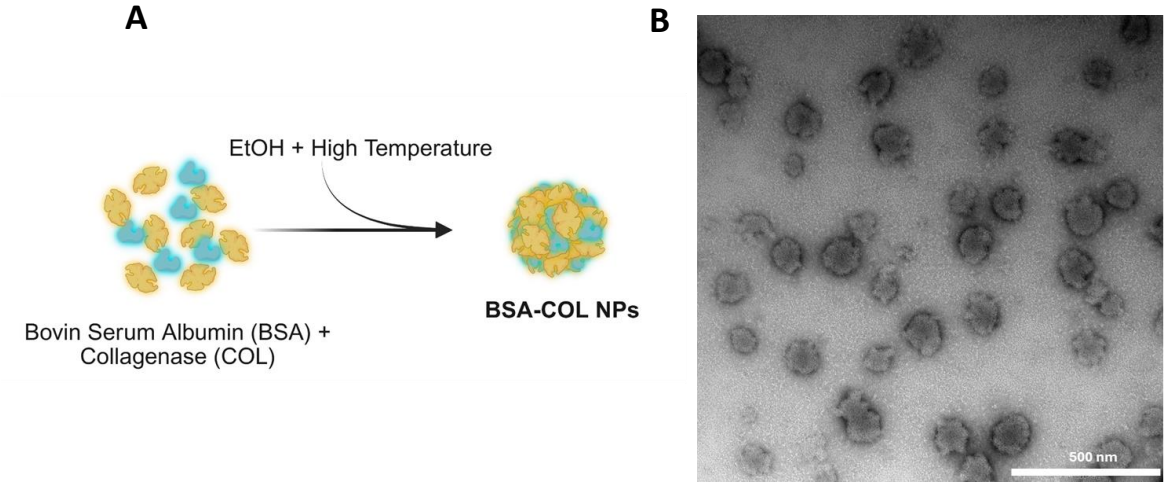

Figure 34: Synthesis and Characterization of BSA Nanoparticles via Thermal Crosslinking. (A) Illustration of the nanoparticle preparation process. (B) TEM image revealing that the thermally crosslinked BSA-nanoparticles are well-defined and predominantly spherical, with a uniform size distribution.

4.3.9 Morphological, Physicochemical, and Biochemical Characterization of BSA-COLH and BSA-COLG Nanoparticles Prepared via Thermal Crosslinking

BSA nanoparticles were synthesized through thermal crosslinking while separately incorporating the two recombinant collagenases, namely COLH and COLG, obtaining the BSA-COLH NPs and BSA-COLG NPs, respectively. The choice to prepare two separate systems allowed for more precise control of their different catalytic activities and specificities both *in vitro* and *in vivo*, facilitating the comparative evaluation of functional performance.

Morphological and dimensional characterization was performed using TEM, DLS, and NTA. TEM revealed that the particles were approximately spherical and not perfectly uniform as the controls, with an average diameter of 80 nm for the BSA-COLH NPs (Fig. 35A) and 91 nm for the BSA-COLG NPs (Fig. 35B). However, unlike the control NPs, the surfaces of the collagenase-containing particles appeared irregular and slightly granular, suggesting a possible interaction between the protein matrix and the enzyme.

DLS analysis showed volume-based average sizes of 131 nm for the BSA-COLH NPs and 128 nm for the BSA-COLG NPs, with a PDI below 0.2 in both cases. Finally, NTA reported average sizes of 90 nm for the BSA-COLH NPs and 89 nm for the BSA-COLG NPs, with concentrations of $4{,}9 \times 10^7 \pm 5.2 \times 10^6$ particles/mL and $5{,}1 \times 10^7 \pm 5{,}7 \times 10^6$ particles/mL. All values are reported.

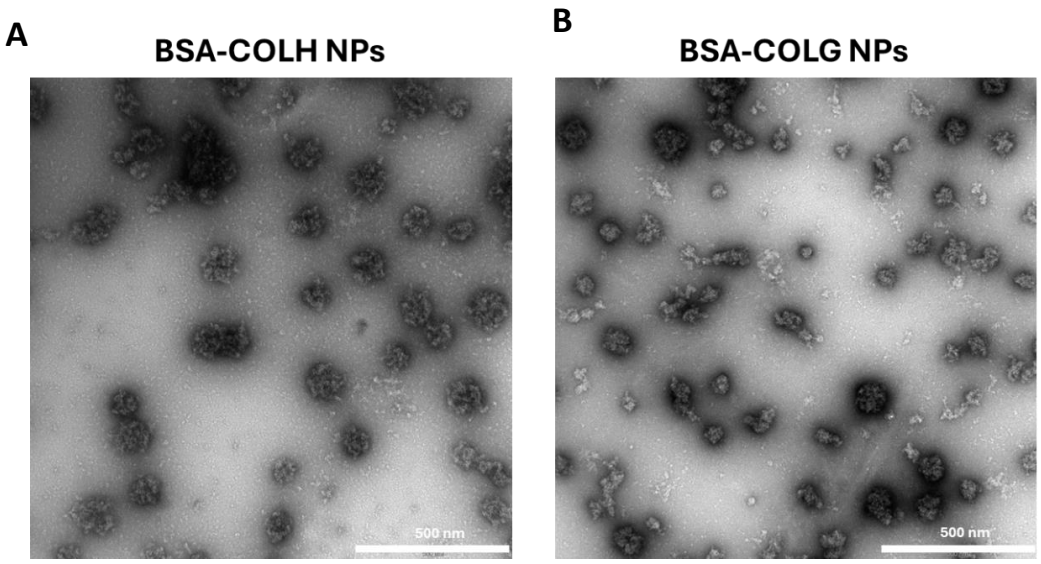

Figure 35: TEM analysis of BSA-COL nanoparticles. (A) BSA-COLH NPs and (B) BSA-COLG NPs. Both nanoparticle types show relatively uniform size distribution, particularly the BSA-COLH NPs. Although the particles are not perfectly spherical, exhibit a granular surface, suggesting possible interactions between the protein matrix and the incorporated enzyme.

To verify enzymatic activity after synthesis, a zymography assay was performed for both nanoparticles. The results showed the presence of a degradation halo in both cases, indicating that the collagenase remained partially active, albeit with reduced activity compared to the free enzymes (Fig. 36). This confirms that thermal crosslinking allows the catalytic function of both constructs to be at least partially preserved, providing a stable platform for future studies and for applications where controlled degradation is required. Notably, this innovative approach could be extended to the conjugation of other proteins, as thermal crosslinking may represent a general strategy to preserve protein structure and functionality while enabling their incorporation into nanoparticulate systems.

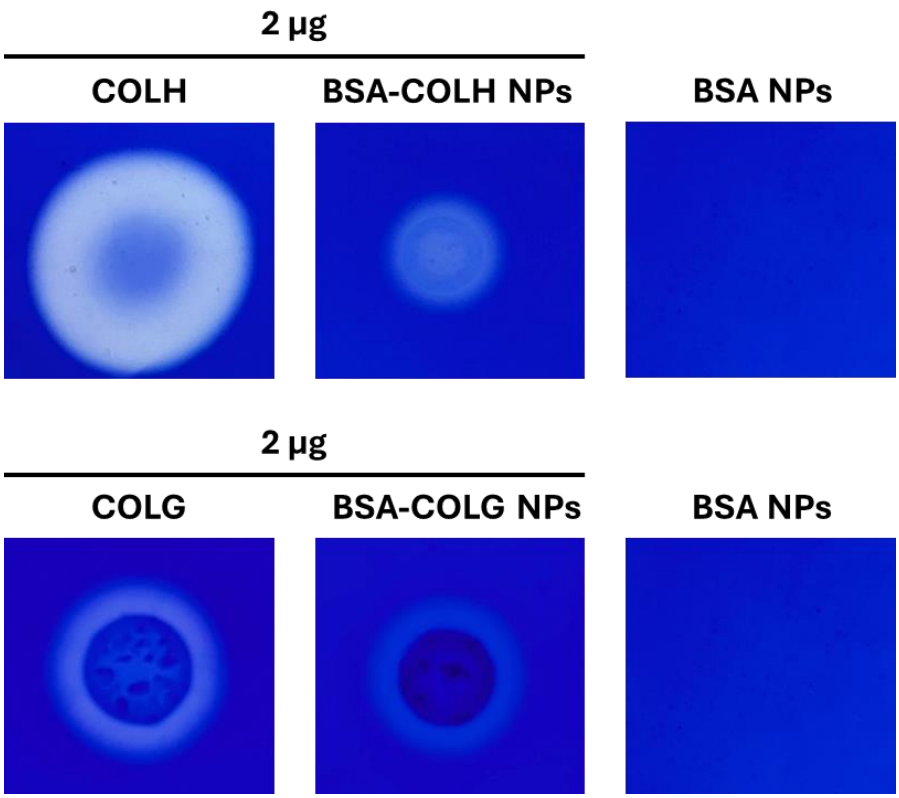

Figure 36: Qualitative analysis of enzymatic activity by spotting zymography. (A) BSA-COLH NPs and (B) BSA-COLG NPs. Both nanoparticle formulations display gelatin degradation, as evidenced by the presence of a digestion halo, indicating that the collagenases retain partial enzymatic activity after incorporation. However, their activity is reduced compared to the free enzyme controls.

4.4 Development and Characterization of 3D Vascularized Tumor Model Integrating Rat Adipose-Derived Microvascular Fragments and Breast Cancer Cells: Evaluation of ABCB1 Expression and Drug Response

4.4.1 Isolation of Adipose-Derived Microvascular Fragments from Rat

Although the model composed of PTCs provides a valuable platform for studying tumor cell behavior and NPs efficacy, it lacks the critical vascular compartment that characterizes solid tumors, limiting its ability to fully replicate the tumor microenvironment and associated physiological processes. This complexity arises from the tumor microenvironment being a highly intricate network, comprising not only malignant cells, but also various stromal components, immune cells, fibroblasts, and a dense ECM. Among these, the vascular system plays a central role in supporting tumor growth and progression by delivering oxygen and nutrients, removing waste products, and positively influencing metastasis [240]. Modeling of tumor vasculature is therefore essential for *in vitro* studies aiming to recapitulate *in vivo* tumor pathophysiology. Traditional 3D tumor models often

incorporate endothelial cells, such as Human Umbilical Vein Endothelial Cells (HUVECs), to recreate vascular networks. However, these systems are limited in their physiological relevance because HUVECs fail to fully replicate the structural and functional complexity of native vasculature, lacking essential accessory cells, such as pericytes [241,242]. In contrast, adipose-derived Microvascular Fragments (MVFs) preserve the full architecture of functional microvessels, including pericytes and small branches [219].

For this reason, in order to generate a 3D tumor model that better mimicked the tumor microenvironment *in vitro* and, in particular, the tumor-associated vascular system, PTCs derived from rat mammary tumors were co-cultured with species-specific MVFs isolated from the visceral adipose tissue of female Wistar rats (Fig.37).

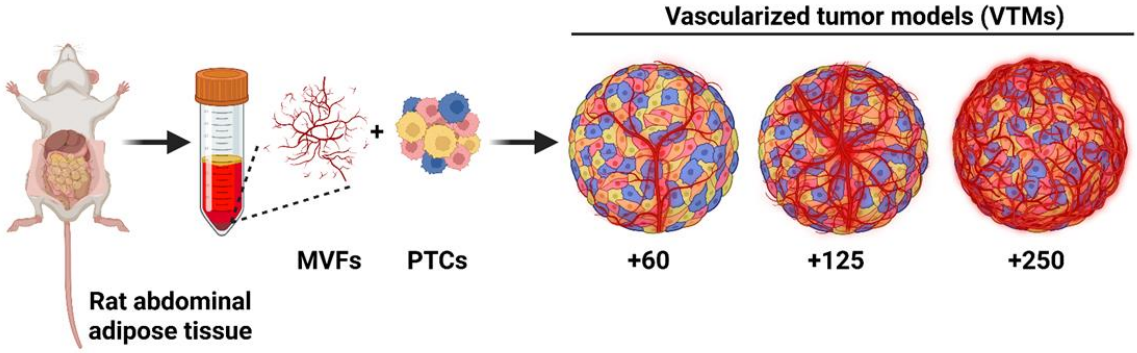

Figure 37: Illustration of the Isolation Process of Microvascular Fragments (MVFs) from Rat Adipose Tissue and Generation of Angiotumoroids in Combination with PTCs.

Tissue digestion was performed using a combination of enzymes, such as ultrapure recombinant collagenase (COLH – Class II) and thermolysin [219]. Following digestion, an average yield of about 2×10^4 microvascular fragments was recovered from each gram of adipose tissue. As observed by optical microscopy (Fig.38A), the MVFs had a length ranging from 50 µm to 300 µm, displaying a mean luminal diameter of approximately 18 µm, and exhibited small lateral branches. Within the vessel lumen, traces of blood residual from the digestion were present (Fig.38B). Accurate visualization and analysis of the morphology of the extracted MVFs were obtained via Scanning Electron Microscopy (SEM) (Fig.38C). The images obtained showed the typical tubular architecture of the MVFs, with no detectable adipocytes present, demonstrating the isolation procedure efficiency. Furthermore, the presence of some erythrocytes adhered to the vessel surface was noted, which were certainly also residues of the digestion process. Notoriously, the vascular apparatus, regardless of tissue type, requires the biomechanical support of a three-

dimensional collagen-based matrix for proper vessel assembly and to fully unleash its angiogenic potential, in terms of sprouting and branching [243].

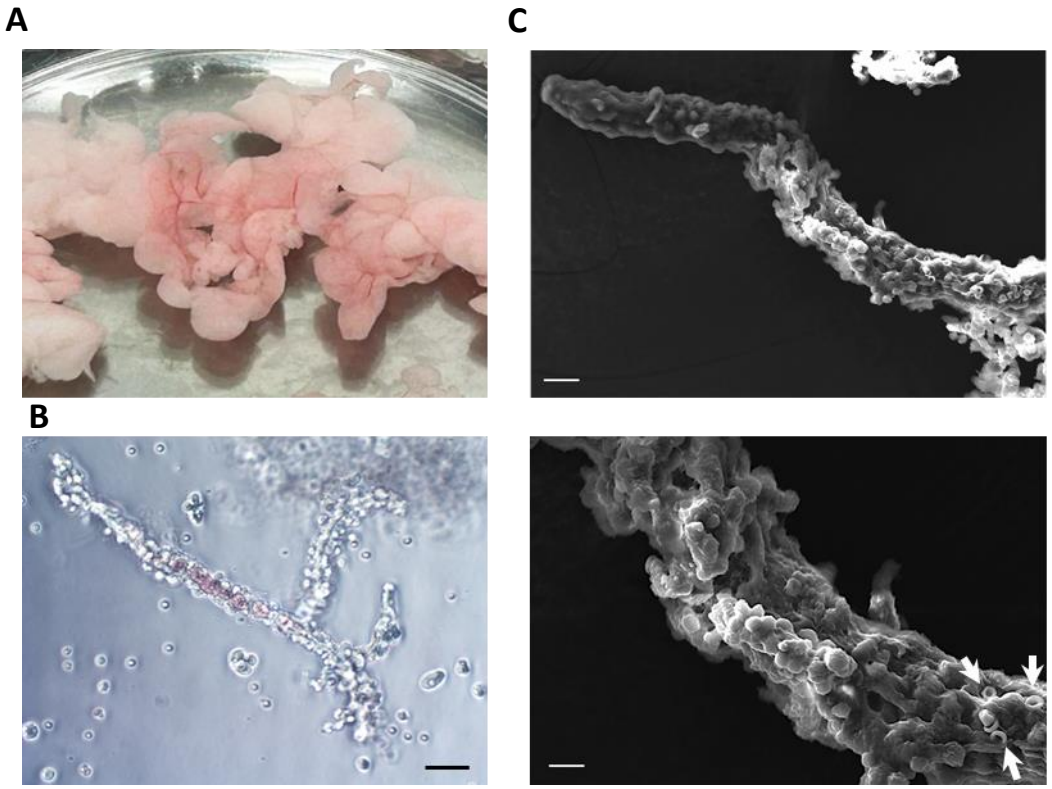

Figure 38: Isolation of adipose-derived microvascular fragments. (A) Rat visceral adipose tissue. (B) Morphological characterization of MVFs by optical microscopy. It's possible to observe blood residual in the vessel lumen. (C) Scanning electron microscopy (SEM) of MVFs.Arrows highlight the presence of erythrocytes in the MVFs surface. Scale bars: 20 µm,10 µm and 5 µm.

Image adapted from Lo Cicero et al: '*Vascularized Three-Dimensional Model Integrating Primary Breast Tumor Cells and Microvascular Fragments: Mimicking the Tumor Microenvironment Involved in Chemoresistance' Cancer Cell Int.* 2026, doi: 10.1186/s12935-025-04154-6 [2]. Copyright via CC BY-NC-ND 4.0 - https://creativecommons.org/licenses/by/4.0/

To evaluate the neoangiogenic potential over time, the MVFs were incorporated into a type I collagen gel matrix and allowed to grow for seven days, already showing sprouting and vascular branching from individual fragments after three days, which progressively increased over time. By day 7, some lateral branches originating from different MVFs fused, a canonical feature in the processes of new vessel formation in tissues (Fig.39).

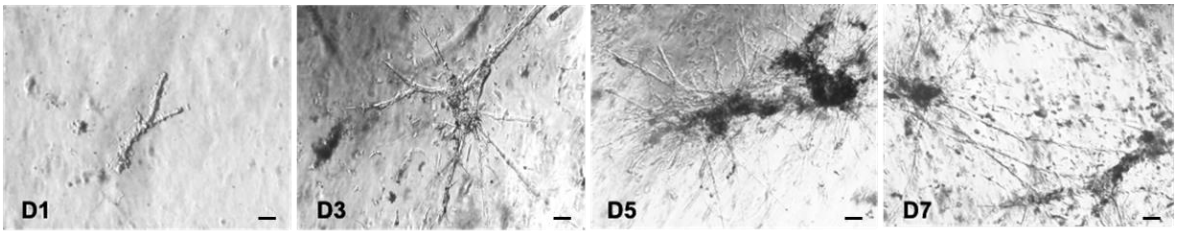

Figure 39: Microvascular fragments MVFs embedded in type I collagen gel at different time points. Optical images of MVFs cultured in type I collagen at day 1 (D1), day 3 (D3), day 5 (D5), and day 7 (D7). The images show a time-dependent increase in MVF sprouting. Scale bar: 10 µm.

Image adapted from Lo Cicero et al: '*Vascularized Three-Dimensional Model Integrating Primary Breast Tumor Cells and Microvascular Fragments: Mimicking the Tumor Microenvironment Involved in Chemoresistance' Cancer Cell Int.* 2026, doi: 10.1186/s12935-025-04154-6 [2]. Copyright via CC BY-NC-ND 4.0 - https://creativecommons.org/licenses/by/4.0/

4.4.2 3D Co-Culture of Species-specific MVFs together with PTCs, in Generation of Angiotumoroids.

Once the proliferative capacity of the extracted vessels was confirmed, PTCs were co-cultured with the MVFs under low-adhesion conditions to generate 3D vascular models, which were named 'angiotumoroids.' These models were prepared with a variable number of MVFs (60, 125, or 250 per condition), while keeping the number of PTCs constant (3×10^3 cells/well) (Fig.40A).

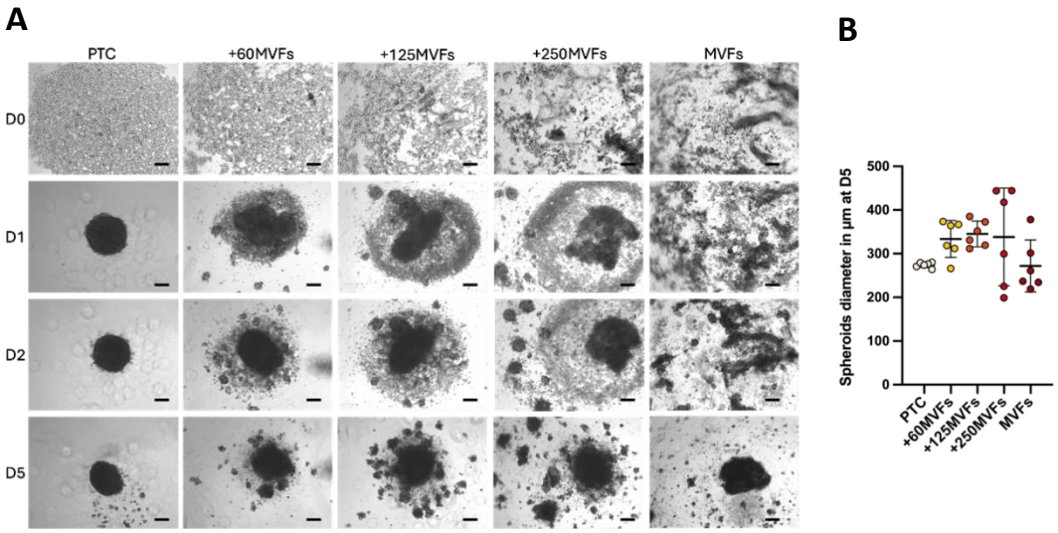

Figure 40: Optical microscopy images of PTCs cocultured with MVFs. (A) Angiotumoroids generated by co-culture with increasing numbers of microvascular fragments (60, 125, or 250 MVFs), PTC spheroids and MVF-only spheroids, monitored at day 0 (D0), day 1 (D1), day 2 (D2), and day 5 (D5). Scale bar: 100 µm. (B) Quantitative analysis of spheroid diameter measured at day 5 (n=6). Results are expressed as mean ± SD.

Image adapted from Lo Cicero et al: '*Vascularized Three-Dimensional Model Integrating Primary Breast Tumor Cells and Microvascular Fragments: Mimicking the Tumor Microenvironment Involved in Chemoresistance' Cancer Cell Int.* 2026, doi: 10.1186/s12935-025-04154-6 [2]. Copyright via CC BY-NC-ND 4.0 - https://creativecommons.org/licenses/by/4.0/

In addition, spheroids composed of PTCs alone or MVFs alone were generated as controls. The inclusion of these controls allowed the specific and independent contribution of each cellular component in the generated models to be evaluated across various assays. Quantitative analysis of spheroid diameter was performed (Fig. 27B). The angiotumoroids and controls were allowed to grow for 5 days, with changes in size, morphology, and spheroid compaction monitored over time. As can be observed from the optical microscopy images, PTC spheroids compacted within 24 hours, maintaining their spherical and compact structure over the following days. Angiotumoroids containing 60 and 125 MVFs also formed by day 1, with progressive compaction, while spheroids with 250 MVFs required an additional 24 hours to achieve a compact structure. As expected, by day 5 post-seeding, the angiotumoroids were larger than the controls composed only of tumor cells. However, co-cultures with 250 MVFs displayed greater size heterogeneity (200–445 µm) compared to those with 125 and 60 MVFs, as shown in the graph. Furthermore, in all co-cultures, small satellite structures were observed around the main spheroid, sequestering part of the cells from the central mass. In angiotumoroids containing 250 MVFs, these

aggregates were more numerous and larger than in the other groups. Finally, spheroids composed of only microvessels required five days to reach compact and spherical structures. For this reason, the data indicate that the presence of tumor cells with an epithelioid phenotype plays a decisive role in the compaction of the 3D model, highlighting the structural synergy established among the various components of a microenvironment and how the quantitative balance between them is fundamental in the formation of a tumor tissue.

4.4.3 Scanning Electron Microscopy (SEM) Analysis of Angiotumoroids

For a more detailed study of the morphology and structural compaction of the different models, images of the various models acquired by Scanning Electron Microscopy (SEM) were analyzed (Fig.41). SEM analysis on day 5 revealed a compact ovoid morphology for PTC spheroids and for angiotumoroids with 60 or 125 MVFs, whereas angiotumoroids with 250 MVFs showed poorly integrated surface cells, indicating reduced structural compaction. Spheroids composed solely of MVFs also exhibited overall compactness, although greater than that observed in the co-cultures with 250 microvessels.

Thus, the acquired images once again suggest that, to obtain a reliable and reproducible model that mimics the tumor microenvironment, it is necessary to quantitatively balance tumor cells and microvessels within the spheroids.

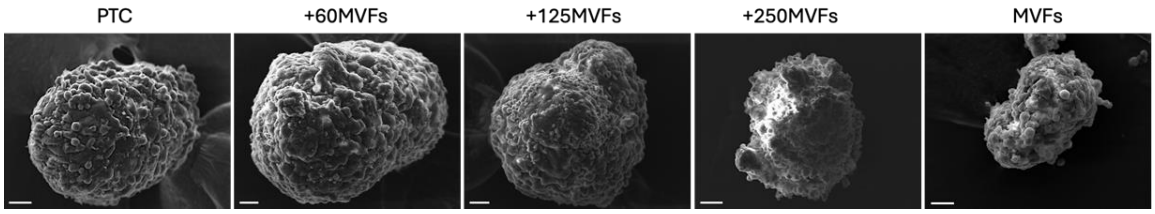

Figure 41: Scanning electron microscopy (SEM) images. Spheroids at day 5 of culture highlight surface morphology and structural organization. Scale bar: 30 µm.

Image adapted from Lo Cicero et al: '*Vascularized Three-Dimensional Model Integrating Primary Breast Tumor Cells and Microvascular Fragments: Mimicking the Tumor Microenvironment Involved in Chemoresistance' Cancer Cell Int.* 2026, doi: 10.1186/s12935-025-04154-6 [2]. Copyright via CC BY-NC-ND 4.0 - https://creativecommons.org/licenses/by/4.0/

4.4.4 MVF Integration and Disposition Detected by CD31

The data obtained through both optical and electron microscopy provided a fundamental contribution to visualizing the morphology of the various models under study. However, it was not clearly possible to visualize the presence of vascular networks within the different

3D models. Therefore, to evaluate the incorporation and distribution of MVFs, immunostaining of the spheroids was performed 5 days post-seeding using the vascular endothelial marker Platelet Endothelial Cell Adhesion Molecule-1 (PECAM-1 or CD31) [244], phenotypically characterizing proliferating and quiescent endothelial cells (Fig.42A). Images obtained via confocal microscopy showed that CD31 (in red) was homogeneously expressed in MVF spheroids and in the angiotumoroids.

Interestingly, in spheroids with 125 MVFs, a well-defined and distributed vascular network was clearly formed (Fig.42B). As expected, no signal was detected in the PTC-only control spheroids.

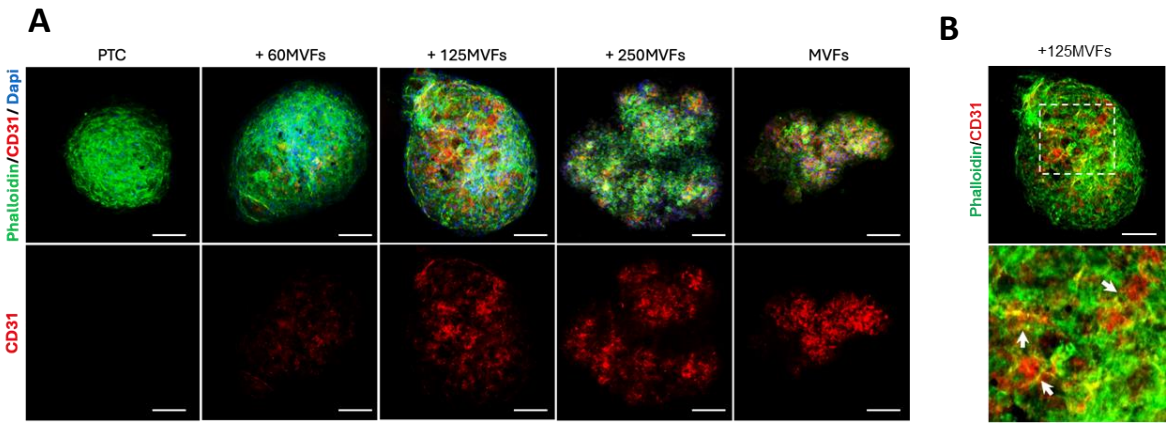

Figure 42: Integration of microvascular fragments within angiotumoroids. (A) Confocal microscopy images of PTC spheroids, angiotumoroids containing 60 (+60 MVFs), 125 (+125 MVFs), or 250 (+250 MVFs), and MVF-only spheroids, at day 5 of seeding. Samples were stained with phalloidin–FITC (green) to label the actin, anti-CD31 antibody (red) to identify endothelial structures, and DAPI (blue) to visualize nuclei. (B) Representative central optical section obtained by confocal microscopy of angiotumoroids containing 125 MVFs. CD31 staining (red) highlights the formation of vessel-like vascular structures within the construct (white arrows), indicating the organization of endothelial cells into microvascular networks. Scale bar: 100 µm.

Image adapted from Lo Cicero et al: '*Vascularized Three-Dimensional Model Integrating Primary Breast Tumor Cells and Microvascular Fragments: Mimicking the Tumor Microenvironment Involved in Chemoresistance' Cancer Cell Int.* 2026, doi: 10.1186/s12935-025-04154-6 [2]. Copyright via CC BY-NC-ND 4.0 - https://creativecommons.org/licenses/by/4.0/

Thus, CD31 expression in the angiotumoroids progressively increased with the density of seeded MVFs, in agreement with Western blot data showing a density-dependent increase in CD31 levels (Fig.43). These images demonstrated effective and proportional integration of MVFs in the 3D co-cultures.

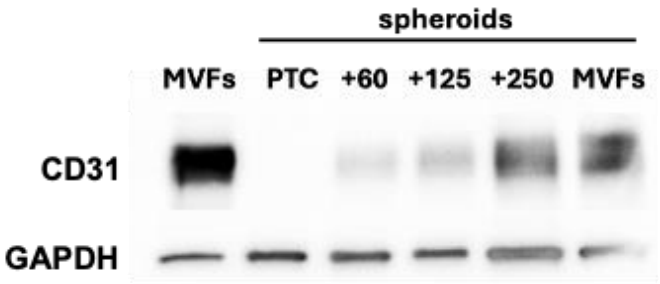

Figure 43: Western blot analysis to detect for CD31. GADPH was used as control.

Image adapted from Lo Cicero et al: '*Vascularized Three-Dimensional Model Integrating Primary Breast Tumor Cells and Microvascular Fragments: Mimicking the Tumor Microenvironment Involved in Chemoresistance' Cancer Cell Int.* 2026, doi: 10.1186/s12935-025-04154-6 [2]. Copyright via CC BY-NC-ND 4.0 - https://creativecommons.org/licenses/by/4.0/

4.4.5 Quantification of Matrix Metalloproteases (MMPs) in Angiotumoroids

Matrix metalloproteinases (MMPs) play a central role in angiogenesis. They degrade the ECM, allowing endothelial cell migration. This remodeling, in which MMP9 and MMP2 are particularly involved, is essential for the formation of new vessels and capillary networks [245,246]. However, few published studies have evaluated MMP expression in 3D *in vitro* models, and the existing ones have been limited to homotypic tumor spheroids, without recreating a complex microenvironment that includes key components such as the vascular compartment [247]. Considering the role of MMPs in angiogenesis, zymography assays were performed to analyze total protein extracts from angiotumoroids and control spheroids. Subsequently, MMP activity levels were quantified and reported, comparing the activities of MMPs in the different models to those detected in PTC-only spheroids (Fig.44).

Zymography analysis showed that the activity of the multimeric enzymatic complex was higher in angiotumoroids with 250 MVFs and in MVF-only spheroids compared to PTC control spheroids, although no statistical significance was observed. In contrast, pro-MMP9 activity was significantly higher in angiotumoroids containing 125 and 250 MVFs, as well as in spheroids composed solely of MVFs, compared to PTC spheroids, which exhibited approximately threefold lower catalytic activity, whereas no significant differences were found in angiotumoroids with 60 MVFs. Similar to the pro form, the active form of MMP9 was overexpressed in angiotumoroids with 125 and 250 MVFs compared not only with PTC spheroids, suggesting that crosstalk between the two components synergistically promotes MMP9 expression.. The described results reflect a

known behavior of tumor cells, which, through factors such as the tyrosine kinase VEGFR-1 (Flt-1), stimulate the overexpression of MMP9 in endothelial cells, establishing a biochemical crosstalk favorable to tumor progression and metastasis [248]. The activity of both the pro- and active forms of MMP2 did not show significant differences among all spheroid models. In summary, it was demonstrated that the quantity of MVFs in angiotumoroids modulates MMPs activity, particularly affecting MMP9, known for its involvement in tumor-associated neoangiogenic processes.

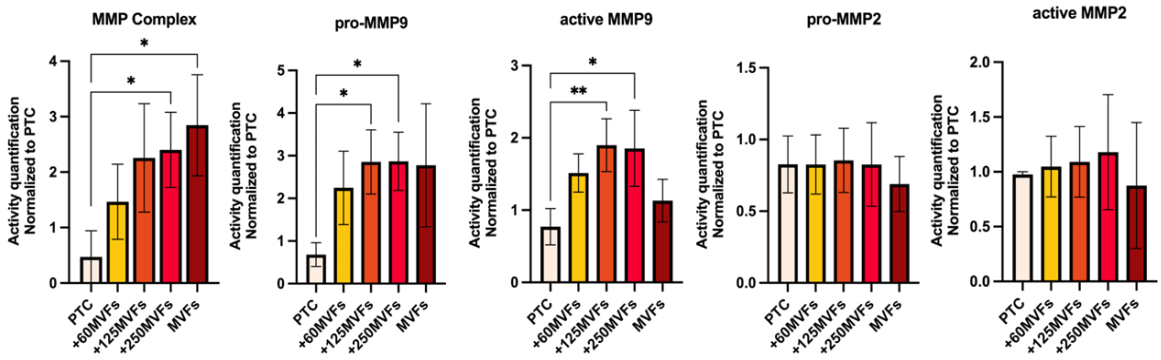

Figure 44: Quantification of zymography assay of protein extracts from PTC spheroids, angiotumoroids containing 60 (+60 MVFs), 125 (+125 MVFs), or 250 (+250 MVFs) MVFs, and MVF-only spheroids. Quantitative analysis of gelatinolytic activity is shown for the following matrix metalloproteases (MMPs): MMP complex (A); pro-MMP9 (B); active MMP9 (C); pro-MMP2 (D); and active MMP2 (E). Data are presented as mean ± SD. Statistical significance was determined using one-way ANOVA (n = 3; *p < 0.05, **p < 0.01).

Image adapted from Lo Cicero et al: '*Vascularized Three-Dimensional Model Integrating Primary Breast Tumor Cells and Microvascular Fragments: Mimicking the Tumor Microenvironment Involved in Chemoresistance' Cancer Cell Int.* 2026, doi: 10.1186/s12935-025-04154-6 [2]. Copyright via CC BY-NC-ND 4.0 - https://creativecommons.org/licenses/by/4.0/

4.4.6 Angiotumoroid Sprouting in Collagen Gel

Since proliferative activity had previously been observed in MVFs incorporated alone in collagen gel, it was evaluated whether vessels within the co-cultures retained the same behavior. For this reason, angiotumoroids and controls matured for 5 days were embedded in a 3D collagen gel, and vessel formation was monitored via optical microscopy during the 48 hours following embedding (Fig.45A).

In the two days after embedding, no vessel formation was observed in PTC-only spheroids, which progressively became less compact as cells migrated into the surrounding matrix. It is well known that tumor cells composing a spheroid, when incorporated into a collagen matrix, do not remain confined within the 3D structure but progressively migrate into the surrounding matrix [249].

In contrast, MVF-only spheroids and angiotumoroids containing 60 or 125 MVFs exhibited visible sprouts after two days of incubation in the gel. However, angiotumoroids with 60–125 MVFs generated more extensive branching and a higher number of sprouts compared to MVF-only spheroids, suggesting that crosstalk between PTCs and MVFs promotes *in vitro* neoangiogenesis (Fig.45B). Unlike the other two co-cultures, angiotumoroids with 250 MVFs showed reduced compactness, with cells migrating out of the spheroids similar to the control and minimal formation of vascular branches.

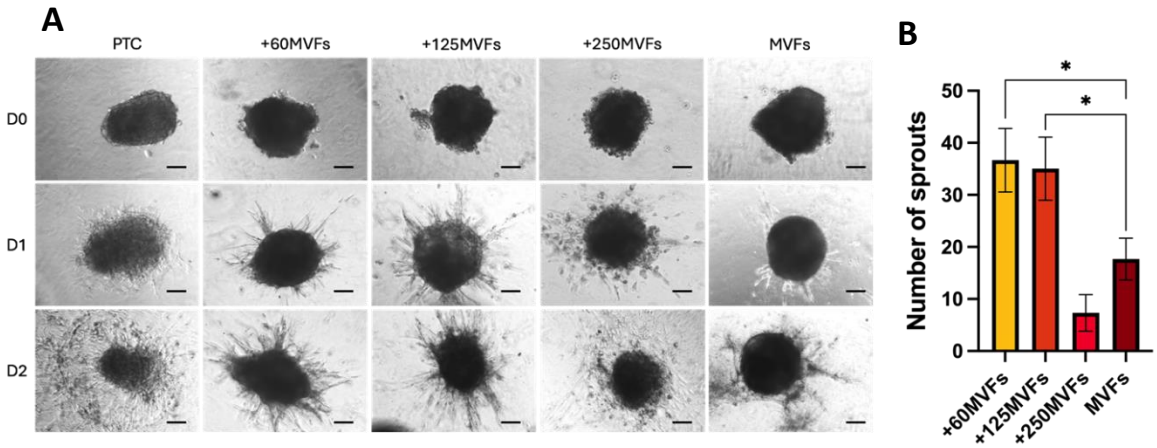

Figure 45: Angiotumoroid sprouting in collagen gel. (A) PTC spheroids, angiotumoroids containing 60 (+60 MVFs), 125 (+125 MVFs), or 250 (+250 MVFs) MVFs, and MVF-only spheroids embedded in collagen gel at day 0 (D0), day 1 (D1), and day 2 (D2). Scale bar: 100 µm. (B) Quantification of the number of sprouts at D2. Data are presented as mean ± SD. Statistical analysis was performed using two-way ANOVA ($n = 3$; $p < 0.05$).

Image adapted from Lo Cicero et al: '*Vascularized Three-Dimensional Model Integrating Primary Breast Tumor Cells and Microvascular Fragments: Mimicking the Tumor Microenvironment Involved in Chemoresistance' Cancer Cell Int.* 2026, doi: 10.1186/s12935-025-04154-6 [2]. Copyright via CC BY-NC-ND 4.0 - https://creativecommons.org/licenses/by/4.0/

Therefore, despite high levels of active MMP9 in both 125- and 250-MVF angiotumoroids, only spheroids with 125 MVFs exhibited effective sprouting and branching.

Furthermore, when two angiotumoroids with 125 MVFs were cultured in the same collagen gel, connections between the vessels of adjacent spheroids within two days were observed, demonstrating the ability to form a coordinated communication network (Fig.46).

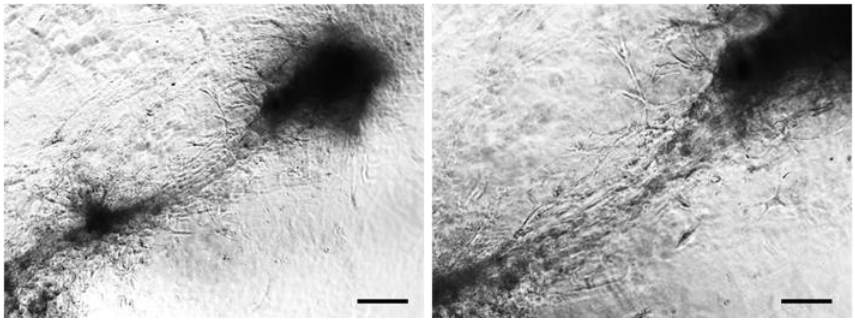

Figure 46: Angiotumoroids containing 125 MVFs (+125 MVFs) forming interconnections within collagen gel. Scale bars: 50 µm and 25 µm.

Image adapted from Lo Cicero et al: '*Vascularized Three-Dimensional Model Integrating Primary Breast Tumor Cells and Microvascular Fragments: Mimicking the Tumor Microenvironment Involved in Chemoresistance' Cancer Cell Int.* 2026, doi: 10.1186/s12935-025-04154-6 [2]. Copyright via CC BY-NC-ND 4.0 - https://creativecommons.org/licenses/by/4.0/

The sprouting in gels was further assessed by CD31 staining (Fig.47). Fluorescence microscopy confirmed the absence of a CD31 signal in PTC spheroids, while in angiotumoroids, the new vessels showed positive signals for CD31. However, even in this case, angiotumoroids with 250 MVFs did not show evident sprouting, but single endothelial cells coming out into the collagen matrix, confirming their reduced neoangiogenic potential compared to the other two models. These findings suggest that angiotumoroids with 60 and 125 MVFs serve as more reliable models for accurately mimicking the neoangiogenic process *in vitro* over time.

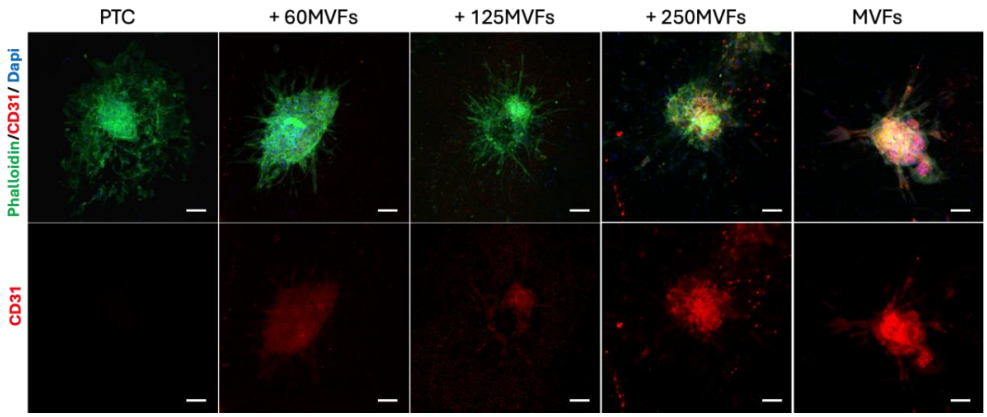

Figure 47: Integration of MVFs into Angiotumoroids Embedded in Collagen Gel. Confocal microscopy of PTC spheroids, angiotumoroids with 60 (+60 MVFs), 125 (+125 MVFs), or 250 (+250 MVFs) MVFs, and MVF-only spheroids embedded in collagen gel, stained with phalloidin-FITC (green), anti-CD31 antibody (red), and DAPI (blue). Scale bar: 100 µm.

4.4.7 PTC Influence on Neoangiogenesis

Several studies have demonstrated that tumor cells actively contribute to neoangiogenesis through the secretion of soluble pro-angiogenic factors, such as Vascular Endothelial Growth Factor (VEGF) and Fibroblast Growth Factor (FGF), and matrix-remodeling molecules [250,251]. These mediators act on endothelial cells, promoting their proliferation, migration, and the formation of new vascular sprouts. Furthermore, interactions between tumor cells and the vascular compartment establish feedback mechanisms that support tumor progression [76].

Based on these findings, this aspect was evaluated in an *in vitro* system, investigating whether PTCs were able to modulate neoangiogenesis not only through direct cell–cell interactions, but also via soluble factors secreted at a distance. To this end, spheroids composed solely of MVFs were embedded in 3D collagen matrices and exposed to PTC-conditioned medium. Optical microscopy images at 24 and 48 hours after embedding were acquired (Fig.48A). After the first 24 hours, MVF spheroids treated with conditioned medium showed a 2.2-fold increase in sprout formation compared to untreated controls, an increase that became statistically significant at 48 hours (Fig.48B). Furthermore, quantitative analysis of vascular branching revealed a marked increase in branching in spheroids treated with conditioned medium (Fig.48C).

Overall, these data indicate that PTCs actively modulate the neoangiogenic process of MVFs, promoting new vessel formation both through direct cellular interactions and via paracrine mechanisms mediated by soluble factors.

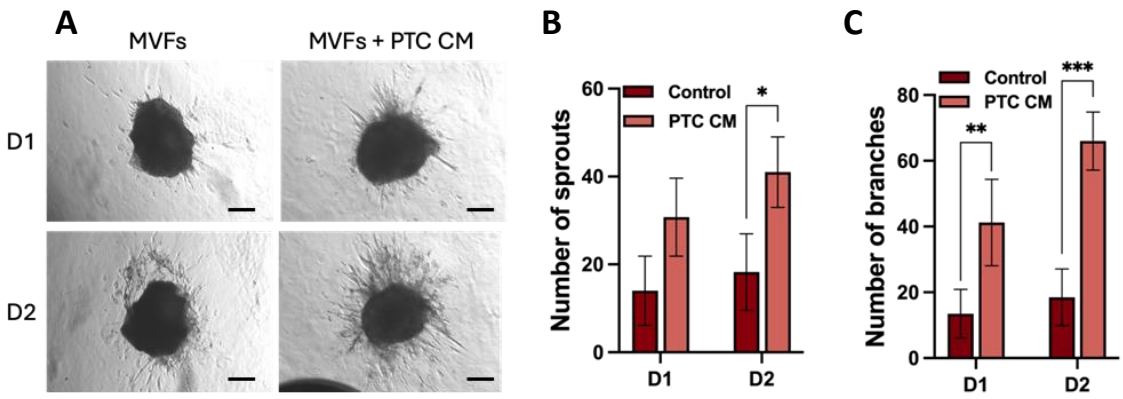

Figure 48: Effect of PTC-Conditioned Medium on MVF Spheroid Angiogenic Sprouting. (A) MVF spheroids embedded in collagen gel with High Glucose-DMEM (control, MVFs) or with conditioned medium from PTCs (MVFs + PTC CM) at day 1 (D1) and day 2 (D2). Scale bar: 100 µm. (B) Quantification of the number of vascular sprouts and (C) branching at D1 and D2 in MVF spheroids embedded in collagen gel with High Glucose DMEM (Control) or PTC-conditioned medium (PTC CM). Data are presented as mean ± SD. Statistical analysis (2-way ANOVA) was performed (n = 3) (*$p < 0.05$; **$p < 0.01$; ***$p < 0.001$).

Image adapted from Lo Cicero et al: '*Vascularized Three-Dimensional Model Integrating Primary Breast Tumor Cells and Microvascular Fragments: Mimicking the Tumor Microenvironment Involved in Chemoresistance' Cancer Cell Int.* 2026, doi: 10.1186/s12935-025-04154-6 [2]. Copyright via CC BY-NC-ND 4.0 - https://creativecommons.org/licenses/by/4.0/

4.4.8 Proteomic Analysis of Angiotumoroids

Based on their compactness, MMP9 expression, and sprouting and branching capability, angiotumoroids with 125 MVFs were identified as the most reproducible tumor models to mimic the tumor vascularization. To analyze the protein expression profile of these models in depth, in collaboration with Dr. Simone Dario Scilabra and Dr. Margot Lo Pinto of Ri.MED Foundation, high-resolution proteomics was performed on angiotumoroids with 125 MVFs, PTC spheroids, and MVF-only spheroids, focusing on angiogenesis mediators, ECM components, and matrix-remodeling proteins (Fig.49A).

The relative expression of proteins in angiotumoroids versus both control spheroids was determined through label-free quantification. A comparison of angiotumoroids with PTC spheroids revealed 1,587 proteins that were significantly different from the 5,093 identified. Among 773 proteins upregulated in angiotumoroids, including: MMP9, MMP10, MMP13, a disintegrin and metalloproteinase with thrombospondin motifs 1 (ADAMTS1), vascular endothelial growth factor A (VEGFA), platelet glycoprotein 4 (CD36), and Adiponectin (Adipoq), indicating enhanced ECM remodeling and metabolic activity. While protein expression involved in mitochondrial respiration and ECM

composition, such as NDUFS1, NDUFV1, NDUFV2, NDUFB7, FOXRED1, CSPG4, and Collagen I (Col1a1), were decreased in angiotumoroids compared to PTC spheroids. When compared with MVF-only spheroids, angiotumoroids displayed 1,070 upregulated and 1,272 downregulated proteins. In this case, ECM remodeling proteins, including MMP3 and MMP10, and protein transporters, such as sodium- and chloride-dependent taurine transporter (Slc6a6), phospholipid-transporting ATPase (Atp8a1), and Sodium/Potassium-Exchanging ATPase Complex (subunits Fxyd2 and Atp1b1), were more abundant, in contrast with ECM-related components, like extracellular superoxide dismutase [Cu-Zn] (SOD3), collectin-12 (COLEC12), tenascin-C (Tnc), and fibrillin-1 (Fbn1). Based on UniProt Gene Ontology, the relative quantification of proteins involved in angiogenesis revealed that VEGFA and Epiregulin (EREG) were significantly upregulated in angiotumoroids relative to PTC spheroids, while neuropilin-1 (NRP1) and MMP2 were downregulated. Compared to MVF spheroids, protein kinase C alpha (PRKCA) and Protein Tyrosine Kinase 2 Beta (PTK2B) were overexpressed. Collectively, these results indicate that the vascularized tumor model represents a distinct biological platform *in vitro*, displaying, increased MMP-mediated remodeling (MMP3, MMP9, MMP10, MMP11, MMP13), angiogenic potential, and enhanced ECM composition (collagen types I and IV) (Fig.49B). Additionally, proteomic analysis revealed significant upregulation of ATP-binding cassette (ABC) transporters (Fig.49C). As can be observed, there is a statistically significant difference in ABCB1 expression between angiotumoroids containing 125 MVFs and spheroids composed solely of PTCs, and even more so compared to spheroids composed only of microvascular fragments. This indicates that the integration of MVFs into the tumor spheroids enhances the expression of ABCB1, suggesting an increased potential for drug efflux and a more pronounced chemoresistant phenotype in the angiotumoroid model.

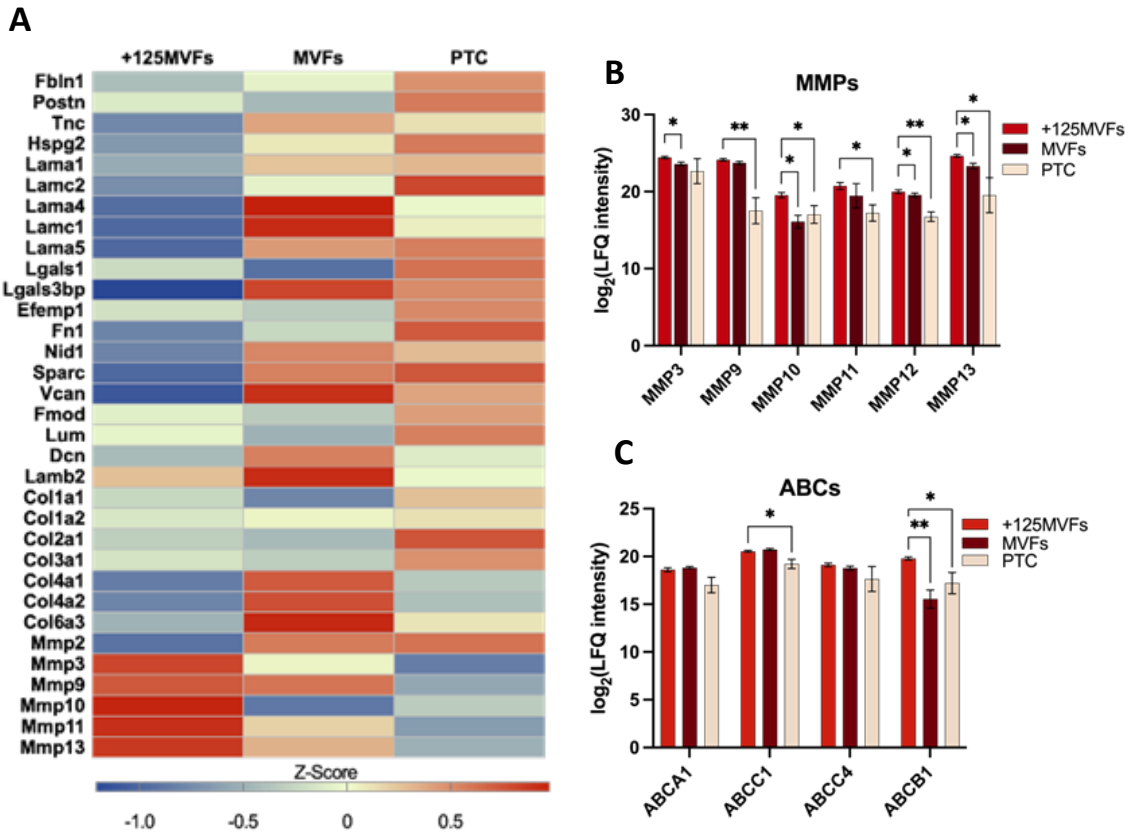

Figure 49: Proteomic Analysis of 125 MVFs (+125 MVFs), MVF spheroids, and PTC spheroids. (A) ECM composition and remodeling were assessed via proteomics, with differences in protein expression, misured as Label-Free Quantification intensity (LFQ). (B) LFQ intensity of the most differentially expressed Matrix Metalloproteinases (MMPs) in angiotumoroids with 125 MVFs (+125 MVFs), MVF spheroids, and PTC spheroids. (C) LFQ intensity of the differentially expressed ABC transporters in the same conditions (n = 4).

Image adapted from Lo Cicero et al: '*Vascularized Three-Dimensional Model Integrating Primary Breast Tumor Cells and Microvascular Fragments: Mimicking the Tumor Microenvironment Involved in Chemoresistance' Cancer Cell Int.* 2026, doi: 10.1186/s12935-025-04154-6 [2]. Copyright via CC BY-NC-ND 4.0 - https://creativecommons.org/licenses/by/4.0/

4.4.9 ABCB1 Expression and Disposition

The behavior observed in our *in vitro* models is consistent with published evidence. Indeed, previous studies have demonstrated that endothelial cells within the tumor neovasculature can express high levels of P-glycoprotein. In human brain tumors, P-gp is specifically detected in endothelial cells of newly formed vessels, indicating the presence of a drug-resistant vascular barrier, while complementary *in vitro* studies have shown that endothelial cells can upregulate ABC transporters, including P-gp, further highlighting the active role of the vascular compartment in therapy resistance [252].

Therefore, to confirm the overexpression of ABCB1 in our 3D models, a western blot assay was conducted using total proteins isolated from angiotumoroids and PTC spheroids. As shown in Figure 50A, Western blot analysis demonstrated that angiotumoroids with 125 MVFs exhibited significantly higher ABCB1 expression than PTC spheroids, suggesting that the presence of MVFs in the tumor in vitro model contributes to the upregulation of this key efflux transporter involved in drug resistance. In addition, to examine the spatial distribution of the protein within the angiotumoroids, immunofluorescence analysis was performed. The confocal microscopy images revealed a homogeneous localization of ABCB1 in angiotumoroids, expressed in both endothelial and tumor cells, while PTC spheroids displayed only minimal signal, supporting its functional relevance within the vascularized tumor microenvironment (Fig.50B).

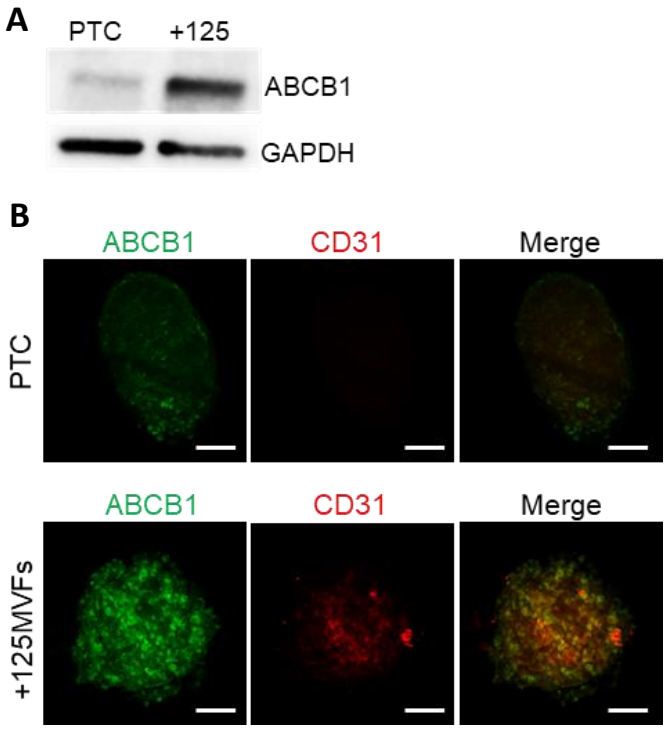

Figure 50: ABCB1 Expression in Angiotumoroid. (A) Western blot showing ABCB1 levels in PTC spheroids and angiotumoroids containing 125 MVFs (+125 MVFs). (B) Confocal microscopy images of PTC spheroids and angiotumoroids containing 125 MVFs at day 5, stained for ABCB1 (green) and CD31 (red). Scale bar: 100 µm.

Image adapted from Lo Cicero et al: '*Vascularized Three-Dimensional Model Integrating Primary Breast Tumor Cells and Microvascular Fragments: Mimicking the Tumor Microenvironment Involved in Chemoresistance' Cancer Cell Int.* 2026, doi: 10.1186/s12935-025-04154-6 [2]. Copyright via CC BY-NC-ND 4.0 - https://creativecommons.org/licenses/by/4.0/

4.4.10 Doxorubicin Uptake and Cytotoxicity in Angiotumoroids

Since DOX is a well-established substrate of P-glycoprotein [253] angiotumoroids drug uptake and cytotoxic response were analyzed and compared to PTC spheroids. Time-course monitoring of DOX autofluorescence at 30 minutes, 1 hour, 2 hours, and 4 hours was performed by confocal microscopy (Fig.51A). The quantitative fluorescence intensity analysis showed a markedly faster and more pronounced accumulation of doxorubicin in angiotumoroids compared to control spheroids (Fig.51B). This enhanced uptake highlights the impact of the integrated microvascular fragments on drug delivery, suggesting that the presence of a vascular-like network facilitates deeper penetration and more efficient retention of the chemotherapeutic agent within the 3D tumor-like structures. The findings indicate that angiotumoroids better recapitulate the *in vivo* tumor microenvironment, providing a more physiologically relevant model for assessing drug distribution and efficacy.

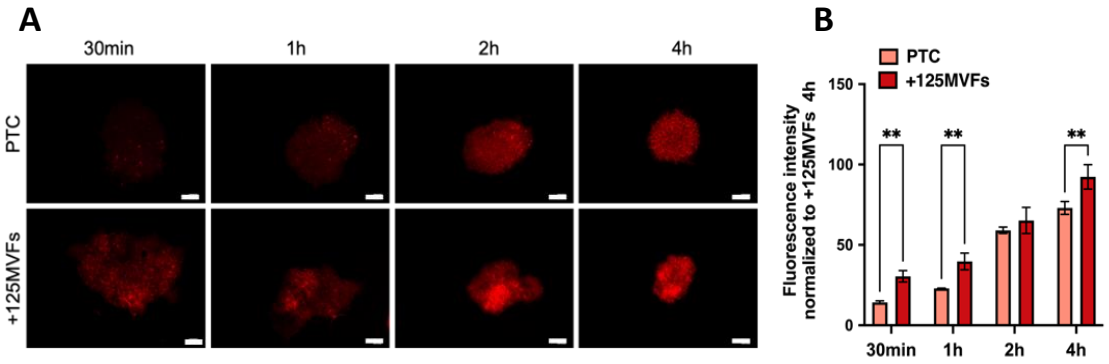

Figure 51: Doxorubicin Uptake in PTC and Angiotumoroids. (A) Fluorescence analysis of doxorubicin in red (10 µM) uptake in PTC spheroids (PTC) and PTC spheroids with 125 MVFs (+125 MVFs) monitored at 30 min, 1 h, 2 h, and 4 h. Scale bar: 30 µm. (B) Quantification of fluorescence intensity of doxorubicin, normalized to angiotumoroids +125 MVFs at 4 h. Data are mean ± SD. Statistical analysis (2-way ANOVA) was performed (n = 3) (**p < 0.01).

Image adapted from Lo Cicero et al: '*Vascularized Three-Dimensional Model Integrating Primary Breast Tumor Cells and Microvascular Fragments: Mimicking the Tumor Microenvironment Involved in Chemoresistance' Cancer Cell Int.* 2026, doi: 10.1186/s12935-025-04154-6 [2]. Copyright via CC BY-NC-ND 4.0 - https://creativecommons.org/licenses/by/4.0/

Interestingly, the doxorubicin detected was mainly concentrated in MVF-rich areas, as indicated by its colocalization with CD31 (Fig. 52). These results suggest that the vascular components facilitate drug uptake, compartmentalization, and local transport, more accurately reflecting drug distribution *in vivo*.

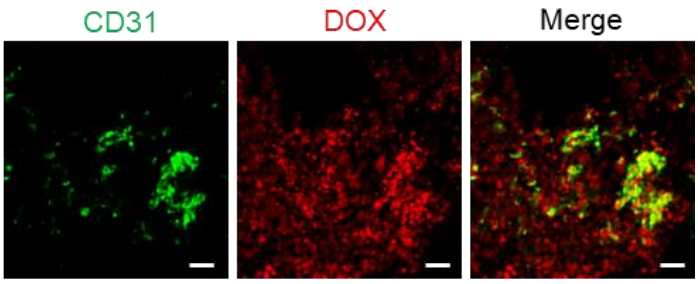

Figure 52: CD31 and Doxorubicin Colocalization in Angiotumoroids. Confocal microscopy images of angiotumoroids containing 125 MVFs, stained with anti-CD31 antibody (green) and doxorubicin (red), showing the spatial relationship between endothelial structures and the drug.

Image adapted from Lo Cicero et al: '*Vascularized Three-Dimensional Model Integrating Primary Breast Tumor Cells and Microvascular Fragments: Mimicking the Tumor Microenvironment Involved in Chemoresistance' Cancer Cell Int.* 2026, doi: 10.1186/s12935-025-04154-6 [2]. Copyright via CC BY-NC-ND 4.0 - https://creativecommons.org/licenses/by/4.0/

However, after treatment with doxorubicin at day 5 post-seeding, a clear difference between angiotumoroids and PTC spheroids was observed. As shown by optical microscopy images (Fig.53A), the angiotumoroids remained more compact and cohesive after 24 h of doxorubicin incubation, with fewer dead cells around them, while PTC spheroids appeared less compact, with a clear halo of dead cells surrounding the spheroids. This observation is supported by the cell viability assay (Fig.53B), indicating that approximately 60% of cells within the angiotumoroids were viable after 24 hours of doxorubicin exposure, compared to only 23% in the PTC spheroids. This increased resistance is likely associated with the elevated expression of ABCB1 observed in angiotumoroids, which could enhance drug efflux and reduce intracellular accumulation of doxorubicin, thereby contributing to their greater resilience against chemotherapeutic treatment.

To sum up, the inclusion of MVFs markedly influences both the distribution and effectiveness of chemotherapeutic agents such as doxorubicin, as reflected by altered uptake patterns and cytotoxic responses. These results underscore the potential of angiotumoroids as a robust *in vitro* platform for studying solid tumors, in particular the interactions between tumor cells and vessels and the evaluation of drug delivery strategies designed to target the tumor microenvironment.

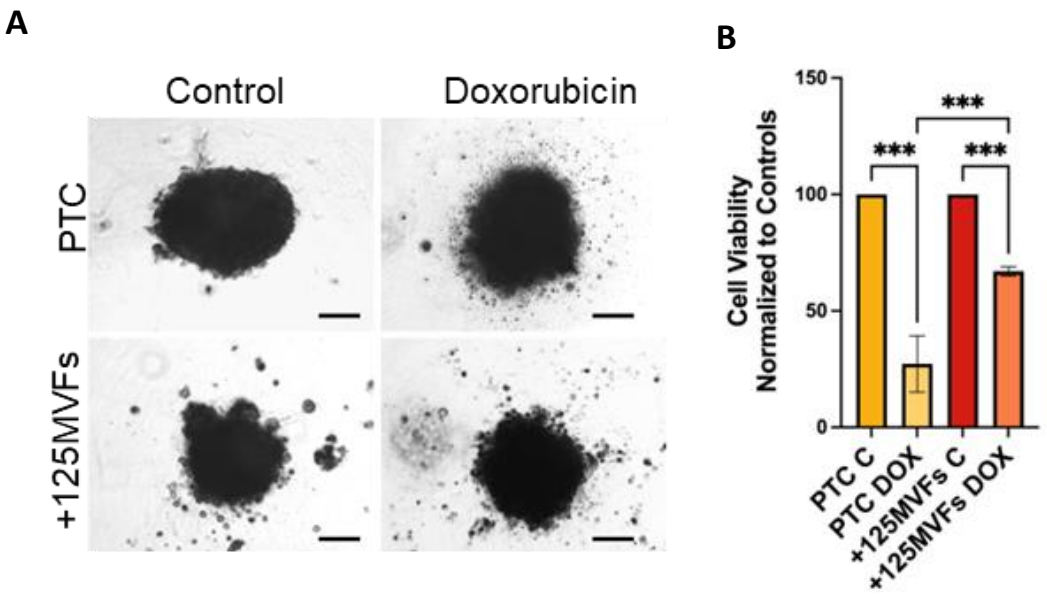

Figure 53: Effect of Doxorubicin on PTC and +125 MVFs Spheroids. (A) PTC spheroids and angiotumoroids containing 125 MVFs (+125 MVFs) following 24 h treatment with 10 µM doxorubicin. Scale bar: 100 µm. (B) Cell viability was assessed in PTC spheroids and +125 MVFs angiotumoroids following 24 h treatment with 10 µM doxorubicin (DOX), where PTC C and +125 MVFs C were used as untreated controls. Data are presented as mean ± SD. Statistical analysis was performed using 2-way ANOVA (n = 3) (***p < 0.001).

Image adapted from Lo Cicero et al: '*Vascularized Three-Dimensional Model Integrating Primary Breast Tumor Cells and Microvascular Fragments: Mimicking the Tumor Microenvironment Involved in Chemoresistance' Cancer Cell Int.* 2026, doi: 10.1186/s12935-025-04154-6 [2]. Copyright via CC BY-NC-ND 4.0 - https://creativecommons.org/licenses/by/4.0/

Chapter 5

CONCLUSIONS AND FUTURE PROSPECTIVES

5.1 Conclusions

This PhD thesis focused on the investigation of the biomechanical and biochemical barriers defining the tumor microenvironment (TME), with the central hypothesis that the extracellular matrix (ECM) constitutes the primary determinant of drug resistance in solid tumors. Furthermore, the work aimed to validate innovative strategies to overcome these barriers. The results obtained not only confirm this hypothesis but also open new perspectives in the fields of precision medicine and nanosystem-based drug delivery. The multidisciplinary approach adopted allowed for the connection of advanced cell biology, proteomic characterization, and the engineering of vascularized three-dimensional models, providing a technically solid overview consistent with the bibliographic sources present in the literature.

A primary cornerstone lies in the validation of three-dimensional (3D) models to mimic the tumor microenvironment in vitro. The induction of breast tumor mass via 7-12 dimethylbenz[a]anthracene (DMBA) in immunocompetent female Wistar rats allowed for operation on a biological substrate of high complexity, overcoming the limitations of immortalized cell lines that often lose the ability to synthesize an endogenous matrix, compatible with solid tumors. Indeed, the isolation of PTCs guaranteed the maintenance of intrinsic cellular heterogeneity, including stromal populations essential for the deposition and remodeling of the ECM. It was observed, via uHPLC–MS/MS mass spectrometry data, a radically different proteomic profile between two-dimensional (2D) systems and the respective three-dimensional models, with the overexpression of over 1128 proteins in the spheroids. Among these, the identification of specific matrix markers, such as the collagen isoforms Col1a1, Col4a1, and Col5a2, together with the overexpression of matrix MMPs with the exclusive detection of MMP-9 and MMP-13 in PTC spheroids, confirms that three-dimensional architecture is a fundamental condition for faithfully replicating the density and rigidity of the tumor stroma observed *in vivo* [226].

The most significant evidence emerged regarding the function of collagenase as a "tumor priming" agent. Characterization via confocal microscopy and immunofluorescence clearly showed how the spheroids produce a dense peripheral shell of type I collagen, which acts as a biomechanical shield against drugs and immune system cells. In response to this barrier, the enzymatic degradation strategy demonstrated that only the combination of recombinant Class I (ColG) and Class II (ColH) collagenases guarantees a complete lysis of the collagen fibrils. This enzymatic administration induced a total digestion of type I collagen in the spheroids, with an immediate effect on the *in vitro* pharmacokinetics. In

fact, the uptake over time of free doxorubicin (DOX) increased significantly in the pre-treated spheroids compared to the untreated control, demonstrating that resistance is not only a genetic-molecular phenomenon, but a problem of physical transport conditioned by the reduced permeability of the tumor matrix. This tangible increase in drug uptake proved fundamental in increasing the cytotoxicity of PTC spheroids, confirming the importance of ECM, and particularly of collagen, in drug resistance.

The transition from the free drug administration to drug delivery systems (DDS) represented a strength of this research. The aim was to overcome the dose-dependent cardiotoxicity of doxorubicin and the immunoreactivity of collagenases *in vivo*. The synthesis of nanoparticles based on bovine serum albumin (BSA) exploited the intrinsic biocompatibility of this protein and its capacity for selective accumulation at tumor sites [235]. A primary technical challenge was the development of a stabilization protocol that would not compromise the functional integrity of the incorporated collagenases. The comparison between chemical crosslinking with glutaraldehyde and thermal crosslinking highlighted that the latter, conducted at 65°C, allows for the partial preservation of the enzyme's catalytic activity. Zymography analyses indeed confirmed the persistence of gelatin degradation halos for the thermally stabilized nanoparticles, in contrast to those chemically stabilized, which were catalytically inactive.

Furthermore, a fundamental contribution of this project lies in the comparison between different DDS conjugated to the chemotherapeutic, using doxorubicin as a drug model. Under acidic conditions mimicking the tumor microenvironment, BSA nanoparticles showed aggregation phenomena associated with reduced colloidal stability, which may contribute to increased intratumoral retention [254]. On the other hand, the use of polyvinylpyrrolidone (PVP) nanoparticles conjugated via the AEDP linker allows for redox sensitivity to intracellular glutathione (GSH) levels, achieving a selective release within the tumor cytoplasmic compartment [207]. Moreover, cytotoxicity data on primary cell tumor spheroids confirmed that the combination of collagenase pre-treatment and drug administration by nanoplatform (both BSA-DOX and PVP-AEDP-DOX) produces a higher synergistic effect, reducing spheroid cell viability compared to controls not treated enzymatically, further confirming the fundamental role of the matrix in solid tumors.

The integration of the vascular compartment using microvascular fragments (MVFs) isolated from rat adipose tissue allowed for an elevated degree of *in vitro* model reliability. In fact, the angiotumoroids generated preserved the architecture of native microvessels, overcoming the limits of models based on HUVEC. The formation of organized vascular

networks within the spheroid, confirmed by CD31 staining, revealed a dynamic interaction with tumor cells that was both physical and paracrine, stimulating neoangiogenesis through the secretion of factors such as VEGF. A particular incisive result of this research was the detection of high levels of ABCB1 (P-gp) transporter in both the tumor cells and the endothelial cells of the angiotumoroids. This drug-resistant vascular barrier, together with the matrix collagen, defines how *in vitro* solid tumor models acquire resistance to chemotherapeutics both mechanically and biochemically. Indeed, it was observed that doxorubicin was localized predominantly in MVF-rich regions, suggesting that vascularization facilitates initial uptake. However, the subsequent diffusion is limited by efflux pumps and matrix density.

In conclusion, the present study demonstrates that effective oncological therapy cannot ignore a "tumor priming" strategy aimed at normalizing the stroma. The combination of recombinant collagenases and chemotherapeutics conjugated to nanoparticles sensitive to environmental stimuli represents a viable pathway for breaking down the physical and biochemical resistance of solid tumors, increasing specificity, and potentially decreasing systemic toxicity *in vivo*. The validation of species-specific vascularized models also lays the foundations for the development of personalized screening systems, where cells derived from human biopsies and autologous MVFs can be employed to predict individual clinical response, accelerating the transition from basic research to oncological clinical practice.

5.2 Future Prospectives

The strategies outlined in this thesis open scenarios of considerable interest, both regarding the optimization of nanotechnological platforms and the evolution of three-dimensional preclinical models. One of the main directions for future research lies in the refinement of the molecular targeting of albumin nanoparticles (BSA). Although the results confirmed the therapeutic efficacy of the nanoparticles *in vitro*, the integration of specific ligands on the surface of the nanoparticles could further increase specificity, using, for example, molecules such as folic acid or bombesin, whose receptors are widely expressed in tumor cells [255,256]. In parallel, the "tumor priming" strategy based on recombinant collagenases requires a further validation phase to establish the ideal concentration in *in vitro* models and the optimal therapeutic window *in vivo*. It will be essential to determine the latency time between the administration of the enzyme (whether free or encapsulated) and the injection of the chemotherapeutic agent. Excessive or prolonged degradation of the ECM could, in fact, theoretically favor epithelial-mesenchymal transition (EMT) processes

and subsequent cellular extravasation, increasing the risk of metastasis [257,258]. Therefore, the development of a programmed release nanoplatform in synergy with collagenases able to digest the matrix only in a transitory manner at the tumor mass site will be a bioengineering challenge of primary importance to enhance treatment safety. Another area of future development concerns the implementation of the "angiotumoroid" as models, toward an even higher multicellular complexity. For example, the integration of immune system components, such as tumor-associated macrophages (TAMs) increase reliability, since these components are fundamental in the tumor progression [259]. From the diagnostics and personalized medicine perspective, the methodological approach validated here in Wistar rats represents the foundation for the creation of patient-specific screening platforms. More specifically, the prospect is to use human biopsies to generate autologous angiotumoroids, integrating the patient’s tumor cells with microvascular fragments obtained from their own adipose tissue. Such models could be employed to test *ex vivo* different therapeutic combinations and collagenase doses, allowing the oncologist to predict the individual's response with greater accuracy. This would reduce the reliance on empirical therapeutic approaches, which are often onerous for the patient’s health. In summary, future research aims at the development of an integrated multimodal therapeutic protocol, in which biomechanical matrix modulation is no longer an isolated intervention but a synergistic component of a two-step treatment strategy, designed to overcome genetic heterogeneity, stromal barriers, and vascular complexity in solid tumors.

BIBLIOGRAPHY

1. Lo Cicero, A.; Campora, S.; Lo Buglio, G.; Cinà, P.; Lo Pinto, M.; Scilabra, S.D.; Ghersi, G. Enhancing Therapeutic Efficacy through Degradation of Endogenous Extracellular Matrix in Primary Breast Tumor Spheroids. *FEBS J.* 2025, *292*, 3494–3507, doi:10.1111/febs.70069.

2. Lo Cicero, A.; La Monica, F.; Lo Buglio, G.; Campora, S.; Gangemi, F.; Cinà, P.; Salamone, M.; Lo Pinto, M.; Scilabra, S.D.; Ghersi, G. A Vascularized Three-Dimensional Model Integrating Primary Breast Tumor Cells and Microvascular Fragments: Mimicking the Tumor Microenvironment Involved in Chemoresistance. *Cancer Cell Int.* 2026, doi:10.1186/s12935-025-04154-6.

3. Force, L.M.; Kocarnik, J.M.; May, M.L.; Bhangdia, K.; Crist, A.; Penberthy, L.; Pritchett, N.; Acheson, A.; Deitesfeld, L.; A, B.; et al. The Global, Regional, and National Burden of Cancer, 1990–2023, with Forecasts to 2050: A Systematic Analysis for the Global Burden of Disease Study 2023. *The Lancet* 2025, *406*, 1565–1586, doi:10.1016/S0140-6736(25)01635-6.

4. Hu, J.; Dong, H.; Dong, Y.; Zhou, R.; Teixeira, W.; He, X.; Ye, D.-W.; Ti, G. Cancer Burden Attributable to Risk Factors, 1990–2019: A Comparative Risk Assessment. *iScience* 2024, *27*, 109430, doi:10.1016/j.isci.2024.109430.

5. Anand, P.; Kunnumakara, A.B.; Sundaram, C.; Harikumar, K.B.; Tharakan, S.T.; Lai, O.S.; Sung, B.; Aggarwal, B.B. Cancer Is a Preventable Disease That Requires Major Lifestyle Changes. *Pharm. Res.* 2008, *25*, 2097–2116, doi:10.1007/s11095-008-9661-9.

6. Tran, K.B.; Lang, J.J.; Compton, K.; Xu, R.; Acheson, A.R.; Henrikson, H.J.; Kocarnik, J.M.; Penberthy, L.; Aali, A.; Abbas, Q.; et al. The Global Burden of Cancer Attributable to Risk Factors, 2010–19: A Systematic Analysis for the Global Burden of Disease Study 2019. *The Lancet* 2022, *400*, 563–591, doi:10.1016/S0140-6736(22)01438-6.

7. Carbone, A. Cancer Classification at the Crossroads. *Cancers (Basel).* 2020, *12*, 980, doi:10.3390/cancers12040980.

8. Halbrook, C.J.; Lyssiotis, C.A.; Pasca di Magliano, M.; Maitra, A. Pancreatic Cancer: Advances and Challenges. *Cell* 2023, *186*, 1729–1754, doi:10.1016/j.cell.2023.02.014.

9. Cai, J.; Lan, Y.; Wang, Y.; Cheng, H.; Xu, S. Liver Cancer Burden Attributable to High Body Mass Index and High Fasting Plasma Glucose in BRICS Countries (1990–2021): A Global Burden of Disease 2021 Analysis with Projections to 2050. *Front. Oncol.* 2025, *15*, doi:10.3389/fonc.2025.1627282.

10. Zafar, A.; Khatoon, S.; Khan, M.J.; Abu, J.; Naeem, A. Advancements and Limitations in Traditional Anti-Cancer Therapies: A Comprehensive Review of Surgery, Chemotherapy, Radiation Therapy, and Hormonal Therapy. *Discover Oncology* 2025, *16*, 607, doi:10.1007/s12672-025-02198-8.

11. Souri, M.; Soltani, M.; Moradi Kashkooli, F.; Kiani Shahvandi, M. Engineered Strategies to Enhance Tumor Penetration of Drug-Loaded Nanoparticles. *Journal of Controlled Release* 2022, *341*, 227–246, doi:10.1016/j.jconrel.2021.11.024.

12. Fu, Y.-C.; Liang, S.-B.; Luo, M.; Wang, X.-P. Intratumoral Heterogeneity and Drug Resistance in Cancer. *Cancer Cell Int.* 2025, *25*, 103, doi:10.1186/s12935-025-03734-w.

13. Hass, R.; von der Ohe, J.; Ungefroren, H. Impact of the Tumor Microenvironment on Tumor Heterogeneity and Consequences for Cancer Cell Plasticity and Stemness. *Cancers (Basel).* 2020, *12*, 3716, doi:10.3390/cancers12123716.

14. Naba, A. Mechanisms of Assembly and Remodelling of the Extracellular Matrix. *Nat. Rev. Mol. Cell Biol.* 2024, *25*, 865–885, doi:10.1038/s41580-024-00767-3.

15. Salavati, H.; Debbaut, C.; Pullens, P.; Ceelen, W. Interstitial Fluid Pressure as an Emerging Biomarker in Solid Tumors. *Biochimica et Biophysica Acta (BBA) - Reviews on Cancer* 2022, *1877*, 188792, doi:10.1016/j.bbcan.2022.188792.

16. Strambi, A.; De Milito, A. Contribution of PH Alterations to the Tumor Microenvironment. In *Tumor Cell Metabolism*; Springer Vienna: Vienna, 2015; pp. 173–196.

17. Pandkar, M.R.; Dhamdhere, S.G.; Shukla, S. Oxygen Gradient and Tumor Heterogeneity: The Chronicle of a Toxic Relationship. *Biochimica et Biophysica Acta (BBA) - Reviews on Cancer* 2021, *1876*, 188553, doi:10.1016/j.bbcan.2021.188553.

18. Dagogo-Jack, I.; Shaw, A.T. Tumour Heterogeneity and Resistance to Cancer Therapies. *Nat. Rev. Clin. Oncol.* 2018, *15*, 81–94, doi:10.1038/nrclinonc.2017.166.

19. El-Tanani, M.; Rabbani, S.A.; Babiker, R.; Rangraze, I.; Kapre, S.; Palakurthi, S.S.; Alnuqaydan, A.M.; Aljabali, A.A.; Rizzo, M.; El-Tanani, Y.; et al. Unraveling the Tumor Microenvironment: Insights into Cancer Metastasis and Therapeutic Strategies. *Cancer Lett.* 2024, *591*, 216894, doi:10.1016/j.canlet.2024.216894.

20. Yuan, Z.; Li, Y.; Zhang, S.; Wang, X.; Dou, H.; Yu, X.; Zhang, Z.; Yang, S.; Xiao, M. Extracellular Matrix Remodeling in Tumor Progression and Immune Escape: From Mechanisms to Treatments. *Mol. Cancer* 2023, *22*, 48, doi:10.1186/s12943-023-01744-8.

21. Hanahan, D.; Weinberg, R.A. Hallmarks of Cancer: The Next Generation. *Cell* 2011, *144*, 646–674, doi:10.1016/j.cell.2011.02.013.

22. Belli, C.; Trapani, D.; Viale, G.; D'Amico, P.; Duso, B.A.; Della Vigna, P.; Orsi, F.; Curigliano, G. Targeting the Microenvironment in Solid Tumors. *Cancer Treat. Rev.* 2018, *65*, 22–32, doi:10.1016/j.ctrv.2018.02.004.

23. Boedtkjer, E.; Pedersen, S.F. The Acidic Tumor Microenvironment as a Driver of Cancer. *Annu. Rev. Physiol.* 2020, *82*, 103–126, doi:10.1146/annurev-physiol-021119-034627.

24. Suvac, A.; Ashton, J.; Bristow, R.G. Tumour Hypoxia in Driving Genomic Instability and Tumour Evolution. *Nat. Rev. Cancer* 2025, doi:10.1038/s41568-024-00781-9.

25. Lo Buglio, G.; Lo Cicero, A.; Campora, S.; Ghersi, G. The Multifaced Role of Collagen in Cancer Development and Progression. *Int. J. Mol. Sci.* 2024, *25*, 13523, doi:10.3390/ijms252413523.

26. Cords, L.; Engler, S.; Haberecker, M.; Rüschoff, J.H.; Moch, H.; de Souza, N.; Bodenmiller, B. Cancer-Associated Fibroblast Phenotypes Are Associated with Patient Outcome in Non-Small Cell Lung Cancer. *Cancer Cell* 2024, *42*, 396-412.e5, doi:10.1016/j.ccell.2023.12.021.

27. Forsthuber, A.; Aschenbrenner, B.; Korosec, A.; Jacob, T.; Annusver, K.; Krajic, N.; Kholodniuk, D.; Frech, S.; Zhu, S.; Purkhauser, K.; et al. Cancer-Associated Fibroblast Subtypes Modulate the Tumor-Immune Microenvironment and Are Associated with Skin Cancer Malignancy. *Nat. Commun.* 2024, *15*, 9678, doi:10.1038/s41467-024-53908-9.

28. Xing, F. Cancer Associated Fibroblasts (CAFs) in Tumor Microenvironment. *Frontiers in Bioscience* 2010, *15*, 166, doi:10.2741/3613.

29. Liao, Z.; Tan, Z.W.; Zhu, P.; Tan, N.S. Cancer-Associated Fibroblasts in Tumor Microenvironment – Accomplices in Tumor Malignancy. *Cell. Immunol.* 2019, *343*, 103729, doi:10.1016/j.cellimm.2017.12.003.

30. Tajaldini, M.; Saeedi, M.; Amiriani, T.; Amiriani, A.H.; Sedighi, S.; Mohammad zadeh, F.; Dehghan, M.; Jahanshahi, M.; Zanjan Ghandian, M.; Khalili, P.; et al. Cancer-Associated Fibroblasts (CAFs) and Tumor-Associated Macrophages (TAMs); Where Do They Stand in Tumorigenesis and How They Can Change the Face of Cancer Therapy? *Eur. J. Pharmacol.* 2022, *928*, 175087, doi:10.1016/j.ejphar.2022.175087.

31. Cancer-Associated Fibroblasts in Intrahepatic Cholangiocarcinoma Progression and Therapeutic Resistance. In; 2022; pp. 201–226.

32. Glabman, R.A.; Choyke, P.L.; Sato, N. Cancer-Associated Fibroblasts: Tumorigenicity and Targeting for Cancer Therapy. *Cancers (Basel).* 2022, *14*, 3906, doi:10.3390/cancers14163906.

33. Hu, D.; Li, Z.; Zheng, B.; Lin, X.; Pan, Y.; Gong, P.; Zhuo, W.; Hu, Y.; Chen, C.; Chen, L.; et al. Cancer-associated Fibroblasts in Breast Cancer: Challenges and Opportunities. *Cancer Commun.* 2022, *42*, 401–434, doi:10.1002/cac2.12291.

34. Zhang, T.; Li, X.; He, Y.; Wang, Y.; Shen, J.; Wang, S.; You, Q.; Zhai, J.; Shen, L. Cancer-Associated Fibroblasts-Derived HAPLN1 Promotes Tumour Invasion through Extracellular Matrix Remodeling in Gastric Cancer. *Gastric Cancer* 2022, *25*, 346–359, doi:10.1007/s10120-021-01259-5.

35. Long, K.R.; Newland, B.; Florio, M.; Kalebic, N.; Langen, B.; Kolterer, A.; Wimberger, P.; Huttner, W.B. Extracellular Matrix Components HAPLN1, Lumican, and Collagen I Cause Hyaluronic Acid-Dependent Folding of the Developing

Human Neocortex. *Neuron* 2018, *99*, 702-719.e6, doi:10.1016/j.neuron.2018.07.013.

36. Joshi, R.S.; Kanugula, S.S.; Sudhir, S.; Pereira, M.P.; Jain, S.; Aghi, M.K. The Role of Cancer-Associated Fibroblasts in Tumor Progression. *Cancers (Basel).* 2021, *13*, 1399, doi:10.3390/cancers13061399.

37. Zarin, B.; Rafiee, L.; Daneshpajouhnejad, P.; Haghjooy Javanmard, S. A Review on the Role of CAFs and CAF-Derived Exosomes in Progression and Metastasis of Digestive System Cancers. *Tumor Biology* 2021, *43*, 141–157, doi:10.3233/TUB-200075.

38. Erdogan, B.; Webb, D.J. Cancer-Associated Fibroblasts Modulate Growth Factor Signaling and Extracellular Matrix Remodeling to Regulate Tumor Metastasis. *Biochem. Soc. Trans.* 2017, *45*, 229–236, doi:10.1042/BST20160387.

39. Kohli, K.; Pillarisetty, V.G.; Kim, T.S. Key Chemokines Direct Migration of Immune Cells in Solid Tumors. *Cancer Gene Ther.* 2022, *29*, 10–21, doi:10.1038/s41417-021-00303-x.

40. Ohno, S.; Tachibana, M.; Fujii, T.; Ueda, S.; Kubota, H.; Nagasue, N. Role of Stromal Collagen in Immunomodulation and Prognosis of Advanced Gastric Carcinoma. *Int. J. Cancer* 2002, *97*, 770–774, doi:10.1002/ijc.10144.

41. Kuczek, D.E.; Larsen, A.M.H.; Thorseth, M.-L.; Carretta, M.; Kalvisa, A.; Siersbæk, M.S.; Simões, A.M.C.; Roslind, A.; Engelholm, L.H.; Noessner, E.; et al. Collagen Density Regulates the Activity of Tumor-Infiltrating T Cells. *J. Immunother. Cancer* 2019, *7*, 68, doi:10.1186/s40425-019-0556-6.

42. Pascoal Ramos, M.I.; van der Vlist, M.; Meyaard, L. Inhibitory Pattern Recognition Receptors: Lessons from LAIR1. *Nat. Rev. Immunol.* 2025, *25*, 711–724, doi:10.1038/s41577-025-01181-2.

43. Chen, Y.; Yang, S.; Tavormina, J.; Tampe, D.; Zeisberg, M.; Wang, H.; Mahadevan, K.K.; Wu, C.-J.; Sugimoto, H.; Chang, C.-C.; et al. Oncogenic Collagen I Homotrimers from Cancer Cells Bind to A3β1 Integrin and Impact Tumor Microbiome and Immunity to Promote Pancreatic Cancer. *Cancer Cell* 2022, *40*, 818-834.e9, doi:10.1016/j.ccell.2022.06.011.

44. Saad, E.E.; Michel, R.; Borahay, M.A. Immunosuppressive Tumor Microenvironment and Uterine Fibroids: Role in Collagen Synthesis. *Cytokine Growth Factor Rev.* 2024, *75*, 93–100, doi:10.1016/j.cytogfr.2023.10.002.

45. Deng, J.; Kang, Y.; Cheng, C.-C.; Li, X.; Dai, B.; Katz, M.H.; Men, T.; Kim, M.P.; Koay, E.A.; Huang, H.; et al. DDR1-Induced Neutrophil Extracellular Traps Drive Pancreatic Cancer Metastasis. *JCI Insight* 2021, *6*, doi:10.1172/jci.insight.146133.

46. Santoni, M.; Massari, F.; Amantini, C.; Nabissi, M.; Maines, F.; Burattini, L.; Berardi, R.; Santoni, G.; Montironi, R.; Tortora, G.; et al. Emerging Role of Tumor-Associated Macrophages as Therapeutic Targets in Patients with Metastatic Renal Cell Carcinoma. *Cancer Immunology, Immunotherapy* 2013, *62*, 1757–1768, doi:10.1007/s00262-013-1487-6.

47. Humphrey, J.D.; Dufresne, E.R.; Schwartz, M.A. Mechanotransduction and Extracellular Matrix Homeostasis. *Nat. Rev. Mol. Cell Biol.* 2014, *15*, 802–812, doi:10.1038/nrm3896.

48. Saad, E.E.; Michel, R.; Borahay, M.A. Senescence-Associated Secretory Phenotype (SASP) and Uterine Fibroids: Association with PD-L1 Activation and Collagen Deposition. *Ageing Res. Rev.* 2024, *97*, 102314, doi:10.1016/j.arr.2024.102314.

49. Walker, C.; Mojares, E.; Del Río Hernández, A. Role of Extracellular Matrix in Development and Cancer Progression. *Int. J. Mol. Sci.* 2018, *19*, 3028, doi:10.3390/ijms19103028.

50. Ye, Z.; Yu, Z.; Chen, G.; Jia, J. Extracellular Vesicles in Tumor Angiogenesis and Resistance to Anti-angiogenic Therapy. *Cancer Sci.* 2023, *114*, 2739–2749, doi:10.1111/cas.15801.

51. Ouarné, M.; Pena, A.; Franco, C.A. From Remodeling to Quiescence: The Transformation of the Vascular Network. *Cells & Development* 2021, *168*, 203735, doi:10.1016/j.cdev.2021.203735.

52. Sandoo, A.; Veldhuijzen van Zanten, J.J.C.S.; Metsios, G.S.; Carroll, D.; Kitas, G.D. The Endothelium and Its Role in Regulating Vascular Tone. *Open Cardiovasc. Med. J.* 2010, *4*, 302–312, doi:10.2174/1874192401004010302.

53. Libby, J.R.; Royce, H.; Walker, S.R.; Li, L. The Role of Extracellular Matrix in Angiogenesis: Beyond Adhesion and Structure. *Biomaterials and Biosystems* 2024, *15*, 100097, doi:10.1016/j.bbiosy.2024.100097.

54. Kretschmer, M.; Rüdiger, D.; Zahler, S. Mechanical Aspects of Angiogenesis. *Cancers (Basel).* 2021, *13*, 4987, doi:10.3390/cancers13194987.

55. Vagena, I.-A.; Malapani, C.; Gatou, M.-A.; Lagopati, N.; Pavlatou, E.A. Enhancement of EPR Effect for Passive Tumor Targeting: Current Status and Future Perspectives. *Applied Sciences* 2025, *15*, 3189, doi:10.3390/app15063189.

56. Belyaev, I.B.; Griaznova, O.Yu.; Yaremenko, A. V.; Deyev, S.M.; Zelepukin, I. V. Beyond the EPR Effect: Intravital Microscopy Analysis of Nanoparticle Drug Delivery to Tumors. *Adv. Drug Deliv. Rev.* 2025, *219*, 115550, doi:10.1016/j.addr.2025.115550.

57. Sun, R.; Xiang, J.; Zhou, Q.; Piao, Y.; Tang, J.; Shao, S.; Zhou, Z.; Bae, Y.H.; Shen, Y. The Tumor EPR Effect for Cancer Drug Delivery: Current Status, Limitations, and Alternatives. *Adv. Drug Deliv. Rev.* 2022, *191*, 114614, doi:10.1016/j.addr.2022.114614.

58. Heldin, C.-H.; Rubin, K.; Pietras, K.; Östman, A. High Interstitial Fluid Pressure — an Obstacle in Cancer Therapy. *Nat. Rev. Cancer* 2004, *4*, 806–813, doi:10.1038/nrc1456.

59. Böckelmann, L.C.; Schumacher, U. Targeting Tumor Interstitial Fluid Pressure: Will It Yield Novel Successful Therapies for Solid Tumors? *Expert Opin. Ther. Targets* 2019, *23*, 1005–1014, doi:10.1080/14728222.2019.1702974.

60. Rickard, B.P.; Conrad, C.; Sorrin, A.J.; Ruhi, M.K.; Reader, J.C.; Huang, S.A.; Franco, W.; Scarcelli, G.; Polacheck, W.J.; Roque, D.M.; et al. Malignant Ascites in Ovarian Cancer: Cellular, Acellular, and Biophysical Determinants of Molecular Characteristics and Therapy Response. *Cancers (Basel).* 2021, *13*, 4318, doi:10.3390/cancers13174318.

61. Lunt, S.J.; Fyles, A.; Hill, R.P.; Milosevic, M. Interstitial Fluid Pressure in Tumors: Therapeutic Barrier and Biomarker of Angiogenesis. *Future Oncology* 2008, *4*, 793–802, doi:10.2217/14796694.4.6.793.

62. Debnath, G.; Vasu, B.; Gorla, R.S.R. Finite Element Simulation of Interstitial–Lymphatic Fluid Flow and Nanodrug Transport in a Solid Tumor: An Intratumoral Injection Approach. *BME Front.* 2025, *6*, doi:10.34133/bmef.0119.

63. Vimalraj, S. A Concise Review of VEGF, PDGF, FGF, Notch, Angiopoietin, and HGF Signalling in Tumor Angiogenesis with a Focus on Alternative Approaches and Future Directions. *Int. J. Biol. Macromol.* 2022, *221*, 1428–1438, doi:10.1016/j.ijbiomac.2022.09.129.

64. Apte, R.S.; Chen, D.S.; Ferrara, N. VEGF in Signaling and Disease: Beyond Discovery and Development. *Cell* 2019, *176*, 1248–1264, doi:10.1016/j.cell.2019.01.021.

65. Dudley, A.C.; Griffioen, A.W. Pathological Angiogenesis: Mechanisms and Therapeutic Strategies. *Angiogenesis* 2023, *26*, 313–347, doi:10.1007/s10456-023-09876-7.

66. Dor, Y.; Porat, R.; Keshet, E. Vascular Endothelial Growth Factor and Vascular Adjustments to Perturbations in Oxygen Homeostasis. *American Journal of Physiology-Cell Physiology* 2001, *280*, C1367–C1374, doi:10.1152/ajpcell.2001.280.6.C1367.

67. Conway, E. Molecular Mechanisms of Blood Vessel Growth. *Cardiovasc. Res.* 2001, *49*, 507–521, doi:10.1016/S0008-6363(00)00281-9.

68. Masoud, G.N.; Li, W. HIF-1α Pathway: Role, Regulation and Intervention for Cancer Therapy. *Acta Pharm. Sin. B* 2015, *5*, 378–389, doi:10.1016/j.apsb.2015.05.007.

69. Kureshi, C.T.; Dougan, S.K. Cytokines in Cancer. *Cancer Cell* 2025, *43*, 15–35, doi:10.1016/j.ccell.2024.11.011.

70. Levin, L.I.; Breen, E.C.; Birmann, B.M.; Batista, J.L.; Magpantay, L.I.; Li, Y.; Ambinder, R.F.; Mueller, N.E.; Martínez-Maza, O. Elevated Serum Levels of SCD30 and IL6 and Detectable IL10 Precede Classical Hodgkin Lymphoma Diagnosis. *Cancer Epidemiology, Biomarkers & Prevention* 2017, *26*, 1114–1123, doi:10.1158/1055-9965.EPI-16-1012.

71. Unver, N.; McAllister, F. IL-6 Family Cytokines: Key Inflammatory Mediators as Biomarkers and Potential Therapeutic Targets. *Cytokine Growth Factor Rev.* 2018, *41*, 10–17, doi:10.1016/j.cytogfr.2018.04.004.

72. Derynck, R.; Turley, S.J.; Akhurst, R.J. TGFβ Biology in Cancer Progression and Immunotherapy. *Nat. Rev. Clin. Oncol.* 2021, *18*, 9–34, doi:10.1038/s41571-020-0403-1.

73. Lee, C.; Kim, M.-J.; Kumar, A.; Lee, H.-W.; Yang, Y.; Kim, Y. Vascular Endothelial Growth Factor Signaling in Health and Disease: From Molecular Mechanisms to Therapeutic Perspectives. *Signal Transduct. Target. Ther.* 2025, *10*, 170, doi:10.1038/s41392-025-02249-0.

74. Desai, S.A.; Patel, V.P.; Bhosle, K.P.; Nagare, S.D.; Thombare, K.C. The Tumor Microenvironment: Shaping Cancer Progression and Treatment Response. *Journal of Chemotherapy* 2025, *37*, 15–44, doi:10.1080/1120009X.2023.2300224.

75. Campora, S.; Lo Cicero, A. The 3D Language of Cancer: Communication via Extracellular Vesicles from Tumor Spheroids and Organoids. *Int. J. Mol. Sci.* 2025, *26*, 7104, doi:10.3390/ijms26157104.

76. da Silva Correia, A.B.A.; de Souza Melo, B.M.; da Silva, B.A.; Maciel, G.C.; Cavalcante, G.M.S.M.; Almeida dos Santos, J.P.; Silva, L.M.B.; Rocha, L.F.P.; Brêda, M.B.C.; de Oliveira, M.E.T.; et al. Physical Interactions between Cancer Cells and Tumor Microenvironment. *Cell Biochem. Biophys.* 2025, doi:10.1007/s12013-025-01900-5.

77. Bonnans, C.; Chou, J.; Werb, Z. Remodelling the Extracellular Matrix in Development and Disease. *Nat. Rev. Mol. Cell Biol.* 2014, *15*, 786–801, doi:10.1038/nrm3904.

78. Prasad, N.; Topping, R.S.; Decker, S.J. Src Family Tyrosine Kinases Regulate Adhesion-Dependent Tyrosine Phosphorylation of 5′-Inositol Phosphatase SHIP2 during Cell Attachment and Spreading on Collagen I. *J. Cell Sci.* 2002, *115*, 3807–3815, doi:10.1242/jcs.00070.

79. Theocharis, A.D.; Skandalis, S.S.; Gialeli, C.; Karamanos, N.K. Extracellular Matrix Structure. *Adv. Drug Deliv. Rev.* 2016, *97*, 4–27, doi:10.1016/j.addr.2015.11.001.

80. Vaday, G.G.; Lider, O. Extracellular Matrix Moieties, Cytokines, and Enzymes: Dynamic Effects on Immune Cell Behavior and Inflammation. *J. Leukoc. Biol.* 2000, *67*, 149–159, doi:10.1002/jlb.67.2.149.

81. Li, J.; Fan, X.; Wang, Y.; Han, L.; Lin, Y.; Shi, Z.; Liu, W.; Zheng, F.; Wang, H.-S. Targeted Europium Chelation: A Strategy for Intervening Tumor Extracellular Matrix. *Nano Lett.* 2025, *25*, 11440–11448, doi:10.1021/acs.nanolett.5c02693.

82. Jiang, Y.; Zhang, H.; Wang, J.; Liu, Y.; Luo, T.; Hua, H. Targeting Extracellular Matrix Stiffness and Mechanotransducers to Improve Cancer Therapy. *J. Hematol. Oncol.* 2022, *15*, 34, doi:10.1186/s13045-022-01252-0.

83. Xiong, J.; Yan, L.; Zou, C.; Wang, K.; Chen, M.; Xu, B.; Zhou, Z.; Zhang, D. Integrins Regulate Stemness in Solid Tumor: An Emerging Therapeutic Target. *J. Hematol. Oncol.* 2021, *14*, 177, doi:10.1186/s13045-021-01192-1.

84. Piersma, B.; Hayward, M.-K.; Weaver, V.M. Fibrosis and Cancer: A Strained Relationship. *Biochimica et Biophysica Acta (BBA) - Reviews on Cancer* 2020, *1873*, 188356, doi:10.1016/j.bbcan.2020.188356.

85. Lu, P.; Takai, K.; Weaver, V.M.; Werb, Z. Extracellular Matrix Degradation and Remodeling in Development and Disease. *Cold Spring Harb. Perspect. Biol.* 2011, *3*, a005058–a005058, doi:10.1101/cshperspect.a005058.

86. Costa, S.; Ragusa, M.A.; Lo Buglio, G.; Scilabra, S.D.; Nicosia, A. The Repertoire of Tissue Inhibitors of Metalloproteases: Evolution, Regulation of Extracellular Matrix Proteolysis, Engineering and Therapeutic Challenges. . 2022, *12*, 1145, doi:10.3390/life12081145.

87. ZHANG, X.; HUANG, S.; GUO, J.; ZHOU, L.; YOU, L.; ZHANG, T.; ZHAO, Y. Insights into the Distinct Roles of MMP-11 in Tumor Biology and Future Therapeutics (Review). *Int. J. Oncol.* 2016, *48*, 1783–1793, doi:10.3892/ijo.2016.3400.

88. Gommes, C.J.; Louis, T.; Bourgot, I.; Noël, A.; Blacher, S.; Maquoi, E. Remodelling of the Fibre-Aggregate Structure of Collagen Gels by Cancer-Associated Fibroblasts: A Time-Resolved Grey-Tone Image Analysis Based on Stochastic Modelling. *Front. Immunol.* 2023, *13*, doi:10.3389/fimmu.2022.988502.

89. Cannone, S.; Greco, M.R.; Carvalho, T.M.A.; Guizouarn, H.; Soriani, O.; Di Molfetta, D.; Tomasini, R.; Zeeberg, K.; Reshkin, S.J.; Cardone, R.A. Cancer Associated Fibroblast (CAF) Regulation of PDAC Parenchymal (CPC) and CSC Phenotypes Is Modulated by ECM Composition. *Cancers (Basel).* 2022, *14*, 3737, doi:10.3390/cancers14153737.

90. Myllyharju, J.; Schipani, E. Extracellular Matrix Genes as Hypoxia-Inducible Targets. *Cell Tissue Res.* 2010, *339*, 19–29, doi:10.1007/s00441-009-0841-7.

91. Gilkes, D.M.; Bajpai, S.; Chaturvedi, P.; Wirtz, D.; Semenza, G.L. Hypoxia-Inducible Factor 1 (HIF-1) Promotes Extracellular Matrix Remodeling under Hypoxic Conditions by Inducing P4HA1, P4HA2, and PLOD2 Expression in Fibroblasts. *Journal of Biological Chemistry* 2013, *288*, 10819–10829, doi:10.1074/jbc.M112.442939.

92. Eisinger-Mathason, T.S.K.; Zhang, M.; Qiu, Q.; Skuli, N.; Nakazawa, M.S.; Karakasheva, T.; Mucaj, V.; Shay, J.E.S.; Stangenberg, L.; Sadri, N.; et al. Hypoxia-Dependent Modification of Collagen Networks Promotes Sarcoma Metastasis. *Cancer Discov.* 2013, *3*, 1190–1205, doi:10.1158/2159-8290.CD-13-0118.

93. Gilkes, D.M.; Bajpai, S.; Wong, C.C.; Chaturvedi, P.; Hubbi, M.E.; Wirtz, D.; Semenza, G.L. Procollagen Lysyl Hydroxylase 2 Is Essential for Hypoxia-Induced Breast Cancer Metastasis. *Molecular Cancer Research* 2013, *11*, 456–466, doi:10.1158/1541-7786.MCR-12-0629.

94. Xiong, G.; Deng, L.; Zhu, J.; Rychahou, P.G.; Xu, R. Prolyl-4-Hydroxylase α Subunit 2 Promotes Breast Cancer Progression and Metastasis by Regulating Collagen Deposition. *BMC Cancer* 2014, *14*, 1, doi:10.1186/1471-2407-14-1.

95. Petrova, V.; Annicchiarico-Petruzzelli, M.; Melino, G.; Amelio, I. The Hypoxic Tumour Microenvironment. *Oncogenesis* 2018, *7*, 10, doi:10.1038/s41389-017-0011-9.

96. Desai, N.; Sahel, D.; Kubal, B.; Postwala, H.; Shah, Y.; Chavda, V.P.; Fernandes, C.; Khatri, D.K.; Vora, L.K. Role of the Extracellular Matrix in Cancer: Insights into Tumor Progression and Therapy. *Adv. Ther. (Weinh).* 2025, *8*, doi:10.1002/adtp.202400370.

97. Wang, Y.; Wen, X.; Su, C.; You, Y.; Jiang, Z.; Fan, Q.; Zhu, D. The Role of Tenascin-C in Tumor Microenvironments and Its Potential as a Therapeutic Target. *Front. Cell Dev. Biol.* 2025, *13*, doi:10.3389/fcell.2025.1554312.

98. Xue, M.; Jackson, C.J. Extracellular Matrix Reorganization During Wound Healing and Its Impact on Abnormal Scarring. *Adv. Wound Care (New Rochelle).* 2015, *4*, 119–136, doi:10.1089/wound.2013.0485.

99. He, X.; Lee, B.; Jiang, Y. Extracellular Matrix in Cancer Progression and Therapy. *Medical Review* 2022, *2*, 125–139, doi:10.1515/mr-2021-0028.

100. Elgundi, Z.; Papanicolaou, M.; Major, G.; Cox, T.R.; Melrose, J.; Whitelock, J.M.; Farrugia, B.L. Cancer Metastasis: The Role of the Extracellular Matrix and the Heparan Sulfate Proteoglycan Perlecan. *Front. Oncol.* 2020, *9*, doi:10.3389/fonc.2019.01482.

101. Mahout, M.; Schwartz, L.; Attal, R.; Bakkar, A.; Peres, S. Metabolic Modelling Links Warburg Effect to Collagen Formation, Angiogenesis and Inflammation in the Tumoral Stroma. *PLoS One* 2024, *19*, e0313962, doi:10.1371/journal.pone.0313962.

102. Zhang, M.; Zhang, B. Extracellular Matrix Stiffness: Mechanisms in Tumor Progression and Therapeutic Potential in Cancer. *Exp. Hematol. Oncol.* 2025, *14*, 54, doi:10.1186/s40164-025-00647-2.

103. Brizzi, M.F.; Tarone, G.; Defilippi, P. Extracellular Matrix, Integrins, and Growth Factors as Tailors of the Stem Cell Niche. *Curr. Opin. Cell Biol.* 2012, *24*, 645–651, doi:10.1016/j.ceb.2012.07.001.

104. Liu, X.; To, K.K.W.; Zeng, Q.; Fu, L. Effect of Extracellular Vesicles Derived From Tumor Cells on Immune Evasion. *Advanced Science* 2025, *12*, doi:10.1002/advs.202417357.

105. Mai, Z.; Lin, Y.; Lin, P.; Zhao, X.; Cui, L. Modulating Extracellular Matrix Stiffness: A Strategic Approach to Boost Cancer Immunotherapy. *Cell Death Dis.* 2024, *15*, 307, doi:10.1038/s41419-024-06697-4.

106. Liu, Y.; Yao, X.; Zhao, Y.; Fang, D.; Shi, L.; Yang, L.; Song, G.; Cai, K.; Li, L.; Deng, Q.; et al. Mechanotransduction in Response to ECM Stiffening Impairs CGAS Immune Signaling in Tumor Cells. *Cell Rep.* 2023, *42*, 113213, doi:10.1016/j.celrep.2023.113213.

107. Feng, X.; Cao, F.; Wu, X.; Xie, W.; Wang, P.; Jiang, H. Targeting Extracellular Matrix Stiffness for Cancer Therapy. *Front. Immunol.* 2024, *15*, doi:10.3389/fimmu.2024.1467602.

108. Dwairy, M.; Reddy, J.N.; Righetti, R. Predicting Stress and Interstitial Fluid Pressure in Tumors Based on Biphasic Theory. *Comput. Biol. Med.* 2023, *167*, 107651, doi:10.1016/j.compbiomed.2023.107651.

109. Ren, R.; Zhang, S.; Peng, Z.; Ji, X.; Song, H.; Wang, Q.; Sun, X.; Wang, H.; Dong, Y. Matrix Stiffness Regulates Glucose-6-Phosphate Dehydrogenase Expression to Mediate Sorafenib Resistance in Hepatocellular Carcinoma through the ITGB1-PI3K/AKT Pathway. *Cell Death Dis.* 2025, *16*, 538, doi:10.1038/s41419-025-07842-3.

110. He, X.; Zhong, L.; Wang, N.; Zhao, B.; Wang, Y.; Wu, X.; Zheng, C.; Ruan, Y.; Hou, J.; Luo, Y.; et al. Gastric Cancer Actively Remodels Mechanical Microenvironment to Promote Chemotherapy Resistance via MSCs-Mediated Mitochondrial Transfer. *Advanced Science* 2024, *11*, doi:10.1002/advs.202404994.

111. Winkler, J.; Abisoye-Ogunniyan, A.; Metcalf, K.J.; Werb, Z. Concepts of Extracellular Matrix Remodelling in Tumour Progression and Metastasis. *Nat. Commun.* 2020, *11*, 5120, doi:10.1038/s41467-020-18794-x.

112. Vallet, S.D.; Ricard-Blum, S. Lysyl Oxidases: From Enzyme Activity to Extracellular Matrix Cross-Links. *Essays Biochem.* 2019, *63*, 349–364, doi:10.1042/EBC20180050.

113. Fontana, F.; Giannitti, G.; Marchesi, S.; Limonta, P. The PI3K/Akt Pathway and Glucose Metabolism: A Dangerous Liaison in Cancer. *Int. J. Biol. Sci.* 2024, *20*, 3113–3125, doi:10.7150/ijbs.89942.

114. Lee, B.Y.; Timpson, P.; Horvath, L.G.; Daly, R.J. FAK Signaling in Human Cancer as a Target for Therapeutics. *Pharmacol. Ther.* 2015, *146*, 132–149, doi:10.1016/j.pharmthera.2014.10.001.

115. Guo, X.; Bu, X.; Yuan, L.; Ji, L. Collagen Type V Alpha 2 Promotes the Development of Gastric Cancer via M2 Macrophage Polarization. *Chinese Journal of Physiology* 2023, *66*, 93–102, doi:10.4103/cjop.CJOP-D-22-00078.

116. Goenka, A.; Khan, F.; Verma, B.; Sinha, P.; Dmello, C.C.; Jogalekar, M.P.; Gangadaran, P.; Ahn, B. Tumor Microenvironment Signaling and Therapeutics in Cancer Progression. *Cancer Commun.* 2023, *43*, 525–561, doi:10.1002/cac2.12416.

117. Valdembri, D.; Serini, G. The Roles of Integrins in Cancer. *Fac. Rev.* 2021, *10*, doi:10.12703/r/10-45.

118. Sun, Z.; Guo, S.S.; Fässler, R. Integrin-Mediated Mechanotransduction. *Journal of Cell Biology* 2016, *215*, 445–456, doi:10.1083/jcb.201609037.

119. Pang, X.; He, X.; Qiu, Z.; Zhang, H.; Xie, R.; Liu, Z.; Gu, Y.; Zhao, N.; Xiang, Q.; Cui, Y. Targeting Integrin Pathways: Mechanisms and Advances in Therapy. *Signal Transduct. Target. Ther.* 2023, *8*, 1, doi:10.1038/s41392-022-01259-6.

120. Sloan, E.K.; Pouliot, N.; Stanley, K.L.; Chia, J.; Moseley, J.M.; Hards, D.K.; Anderson, R.L. Tumor-Specific Expression of Avβ3 Integrin Promotes Spontaneous Metastasis of Breast Cancer to Bone. *Breast Cancer Research* 2006, *8*, R20, doi:10.1186/bcr1398.

121. Mao, L.; Wang, L.; Xu, J.; Zou, J. The Role of Integrin Family in Bone Metabolism and Tumor Bone Metastasis. *Cell Death Discov.* 2023, *9*, 119, doi:10.1038/s41420-023-01417-x.

122. Hill, B.S.; Sarnella, A.; Capasso, D.; Comegna, D.; Del Gatto, A.; Gramanzini, M.; Albanese, S.; Saviano, M.; Zaccaro, L.; Zannetti, A. Therapeutic Potential of a Novel Avβ3 Antagonist to Hamper the Aggressiveness of Mesenchymal Triple Negative Breast Cancer Sub-Type. *Cancers (Basel).* 2019, *11*, 139, doi:10.3390/cancers11020139.

123. Yang, L.; Hou, Y.; Yuan, J.; Tang, S.; Zhang, H.; Zhu, Q.; Du, Y.; Zhou, M.; Wen, S.; Xu, L.; et al. Twist Promotes Reprogramming of Glucose Metabolism in Breast Cancer Cells through PI3K/AKT and P53 Signaling Pathways. *Oncotarget* 2015, *6*, 25755–25769, doi:10.18632/oncotarget.4697.

124. Artym, V. V.; Swatkoski, S.; Matsumoto, K.; Campbell, C.B.; Petrie, R.J.; Dimitriadis, E.K.; Li, X.; Mueller, S.C.; Bugge, T.H.; Gucek, M.; et al. Dense Fibrillar Collagen Is a Potent Inducer of Invadopodia via a Specific Signaling Network. *Journal of Cell Biology* 2015, *208*, 331–350, doi:10.1083/jcb.201405099.

125. Medici, D.; Nawshad, A. Type I Collagen Promotes Epithelial–Mesenchymal Transition through ILK-Dependent Activation of NF-KB and LEF-1. *Matrix Biology* 2010, *29*, 161–165, doi:10.1016/j.matbio.2009.12.003.

126. Su, H.; Yang, F.; Fu, R.; Trinh, B.; Sun, N.; Liu, J.; Kumar, A.; Baglieri, J.; Siruno, J.; Le, M.; et al. Collagenolysis-Dependent DDR1 Signalling Dictates Pancreatic Cancer Outcome. *Nature* 2022, *610*, 366–372, doi:10.1038/s41586-022-05169-z.

127. Wu, Y.; Liu, X.; Zhu, Y.; Qiao, Y.; Gao, Y.; Chen, J.; Ge, G. Type IV Collagen α 5 Chain Promotes Luminal Breast Cancer Progression through c-Myc-Driven Glycolysis. *J. Mol. Cell Biol.* 2023, *14*, doi:10.1093/jmcb/mjac068.

128. Sharom, F.J. ABC Multidrug Transporters: Structure, Function and Role in Chemoresistance. *Pharmacogenomics* 2008, *9*, 105–127, doi:10.2217/14622416.9.1.105.

129. Baltes, F.; Pfeifer, V.; Silbermann, K.; Caspers, J.; Wantoch von Rekowski, K.; Schlesinger, M.; Bendas, G. B1-Integrin Binding to Collagen Type 1 Transmits Breast Cancer Cells into Chemoresistance by Activating ABC Efflux Transporters. *Biochimica et Biophysica Acta (BBA) - Molecular Cell Research* 2020, *1867*, 118663, doi:10.1016/j.bbamcr.2020.118663.

130. Wu, Y.-H.; Huang, Y.-F.; Wu, P.-Y.; Chang, T.-H.; Huang, S.-C.; Chou, C.-Y. The Downregulation of MiR-509-3p Expression by Collagen Type XI Alpha 1-Regulated Hypermethylation Facilitates Cancer Progression and Chemoresistance via the DNA Methyltransferase 1/Small Ubiquitin-like Modifier-3 Axis in Ovarian Cancer Cells. *J. Ovarian Res.* 2023, *16*, 124, doi:10.1186/s13048-023-01191-5.

131. Liu, J.; Chiang, H.-C.; Xiong, W.; Laurent, V.; Griffiths, S.C.; Dülfer, J.; Deng, H.; Sun, X.; Yin, Y.W.; Li, W.; et al. A Highly Selective Humanized DDR1 MAb Reverses Immune Exclusion by Disrupting Collagen Fiber Alignment in Breast Cancer. *J. Immunother. Cancer* 2023, *11*, e006720, doi:10.1136/jitc-2023-006720.

132. Rodriguez, B.L.; Huang, J.; Gibson, L.; Fradette, J.J.; Chen, H.-I.H.; Koyano, K.; Cortez, C.; Li, B.; Ho, C.; Ashique, A.M.; et al. Antitumor Activity of a Novel LAIR1 Antagonist in Combination with Anti-PD1 to Treat Collagen-Rich Solid

Tumors. *Mol. Cancer Ther.* 2024, *23*, 1144–1158, doi:10.1158/1535-7163.MCT-23-0866.

133. Vijver, S. V.; Singh, A.; Mommers-Elshof, E.T.A.M.; Meeldijk, J.; Copeland, R.; Boon, L.; Langermann, S.; Flies, D.; Meyaard, L.; Ramos, M.I.P. Collagen Fragments Produced in Cancer Mediate T Cell Suppression Through Leukocyte-Associated Immunoglobulin-Like Receptor 1. *Front. Immunol.* 2021, *12*, doi:10.3389/fimmu.2021.733561.

134. Provenzano, P.P.; Hingorani, S.R. Hyaluronan, Fluid Pressure, and Stromal Resistance in Pancreas Cancer. *Br. J. Cancer* 2013, *108*, 1–8, doi:10.1038/bjc.2012.569.

135. Stylianopoulos, T.; Martin, J.D.; Chauhan, V.P.; Jain, S.R.; Diop-Frimpong, B.; Bardeesy, N.; Smith, B.L.; Ferrone, C.R.; Hornicek, F.J.; Boucher, Y.; et al. Causes, Consequences, and Remedies for Growth-Induced Solid Stress in Murine and Human Tumors. *Proceedings of the National Academy of Sciences* 2012, *109*, 15101–15108, doi:10.1073/pnas.1213353109.

136. Yu, B.; Wang, W.; Zhang, Y.; Sun, Y.; Li, C.; Liu, Q.; Zhen, X.; Jiang, X.; Wu, W. Enhancing the Tumor Penetration of Multiarm Polymers by Collagenase Modification. *Biomater. Sci.* 2024, *12*, 2302–2311, doi:10.1039/D3BM02123H.

137. Druzhkova, I.; Nikonova, E.; Ignatova, N.; Koryakina, I.; Zyuzin, M.; Mozherov, A.; Kozlov, D.; Krylov, D.; Kuznetsova, D.; Lisitsa, U.; et al. Effect of Collagen Matrix on Doxorubicin Distribution and Cancer Cells' Response to Treatment in 3D Tumor Model. *Cancers (Basel).* 2022, *14*, 5487, doi:10.3390/cancers14225487.

138. Tsou, S.-H.; Chen, T.-M.; Hsiao, H.-T.; Chen, Y.-H. A Critical Dose of Doxorubicin Is Required to Alter the Gene Expression Profiles in MCF-7 Cells Acquiring Multidrug Resistance. *PLoS One* 2015, *10*, e0116747, doi:10.1371/journal.pone.0116747.

139. Tian, Y.; Lei, Y.; Wang, Y.; Lai, J.; Wang, J.; Xia, F. Mechanism of Multidrug Resistance to Chemotherapy Mediated by P-glycoprotein (Review). *Int. J. Oncol.* 2023, *63*, 119, doi:10.3892/ijo.2023.5567.

140. Sawazaki, H.; Ito, K.; Asano, T.; Kuroda, K.; Horiguchi, A.; Tsuda, H.; Asano, T. Expressions of P-Glycoprotein, Multidrug Resistance Protein 1 and Annexin A2 as Predictive Factors for Intravesical Recurrence of Bladder Cancer after the Initial Transurethral Resection and Immediate Single Intravesical Instillation of Adriamycin. *Asian Pacific Journal of Cancer Prevention* 2021, *22*, 1459–1466, doi:10.31557/APJCP.2021.22.5.1459.

141. Khawar, I.A.; Kim, J.H.; Kuh, H.-J. Improving Drug Delivery to Solid Tumors: Priming the Tumor Microenvironment. *Journal of Controlled Release* 2015, *201*, 78–89, doi:10.1016/j.jconrel.2014.12.018.

142. Wang, J.; Chan, D.K.W.; Sen, A.; Ma, W.W.; Straubinger, R.M. Tumor Priming by SMO Inhibition Enhances Antibody Delivery and Efficacy in a Pancreatic Ductal Adenocarcinoma Model. *Mol. Cancer Ther.* 2019, *18*, 2074–2084, doi:10.1158/1535-7163.MCT-18-0354.

143. He, J.; Liu, Z.; Zhu, X.; Xia, H.; Gao, H.; Lu, J. Ultrasonic Microbubble Cavitation Enhanced Tissue Permeability and Drug Diffusion in Solid Tumor Therapy. *Pharmaceutics* 2022, *14*, 1642, doi:10.3390/pharmaceutics14081642.

144. Xiang, Y.; Tang, L.; Pang, H.; Xu, H.; He, Y.; Feng, Y.; Ju, L.; Zhang, L.; Wang, D. Ultrasound -Induced Thermal Effect Enhances the Efficacy of Chemotherapy and Immunotherapy in Tumor Treatment. *Int. J. Nanomedicine* 2024, *Volume 19*, 6677–6692, doi:10.2147/IJN.S464830.

145. Farr, N.; Wang, Y.-N.; D'Andrea, S.; Starr, F.; Partanen, A.; Gravelle, K.M.; McCune, J.S.; Risler, L.J.; Whang, S.G.; Chang, A.; et al. Hyperthermia-Enhanced Targeted Drug Delivery Using Magnetic Resonance-Guided Focussed Ultrasound: A Pre-Clinical Study in a Genetic Model of Pancreatic Cancer. *International Journal of Hyperthermia* 2018, *34*, 284–291, doi:10.1080/02656736.2017.1336675.

146. Chen, Q.; Liu, S.; Qin, P.; Xue, J.; Deng, P.; Li, Z.; Whitelock, J.; Guo, T.; Liang, K. Improving Extracellular Matrix Penetration with Biocatalytic Metal–Organic Framework Nanoswimmers. *J. Mater. Chem. B* 2025, *13*, 8897–8907, doi:10.1039/D5TB00509D.

147. García-Olmo, D.; Villarejo Campos, P.; Barambio, J.; Gomez-Heras, S.G.; Vega-Clemente, L.; Olmedillas-Lopez, S.; Guadalajara, H.; Garcia-Arranz, M. Intraperitoneal Collagenase as a Novel Therapeutic Approach in an Experimental Model of Colorectal Peritoneal Carcinomatosis. *Sci. Rep.* 2021, *11*, 503, doi:10.1038/s41598-020-79721-0.

148. Zhao, Z.; Li, Q.; Qu, C.; Jiang, Z.; Jia, G.; Lan, G.; Luan, Y. A Collagenase Nanogel Backpack Improves CAR-T Cell Therapy Outcomes in Pancreatic Cancer. *Nat. Nanotechnol.* 2025, *20*, 1131–1141, doi:10.1038/s41565-025-01924-1.

149. Pan, A.; Wang, Z.; Chen, B.; Dai, W.; Zhang, H.; He, B.; Wang, X.; Wang, Y.; Zhang, Q. Localized Co-Delivery of Collagenase and Trastuzumab by Thermosensitive Hydrogels for Enhanced Antitumor Efficacy in Human Breast Xenograft. *Drug Deliv.* 2018, *25*, 1495–1503, doi:10.1080/10717544.2018.1474971.

150. Wang, Y.; Zhou, Q.; Luo, W.; Yang, X.; Zhang, J.; Lou, Y.; Mao, J.; Chen, J.; Wu, F.; Hou, J.; et al. A Collagenase-Decorated Cu-Based Nanotheranostics: Remodeling Extracellular Matrix for Optimizing Cuproptosis and MRI in Pancreatic Ductal Adenocarcinoma. *J. Nanobiotechnology* 2024, *22*, 689, doi:10.1186/s12951-024-02968-6.

151. Li, J.; Gong, C.; Chen, X.; Guo, H.; Tai, Z.; Ding, N.; Gao, S.; Gao, Y. Biomimetic Liposomal Nanozymes Improve Breast Cancer Chemotherapy with Enhanced Penetration and Alleviated Hypoxia. *J. Nanobiotechnology* 2023, *21*, 123, doi:10.1186/s12951-023-01874-7.

152. Wang, J.; Wu, Q.; Wang, Y.; Xiang, L.; Feng, J.; Zhou, Z.; Fu, Q.; Zhang, L. Collagenase-Loaded PH-Sensitive Nanocarriers Efficiently Remodeled Tumor Stroma Matrixes and Improved the Enrichment of Nanomedicines. *Nanoscale* 2021, *13*, 9402–9414, doi:10.1039/D1NR00950H.

153. Huang, H.-Y.; Chen, L.-Q.; Sun, W.; Du, H.-H.; Dong, S.; Ahmed, A.M.Q.; Cao, D.; Cui, J.-H.; Zhang, Y.; Cao, Q.-R. Collagenase IV and Clusterin-Modified

Polycaprolactone-Polyethylene Glycol Nanoparticles for Penetrating Dense Tumor Tissues. *Theranostics* 2021, *11*, 906–924, doi:10.7150/thno.47446.

154. Hauge, A.; Rofstad, E.K. Antifibrotic Therapy to Normalize the Tumor Microenvironment. *J. Transl. Med.* 2020, *18*, 207, doi:10.1186/s12967-020-02376-y.

155. Wang, S.; Li, J.; Zhao, Y. Targeting Collagen in "Armored and Cold" Tumors: Overcoming Barriers to Cancer Therapy. *Cancer Pathogenesis and Therapy* 2025, *3*, 383–391, doi:10.1016/j.cpt.2024.11.001.

156. Alderton, G.K. Hedgehog Doesn't... *Nat. Rev. Cancer* 2009, *9*, 455–455, doi:10.1038/nrc2688.

157. Cetin, M.; Saatci, O.; Rezaeian, A.-H.; Rao, C.N.; Beneker, C.; Sreenivas, K.; Taylor, H.; Pederson, B.; Chatzistamou, I.; Buckley, B.; et al. A Highly Potent Bi-Thiazole Inhibitor of LOX Rewires Collagen Architecture and Enhances Chemoresponse in Triple-Negative Breast Cancer. *Cell Chem. Biol.* 2024, *31*, 1926-1941.e11, doi:10.1016/j.chembiol.2024.06.012.

158. Sarohi, V. Comprehensive Analysis of the Effects of P4ha1 and P4ha2 Deletion on Post-Translational Modifications of Fibrillar Collagens in Mouse Skin. *Front. Cell Dev. Biol.* 2025, *13*, doi:10.3389/fcell.2025.1527839.

159. Ong, C.H.; Tham, C.L.; Harith, H.H.; Firdaus, N.; Israf, D.A. TGF-β-Induced Fibrosis: A Review on the Underlying Mechanism and Potential Therapeutic Strategies. *Eur. J. Pharmacol.* 2021, *911*, 174510, doi:10.1016/j.ejphar.2021.174510.

160. Berestjuk, I.; Lecacheur, M.; Carminati, A.; Diazzi, S.; Rovera, C.; Prod'homme, V.; Ohanna, M.; Popovic, A.; Mallavialle, A.; Larbret, F.; et al. Targeting Discoidin Domain Receptors DDR1 and DDR2 Overcomes Matrix-mediated Tumor Cell Adaptation and Tolerance to BRAF-targeted Therapy in Melanoma. *EMBO Mol. Med.* 2022, *14*, doi:10.15252/emmm.201911814.

161. Hunter, E.J.; Hamaia, S.W.; Gullberg, D.; Malcor, J.-D.; Farndale, R.W. Selectivity of the Collagen-Binding Integrin Inhibitors, TC-I-15 and Obtustatin. *Toxicol. Appl. Pharmacol.* 2021, *428*, 115669, doi:10.1016/j.taap.2021.115669.

162. Brassart-Pasco, S.; Sénéchal, K.; Thevenard, J.; Ramont, L.; Devy, J.; Di Stefano, L.; Dupont-Deshorgue, A.; Brézillon, S.; Feru, J.; Jazeron, J.-F.; et al. Tetrastatin, the NC1 Domain of the A4(IV) Collagen Chain: A Novel Potent Anti-Tumor Matrikine. *PLoS One* 2012, *7*, e29587, doi:10.1371/journal.pone.0029587.

163. Paturel, V.; Baud, S.; Schneider, C.; Brassart-Pasco, S. In Silico Prediction of Tetrastatin-Derived Peptide Interactions with Avβ3 and A5β1 Integrins. *Pharmaceuticals* 2025, *18*, 940, doi:10.3390/ph18070940.

164. Martin, E.M.; Chang, J.; González, A.; Genovese, F. Circulating Collagen Type I Fragments as Specific Biomarkers of Cardiovascular Outcome Risk: Where Are the Opportunities? *Matrix Biology* 2025, *137*, 19–32, doi:10.1016/j.matbio.2025.03.001.

165. Cheng, J.; Sauthoff, H.; Huang, Y.; Kutler, D.I.; Bajwa, S.; Rom, W.N.; Hay, J.G. Human Matrix Metalloproteinase-8 Gene Delivery Increases the Oncolytic Activity

of a Replicating Adenovirus. *Molecular Therapy* 2007, *15*, 1982–1990, doi:10.1038/sj.mt.6300264.

166. Ebelt, N.D.; Zamloot, V.; Zuniga, E.; Passi, K.B.; Sobocinski, L.J.; Young, C.A.; Blazar, B.R.; Manuel, E.R. Collagenase-Expressing Salmonella Targets Major Collagens in Pancreatic Cancer Leading to Reductions in Immunosuppressive Subsets and Tumor Growth. *Cancers (Basel).* 2021, *13*, 3565, doi:10.3390/cancers13143565.

167. Wang, Y.; Zhang, F.; Qian, Z.; Jiang, Y.; Wu, D.; Liu, L.; Ning, X.; Mei, J.; Chen, D.; Zhang, Y. Targeting Collagen to Optimize Cancer Immunotherapy. *Exp. Hematol. Oncol.* 2025, *14*, 101, doi:10.1186/s40164-025-00691-y.

168. Yang, C.; Liao, X.; Zhou, K.; Yao, Y.; He, X.; Zhong, W.; Zheng, D.; Yang, Y.; Li, M.; Zhou, M.; et al. Multifunctional Nanoparticles and Collagenase Dual Loaded Thermosensitive Hydrogel System for Enhanced Tumor-Penetration, Reversed Immune Suppression and Photodynamic-Immunotherapy. *Bioact. Mater.* 2025, *48*, 1–17, doi:10.1016/j.bioactmat.2025.02.014.

169. Dolor, A.; Szoka, F.C. Digesting a Path Forward: The Utility of Collagenase Tumor Treatment for Improved Drug Delivery. *Mol. Pharm.* 2018, *15*, 2069–2083, doi:10.1021/acs.molpharmaceut.8b00319.

170. Warwick, D.; Arandes-Renú, J.M.; Pajardi, G.; Witthaut, J.; Hurst, L.C. *Collagenase Clostridium Histolyticum :* Emerging Practice Patterns and Treatment Advances. *J. Plast. Surg. Hand Surg.* 2016, *50*, 251–261, doi:10.3109/2000656X.2016.1159568.

171. de la Fuente, M.; Lombardero, L.; Gómez-González, A.; Solari, C.; Angulo-Barturen, I.; Acera, A.; Vecino, E.; Astigarraga, E.; Barreda-Gómez, G. Enzyme Therapy: Current Challenges and Future Perspectives. *Int. J. Mol. Sci.* 2021, *22*, 9181, doi:10.3390/ijms22179181.

172. Costas, B.; Coleman, S.; Kaufman, G.; James, R.; Cohen, B.; Gaston, R.G. Efficacy and Safety of Collagenase Clostridium Histolyticum for Dupuytren Disease Nodules: A Randomized Controlled Trial. *BMC Musculoskelet. Disord.* 2017, *18*, 374, doi:10.1186/s12891-017-1713-z.

173. Wang, Z.-Z.; Wang, K.; Xu, L.-F.; Su, C.; Gong, J.-S.; Shi, J.-S.; Ma, X.-D.; Xie, N.; Qian, J.-Y. Unlocking the Potential of Collagenases: Structures, Functions, and Emerging Therapeutic Horizons. *BioDesign Research* 2024, *6*, 0050, doi:10.34133/bdr.0050.

174. Boneva, B.; Ralchev, N.; Ganova, P.; Tchorbanov, A.; Mihaylova, N. Collagenase-Induced Mouse Model of Osteoarthritis—A Thorough Flow Cytometry Analysis. . 2022, *12*, 1938, doi:10.3390/life12111938.

175. Yata, T.; Lee, E.L.Q.; Suwan, K.; Syed, N.; Asavarut, P.; Hajitou, A. Modulation of Extracellular Matrix in Cancer Is Associated with Enhanced Tumor Cell Targeting by Bacteriophage Vectors. *Mol. Cancer* 2015, *14*, 110, doi:10.1186/s12943-015-0383-4.

176. Baldari, S.; Di Modugno, F.; Nisticò, P.; Toietta, G. Strategies for Efficient Targeting of Tumor Collagen for Cancer Therapy. *Cancers (Basel).* 2022, *14*, 4706, doi:10.3390/cancers14194706.

177. Paradiso, F.; Serpelloni, S.; Francis, L.W.; Taraballi, F. Mechanical Studies of the Third Dimension in Cancer: From 2D to 3D Model. *Int. J. Mol. Sci.* 2021, *22*, 10098, doi:10.3390/ijms221810098.

178. Steinberg, T.; Dieterle, M.P.; Ramminger, I.; Klein, C.; Brossette, J.; Husari, A.; Tomakidi, P. On the Value of In Vitro Cell Systems for Mechanobiology from the Perspective of Yes-Associated Protein/Transcriptional Co-Activator with a PDZ-Binding Motif and Focal Adhesion Kinase and Their Involvement in Wound Healing, Cancer, Aging, and Senescence. *Int. J. Mol. Sci.* 2023, *24*, 12677, doi:10.3390/ijms241612677.

179. Guerrero-López, P.; Martín-Pardillos, A.; Bonet-Aleta, J.; Mosseri, A.; Hueso, J.L.; Santamaria, J.; Garcia-Aznar, J.M. 2D versus 3D Tumor-on-Chip Models to Study the Impact of Tumor Organization on Metabolic Patterns in Vitro. *Sci. Rep.* 2025, *15*, 19506, doi:10.1038/s41598-025-03504-8.

180. Habanjar, O.; Diab-Assaf, M.; Caldefie-Chezet, F.; Delort, L. 3D Cell Culture Systems: Tumor Application, Advantages, and Disadvantages. *Int. J. Mol. Sci.* 2021, *22*, 12200, doi:10.3390/ijms222212200.

181. Pinto, B.; Henriques, A.C.; Silva, P.M.A.; Bousbaa, H. Three-Dimensional Spheroids as In Vitro Preclinical Models for Cancer Research. *Pharmaceutics* 2020, *12*, 1186, doi:10.3390/pharmaceutics12121186.

182. Arora, S.; Singh, S.; Mittal, A.; Desai, N.; Khatri, D.K.; Gugulothu, D.; Lather, V.; Pandita, D.; Vora, L.K. Spheroids in Cancer Research: Recent Advances and Opportunities. *J. Drug Deliv. Sci. Technol.* 2024, *100*, 106033, doi:10.1016/j.jddst.2024.106033.

183. Garnique, A. del M.B.; Parducci, N.S.; de Miranda, L.B.L.; de Almeida, B.O.; Sanches, L.; Machado-Neto, J.A. Two-Dimensional and Spheroid-Based Three-Dimensional Cell Culture Systems: Implications for Drug Discovery in Cancer. *Drugs and Drug Candidates* 2024, *3*, 391–409, doi:10.3390/ddc3020024.

184. Vakhshiteh, F.; Bagheri, Z.; Soleimani, M.; Ahvaraki, A.; Pournemat, P.; Alavi, S.E.; Madjd, Z. Heterotypic Tumor Spheroids: A Platform for Nanomedicine Evaluation. *J. Nanobiotechnology* 2023, *21*, 249, doi:10.1186/s12951-023-02021-y.

185. Hofmann, S.; Cohen-Harazi, R.; Maizels, Y.; Koman, I. Patient-Derived Tumor Spheroid Cultures as a Promising Tool to Assist Personalized Therapeutic Decisions in Breast Cancer. *Transl. Cancer Res.* 2022, *11*, 134–147, doi:10.21037/tcr-21-1577.

186. Moskovits, N.; Itzhaki, E.; Tarasenko, N.; Chausky, E.; Bareket-Samish, A.; Kaufman, A.; Meerson, R.; Stemmer, S.M. Establishing 3-Dimensional Spheroids from Patient-Derived Tumor Samples and Evaluating Their Sensitivity to Drugs. *Journal of Visualized Experiments* 2022, doi:10.3791/64564.

187. Shin, S.; Choi, Y.; Jang, W.; Ulziituya, B.; Ha, G.; Kang, R.; Park, S.; Kim, M.; Zhang, Y.S.; Kim, H.-J.; et al. A Vascularized Tumors-on-a-Chip Model for Studying

Tumor-Angiogenesis Interplay, Heterogeneity and Drug Responses. *Mater. Today Bio* 2025, *32*, 101741, doi:10.1016/j.mtbio.2025.101741.

188. Subia, B.; Patel, A.; Nathwani, S.; Ghoshdastidar, K.; Jain, M.; Viswanathan, K. Simulating Tumor Complexity: 3D Pancreatic Tumor Spheroid Model for Improved Drug Screening. *Hum. Cell* 2025, *38*, 149, doi:10.1007/s13577-025-01277-w.

189. Bang, J.; Yeo, J.; Lee, S.J.; Lee, H.; Kim, J.; Jeong, S.; Kang, E.; Rho, H.S.; Kim, Y.; Park, J.-O. A 3D Vascularized Tumor Spheroid Microfluidic Platform for Head and Neck Cancer Research: New Insights. *Biomed. Microdevices* 2025, *27*, 25, doi:10.1007/s10544-025-00748-z.

190. Nakod, P.S.; Kim, Y.; Rao, S.S. The Impact of Astrocytes and Endothelial Cells on Glioblastoma Stemness Marker Expression in Multicellular Spheroids. *Cell. Mol. Bioeng.* 2021, *14*, 639–651, doi:10.1007/s12195-021-00691-y.

191. Campora, S.; Ghersi, G. Recent Developments and Applications of Smart Nanoparticles in Biomedicine. *Nanotechnol. Rev.* 2022, *11*, 2595–2631, doi:10.1515/ntrev-2022-0148.

192. Badparvar, F.; Marjani, A.P.; Salehi, R.; Ramezani, F. PH/Redox Responsive Size-switchable Intelligent Nanovehicle for Tumor Microenvironment Targeted DOX Release. *Sci. Rep.* 2023, *13*, 22475, doi:10.1038/s41598-023-49446-x.

193. Bravo, M.; Fortuni, B.; Mulvaney, P.; Hofkens, J.; Uji-i, H.; Rocha, S.; Hutchison, J.A. Nanoparticle-Mediated Thermal Cancer Therapies: Strategies to Improve Clinical Translatability. *Journal of Controlled Release* 2024, *372*, 751–777, doi:10.1016/j.jconrel.2024.06.055.

194. Xu, M.; Qi, Y.; Liu, G.; Song, Y.; Jiang, X.; Du, B. Size-Dependent *In Vivo* Transport of Nanoparticles: Implications for Delivery, Targeting, and Clearance. *ACS Nano* 2023, *17*, 20825–20849, doi:10.1021/acsnano.3c05853.

195. Suk, J.S.; Xu, Q.; Kim, N.; Hanes, J.; Ensign, L.M. PEGylation as a Strategy for Improving Nanoparticle-Based Drug and Gene Delivery. *Adv. Drug Deliv. Rev.* 2016, *99*, 28–51, doi:10.1016/j.addr.2015.09.012.

196. Xu, B.; Li, S.; Shi, R.; Liu, H. Multifunctional Mesoporous Silica Nanoparticles for Biomedical Applications. *Signal Transduct. Target. Ther.* 2023, *8*, 435, doi:10.1038/s41392-023-01654-7.

197. Mashima, R.; Takada, S. Lipid Nanoparticles: A Novel Gene Delivery Technique for Clinical Application. *Curr. Issues Mol. Biol.* 2022, *44*, 5013–5027, doi:10.3390/cimb44100341.

198. Eltaib, L. Polymeric Nanoparticles in Targeted Drug Delivery: Unveiling the Impact of Polymer Characterization and Fabrication. *Polymers (Basel).* 2025, *17*, 833, doi:10.3390/polym17070833.

199. Zha, S.; Liu, H.; Li, H.; Li, H.; Wong, K.-L.; All, A.H. Functionalized Nanomaterials Capable of Crossing the Blood–Brain Barrier. *ACS Nano* 2024, *18*, 1820–1845, doi:10.1021/acsnano.3c10674.

200. Bu, X.; Ji, N.; Dai, L.; Dong, X.; Chen, M.; Xiong, L.; Sun, Q. Self-Assembled Micelles Based on Amphiphilic Biopolymers for Delivery of Functional Ingredients. *Trends Food Sci. Technol.* 2021, *114*, 386–398, doi:10.1016/j.tifs.2021.06.001.

201. Sand, K.M.K.; Bern, M.; Nilsen, J.; Noordzij, H.T.; Sandlie, I.; Andersen, J.T. Unraveling the Interaction between FcRn and Albumin: Opportunities for Design of Albumin-Based Therapeutics. *Front. Immunol.* 2015, *5*, doi:10.3389/fimmu.2014.00682.

202. Ji, Q.; Zhu, H.; Qin, Y.; Zhang, R.; Wang, L.; Zhang, E.; Zhou, X.; Meng, R. GP60 and SPARC as Albumin Receptors: Key Targeted Sites for the Delivery of Antitumor Drugs. *Front. Pharmacol.* 2024, *15*, doi:10.3389/fphar.2024.1329636.

203. Yang, Z.; Zhang, N.; Ma, T.; Liu, L.; Zhao, L.; Xie, H. Engineered Bovine Serum Albumin-Based Nanoparticles with PH-Sensitivity for Doxorubicin Delivery and Controlled Release. *Drug Deliv.* 2020, *27*, 1156–1164, doi:10.1080/10717544.2020.1797243.

204. Sánchez-Segura, L.; Zaina, S.; Kú-González, A.F.; Guzmán-López, J.A.; Zavala-García, L.E.; López, M.G. Effect of Crosslinking Using Heat on the Physicochemical Features of Bsa–Capsaicin Nanoparticles. *Pharmaceutics* 2025, *17*, 1306, doi:10.3390/pharmaceutics17101306.

205. Yadav, P.; Yadav, A.B. Preparation and Characterization of BSA as a Model Protein Loaded Chitosan Nanoparticles for the Development of Protein-/Peptide-Based Drug Delivery System. *Futur. J. Pharm. Sci.* 2021, *7*, 200, doi:10.1186/s43094-021-00345-w.

206. Yu, Y.; Ghalandari, B.; Shen, G.; Wang, L.; Liu, X.; Wang, A.; Li, S.; Xie, H.; Ding, X. Poly (N-Vinylpyrrolidone) Modification Mitigates Plasma Protein Corona Formation on Phosphomolybdate-Based Nanoparticles. *J. Nanobiotechnology* 2021, *19*, 445, doi:10.1186/s12951-021-01140-8.

207. Adamo, G.; Grimaldi, N.; Campora, S.; Bulone, D.; Bondì, M.; Al-Sheikhly, M.; Sabatino, M.; Dispenza, C.; Ghersi, G. Multi-Functional Nanogels for Tumor Targeting and Redox-Sensitive Drug and SiRNA Delivery. *Molecules* 2016, *21*, 1594, doi:10.3390/molecules21111594.

208. Vauthier, C.; Bouchemal, K. Methods for the Preparation and Manufacture of Polymeric Nanoparticles. *Pharm. Res.* 2009, *26*, 1025–1058, doi:10.1007/s11095-008-9800-3.

209. An, J.-C.; Weaver, A.; Kim, B.; Barkatt, A.; Poster, D.; Vreeland, W.N.; Silverman, J.; Al-Sheikhly, M. Radiation-Induced Synthesis of Poly(Vinylpyrrolidone) Nanogel. *Polymer (Guildf).* 2011, *52*, 5746–5755, doi:10.1016/j.polymer.2011.09.056.

210. Kuskov, A.; Nikitovic, D.; Berdiaki, A.; Shtilman, M.; Tsatsakis, A. Amphiphilic Poly-N-Vinylpyrrolidone Nanoparticles as Carriers for Nonsteroidal, Anti-Inflammatory Drugs: Pharmacokinetic, Anti-Inflammatory, and Ulcerogenic Activity Study. *Pharmaceutics* 2022, *14*, 925, doi:10.3390/pharmaceutics14050925.

211. Di Pasquale, R.; Vaccaro, S.; Caputo, M.; Cuppari, C.; Caruso, S.; Catania, A.; Messina, L. Collagenase-assisted Wound Bed Preparation: An in Vitro Comparison between *Vibrio Alginolyticus* and *Clostridium Histolyticum* Collagenases on Substrate Specificity. *Int. Wound J.* 2019, *16*, 1013–1023, doi:10.1111/iwj.13148.

212. Vargas, F.; Vives-Pi, M.; Somoza, N.; Armengol, P.; Alcalde, L.; Mart??, M.; Costa, M.; Serradell, L.; Dominguez, O.; Fern??ndez-Llamazares, J.; et al. ENDOTOXIN CONTAMINATION MAY BE RESPONSIBLE FOR THE UNEXPLAINED FAILURE OF HUMAN PANCREATIC ISLET TRANSPLANTATION1. *Transplantation* 1998, *65*, 722–727, doi:10.1097/00007890-199803150-00020.

213. Malla, S.; Prasad Niraula, N.; Singh, B.; Liou, K.; Kyung Sohng, J. Limitations in Doxorubicin Production from Streptomyces Peucetius. *Microbiol. Res.* 2010, *165*, 427–435, doi:10.1016/j.micres.2009.11.006.

214. Sheibani, M.; Azizi, Y.; Shayan, M.; Nezamoleslami, S.; Eslami, F.; Farjoo, M.H.; Dehpour, A.R. Doxorubicin-Induced Cardiotoxicity: An Overview on Pre-Clinical Therapeutic Approaches. *Cardiovasc. Toxicol.* 2022, *22*, 292–310, doi:10.1007/s12012-022-09721-1.

215. Heffelfinger, S.C.; Gear, R.B.; Taylor, K.; Ann Miller, M.; Schneider, J.; LaDow, K.; Warshawsky, D. DMBA-Induced Mammary Pathologies Are Angiogenic In Vivo and In Vitro. *Laboratory Investigation* 2000, *80*, 485–492, doi:10.1038/labinvest.3780054.

216. Wiśniewski, J.R.; Zougman, A.; Nagaraj, N.; Mann, M. Universal Sample Preparation Method for Proteome Analysis. *Nat. Methods* 2009, *6*, 359–362, doi:10.1038/nmeth.1322.

217. Rappsilber, J.; Ishihama, Y.; Mann, M. Stop and Go Extraction Tips for Matrix-Assisted Laser Desorption/Ionization, Nanoelectrospray, and LC/MS Sample Pretreatment in Proteomics. *Anal. Chem.* 2003, *75*, 663–670, doi:10.1021/ac026117i.

218. Rabienezhad Ganji, N.; Urzì, O.; Tinnirello, V.; Costanzo, E.; Polito, G.; Palumbo Piccionello, A.; Manno, M.; Raccosta, S.; Gallo, A.; Lo Pinto, M.; et al. Proof-of-Concept Study on the Use of Tangerine-Derived Nanovesicles as SiRNA Delivery Vehicles toward Colorectal Cancer Cell Line SW480. *Int. J. Mol. Sci.* 2023, *25*, 546, doi:10.3390/ijms25010546.

219. Salamone, M.; Rigogliuso, S.; Nicosia, A.; Campora, S.; Bruno, C.M.; Ghersi, G. 3D Collagen Hydrogel Promotes In Vitro Langerhans Islets Vascularization through Ad-MVFs Angiogenic Activity. *Biomedicines* 2021, *9*, 739, doi:10.3390/biomedicines9070739.

220. Adefisan-Adeoye, A.O.; Ayanbanjo, O.O.; Adeoye, T.D.; Jayesimi, T.E.; Unuofin, J.O.; Lebelo, S.L.; Adaramoye, O.A. Bisdemethoxycurcumin Chemoprevents 7,12-Dimethylbenz(a)Anthracene-Induced Mammary Toxicity via Modulation of Oxidative Processes. *Sci. Rep.* 2025, *15*, 9170, doi:10.1038/s41598-025-94168-x.

221. Kerslake, R.; Belay, B.; Panfilov, S.; Hall, M.; Kyrou, I.; Randeva, H.S.; Hyttinen, J.; Karteris, E.; Sisu, C. Transcriptional Landscape of 3D vs. 2D Ovarian Cancer Cell Models. *Cancers (Basel).* 2023, *15*, 3350, doi:10.3390/cancers15133350.

222. Dutta, S.; Ghosh, S.; Sen, S. Proteolytic and Non-Proteolytic Functions of MMP9 in Cancer Invasion. *Biophys. J.* 2024, *123*, 2a, doi:10.1016/j.bpj.2023.11.143.

223. Li, S.; Pritchard, D.M.; Yu, L.-G. Regulation and Function of Matrix Metalloproteinase-13 in Cancer Progression and Metastasis. *Cancers (Basel).* 2022, *14*, 3263, doi:10.3390/cancers14133263.

224. Zhou, Y.; Jiang, Z.; Cao, L.; Yang, J. The Role of Various Collagen Types in Tumor Biology: A Review. *Front. Oncol.* 2025, *15*, doi:10.3389/fonc.2025.1549797.

225. Franco, P.; De Marco, I. The Use of Poly(N-Vinyl Pyrrolidone) in the Delivery of Drugs: A Review. *Polymers (Basel).* 2020, *12*, 1114, doi:10.3390/polym12051114.

226. Rauner, G.; Gupta, P.B.; Kuperwasser, C. From 2D to 3D and beyond: The Evolution and Impact of in Vitro Tumor Models in Cancer Research. *Nat. Methods* 2025, *22*, 1776–1787, doi:10.1038/s41592-025-02769-1.

227. H.-Alcántara, A.; Kourani, O.; Marcos-Jiménez, A.; Martínez-Núñez, P.; Herranz-Martín, E.; Fuentes, P.; Toribio, M.L.; Muñoz-Calleja, C.; Iglesias, T.; Campanero, M.R. Glutathione Overproduction Mediates Lymphoma Initiating Cells Survival and Has a Sex-Dependent Effect on Lymphomagenesis. *Cell Death Dis.* 2024, *15*, 534, doi:10.1038/s41419-024-06923-z.

228. Ciufolini, G.; Zampieri, S.; Cesaroni, S.; Pasquale, V.; Bonanomi, M.; Gaglio, D.; Sacco, E.; Vanoni, M.; Pastore, M.; Marra, F.; et al. 3D Modeling: Insights into the Metabolic Reprogramming of Cholangiocarcinoma Cells. *Cells* 2024, *13*, 1536, doi:10.3390/cells13181536.

229. Gamcsik, M.P.; Kasibhatla, M.S.; Teeter, S.D.; Colvin, O.M. Glutathione Levels in Human Tumors. *Biomarkers* 2012, *17*, 671–691, doi:10.3109/1354750X.2012.715672.

230. Kennedy, L.; Sandhu, J.K.; Harper, M.-E.; Cuperlovic-Culf, M. Role of Glutathione in Cancer: From Mechanisms to Therapies. *Biomolecules* 2020, *10*, 1429, doi:10.3390/biom10101429.

231. Mardikasari, S.A.; Katona, G.; Csóka, I. Bovine Serum Albumin Nanoparticles: A Promising Platform for Nasal Drug Delivery. *Expert Opin. Drug Deliv.* 2025, *22*, 7–10, doi:10.1080/17425247.2024.2436117.

232. Bashiri, G.; Shojaosadati, S.A.; Abdollahi, M. Synthesis and Characterization of Schiff Base Containing Bovine Serum Albumin-Gum Arabic Aldehyde Hybrid Nanogels via Inverse Miniemulsion for Delivery of Anticancer Drug. *Int. J. Biol. Macromol.* 2021, *170*, 222–231, doi:10.1016/j.ijbiomac.2020.12.150.

233. Szota, M.; Szwedowicz, U.; Rembialkowska, N.; Janicka-Klos, A.; Doveiko, D.; Chen, Y.; Kulbacka, J.; Jachimska, B. Dendrimer Platforms for Targeted Doxorubicin Delivery—Physicochemical Properties in Context of Biological Responses. *Int. J. Mol. Sci.* 2024, *25*, 7201, doi:10.3390/ijms25137201.

234. Long, X.; Ren, J.; Zhang, C.; Ji, F.; Jia, L. Facile and Controllable Fabrication of Protein-Only Nanoparticles through Photo-Induced Crosslinking of Albumin and Their Application as DOX Carriers. *Nanomaterials* 2019, *9*, 797, doi:10.3390/nano9050797.

235. Hemlata; Hariharan, A.; Murali, N.; Roy, S.; Betal, S.; Kumar, S.; Minocha, S. Engineered BSA Nanoparticles: Synthesis, Drug Loading, and Advanced Characterization. *Biol. Methods Protoc.* 2025, *10*, doi:10.1093/biomethods/bpaf066.

236. Chouhan, R.; Bajpai, A. Real Time in Vitro Studies of Doxorubicin Release from PHEMA Nanoparticles. *J. Nanobiotechnology* 2009, *7*, 5, doi:10.1186/1477-3155-7-5.

237. Singh, N.; Bhattacharyya, D. Collagenases in an Ether Extract of Bacterial Metabolites Used as an Immunostimulator Induces TNF-α and IFN-γ. *Int. Immunopharmacol.* 2014, *23*, 211–221, doi:10.1016/j.intimp.2014.08.026.

238. Muhammad, Q.; Jang, Y.; Kang, S.H.; Moon, J.; Kim, W.J.; Park, H. Modulation of Immune Responses with Nanoparticles and Reduction of Their Immunotoxicity. *Biomater. Sci.* 2020, *8*, 1490–1501, doi:10.1039/C9BM01643K.

239. Asghar, S.; Salmani, J.M.M.; Hassan, W.; Xie, Y.; Meng, F.; Su, Z.; Sun, M.; Xiao, Y.; Ping, Q. A Facile Approach for Crosslinker Free Nano Self Assembly of Protein for Anti-Tumor Drug Delivery: Factors' Optimization, Characterization and in Vitro Evaluation. *European Journal of Pharmaceutical Sciences* 2014, *63*, 53–62, doi:10.1016/j.ejps.2014.06.022.

240. De Palma, M.; Hanahan, D. Milestones in Tumor Vascularization and Its Therapeutic Targeting. *Nat. Cancer* 2024, *5*, 827–843, doi:10.1038/s43018-024-00780-7.

241. Urbanczyk, M.; Zbinden, A.; Schenke-Layland, K. Organ-Specific Endothelial Cell Heterogenicity and Its Impact on Regenerative Medicine and Biomedical Engineering Applications. *Adv. Drug Deliv. Rev.* 2022, *186*, 114323, doi:10.1016/j.addr.2022.114323.

242. Acimovic, I.; Chochola, V.; Herrera, J.L.; Hampl, A.; Jaros, J. 3D Endothelial Network Formation in Hydrogels Improved by Stromal Cells and Specific Growth Factors. *Sci. Rep.* 2025, *15*, 41524, doi:10.1038/s41598-025-25381-x.

243. Sorg, H.; Harder, Y.; Krueger, C.; Reimers, K.; Vogt, P.M. The Nonhematopoietic Effects of Erythropoietin in Skin Regeneration and Repair: From Basic Research to Clinical Use. *Med. Res. Rev.* 2013, *33*, 637–664, doi:10.1002/med.21259.

244. Righi, L.; Deaglio, S.; Pecchioni, C.; Gregorini, A.; Horenstein, A.L.; Bussolati, G.; Sapino, A.; Malavasi, F. Role of CD31/Platelet Endothelial Cell Adhesion Molecule-1 Expression in in Vitro and in Vivo Growth and Differentiation of Human Breast Cancer Cells. *Am. J. Pathol.* 2003, *162*, 1163–1174, doi:10.1016/S0002-9440(10)63912-0.

245. Quintero-Fabián, S.; Arreola, R.; Becerril-Villanueva, E.; Torres-Romero, J.C.; Arana-Argáez, V.; Lara-Riegos, J.; Ramírez-Camacho, M.A.; Alvarez-Sánchez, M.E. Role of Matrix Metalloproteinases in Angiogenesis and Cancer. *Front. Oncol.* 2019, *9*, doi:10.3389/fonc.2019.01370.

246. Siddhartha, R.; Goel, A.; Singhai, A.; Garg, M. Matrix Metalloproteinases -2 and -9, Vascular Endothelial Growth Factor, Basic Fibroblast Growth Factor and CD105-Micro-Vessel Density Are Predictive Markers of Non-Muscle Invasive Bladder

Cancer and Muscle Invasive Bladder Cancer Subtypes. *Biochem. Genet.* 2025, *63*, 4057–4112, doi:10.1007/s10528-024-10921-3.

247. Majo, S.; Redoute-Timonnier, C.; Lacour, A.; Challeat, L.; Epinette, E.; Teillon, J.; Grosset, C.F.; Auguste, P. Optimized Zymogram Protocol from 3D Spheroid Cultures to Study MMP-2 and -9 Activities in Tumor Cells. *BMC Biotechnol.* 2025, *25*, 28, doi:10.1186/s12896-025-00961-x.

248. Hiratsuka, S.; Nakamura, K.; Iwai, S.; Murakami, M.; Itoh, T.; Kijima, H.; Shipley, J.M.; Senior, R.M.; Shibuya, M. MMP9 Induction by Vascular Endothelial Growth Factor Receptor-1 Is Involved in Lung-Specific Metastasis. *Cancer Cell* 2002, *2*, 289–300, doi:10.1016/S1535-6108(02)00153-8.

249. Nazari, S.S.; Doyle, A.D.; Yamada, K.M. Mechanisms of Basement Membrane Micro-Perforation during Cancer Cell Invasion into a 3D Collagen Gel. *Gels* 2022, *8*, 567, doi:10.3390/gels8090567.

250. Chen, Y.; Gou, X.; Ke, X.; Cui, H.; Chen, Z. Human Tumor Cells Induce Angiogenesis through Positive Feedback between CD147 and Insulin-Like Growth Factor-I. *PLoS One* 2012, *7*, e40965, doi:10.1371/journal.pone.0040965.

251. Jiang, X.; Wang, J.; Deng, X.; Xiong, F.; Zhang, S.; Gong, Z.; Li, X.; Cao, K.; Deng, H.; He, Y.; et al. The Role of Microenvironment in Tumor Angiogenesis. *Journal of Experimental & Clinical Cancer Research* 2020, *39*, 204, doi:10.1186/s13046-020-01709-5.

252. Huang, L.; Perrault, C.; Coelho-Martins, J.; Hu, C.; Dulong, C.; Varna, M.; Liu, J.; Jin, J.; Soria, C.; Cazin, L.; et al. Induction of Acquired Drug Resistance in Endothelial Cells and Its Involvement in Anticancer Therapy. *J. Hematol. Oncol.* 2013, *6*, 49, doi:10.1186/1756-8722-6-49.

253. Mirzaei, S.; Gholami, M.H.; Hashemi, F.; Zabolian, A.; Farahani, M.V.; Hushmandi, K.; Zarrabi, A.; Goldman, A.; Ashrafizadeh, M.; Orive, G. Advances in Understanding the Role of P-Gp in Doxorubicin Resistance: Molecular Pathways, Therapeutic Strategies, and Prospects. *Drug Discov. Today* 2022, *27*, 436–455, doi:10.1016/j.drudis.2021.09.020.

254. Zhang, B.; Wan, S.; Peng, X.; Zhao, M.; Li, S.; Pu, Y.; He, B. Human Serum Albumin-Based Doxorubicin Prodrug Nanoparticles with Tumor PH-Responsive Aggregation-Enhanced Retention and Reduced Cardiotoxicity. *J. Mater. Chem. B* 2020, *8*, 3939–3948, doi:10.1039/D0TB00327A.

255. Young, O.; Ngo, N.; Lin, L.; Stanbery, L.; Creeden, J.F.; Hamouda, D.; Nemunaitis, J. Folate Receptor as a Biomarker and Therapeutic Target in Solid Tumors. *Curr. Probl. Cancer* 2023, *47*, 100917, doi:10.1016/j.currproblcancer.2022.100917.

256. Pooja, D.; Gunukula, A.; Gupta, N.; Adams, D.J.; Kulhari, H. Bombesin Receptors as Potential Targets for Anticancer Drug Delivery and Imaging. *Int. J. Biochem. Cell Biol.* 2019, *114*, 105567, doi:10.1016/j.biocel.2019.105567.

257. Paolillo, M.; Schinelli, S. Extracellular Matrix Alterations in Metastatic Processes. *Int. J. Mol. Sci.* 2019, *20*, 4947, doi:10.3390/ijms20194947.

258. Radisky, E.S.; Radisky, D.C. Matrix Metalloproteinase-Induced Epithelial-Mesenchymal Transition in Breast Cancer. *J. Mammary Gland Biol. Neoplasia* 2010, *15*, 201–212, doi:10.1007/s10911-010-9177-x.

259. Tang, W.; Wang, X.; Han, B.; Jiang, S.-H.; Cao, H. Tumor-Associated Macrophages in Cancer: From Mechanisms to Application. *Molecular Biomedicine* 2025, *6*, 145, doi:10.1186/s43556-025-00396-y.

EDUCATIONAL ACTIVITIES AND CONFERENCES

Training and Dissemination Activities:

- **Courses at the University of Palermo**

- Confocal microscopy Training (6 hours)
- Applications of Physics to Medicine (8 hours)
- Fundamentals for approaching the use of animal models in preclinical research (8 hours)
- Structural Biology and its applications in Drug Discovery (10 hours)
- Applications of cell culture-based models for the initial characterization of the mechanisms of action of molecules to be adopted in clinical trials (5 hours)
- Writing a Scientific Research Project Proposal (6 hours)
- Antibacterial, antitumor activity and drug-resistance acquisition: cellular targets and molecular mechanisms (12 hours)
- Epigenetic mechanisms of gene regulation (8 hours)

- **Courses at the University of Copenhagen**

- Scientific Project Planning and Management 1 (20-21/02/2024)
- Academic writing - How to create good texts (04-05/03/2024)
- Responsible Conduct of Research 1: An Introduction (04/04/2024)
- Molecular Pharmacology (15-19/04/2024)
- Drug Delivery (13-17/05/2024)
- Introduction to University Pedagogy (20-21/02/2024)
- Receptor Structure and Function (24-28/06/2025)
- Intensive Medical Writing: Learn how to write papers that get published (11-12/08/2025)
- Responsible Conduct of Research 2: Getting Ready for Submission (25/08/2025)
- Scientific Project Planning and Management 2 - Finishing your PhD (28-29/10/2025)

Workshop and School

- "Technologies and Sciences for Human Health (II Edition)" – PhD Workshop (23-26/10/2023, Palermo, Italy) – Poster Presentation
- "Technologies and Sciences for Human Health (III Edition) – PhD Workshop (28-30/10/2024, Palermo, Italy) – Oral Presentation
- "Tech4Health (IV Edition) – PhD Workshop (07-08/10/2025) – Workshop

planning and coordination

- “DRA Summer School for the PhD Students in Pharmaceutical Sciences (21-22/08/2023, Copenhagen, Denmark) – Attended
- “DRA summer school for PhD students in Pharmaceutical Sciences (19-20/08/2025, Copenhagen, Denmark) – Oral presentation
- The Horizon Europe framework program: opportunities to support young researchers and develop their early-stage careers” (5/02/2024, Palermo, Italy)
- “Pubblicare la tesi di Dottorato con UNIPA-SPRINGER” (12/03/2024, Palermo, Italy)
- “Come si comunica la ricerca?!” (14/10/2024, Palermo, Italy)
- “Breve e agile introduzione ai processi di qualità. Perché è importante e come può migliorare la ricerca e la didattica nei dottorati, diritti e doveri dei dottorandi” (2/12/2024, Palermo, Italy)
- "Dalle reti neurali all'intelligenza artificiale, passando per un paio di premi nobel" (3/02/2025, Palermo, Italy)
- "Il sostegno all'innovazione nella programmazione Europea: la politica di coesione 2021-2027 in Sicilia e Horizon Europe" - (7/04/2025, Palermo, Italy)
- “Comunicare la ricerca” (9/06/2025, Palermo, Italy)
- “Scienza e innovazione nelle tecnologie quantistiche” (6/10/2025, Palermo, Italy)

Presentations at conferences/seminars

- “Meeting intersezioni SIB (Società Italiana di Biochimica e Biologia Molecolare)” (interregionale) (03-05/10/2024, Messina, Italy) – Oral presentation
- “63° SIB (Società Italiana di Biochimica e Biologia Molecolare) National Congress” (10-12/09/2025, Palermo, Italy) – Poster presentation
- “97° SIBS (Società Italiana di Biologia Sperimentale) National Congress” (10—13/04/2025, Palermo, Italy) – Oral Presentation
- “Seminario Vivere Ingegneria: Nanotecnologie e Modelli 3D per la Terapia Antitumorale” (08/05/2025, Palermo, Italy) – Oral Presentation

Mobility and Collaborations:

- University of Copenhagen – Department of Pharmacy (19/08/2023 – 23/08/2023)
- University of Copenhagen – Department of Pharmacy (05/02/2024 – 01/08/2024)
- University of Copenhagen – Department of Pharmacy (16/05/2025 – 24/05/2025)

- University of Copenhagen – Department of Pharmacy (19/08/2025 – 27/08/2025)
- University of Copenhagen – Department of Pharmacy (26/10/2025 – 31/10/2025)

Other Activities / Achievements:

- **Best Oral Presentation Award** at the "Meeting intersezioni SIB (Società Italiana di Biochimica e Biologia Molecolare)" (interregional) (03-05/10/2024, Messina, Italy)
- **Best Oral Presentation Award** at the "97° SIBS (Società Italiana di Biologia Sperimentale) National Congress" (10—13/04/2025, Palermo, It

APPENDIX V

PUBLICATIONS

International Journal of
Molecular Sciences

MDPI

Review

The Multifaced Role of Collagen in Cancer Development and Progression

Gabriele Lo Buglio [1,2], Alessandra Lo Cicero [1,*], Simona Campora [1] and Giulio Ghersi [1,3,*]

[1] Department of Biological, Chemical and Pharmaceutical Sciences and Technologies (STEBICEF), University of Palermo, 90128 Palermo, Italy; gabriele.lobuglio@unipa.it (G.L.B.); simona.campora@unipa.it (S.C.)
[2] Department of Pharmacy, University of Copenhagen, Universitetsparken 2, 2100 Copenhagen, Denmark
[3] Abiel srl, 90128 Palermo, Italy
* Correspondence: alessandra.locicero@unipa.it (A.L.C.); giulio.ghersi@unipa.it (G.G.)

Abstract: Collagen is a crucial protein in the extracellular matrix (ECM) essential for preserving tissue architecture and supporting crucial cellular functions like proliferation and differentiation. There are twenty-eight identified types of collagen, which are further divided into different subgroups. This protein plays a critical role in regulating tissue homeostasis. However, in solid tumors, the balance can be disrupted, due to an abundance of collagen in the tumor microenvironment, which significantly affects tumor growth, cell invasion, and metastasis. It is important to investigate the specific types of collagens in cancer ECM and their distinct roles in tumor progression to comprehend their unique contribution to tumor behavior. The diverse pathophysiological functions of different collagen types in cancers illustrate collagen's dual roles, offering potential therapeutic options and serving as prognostic markers.

Keywords: collagen; extracellular matrix; solid tumor; tumor microenvironment

Citation: Lo Buglio, G.; Lo Cicero, A.; Campora, S.; Ghersi, G. The Multifaced Role of Collagen in Cancer Development and Progression. *Int. J. Mol. Sci.* **2024**, *25*, 13523. https://doi.org/10.3390/ijms252413523

Academic Editor: Andrea Disanza

Received: 20 November 2024
Revised: 10 December 2024
Accepted: 13 December 2024
Published: 17 December 2024

1. Introduction

Collagen is the most abundant protein in the human body, accounting for 25–30% of its total protein content and is the main constituent of various tissues, including bones, ligaments, and skin [1]. As the fundamental component of the extracellular matrix (ECM), collagen plays a crucial role in the structural and functional organization of all tissues [2,3]. The ECM is a dynamic three-dimensional network of macromolecules, such as glycoproteins, proteoglycans, fibronectin, and laminin, with functions that are highly dependent on protein compositions. These functions include pH maintaining, regulating cell proliferation and differentiation, and providing support and anchorage for cells [4,5]. Collagen and other ECM components vary in structure and function, thereby regulating tissue homeostasis.

The equilibrium of ECM can be affected by injuries, aging, and various diseases [6]. Recent research studies have focused on understanding the role of ECM and collagen in the formation and progression of solid tumors. Together with tumor vasculature, associated connective tissues, infiltrating immune cells, and cancer-associated fibroblasts (CAFs), the component of ECM constitutes the tumor microenvironment (TME) of solid tumors [7]. Therefore, solid tumors are characterized by ECM rich in collagen, which encapsulates tumor cells, influencing cell accessibility and metabolism, and promoting tumor cell progression, invasion, and migration. This high collagen density leads to a TME stiffness that is significantly stronger compared to healthy tissues [8,9]. This condition is also influenced by the orientation of collagen fibers, which form a random reticle, dynamically remodeled during disease progression [10–12]. Excessive deposition and specific orientation of collagen are considered the major pathological features of solid tumors, allowing collagens to play active roles in cancer [13,14]. Increasing evidence suggests that the various types of collagens in the tumor ECM promote tumor proliferation and invasion and create conditions that enhance metastatic dissemination [15].

This review aims to provide an overview of the pathological role of different types of collagens in solid tumors, highlighting how these molecules represent excellent therapeutic targets and reliable prognostic markers. By exploring the diverse functions of collagen within the ECM, it is possible to better understand its impact on tumor biology and identify novel approaches to modulate the ECM for improved cancer treatment outcomes.

2. Collagen: Role and Structure

Along with fibronectin, laminin, and elastin, collagen constitutes the matrisome of the ECM, composed of approximately 300 proteins [16]. Collagen is a complex and dynamic macromolecule, assuming various structures in different tissues, conferring them a range of biological functions. To date, 28 collagen subtypes have been identified, with type I collagen representing over 90%, being the primary component of organs and connective tissues [6]. As a key component of connective tissues, collagen plays an essential role in maintaining their structural and biological integrity [17]. The synthesis and remodeling of collagens are dynamic mechanisms that are closely dependent on the physiological and, in some cases, pathological conditions of the tissue. These processes primarily involve fibroblasts, chondrocytes, osteoblasts, smooth muscle cells (SMCs), epithelial cells, endothelial cells, hepatic stellate cells, and cardiac myocytes [18–24]. The α chains of various types of collagen are used to build trimeric molecules, which intertwine into a 300 nm long triple helix and subsequently assemble into fibrils. Some types, such as type II collagen, form homotrimeric molecules, while others, such as types I and V, form heterotrimers [25,26]. The collagen components interact in a specific sequence with each other and with other tissue proteins and cells, producing higher-order structures. For example, continuous crosstalk occurs between collagen fibers and resident fibroblasts, allowing for a balance of tensile and recoil energy in a tissue, and modulating mechanotransduction pathways [27]. The modulation of the intracellular signaling pathways also depends on the turnover of the various collagens within the extracellular matrix. This process is highly dependent on the activity of specific proteases, particularly matrix metalloproteinases (MMPs) secreted by resident cells [28,29]. These enzymes modify the different extracellular matrix components, altering the density of the microenvironment and leading to mechanical loads perceived by the cells. Several studies have examined the influence of mechanical force on the extracellular matrix formation. However, the complexity of controlling and assembling collagen fibrils is still not well understood. Some studies suggest both cell-dependent and cell-independent models for collagen organization, highlighting the importance of mechanochemistry in determining fibril arrangement under mechanical stress [30].

3. Biosynthesis

The different types of collagen share the canonical sequence domain Gly-X-Y, where X and Y can vary with a consistent presence of proline and hydroxyproline residues [31]. Hydroxyproline is an amino acid not commonly found in the amino acid sequence of proteins; however, it may account for more than 50% of the total amino acid content of collagen [32]. The high percentage of these residues is critical for reducing the entropic contribution during collagen filament folding [33]. Collagen synthesis is a multi-step process involving several enzymes. After synthesis, pre-collagen undergoes disulfide bond formation at the N- and C-terminal propeptide regions followed by post-translational modifications, mainly on lysines and prolines, such as hydroxylation (via lysyl hydroxylase activity) and glycosylation (through the addition of glucose and galactose oligosaccharides), leading to the formation of pro-collagen α chains [34]. Lysine hydroxylation induces the formation of triple helices, which are then secreted into the extracellular environment via Golgi vesicles [15]. Once secreted, collagen undergoes a combined activity of lysyl oxidases (LOX) and some classes of LOX-like proteins (LOXL) [35], which function as cross-linking agents found both in the intracellular and extracellular environment. They are necessary for collagen's mechanical properties acquisition, such as tensile strength, contributing to the regulation of ECM stiffness [36,37].

4. Tumoral Extracellular Matrix

Tumorigenesis is a complex and dynamic process involving the cooperation of various elements within the tumor microenvironment (TME) [7]. The TME components play several critical roles in promoting and sustaining tumor progression. These roles include the deregulation of proliferative signals and the evasion of growth suppression control. Consequently, tumor cells acquire several characteristics: resistance to apoptosis, uncontrolled proliferation, promotion of tissue colonization, modulation of cellular metabolism, stimulation of angiogenesis, and evasion from the immune system [38]. The TME is composed of multiple cellular components, such as endothelial cells (ECs), immunocytes, adipocytes, cancer-associated fibroblasts (CAFs), and the ECM [3] (Figure 1).

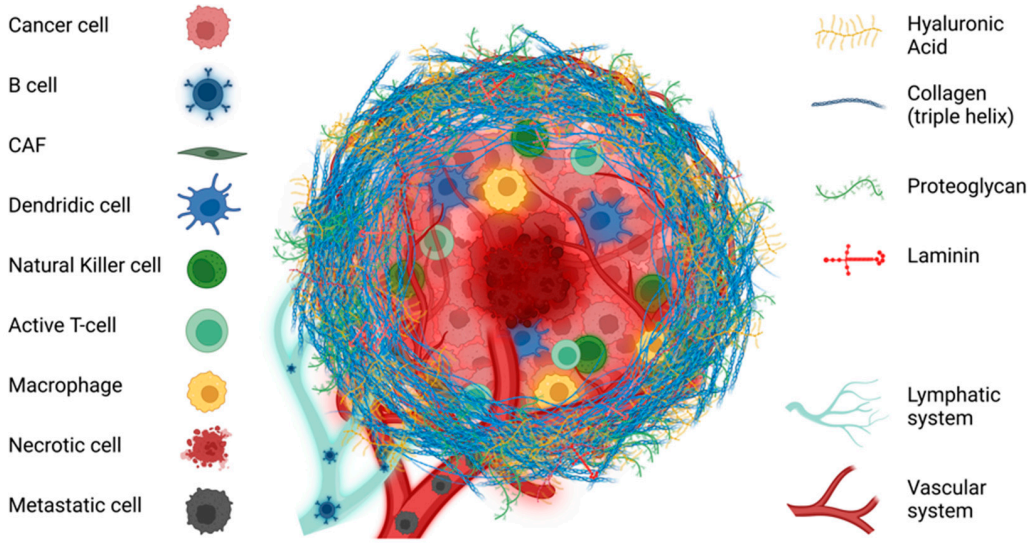

Figure 1. Schematic representation of the major components of tumor microenvironment in solid tumors. The tumor microenvironment mainly consists of tumor cells, immune cells, stromal cells, and extracellular matrix. The primary factor contributing to matrix stiffness is the excessive presence of collagen, which significantly impacts various crucial biological processes throughout tumor development.

CAFs are pivotal components of the TME with enhanced functional properties, such as proliferation, migration, and secretion. They persist in a hyperactivated condition and exhibit elevated metabolic activity. Their activity contributes to shaping a thick tumoral extracellular matrix, through synthesis and abnormal deposition of fibronectin, laminin, hyaluronic acid, and collagen types I, III, IV, and V, above all collagen type I [39–41].

The ECM plays a key role in the TME, encapsulating tumor cells within an acidic and hypoxic extracellular matrix, which reduces cell accessibility and influences their metabolism. From a structural point of view, the ECM of solid tumors is an envelope that surrounds, protects, and interacts with tumor cells. Moreover, due to its macromolecular composition, the tumor ECM exhibits abnormal rigidity compared to the ECM of healthy tissues. For example, while the stiffness of the ECM in healthy tissues such as the breast, brain, liver, lung, and pancreas is typically around 1000 Pa, it can reach values between 4 and 10 kPa in tumors located in these same sites [8]. This increased stiffness can result from different biomechanical factors, including an imbalance between matrix deposition and degradation, the presence of contractile actomyosin in CAFs, interactions between tumor and normal cells, and especially altered collagen cross-linking [42,43]. Tumor ECM shares several components with healthy tissues ECM, such as collagens, elastin, proteoglycans, and glycoproteins like tenascin-C, laminins, and fibronectins [44]. However, changes in the relative composition of these elements lead to structural and functional alterations that promote tumor development [45]. The ECM components contribute to a fibrotic extracellular environment, modified by multiple factors, such as MMPs. MMPs actively

contribute to tumor progression by participating in ECM turnover, which influences tumor cell proliferation, angiogenesis, and invasion, as well as apoptosis inhibition [46].

5. Collagens in Solid Tumors

Collagen is a key component of the ECM in the TME, significantly contributing to tumors' physical and biochemical properties. The organization and density of collagen fibers can significantly affect the progression and spread of tumors. Collagen provides structural support to tumors, creating a scaffold that aids tumor growth. Increased collagen deposition leads to a stiffer ECM, promoting tumor cell proliferation and survival. Cancer cells interact with collagen through integrins and other receptors, transducing signals that influence tumor cell behavior, leading to cell growth, invasion, resistance to chemotherapy, metabolism variation, invasion, migration, and evasion to the immune system.

5.1. Collagen and Cancer Cell Proliferation

Collagen and other ECM components interact directly with tumor cells, influencing their growth. These molecules play an important role in regulating the cell cycle. Some fibrillar collagens suppress tumor growth by interacting with Discoidin Domain Receptor 2 (DDR2), a transmembrane receptor tyrosine kinase (RTK). Along with Discoidin Domain Receptor 1 (DDR1), DDR2 binds collagen in the extracellular matrix of various tissues. This interaction leads to cell cycle arrest at the G1/S checkpoint [47]. Other collagens, such as type III collagen, induce tumor cells into dormancy via the DDR1/Signal Transducer and Activator of Transcription 1 (STAT1) signaling pathway [48]. However, most of them promote tumor cell proliferation through various pathways. For instance, it has been shown that monomeric collagen can inhibit the expression of p21 in tumor cells in vitro, altering cell cycle restrictions [49]. Moreover, collagen interaction with integrin beta-1 leads to increased tumor cell proliferation, through the activation of β-catenin [50,51] However, collagen regulates tumor cell proliferation through several mechanisms, including diverse metabolic pathways.

5.2. Collagen and Tumor Metabolism

One of the aspects that over the years led to significant attention in the scientific community is tumor glucose metabolism. Tumor cells can absorb more glucose than their healthy tissue counterparts, converting it into lactate [52]. This process, known as the Warburg effect, is regulated by numerous factors, including matrix collagen. It has been demonstrated in vitro that increased collagen density promotes aerobic glycolysis in human breast cancer cell lines, stimulating integrin activation [53]. This activates the Posphoinositide 3-Kinase (PI3K)/Protein Kinase B (Akt) signaling pathway, which positively modulates the activity of various factors upstream, such as Glucose Transporter 1 (GLUT1) and pyruvate kinase M2 (PKM2) [54,55]. Furthermore, these metabolic anomalies modify glutamine uptake and its fate in tumors. In this context, a recent in silico study focused on the increased glutamine uptake in tumor cells exploiting the Warburg effect, noting that this metabolite is directed toward stromal collagen production.

Thus, through positive feedback mechanisms, tumor cells link collagen with glucose and lipid metabolism, promoting tumor progression [56–58].

5.3. Collagen and Apoptosis

Apoptosis represents a highly regulated cell death process governed by various endogenous or exogenous stimuli. However, in the tumorigenesis contest, this mechanism is completely dysregulated, promoting tumor growth at the expense of surrounding tissues [59]. The involvement of matrix collagen in anti-apoptotic processes is not fully understood. The presence of collagen in gastric cancer has been shown to upregulate, both in vitro and in vivo, the expression of anti-apoptotic factors, such as B-cell lymphoma 2 (BCL2), increased by the β-catenin pathway [60]. Moreover, DDR1 pathway activation mediated by type I collagen inhibits tumor cell growth, through the pro-apoptotic

factor BCL-2 interacting killer (BIK), a member of the BCL2 family [61,62]. Collagen can also suppress tumor growth by negatively modulating certain cell cycle factors, such as p21 and CDKs, and regulating caspase expression [63]. In addition to collagen, some of its peptide derivatives can induce apoptosis, by Bcl-2 and BCL-extra large (BCLxL) pathways [64].

To resume, the dual role of collagen raises many questions about its actual function in solid tumors. Given its pleiotropic effects on malignancy, different factors may play crucial roles, such as tumor type, staging, and the specific type of matrix collagen.

5.4. Collagen and Tumor Cell Invasion

Among the hallmarks of solid tumors, the invasion of tumor cells is one of the most determining factors for patient prognosis since this mechanism plays a crucial role in tumor progression and metastasis formation [65]. For instance, collagen regulates the extension of invadopodia through the integrin αvβ3/Dishevelled-associated activator of morphogenesis 1 (DAAM1)/Ras Homolog family member A (RHOA)-dependent cascade [66], which are small actin-rich protrusions that mediate the invasion of tumor cells [67]. From a biophysical perspective, the increased stromal tension caused by matrix collagen accumulation in breast cancers enhances the integrin β1-mediated signaling pathway, leading to the activation of the Focal Adhesion Kinase (FAK)/Yes-Associated Protein (YAP) pathway [68]. Activation of integrin β1 can be triggered by mutated collagens at one or more sites, which accelerate the tumor cell invasion, as observed in invasive epithelial tumors [69]. However, YAP activation must be corroborated by collagen matrix remodeling, mediated by Lox3 and MMPs, which are regulated by the microenvironment stiffness [70]. On the other hand, collagen degradation, or the loss of ECM stiffness induced by ultraviolet radiation (UVR) against fibroblasts, could surprisingly increase the survival of melanoma patients due to the lack of matrix support for invasiveness [71].

5.5. Collagen and Metastasis

Besides driving tumors to cell invasion, collagen plays a key role in cell migration. The ECM of solid tumors changes the acquisition of metastatic potential [72], and the collagen within it acts as a "molecular binary" to increase the tumor cell's escape from the primary site [73,74]. However, cancer research has recently focused on the pathways regulated by stromal collagen implicated in this process. For instance, the DDR1 or DDR2 activation mediated by collagen positively regulates the metastatic process involving tumor-associated neutrophils (TANs) and CAFs [75,76]. Upregulation of collagen prolyl-4-hydroxylases (P4HA) of class I and II, whose expression is increased by tissue hypoxia [77], could drive collagen deposition in metastatic ovarian tumors, leading to neo-angiogenesis and tumor cell migration [78].

Thus, metastasis is a complex process involving multiple converging and diverging signaling pathways, often upstream regulated by collagen. Some pathways are even independent, such as versican (VCAN)/Extracellular signal-Regulated Kinase (ERK) and poly [ADP-ribose] polymerase 1 (PARP1)/Zinc finger E-box-Binding homeobox 1 (ZEB1) pathways, which promote the proliferation and migration of colorectal cancer cells, regulated directly or indirectly by collagen [79]. In other cases, collagen can be secreted into exosomes to promote metastasis, as observed in osteosarcomas [80].

5.6. Collagen and Tumor Angiogenesis

Increased collagen deposition and its alignment are characteristics that impact neovascularization [81,82]. More specifically, the high density of collagen and other matrix components creates a hypoxic environment at the tumor core, activating the hypoxia-inducible factor (HIF-1) [83]. HIF-1 is a pivotal transcription factor for vascular endothelial growth factor (VEGF), which stimulates neo-angiogenesis and actively contributes to tumor progression [84]. Additionally, HIF-1 is involved in immune evasion mechanisms through the expression of immunosuppressors, such as those regulating antigen presentation to Natural Killer (NK) cells [85].

Thus, collagen plays a physical role in tumor vascular system formation. However, some studies have also examined the biochemical role of collagen in neo-angiogenesis, investigating the pathways in which this protein is involved. More specifically, some of its peptide derivatives exhibit anti-angiogenic effects involving integrins αvβ3 and α5β1 [86]. Other peptides, including those derived from type IV collagen, inhibit endothelial cell proliferation stimulated by basic fibroblast growth factor (bFGF) or induce apoptosis in endothelial cells via a Fas-dependent mechanism [87], confirming the pleiotropic nature of tumor-associated collagen.

5.7. Collagen and Chemoresistance

Despite the significant advancements in research, chemoresistance remains the main challenge in tumor relapse and therapeutic ineffectiveness [88]. ECM, particularly collagen, plays a crucial role in chemoresistance, acting as a physical barrier against drugs. Additionally, collagen can influence various biochemical processes, such as dormancy, where tumor cells enter a quiescent state and become desensitized to chemotherapeutic agents before re-entering the G1/S phase [89,90]. Another important mechanism of chemoresistance is drug efflux, mediated by the upregulation of the ATP-binding cassette (ABC) superfamily, with P-glycoprotein (ABCB1) being the most well-known factor [91]. Specifically, ABCs can be positively modulated by α2β1-integrin, which is activated by the stromal collagen [92]. Moreover, collagen can also affect the transcription of certain genes to promote chemoresistance. In ovarian carcinoma, collagen can stabilize and activate DNA methyltransferase 1 (DNMT1), which leads to methylation and downregulation of miR-509-3p promoter, an anti-tumor miRNA that also suppresses chemoresistance [93].

Therefore, in addition to physically preventing drug entry, collagen in the tumor matrix can access multiple signaling pathways that reduce therapeutic efficacy.

5.8. Collagen and Immunomodulation

ECM plays an immunomodulatory role in solid tumors. This dense and fibrotic structure, rich in collagen, creates barriers that hinder the infiltration of chemotherapeutics and immune cells. For instance, the ECM can influence leukocyte localization and transmigration, reducing their accessibility to the tumor mass [94,95]. Among the matrix components, collagen regulates immune cell activity, such as T lymphocytes and macrophages, often favoring tumor progression [96,97]. The increased matrix density and collagen alignment suppress the tumor-infiltrating T lymphocyte (TIL) activity [98]. It has been shown in vivo that tumor collagen alignment mediated by the DDR1 extracellular domain binding hinders the infiltration of CD4+ and CD8+ T lymphocytes [99]. Supporting this study, the use of PRTH-101 (monoclonal anti-DDR1 antibodies) in breast cancer mouse models disrupted stromal collagen organization, increasing immune infiltration and, consequently, survival [100]. Beyond DDRs, collagen has receptors on leukocytes, such as leukocyte-associated immunoglobulin-like receptor 1 (LAIR-1). This receptor has an essential physiological role in preventing the immune system's uncontrolled responses, such as autoimmune reactions [101]. However, when LAIR-1 binds collagen of the tumor microenvironment, the antitumor potential of cytotoxic T lymphocytes is suppressed in an SHP-1-dependent pathway, as seen in gliomas [102]. Therefore, LAIR-1 has recently become a therapeutic target to counteract immune evasion in solid tumors [103,104]. Similarly, collagen fragments generated by MMP1 and MMP9 can bind LAIR-1, leading to immune suppression. LAIR-2, a soluble homolog of LAIR-1, reverses T lymphocyte collagen-mediated suppression through a competitive mechanism [105].

Thus, tumor collagen and the other associated factors, such as lysyl oxidase, represent important therapeutic targets to enhance immune responses against solid tumors [106–110]. However, some cytokines, such as chemokines produced by immune cells, can contribute to tumor matrix formation or even interfere with the antitumor activity of the immune system. Indeed, specific interleukins (IL), such as IL-4, IL-6, and IL-13, induce collagen synthesis, contributing to tissue fibrosis and tumor progression. In addition, other factors, such

as IL-10 and Transforming Growth Factor Beta-1 (TGF-β), secreted by M2 macrophages, inhibit Th1 lymphocyte responses and immune cell activation, creating an environment that supports tumor growth and immune evasion [111,112]. Moreover, it has been studied that the collagen I/DDR1 axis activates the Protein Kinase C theta (PKCθ)/Spleen tyrosine kinase (SYK)/Nuclear Factor kappa-light-chain-enhancer of activated B cells (NF-κB) cascade, resulting in the upregulation of the chemokine C-X-C motif chemokine 5 (CXCL5). This chemokine leads to the formation of neutrophils extracellular traps (NETs) by TANs, a key mechanism driving the metastatic process [113,114].

Therefore, the relationship between the immune system and the stromal collagen in solid tumors is ambiguous, where even some immune cells can actively participate in the ECM formation and tumor progression. A striking example is tumor-associated macrophages (TAMs). These macrophages acquire specific phenotypic characteristics, polarizing from antitumoral (M1) to protumoral (M2) states through a mechanism induced by IL-4 secreted by CD4+ T cells [75]. These cells influence the tumor progression, enhancing neo-angiogenesis or tumor cell migration [115,116]. Additionally, TAM2s can secrete collagen I to activate the α2β1 integrin/PI3K/Akt axis, supporting tumor progression [117,118].

For this reason, continued studies on the relationship between stromal collagen and the immune system may uncover targeted therapies against solid tumors.

6. Mechanotransduction Mediated by Collagen in Cancer

Mechanotransduction is a complex process in which the mechanical properties of a tissue modulate intracellular signaling pathways, essential for the homeostasis of its constituent cells [119]. Mechanical homeostasis is regulated by the deposition and orientation of matrix components, such as collagens and fibronectin. The balance of stretching and tensile forces determines the elasticity or stiffness of the microenvironment. In this contest, resident cells can perceive the stiffness by acting as mechanosensors [120]. Moreover, focal adhesions are fundamental to the mechanical stimuli reception, mediating cell–matrix contacts in synergy with specific linker proteins, such as integrins and actin cytoskeleton components [121,122]. Additionally, the modulation of mechanical stimuli within the tissue microenvironment can be influenced by the cells, neighboring tissues, or the hydrostatic pressures of surrounding fluids [123]. Within this context, signaling pathways arising from the intricate relationship between a tissue's biochemistry and physical properties regulate gene expression, modulating the phenotype and primary metabolic activities of resident cells, including proliferation, differentiation, migration, and programmed cell death mechanisms [124]. However, mechanotransduction is also fundamental in the pathology of various diseases. For instance, in tumors, the heterogeneous increase in density and cross-linking of ECM components leads to abnormal stiffness compared to healthy tissue [125]. Generally, receptor tyrosine kinases (RTKs), such as AXL receptor tyrosine kinase (AXL), Receptor Tyrosine Kinase Like Orphan Receptor 2 (ROR2), and ephrin receptors (EPHs), detect matrix contractions across different hotspot regions, working as mechanosensors [126]. For instance, it has been demonstrated that EPHA2, in the absence of its canonical ligand and in cooperation with integrin beta-1, senses the stiffening of the tumor microenvironment. This detection activates the Lck/yes-related protein tyrosine kinase (LYN) signaling pathway, resulting in the phosphorylation and nuclear translocation of the transcription cofactor Twist-related protein 1 (TWIST1). Consequently, the activated pathway triggers the epithelial–mesenchymal transition (EMT) required for tumor cell invasion [127].

The interactions in the cell–matrix interface between cancer cells and collagen can activate the transcriptional coactivator YAP. YAP selectively reprograms tumor cells, promoting the transition of outer basal tumor cells into leader cells with invasive capacities. Furthermore, YAP activation enhances the transcription of ECM remodelers involved in collagen cross-linking, establishing a positive feedback mechanism that amplifies the invasive potential of tumor cells [128,129]. Different studies have highlighted that YAP nuclear translocation is facilitated by morphological modifications of nuclear pores, induced by increased stress fibers in the perinuclear region connected to the tumor ECM [130–132].

Mechanical signals from the tumor microenvironment also amplify tumor cell proliferation through positive feedback mechanisms. For instance, excessive collagen deposition and other tumor matrix components are physically sensed by stromal mesenchymal stem cells (MSCs). In response, MSCs start to secrete the protein prosaposin (PSAP), which promotes tumor growth via activation of the Toll-Like Receptor (TLR)/NF-κB signaling pathway [133–135]. Additionally, matrix stiffness drives the differentiation of MSCs into cancer-associated fibroblasts (CAFs), which are primary contributors to collagen secretion, further reinforcing overall matrix stiffness in a self-perpetuating cycle [136].

Beyond cell invasiveness and proliferation, continuous remodeling and stiffening of the tumor-associated extracellular collagen activate angiogenic signaling necessary for new vessel development. This process engages the integrin β1/PI3K/Akt signaling pathway, promoting the secretion of factors such as activin A, amphiregulin, artemin, interleukin (IL-1β), persephin, urokinase-type plasminogen activator (uPA), and vascular endothelial growth factor (VEGF) [127,137,138]. Thus, mechanotransduction triggered by matrix components, specifically collagen, underlies cancer pathology by driving processes such as differentiation, proliferation, invasion, and angiogenesis.

7. Collagen Classification

The collagen superfamily is characterized by twenty-eight types of collagens, which are further divided into different subgroups [139]. In vertebrates, collagens are numbered using Roman numerals (I–XXVIII) [140] and are classified into fibrillar and non-fibrillar types. The predominant category is represented by fibrillar collagens, which constitute 90% of the total. These fibrillar collagens have elongated fibril-like structures (rods or bands) and include types I, II, III, V, XI, XXIV, and XXVII. On the other hand, non-fibrillar collagens form various supramolecular structures and are divided into different categories, including fibrils-associated collagens with interrupted triple helices (FACITs) (types IX, XII, XIV, XVI, XIX, XX, XXI, and XXII), network-forming collagens (types IV, VIII, and X), beaded filament-forming collagens (types VI, XXVI, and XXVIII), anchoring fibrils (type VII), transmembrane collagens (types XIII, XVII, XXIII, and XXV), and multiplexins (types XV and XVIII) [141,142]. Various collagens contribute uniquely to the tumor microenvironment, affecting tumor behavior and metastasis through different pathways, such as mechanotransduction (Figure 2).

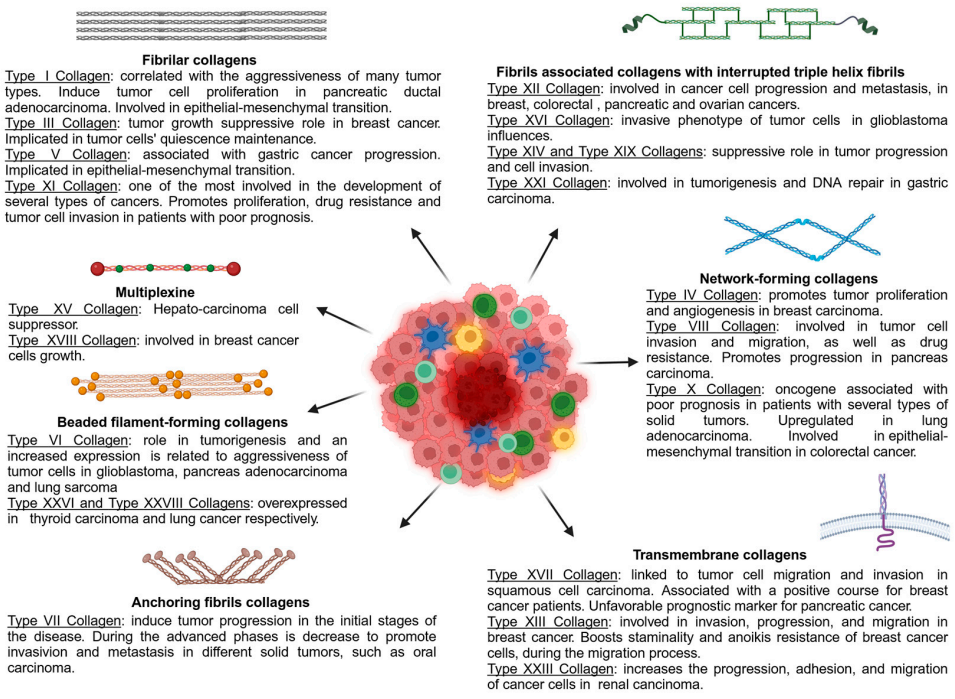

Figure 2. Classification of collagens based on supramolecular assembly and a schematic overview of the major roles of each collagen type in tumorigenesis.

7.1. Fibrillar Collagens

Fibrillar collagens have a continuous triple-helix structure of approximately 300 nm ø, followed by a chain of 1000 amino acids. This group includes types I, II, III, V, XI, XXIV, and XXVII collagens, which promote the development of solid tumors [143]. Several studies have analyzed collagen fibers' architecture, characteristic of the solid tumor ECM. While it is well established that tissue fibrosis precedes neoplasms, recent findings increasingly confirm that the stratification and elongation of stromal fibers, particularly their orientation, are statistically associated with a highly aggressive tumor cell phenotype [144]. This is because the orientation of collagen fibers in the tumor ECM differs from that of healthy tissues. Specifically, while in healthy tissues collagen is isotropically oriented, tumor tissues often exhibit an anisotropic orientation, mainly due to an increased ratio of type I to type III collagen [145]. Type I collagen is not only the most abundant protein in the body, but it is also prevalent in solid tumors. Increased deposition of type I collagen (COL1) in the tumor ECM is closely correlated with the aggressiveness of many tumor types, such as triple-negative breast carcinoma, pancreatic ductal adenocarcinoma (PDAC), or gastric carcinoma [146]. For example, COL1 induces cells to spread and reorganize their cytoskeleton in gastric carcinoma, promoting metastasis. This occurs because COL1 decreases adhesion between cells by disassembling the E-cadherin/catenin complex, which is known to be involved in the process of cell adhesion [147,148]. Furthermore, in pancreatic ductal adenocarcinoma, COL1 interacts with Discoidin Domain Receptor 1 (DDR1) [149]. When active, DDRs trigger cellular signals in tumors that affect various functions, including extracellular matrix homeostasis, tumor cell proliferation, and migration [150]. For instance, when DDR1 binds COLI, the proliferation and invasion of tumor cells are promoted through the activation of FAK-related protein tyrosine kinase 2 (PYK2), which consequently downstream activates the Crk-associated substrate (CAS)/Ras-Proximate-1 (RAP1)/c-Jun N-terminal Kinases (JNK1)/c-Jun cascade. Moreover, the cleavage of COL1 by MMPs differently affects the bioenergetics and growth of pancreatic ductal adenocarcinoma via DDR1: matrix-metalloprotease-cleaved COL1 (cCOL1) activates a signaling cascade that promotes tumor growth, while intact COL1 (iCOL1) induces DDR1 degradation, resulting in opposite effects. Patients with enriched iCOL1 exhibit better survival compared to those with tumors enriched in cCOL1 and DDR1, suggesting that targeting the DDR1/NF-κB/Nuclear Factor Erythroid 2-Related factor 2 (NRF2)/Mitochondrial Transcription Factor A (TFAM) pathway could have therapeutic benefits [151]. In addition, COL1 is implicated in the promotion of epithelial–mesenchymal transition (EMT), a key process in embryonic development characterized by the loss of epithelial markers by epithelial cells [152]. Although typically inactive in adults, EMT has been associated with tumor invasion and metastasis. COL1-mediated phosphorylation of IκB is one pathway through which EMT is activated, leading to increased expression of the transcription factors Snail and Lymphoid Enhancer Binding Factor 1 (LEF-1), which decreases the expression of E-cadherin [153]. In addition, COL1 may be a rich source of exploitable metabolic fuel for cancer cells under critical nutrient-deficient conditions [154] and actively involved in tumor progression and metastasis. However, the role of type I collagen produced by CAFs can sometimes be shown to be contradictory since it can also have antitumor activity. The mechanisms underlying these opposing actions remain not entirely clear [139,155].

In contrast to type I collagen, type III collagen (COL3) has been shown to potentially play a tumor growth suppressive role [146]. For instance, in breast cancer patients, COL3 protects the tissues and organs of affected patients, and its reduction enhances the invasiveness of tumor cells. For example, in mice xenografted with breast cancer cells, COL3 inhibited tumor growth [156]. This is because type III collagen is implicated in tumor cells' quiescence (G0 phase) maintenance. The re-entry of quiescence cancer cells into the cell cycle plays an important role in cancer recurrence. A reduction in COL3 leads not only to cell proliferation but also amplifies the metastatic potential of cancer cells, through modulation of the DDR1/STAT1 pathway [48]. However, the concept of quiescence in cancer remains a matter of debate. Indeed, although a state of quiescence might seemingly

be a tumor progression obstacle, some studies claim that in some cases this would represent a defense mechanism from drugs. For example, cancer cells stressed by the presence of drugs enter a long persistence phase, where they can acquire chemoresistance. This drug-tolerance state is reversible as dormant tumor cells can reactivate their proliferation after drug removal; however, this is a process that increases sensitivity [157]. A further study reported that a type III humanized recombinant collagen (rhCOLIII) inhibited breast cancer cell proliferation and invasion in vitro, as well as promoting apoptosis. In addition, rhCOLIII treatment increased DDR1 protein expression, inhibiting autophagy of tumor cells [158]. This is because autophagy regulates cancer stem cell properties and contributes to the maintenance of stemness, development of relapse, and drug resistance [159].

Similar to type I collagen, type V collagen (COL5) created great interest in the scientific community, due to its involvement in tumorigenesis. In particular, type V collagen alpha 2 (COL5A2) has been observed to be associated with gastric cancer progression since this was found to be upregulated in affected patients. COL5A2 has been shown to play a direct role in cell proliferation of gastric cancer cells, where triggering the FAK/PI3K/Akt/mammalian Target Of Rapamycin (mTOR) signaling pathway [160,161]. It is also implicated in epithelial–mesenchymal transition in gastric cancer patients with poor prognosis, by promoting the expression of mesenchymal markers (SNAI1, SNAI2, TWIST, VIM, and MMP2) [162].

Among fibrillar collagens, type XI collagen (COL11) is one of the most involved in the development of several types of cancers, such as papillary thyroid carcinoma, breast cancer, colorectal carcinoma, esophageal cancer, gastric cancer, pancreatic cancer, lung cancer, and ovarian cancer [63,163–169]. Misregulated secretion of COL11 by CAFs creates a crosstalk between tumor cells and the TME, promoting proliferation, drug resistance, and tumor cell invasion in patients with poor prognosis [170–172]. In this context, it has been analyzed that integrin α1β1 and DDR2 act as extracellular Collagen 11 Alpha 1 Chain (COL11A1) receptors, triggering some signaling pathways related to ovarian cancer progression, such as Akt/CCAAT-Enhancer-Binding Proteins (C/EBPβ)/Phosphoinositide-Dependent Kinase-1 (PDK1) [173,174]. Additionally, in mouse models of xenograft with ovarian cancer cells, COL11A1 has been shown to stimulate IL-6 production via induction of TGF-β3, modulating the interaction between CAFs and tumor cells and amplifying tumor invasiveness and progression [172].

A recent study focused on the role of the gene that encodes type XXVII collagen, rather than the role of the collagen itself. Specifically, through an in vitro and in vivo analysis, the study examined the role of a specific miRNA (miRNA-455-3p) located on the gene encoding intron of Alpha Chain 1 of type XXVII collagen (COL271A). Notably, it was observed that in melanoma cells, this miRNA is closely involved in tumor cell dormancy, and its downregulation increased the re-entry of quiescent tumor cells into the cell cycle [175].

7.2. Fibrils-Associated Collagens with Interrupted Triple Helices (FACITs)

Among nonfibrillar collagens, collagens associated with interrupted triple-helix fibrils (FACITs) represent a group of small leucine-rich proteoglycans involved in regulating fibril formation [176]. Unlike fibrillar collagens that form long fibers, FACITs have interruptions in their triple-helix structure. These discontinuities are due to the presence of domains within the collagen molecule that can vary in length and composition, providing binding sites for other components of the extracellular matrix, such as fibrillar collagens [177,178]. Some collagens, such as types XII and XIV, are typically involved in stabilizing the extracellular matrix fibrils, working synergistically with type I. However, the specific organization is disrupted in the tumor microenvironment, resulting in a fibrotic and heterogeneous architecture that plays a functional role in tumorigenesis [59,100,101]. For this reason, several studies have been carried out on the distinct genes encoding for cancer-involved FACITs. For instance, type XII collagen alpha 1 chain (COL12A1) is implicated in cancer cell progression and metastasis [179] and it has been identified as a potential marker of poor

prognosis in patients with breast cancer, colorectal cancer, pancreatic adenocarcinoma, and ovarian cancer. Furthermore, recent studies of temporal changes in breast cancer matrisome profile suggest that high levels of collagen XII in primary tumor ECM can facilitate the spread of lung cancer cells [180]. COL12A1 upregulation has also been correlated with metastasis, such as lymph nodes, and reduced patients' survival with human epidermal growth factor receptor 2 (HER2)-positive breast cancer [181]. Moreover, COL12A1 expression in colorectal cancer has been linked with the regulation of several pathways, such as focal adhesion, and the PI3K-Akt pathway [182]. In patients with poor prognosis pancreatic adenocarcinoma, W. Yao et al. analyzed the relationship between COL12A1 and cytoplasmic poly (A) binding protein-1 (PABPC1), a class of RNA-binding proteins known to modulate tumor progression. PABPC1 acts as an oncogene, accelerating the proliferation and metastasis of human pancreatic cancer cell line BXPC3 through the upregulation of COL12A1 expression [183].

Type XVI Collagen (COL16) has been observed to be upregulated in certain tumor types, such as colorectal cancer (CRC), glioblastoma, and in some dysplastic areas of the mucosal epithelium of patients with oral squamous cell carcinoma [184,185]. In glioblastoma, Col16 expression influences the integrin β1 activation pattern, increasing the invasive phenotype of tumor cells [186].

Vice versa, type XIV (COL14) and type XIX (COL19) collagens exert a suppressive role in tumor progression and cell invasion. Indeed, in MMP14Sf-/- mice, the accumulation of Col14 in peritumoral areas of melanoma is correlated with a reduction in malignancy [187]. Similarly, the NC1 domain of Col19, inhibits tumor cell migration and invasion, as seen on SK-MEL-28 human melanoma cells. NC1 inhibits the FAK/PI3K/Akt/mTOR pathway, reducing the activity of proteins involved in transduction [188].

Information regarding the impact of type XX, XXI, and XXII collagens in tumors is limited. However, recent studies have shown that pancreatic ductal adenocarcinoma patients present elevated levels of circulating type XX and type XXII collagens in their serum, suggesting a possible prognostic value [189]. Another study focused on identifying hub genes and pathways in gastric carcinoma development, found that type XXI collagen alpha chain 1 (Col21a1) might have a direct role in the enrichment of some pathways involved in tumorigenesis, such as DNA repair and KRAS signaling pathway [190].

7.3. Network-Forming Collagens

Among the network-forming collagens, type IV collagen is the most prevalent in basement membranes, is approximately 400 nm in length, and assembles irregularly when forming networks. In contrast, type VIII and X collagens are shorter and form more regular hexagonal networks [191]. The expression mechanisms of network-forming collagens can be regulated by several transcription factors and play a crucial role in the development of solid tumors [143]. Type IV collagen has recently been studied in the ECM of several solid tumors. In mammals, there are six homologous α type IV collagen chains (α1(IV)–α6(IV)) that constitute both the heterotrimeric type IV collagen α1α1α2(IV) and the minor type IV collagens α3α4α5(IV) and α5α5α6(IV). As well as type I collagen, type IV is the most represented in the solid tumor ECM [192]. More specifically, collagen IV reorients within the ECM of various solid tumors, such as hepatocellular carcinoma, breast cancer, and colorectal cancer, conferring tissue stiffness around neoplastic nests. The peritumoral architecture, driven by the dense deposition of collagen IV and the aligned bundling of fibers resulting from the synergistic activation of proteases and lysyl oxidase, creates fibrotic matrix spots with abnormal mechanical properties. These spots attract tumor cells to migrate toward them through a process known as durotaxis [193–195]. This, in turn, strengthens the action of integrins and cytoskeletal interactions, which positively modulate the aggressive phenotype of tumor cells [196].

Moreover, during embryonic development, COL IV plays a crucial role in supporting the architecture of the vascular basement membrane, particularly in maintaining the structural integrity of small vessels, mediated by the non-catalytic activity of lysyl oxidase-like

protein-2 (LOXL2) [197,198]. However, increased COL IV in TEM has a controversial role, as it may negatively or positively impact tumor angiogenesis [199,200].

For instance, some studies have shown that certain peptides derived from the NC1 domains of COL IV used for cancer therapy, such as Arresten (α1 chain), Canstatin (α2 chain), Tumstatin (α3 chain), and Tetrastatin (α4 chain), suppress vessel formation and cell growth in solid tumor [201–203]. These peptides, called collagen-derived antiangiogenic factors (CDAFs), play a critical role in inhibiting angiogenesis by interacting with specific integrin subtypes, influencing neovascularization in different ways [204,205]. Arresten's activity is regulated by p53, as it controls both its transcription and MMP-dependent remodeling activity [206]. Moreover, the activity of Arresten and Canstatin can directly or indirectly influence the pro-angiogenic effects of VEGF or basic fibroblast growth factor [207]. Canstatin can decrease phosphatidylinositol 3-kinase/Akt signaling activity, downregulating VEGF activity, while Arresten can also sensitize endothelial cells to apoptosis by reducing the levels of the anti-apoptotic protein FADD-like IL-1β-converting enzyme)-inhibitory protein (FLIP) [208–210]. However, a recent study indicates that COL4A1 matrix expression and its heightened interaction with integrin beta-1 (ITGB1) in the endothelial cells of the tumor microenvironment is correlated with increased angiogenesis and chemoresistance, raising further questions about COL IV's role in tumor angiogenesis [211].

Beyond influencing vessel development, type IV collagen is widely recognized for its involvement in various tumor processes. It is one of the most extensively studied collagens in the solid tumor ECM. For instance, in luminal breast carcinoma, COLIVα5 promotes tumor proliferation through the non-integrin receptor DDR1. Through interaction with DDR1, COLIVα5 supports the Warburg effect of tumor cells by influencing c-Myc phosphorylation and regulation of p38 Mitogen-Activated Protein Kinase (MAPK), which are essential for breast cancer progression [212]. Moreover, overexpression of type IV collagen mRNA was found not only in human breast cancer tissue but also in metastatic tissues of poor survival patients [213]. Therefore, this type of collagen could also stimulate prometastatic mechanisms. For this reason, similar to type XX, XXI, and XXII collagens, type IV collagen in the serum of patients with colorectal tumors may be a potential biomarker for liver metastases [214].

Type VIII collagen (COL8) is involved in tumor cell invasion and migration, as well as drug resistance [149]. Its expression is determined by tissue hypoxia, and it correlates with the aggressiveness of several solid tumors, as seen in MDA-MB-231 and Hs578T, two cellular subtypes of triple-negative breast cancer [215]. COLVIII regulates various signaling pathways, including the interaction between DDR1 and COL VIII, which promotes pancreatic ductal adenocarcinoma progression, through PI3K-Akt and FAK-NF-κB upregulation [216]. In this context, inhibiting COLVII expression in vitro and in vivo using lentivirus or siRNA has been found to reduce the metastatic potential and gemcitabine resistance of pancreatic ductal adenocarcinoma cells [217].

Finally, type X collagen is associated with a poor prognosis in patients with several types of solid tumors, such as breast cancer, colorectal cancer, gastric cancer, and lung adenocarcinoma [218–220]. In lung adenocarcinoma patients with poor prognosis, COL10A1 is upregulated and could physically interact with DDR2 to maintain a high level of FAK expression [221]. In addition, the direct involvement of COLX in epithelial–mesenchymal transition has been shown by analysis of tissues isolated from patients with aggressive forms of colorectal cancer [219].

7.4. Beaded Filament-Forming Collagens

Beaded filament-forming collagens are a family that includes type VI, XXVI, and XXVIII collagens. The beaded filaments appear as flexible, unbranched structures with a width of approximately 3 nm and a length of at least 2 microns [222]. Among them, type VI collagen (COL6) is a crucial component of the extracellular matrix, located in the basal membrane. Its main isoforms include the chains α1 (VI), α2 (VI), and α3 (VI). Moreover, there are three additional subunits (COL6A4, COL6A5, and COL6A6) that have been identified

subsequently [223]. COL6 forms a microfilamentous network that structurally supports cells and interacts with other ECM molecules, affecting their biological functions, such as tumor response. In solid tumors, acting as a scaffold between different types of collagens and cellular receptors such as integrins, COL6 is involved in the formation of new blood vessels through the assembly of the basement membrane, a unique feature among collagens and a fundamental process in tumorigenesis. The expression levels of collagen VI vary in different cancers such as glioblastoma, ovarian cancer, and pancreatic ductal adenocarcinoma, of which different expression is probably cancer-dependent [224,225]. For example, the increased expression of COL6 is related to the aggressiveness of tumor cells, as seen in bladder cancer of high-grade T1 patients [226]. COL6, mainly produced by fibroblasts and adipocytes, supports tumor stability, and transcriptional program maintenance is related to the aggressiveness of glioblastoma cells. For this reason, its silencing in glioblastoma cells causes a downregulation of genes related to tumor progression and DNA repair mechanisms, including PI3K/AKT, Insulin-like Growth Factor 1(IGF1), Fms-like Tyrosine kinase 3 (FLT3), Platelet-Derived Growth Factor (PDGF), and MAPK [227]. In addition, pancreatic ductal adenocarcinoma cells isolated from areas of low-rigidity tumor tissue have been seen to increase COL6 expression, which has promoted in vitro motility and in vivo metastatic potential of the tumor cells [228]. Similarly, in lung sarcoma metastases, a high expression of COL6 has been detected, suggesting that it is critical for the development of metastatic niches [229].

To date, the roles of cancer of type XXVI collagen (COL26) and type XXVIII collagen (COL28) in cancer remain poorly understood. A recent study showed that in patients with poor prognosis thyroid carcinoma, there was an overexpression of the alpha 1 chain of type XXVI collagen (COL26A1). However, the signaling pathways in which it is involved remain unclear [230]. Moreover, the serum collagen levels of type XXVIII were found to be high in patients with lung cancer, but also in this case the roles are not known yet [231].

7.5. Anchoring Fibrils Collagens

Anchoring fibrils collagens are fibrous structures located in the lamina of different external epithelia that allow the attachment of the epidermal basement membrane to the dermal extracellular matrix [216]. Type VII collagen (COL7) is the only component of this group and its role in tumorigenesis is little understood [232]. Some studies show that hyperexpression promotes tumor progression since this type of collagen creates a scaffold between stroma and tumor epithelium [233]. However, it has been shown that its reduction during the advanced stages of the disease is associated with greater invasiveness of various solid tumors. For example, immunohistochemical studies have demonstrated that COL7A1 is highly expressed in the stroma surrounding tumor cells in solid tumors, such as moderately and poorly differentiated gastric adenocarcinomas, thereby promoting neoplastic processes [234,235]. Moreover, hypomorphic mice with reduced Col7 expression exhibited heightened tumor invasiveness in oral squamous cell carcinoma, suggesting a possible causal link. In addition, the COL7 absence in keratinocytes increases the expression of lysosomal proteases and matrix metalloproteinases, promoting cell invasion [236]. Moreover, in gastric carcinoma immunohistochemistry, it was observed that expression of type VII collagen alpha chain (COL7A1) was higher in tumor tissue than in healthy tissue, mainly localized in the extracellular matrix [234]. An increase in COL7 in the initial stages of the disease may be functional to the progression. On the other hand, its reduction during the more advanced phases can increase the invasive and metastatic potential of the cancer cells of some solid tumors, such as oral carcinoma.

7.6. Transmembrane Collagens

Transmembrane collagen proteins are trimers of α chains and exhibit a characteristic type II membrane protein structure. They are involved in various functions, including cell adhesion and epithelial–mesenchymal interactions [237]. This subgroup includes type XIII, XVII, XXIII, and XXV collagens. Among these, the role of type XVII collagen (COL17), a

component of hemidesmosome, is particularly controversial. This is because its presence may be associated with a risk factor for patients, depending on the cancer type. In particular, the transmembrane COL17 plays a crucial role in anchoring undifferentiated keratinocytes to hemidesmosomes, while its expression is reduced in mature keratinocytes [238,239]. However, its expression significantly increases in melanomas and squamous cell carcinomas, where its deposition at the vertical fronts of the tumor is statistically associated with tumor cell invasiveness [152,153]. Moreover, a high expression of type 17 collagen alpha 1 chain (COL17A1) may be associated with a positive course for breast cancer patients, while it could be an unfavorable prognostic marker for pancreatic cancer patients [240,241]. A recent study showed how COL17 negatively affects the growth and proliferation of breast cancer cells. In particular, the tumor progression was inversely proportional to the expression of COL17, both in MCF7 and MDA-MB-231 cells and in xenotransplanted mice with overexpressed COL17 cells. COL17 inhibited the AKT/mTOR pathway and consequently reduced activation of downstream effectors such as p70S6K and 4EBP1, essential for tumor progression [242]. Furthermore, its role in colorectal cancer has also been analyzed. The absence of COL17A1 positively affected the cell cycle of dormant colorectal cancer stem cells (LGR5p27), leading to a poor prognosis for patients. More specifically, chemotherapy exposure caused a remodeling of the ECM involving COL17A1 degradation. In this way, the absence of COL17A1 promotes the FAK-YAP pathway, restoring the proliferation of dormant LGR5p27 [243]. Finally, COL17A1 can be used as a tumor biomarker, since serum COL17 levels were higher in patients with different solid tumors, including pancreatic cancer, compared to healthy controls [244].

The involvement of type XIII, type XXIII, and type XXV collagens in cancer ECM has been marginally analyzed. However, most recent studies analyze the involvement of type XIII collagen (COL13) in the invasion, progression, and migration of triple-negative breast cancer cells (MDA-MB-231). COL13 interacts with the integrin β1 and active downstream TGF-β contributing to tumor progression, as seen also in the mammosphere. In addition, COL13 boosts staminality and anoikis resistance of breast cancer cells, during the migration process [245]. Anoikis is apoptosis induced by the detachment of cells from the origin environment, through the disassembly of integrin–ECM and cadherin–cell [246]. Resistance to this mechanism plays a fundamental role in the circulating survival of cancer cells with migratory abilities [247].

Recent research has investigated the role of the α1 chain of collagen XXIII (COL23A1) in clear cell renal cell carcinoma (ccRCC). Analysis of tissues from patients with ccRCC with poor prognosis showed that this molecule enhances the progression, adhesion, and migration of cancer cells. Furthermore, knockdown underregulated the adhesion, proliferation, and migration of ccRCC cells, suggesting that COL23A1 plays a crucial role in this context [248].

Finally, the role of type XXV collagen in tumors is not well understood. There is only one study (2022) that identified for the first time the presence of alpha-1 collagen chain type XXV (Col25a1) in the ECM of murine breast tumors, while its expression was not found in the corresponding healthy tissue and human breast cancer tissue [249]. Consequently, its association with healthy and tumor ECM remains unclear.

7.7. Multiplexine

Multiplexins are basement membrane-associated collagens, including type XV (COL15) and type XVIII (COL18) collagens [250]. Despite the structural similarity and localization in the basal membrane, type XV and type XVIII collagens have distinct biological functions. COL15 is involved in the development of muscles and microvessels, while COL18 is in the development of the brain and eyes [251]. Their functions in tumorigenesis have been poorly understood. However, in the past decade, a possible role of COL15 has been identified as a cervical cancer suppressor [252]. Moreover, recent studies have shown its direct involvement in the suppression of hepato-carcinoma cells. More specifically, the silencing of the type XV collagen alpha chain (COL15A1), obtained by small interfering

RNA, significantly enhanced the growth, invasion, and migration of hepato-carcinoma cells induced by the hepatitis B virus [253]. In addition, it has been shown that COL15 could impede hepato-carcinoma cell migration by underregulating the transcription factor Snail/Slug-mediated EMT [254].

In contrast to COL15, COL18 seems to have a positive role in the growth of solid tumors, such as in clear cell renal cell carcinoma and breast cancer [255]. COL18 interacts with the receptor tyrosine kinase of epidermal growth factor and with integrin α6 in breast cancer. The TSP-1 N-terminal domain of COL18 interacts with its receptors, triggering the downstream activation of MAPK/ERK and PI3/AKT pathways. In this way, COLXVIII supports the proliferation and migration of clear cell renal cell carcinoma [256].

Finally, the literature currently lacks the role of type II, IX, and type XXIV collagen in tumor ECM.

The various roles of specific tumor collagens are listed in Table 1.

Table 1. Collagen families, types, and their role in tumor progression.

Collagen Family	Collagen Type	Tumor	Roles	References
Fibrillar Collagen	Type I	Triple-negative breast carcinoma, pancreatic ductal adenocarcinoma, and gastric carcinoma	Increased metastasis, proliferation, and invasion.	[139,146–155]
	Type II *	Not reported	Not reported	Not reported
	Type III	Breast cancer	Reduction in invasiveness, tumor growth suppression; increased cell quiescence; inhibition of autophagy	[48,146,155–159]
	Type V	Gastric cancer	Increased proliferation and epithelial–mesenchymal transition	[160–162]
	Type XI	Papillary thyroid carcinoma, breast cancer, colorectal carcinoma, esophageal cancer, gastric cancer, pancreatic cancer, lung cancer, and ovarian cancer	Promotion of proliferation, drug resistance, and tumor invasiveness	[63,163–174]
	Type XXVII	Melanoma cells	Promotion of tumor cells quiescence	[175]
	Type XXIV *	Not reported	Not reported	Not reported
FACITs	Type XII	Breast cancer, colorectal cancer, pancreatic adenocarcinoma, and ovarian cancer	Promotion of tumor progression and metastasis	[179–183]
	Type XVI	Colorectal cancer (CRC), glioblastoma, and oral squamous cell carcinoma	Increased invasiveness	[184–186]
	Type XIV	Melanoma	Reduction in malignancy	[187]
	Type XIX	Melanoma	Inhibition of tumor cell migration and invasion	[188]
	Type XX	Pancreatic ductal adenocarcinoma	Not reported	[189]
	Type XXII	Pancreatic ductal adenocarcinoma	Not reported	[189]

Table 1. *Cont.*

Collagen Family	Collagen Type	Tumor	Roles	References
	Type XXI	Gastric carcinoma	Increased tumor progression	[190]
	Type IX *	Not reported	Not reported	Not reported
Network-forming collagen	Type IV	Breast carcinoma, colorectal tumor, hepatocellular carcinoma	Promotion of tumor proliferation, durotaxis, angiogenesis, and metastasis. Reduction in angiogenesis	[192–214]
	Type VIII	Breast and pancreatic ductal adenocarcinoma	Promotion of tumor cell invasion and migration, as well as drug resistance	[149,215,257]
	Type X	Breast cancer, colorectal cancer, gastric cancer, and lung adenocarcinoma	Promotion of tumor cell proliferation, migration, and invasion	[218–221]
Beaded filament-forming collagen	Type VI	Glioblastoma, ovarian cancer, and pancreatic ductal adenocarcinoma	Promotion of metastasis, angiogenesis, and tumor progression	[224–229]
	Type XXVI	Thyroid carcinoma	Not reported	[230]
	Type XXVIII	Lung cancer	Not reported	[231]
Anchoring fibril	Type VII	Oral squamous cell carcinoma and gastric carcinoma	Promotion of tumor progression; block invasiveness	[232–236]
Transmembrane collagen	Type XVII	Squamous cell carcinoma; breast cancer, colorectal cancer	Promotion of cell migration and invasion. Block tumor progression	[238–246]
	Type XIII	Breast, clear cell renal cell carcinoma, and prostate cancer	Tumor progression, invasion, resistance to anoikis, and tumor metastasis	[245–247]
	Type XXIII	Clear cell renal cell carcinoma	Promotion of tumor progression, adhesion, and migration	[248]
	Type XXV	Breast cancer	Not reported	[249]
Multiplexin	Type XV	Cervical cancer; hepato-carcinoma	Reduction in growth, invasion, and migration	[251–254]
	Type XVIII	Clear cell renal carcinoma, breast cancer	Increased proliferation and migration	[252,256,257]

* Roles of collagens II, XXIV, and IX in tumor progression uncleared.

8. Conclusions

Collagen is the most common protein in mammals and is the main component of the extracellular matrix. In normal tissues, a dynamic biophysical and biochemical interaction is established between collagen fibers and resident fibroblasts, where tensile and rebound energy in tissue is translated into the activation of appropriate mechanical transduction pathways [27,120,258]. Therefore, the structural changes that collagen undergoes are not only limited to the physical concept of the tissue but also modulate the biochemistry of the cells that compose it. However, these mechanisms are also critical for the development of various diseases, such as cancer [12,259].

In this context, a continuous crosstalk is established between collagen fibers within the tumor microenvironment and cancer cells. Structural modifications and variations in

matrix collagens are perceived by cancer cells, activating mechanotransduction pathways, which modulate tumor progression, invasion, and migration.

For instance, type I collagen promotes epithelial–mesenchymal transition, thereby enhancing cancer cell invasion. Other collagens, such as types V, VI, VIII, and XII, facilitate tumor progression by upregulating the PI3K/Akt signaling pathway. In addition, collagen can modulate the immune system activity, contributing to tumor progression [94], acting as a physical barrier to the infiltration of the immune cells. However, some collagens can suppress these mechanisms in tumors. For instance, a reduction in type III collagen in ECM breast cancer is associated with a poor prognosis. Type XV collagen has also been identified as a tumor suppressor. This is due to its action upstream of EMT-related signaling pathways by downregulating transcription factors Snail/Slug. Furthermore, some peptide fragments derived from collagen type IV can inhibit neo-angiogenesis in tumors, with possible therapeutic applications [204].

Unfortunately, significant data on the role of type II, IX, and XXIV collagens in the extracellular matrix of tumors are still lacking in current scientific research. While other collagen types have been studied over the years, their impact on solid tumors remains uncertain. This review provides an overview of the roles of various collagen types in the extracellular matrix of solid tumors. A deeper understanding of these molecules could lead to significant advancements in the diagnosis, prognosis, and treatment of solid tumors. In recent decades, the use of collagenases in therapeutic applications—both as free enzymes and when conjugated to nanoparticles—has gained attention in the scientific community. These enzymes have the potential to break down the collagen-rich extracellular matrix of tumors, facilitating their treatment. The proteolytic activity of collagenases can improve the permeability of tumors to chemotherapeutic agents and immune cells, resulting in enhanced effectiveness of various cancer therapies. In summary, these innovative approaches represent a new frontier in the treatment of solid tumors, with collagen serving as a primary therapeutic target [260–262].

Author Contributions: G.L.B. and A.L.C., writing—original draft preparation; S.C. and G.G., writing—review and editing; G.G., supervision. All authors have read and agreed to the published version of the manuscript.

Funding: This research was funded by the Italian Ministry of University and Research (MUR) for the PON project on Research and Innovation 2014–2020 (Azione IV.4—Contratti di ricerca su tematiche dell'Innovazione—B75F21002190001). This work has received funding from the European Union-NextGenerationEU through the Italian Ministry of University and Research under PNRR–MUR, PNRR-M4C2, ECS_00000022-SiciliAn MicronanOTecH Research And Innovation CEnter "SAMOTHRACE"—CUP: B73C22000810001. The views and opinions expressed are those of the authors only and do not necessarily reflect those of the European Union or the European Commission. Neither the European Union nor the European Commission can be held responsible for them.

Data Availability Statement: Not applicable.

Conflicts of Interest: Author Giulio Ghersi was employed by the company Abiel srl. The authors declare that this research was conducted in the absence of any commercial or financial relationships that could be construed as a potential conflict of interest. The funders had no role in the design of the study; in the collection, analyses, or interpretation of data; in the writing of the manuscript, or in the decision to publish the results.

References

1. Holwerda, A.M.; van Loon, L.J.C. The Impact of Collagen Protein Ingestion on Musculoskeletal Connective Tissue Remodeling: A Narrative Review. *Nutr. Rev.* **2022**, *80*, 1497–1514. [CrossRef] [PubMed]
2. Zhang, Q.; Sioud, M. Tumor-Associated Macrophage Subsets: Shaping Polarization and Targeting. *Int. J. Mol. Sci.* **2023**, *24*, 7493. [CrossRef] [PubMed]
3. Yuan, Z.; Li, Y.; Zhang, S.; Wang, X.; Dou, H.; Yu, X.; Zhang, Z.; Yang, S.; Xiao, M. Extracellular Matrix Remodeling in Tumor Progression and Immune Escape: From Mechanisms to Treatments. *Mol. Cancer* **2023**, *22*, 48. [CrossRef] [PubMed]
4. Prasad, N.; Topping, R.S.; Decker, S.J. Src Family Tyrosine Kinases Regulate Adhesion-Dependent Tyrosine Phosphorylation of 5′-Inositol Phosphatase SHIP2 during Cell Attachment and Spreading on Collagen I. *J. Cell Sci.* **2002**, *115*, 3807–3815. [CrossRef]

5. Theocharis, A.D.; Skandalis, S.S.; Gialeli, C.; Karamanos, N.K. Extracellular Matrix Structure. *Adv. Drug Deliv. Rev.* **2016**, *97*, 4–27. [CrossRef]
6. Sun, B. The Mechanics of Fibrillar Collagen Extracellular Matrix. *Cell Rep. Phys. Sci.* **2021**, *2*, 100515. [CrossRef]
7. Hanahan, D.; Weinberg, R.A. Hallmarks of Cancer: The Next Generation. *Cell* **2011**, *144*, 646–674. [CrossRef]
8. Piersma, B.; Hayward, M.-K.; Weaver, V.M. Fibrosis and Cancer: A Strained Relationship. *Biochim. Biophys. Acta—Rev. Cancer* **2020**, *1873*, 188356. [CrossRef]
9. Conklin, M.W.; Eickhoff, J.C.; Riching, K.M.; Pehlke, C.A.; Eliceiri, K.W.; Provenzano, P.P.; Friedl, A.; Keely, P.J. Aligned Collagen Is a Prognostic Signature for Survival in Human Breast Carcinoma. *Am. J. Pathol.* **2011**, *178*, 1221–1232. [CrossRef]
10. Sarwar, M.; Sykes, P.H.; Chitcholtan, K.; Evans, J.J. Collagen I Dysregulation Is Pivotal for Ovarian Cancer Progression. *Tissue Cell* **2022**, *74*, 101704. [CrossRef]
11. Nelson, M.S.; Liu, Y.; Wilson, H.M.; Li, B.; Rosado-Mendez, I.M.; Rogers, J.D.; Block, W.F.; Eliceiri, K.W. *Multiscale Label-Free Imaging of Fibrillar Collagen in the Tumor Microenvironment*; Springer: Berlin/Heidelberg, Germany, 2023; pp. 187–235.
12. Xu, S.; Xu, H.; Wang, W.; Li, S.; Li, H.; Li, T.; Zhang, W.; Yu, X.; Liu, L. The Role of Collagen in Cancer: From Bench to Bedside. *J. Transl. Med.* **2019**, *17*, 309. [CrossRef] [PubMed]
13. Du, H.; Pang, M.; Hou, X.; Yuan, S.; Sun, L. PLOD2 in Cancer Research. *Biomed. Pharmacother.* **2017**, *90*, 670–676. [CrossRef] [PubMed]
14. Poonja, S.; Forero Pinto, A.; Lloyd, M.C.; Damaghi, M.; Rejniak, K.A. Dynamics of Fibril Collagen Remodeling by Tumor Cells: A Model of Tumor-Associated Collagen Signatures. *Cells* **2023**, *12*, 2688. [CrossRef] [PubMed]
15. Necula, L.; Matei, L.; Dragu, D.; Pitica, I.; Neagu, A.; Bleotu, C.; Diaconu, C.C.; Chivu-Economescu, M. Collagen Family as Promising Biomarkers and Therapeutic Targets in Cancer. *Int. J. Mol. Sci.* **2022**, *23*, 12415. [CrossRef]
16. Bonnans, C.; Chou, J.; Werb, Z. Remodelling the Extracellular Matrix in Development and Disease. *Nat. Rev. Mol. Cell Biol.* **2014**, *15*, 786–801. [CrossRef]
17. Sorushanova, A.; Delgado, L.M.; Wu, Z.; Shologu, N.; Kshirsagar, A.; Raghunath, R.; Mullen, A.M.; Bayon, Y.; Pandit, A.; Raghunath, M.; et al. The Collagen Suprafamily: From Biosynthesis to Advanced Biomaterial Development. *Adv. Mater.* **2019**, *31*, 1801651. [CrossRef]
18. Hinz, B. Myofibroblasts. *Exp. Eye Res.* **2016**, *142*, 56–70. [CrossRef]
19. Zhang, M.; Serna-Salas, S.; Damba, T.; Borghesan, M.; Demaria, M.; Moshage, H. Hepatic Stellate Cell Senescence in Liver Fibrosis: Characteristics, Mechanisms and Perspectives. *Mech. Ageing Dev.* **2021**, *199*, 111572. [CrossRef]
20. Goldmann, T.; Zissel, G.; Watz, H.; Drömann, D.; Reck, M.; Kugler, C.; Rabe, K.F.; Marwitz, S. Human Alveolar Epithelial Cells Type II Are Capable of TGFβ-Dependent Epithelial-Mesenchymal-Transition and Collagen-Synthesis. *Respir. Res.* **2018**, *19*, 138. [CrossRef]
21. van den Akker, J.; Tuna, B.G.; Pistea, A.; Sleutel, A.J.J.; Bakker, E.N.T.P.; van Bavel, E. Vascular Smooth Muscle Cells Remodel Collagen Matrices by Long-Distance Action and Anisotropic Interaction. *Med. Biol. Eng. Comput.* **2012**, *50*, 701–715. [CrossRef]
22. Zunich, S.M.; Valdovinos, M.; Douglas, T.; Walterhouse, D.; Iannaccone, P.; Lamm, M.L.G. Osteoblast-Secreted Collagen Upregulates Paracrine Sonic Hedgehog Signaling by Prostate Cancer Cells and Enhances Osteoblast Differentiation. *Mol. Cancer* **2012**, *11*, 30. [CrossRef] [PubMed]
23. RHEE, S.; GRINNELL, F. Fibroblast Mechanics in 3D Collagen Matrices. *Adv. Drug Deliv. Rev.* **2007**, *59*, 1299–1305. [CrossRef] [PubMed]
24. Sobierajska, K.; Ciszewski, W.M.; Sacewicz-Hofman, I.; Niewiarowska, J. *Endothelial Cells in the Tumor Microenvironment*; Springer: Berlin/Heidelberg, Germany, 2020; pp. 71–86.
25. Varma, S.; Orgel, J.P.R.O.; Schieber, J.D. Nanomechanics of Type I Collagen. *Biophys. J.* **2016**, *111*, 50–56. [CrossRef] [PubMed]
26. Gordon, M.K.; Hahn, R.A. Collagens. *Cell Tissue Res.* **2010**, *339*, 247–257. [CrossRef]
27. Silver, F.H.; Kelkar, N.; Deshmukh, T. Molecular Basis for Mechanical Properties of ECMs: Proposed Role of Fibrillar Collagen and Proteoglycans in Tissue Biomechanics. *Biomolecules* **2021**, *11*, 1018. [CrossRef]
28. Costa, S.; Ragusa, M.A.; Lo Buglio, G.; Scilabra, S.D.; Nicosia, A. The Repertoire of Tissue Inhibitors of Metalloproteases: Evolution, Regulation of Extracellular Matrix Proteolysis, Engineering and Therapeutic Challenges. *Life* **2022**, *12*, 1145. [CrossRef]
29. Lu, P.; Takai, K.; Weaver, V.M.; Werb, Z. Extracellular Matrix Degradation and Remodeling in Development and Disease. *Cold Spring Harb. Perspect. Biol.* **2011**, *3*, a005058. [CrossRef]
30. Siadat, S.M.; Ruberti, J.W. Mechanochemistry of Collagen. *Acta Biomater.* **2023**, *163*, 50–62. [CrossRef]
31. Fang, M.; Yuan, J.; Peng, C.; Li, Y. Collagen as a Double-Edged Sword in Tumor Progression. *Tumor Biol.* **2014**, *35*, 2871–2882. [CrossRef]
32. Ferreira, A.M.; Gentile, P.; Chiono, V.; Ciardelli, G. Collagen for Bone Tissue Regeneration. *Acta Biomater.* **2012**, *8*, 3191–3200. [CrossRef]
33. Cram, D.J. The Design of Molecular Hosts, Guests, and Their Complexes. *Science* **1988**, *240*, 760–767. [CrossRef] [PubMed]
34. Yamauchi, M.; Sricholpech, M. Lysine Post-Translational Modifications of Collagen. *Essays Biochem.* **2012**, *52*, 113–133. [CrossRef] [PubMed]
35. Vallet, S.D.; Ricard-Blum, S. Lysyl Oxidases: From Enzyme Activity to Extracellular Matrix Cross-Links. *Essays Biochem.* **2019**, *63*, 349–364. [CrossRef] [PubMed]

36. Winkler, J.; Abisoye-Ogunniyan, A.; Metcalf, K.J.; Werb, Z. Concepts of Extracellular Matrix Remodelling in Tumour Progression and Metastasis. *Nat. Commun.* **2020**, *11*, 5120. [CrossRef]
37. Zhang, Q.; An, Z.-Y.; Jiang, W.; Jin, W.-L.; He, X.-Y. Collagen Code in Tumor Microenvironment: Functions, Molecular Mechanisms, and Therapeutic Implications. *Biomed. Pharmacother.* **2023**, *166*, 115390. [CrossRef]
38. Belli, C.; Trapani, D.; Viale, G.; D'Amico, P.; Duso, B.A.; Della Vigna, P.; Orsi, F.; Curigliano, G. Targeting the Microenvironment in Solid Tumors. *Cancer Treat. Rev.* **2018**, *65*, 22–32. [CrossRef]
39. Xing, F. Cancer Associated Fibroblasts (CAFs) in Tumor Microenvironment. *Front. Biosci.* **2010**, *15*, 166. [CrossRef]
40. Chen, Y.; McAndrews, K.M.; Kalluri, R. Clinical and Therapeutic Relevance of Cancer-Associated Fibroblasts. *Nat. Rev. Clin. Oncol.* **2021**, *18*, 792–804. [CrossRef]
41. Hu, D.; Li, Z.; Zheng, B.; Lin, X.; Pan, Y.; Gong, P.; Zhuo, W.; Hu, Y.; Chen, C.; Chen, L.; et al. Cancer-associated Fibroblasts in Breast Cancer: Challenges and Opportunities. *Cancer Commun.* **2022**, *42*, 401–434. [CrossRef]
42. Tian, H.; Shi, H.; Yu, J.; Ge, S.; Ruan, J. Biophysics Role and Biomimetic Culture Systems of ECM Stiffness in Cancer EMT. *Glob. Chall.* **2022**, *6*, 2100094. [CrossRef]
43. Paszek, M.J.; Weaver, V.M. The Tension Mounts: Mechanics Meets Morphogenesis and Malignancy. *J. Mammary Gland Biol. Neoplasia* **2004**, *9*, 325–342. [CrossRef] [PubMed]
44. Jiang, Y.; Zhang, H.; Wang, J.; Liu, Y.; Luo, T.; Hua, H. Targeting Extracellular Matrix Stiffness and Mechanotransducers to Improve Cancer Therapy. *J. Hematol. Oncol.* **2022**, *15*, 34. [CrossRef] [PubMed]
45. Xiong, J.; Yan, L.; Zou, C.; Wang, K.; Chen, M.; Xu, B.; Zhou, Z.; Zhang, D. Integrins Regulate Stemness in Solid Tumor: An Emerging Therapeutic Target. *J. Hematol. Oncol.* **2021**, *14*, 177. [CrossRef] [PubMed]
46. Zhang, X.; Huang, S.; Guo, J.; Zhou, L.; You, L.; Zhang, T.; Zhao, Y. Insights into the Distinct Roles of MMP-11 in Tumor Biology and Future Therapeutics (Review). *Int. J. Oncol.* **2016**, *48*, 1783–1793. [CrossRef]
47. Wall, S.J.; Werner, E.; Werb, Z.; DeClerck, Y.A. Discoidin Domain Receptor 2 Mediates Tumor Cell Cycle Arrest Induced by Fibrillar Collagen. *J. Biol. Chem.* **2005**, *280*, 40187–40194. [CrossRef]
48. Di Martino, J.S.; Nobre, A.R.; Mondal, C.; Taha, I.; Farias, E.F.; Fertig, E.J.; Naba, A.; Aguirre-Ghiso, J.A.; Bravo-Cordero, J.J. A Tumor-Derived Type III Collagen-Rich ECM Niche Regulates Tumor Cell Dormancy. *Nat. Cancer* **2021**, *3*, 90–107. [CrossRef]
49. Koohestani, F.; Braundmeier, A.G.; Mahdian, A.; Seo, J.; Bi, J.; Nowak, R.A. Extracellular Matrix Collagen Alters Cell Proliferation and Cell Cycle Progression of Human Uterine Leiomyoma Smooth Muscle Cells. *PLoS ONE* **2013**, *8*, e75844. [CrossRef]
50. Deka, J.; Wiedemann, N.; Anderle, P.; Murphy-Seiler, F.; Bultinck, J.; Eyckerman, S.; Stehle, J.-C.; André, S.; Vilain, N.; Zilian, O.; et al. Bcl9/Bcl9l Are Critical for Wnt-Mediated Regulation of Stem Cell Traits in Colon Epithelium and Adenocarcinomas. *Cancer Res.* **2010**, *70*, 6619–6628. [CrossRef]
51. Hou, S.; Isaji, T.; Hang, Q.; Im, S.; Fukuda, T.; Gu, J. Distinct Effects of B1 Integrin on Cell Proliferation and Cellular Signaling in MDA-MB-231 Breast Cancer Cells. *Sci. Rep.* **2016**, *6*, 18430. [CrossRef]
52. Liberti, M.V.; Locasale, J.W. The Warburg Effect: How Does It Benefit Cancer Cells? *Trends Biochem. Sci.* **2016**, *41*, 211–218. [CrossRef]
53. Mah, E.J.; Lefebvre, A.E.Y.T.; McGahey, G.E.; Yee, A.F.; Digman, M.A. Collagen Density Modulates Triple-Negative Breast Cancer Cell Metabolism through Adhesion-Mediated Contractility. *Sci. Rep.* **2018**, *8*, 17094. [CrossRef] [PubMed]
54. Fontana, F.; Giannitti, G.; Marchesi, S.; Limonta, P. The PI3K/Akt Pathway and Glucose Metabolism: A Dangerous Liaison in Cancer. *Int. J. Biol. Sci.* **2024**, *20*, 3113–3125. [CrossRef] [PubMed]
55. Yang, L.; Hou, Y.; Yuan, J.; Tang, S.; Zhang, H.; Zhu, Q.; Du, Y.; Zhou, M.; Wen, S.; Xu, L.; et al. Twist Promotes Reprogramming of Glucose Metabolism in Breast Cancer Cells through PI3K/AKT and P53 Signaling Pathways. *Oncotarget* **2015**, *6*, 25755–25769. [CrossRef] [PubMed]
56. Mahout, M.; Schwartz, L.; Attal, R.; Bakkar, A.; Peres, S. Metabolic Modelling Links Warburg Effect to Collagen Formation, Angiogenesis and Inflammation in the Tumoral Stroma. *PLoS ONE* **2024**, *19*, e0313962. [CrossRef] [PubMed]
57. Zheng, Y.; Zhou, R.; Cai, J.; Yang, N.; Wen, Z.; Zhang, Z.; Sun, H.; Huang, G.; Guan, Y.; Huang, N.; et al. Matrix Stiffness Triggers Lipid Metabolic Cross-Talk between Tumor and Stromal Cells to Mediate Bevacizumab Resistance in Colorectal Cancer Liver Metastases. *Cancer Res.* **2023**, *83*, 3577–3592. [CrossRef]
58. Cai, J.; Chen, T.; Jiang, Z.; Yan, J.; Ye, Z.; Ruan, Y.; Tao, L.; Shen, Z.; Liang, X.; Wang, Y.; et al. Bulk and Single-Cell Transcriptome Profiling Reveal Extracellular Matrix Mechanical Regulation of Lipid Metabolism Reprograming through YAP/TEAD4/ACADL Axis in Hepatocellular Carcinoma. *Int. J. Biol. Sci.* **2023**, *19*, 2114–2131. [CrossRef]
59. Morana, O.; Wood, W.; Gregory, C.D. The Apoptosis Paradox in Cancer. *Int. J. Mol. Sci.* **2022**, *23*, 1328. [CrossRef]
60. Lv, Y.; Shan, Y.; Song, L.; Zhao, Y.; Lai, R.; Su, J.; Zhang, X. Type I Collagen Promotes Tumor Progression of Integrin B1 Positive Gastric Cancer through a BCL9L/β-Catenin Signaling Pathway. *Aging* **2021**, *13*, 19064–19076. [CrossRef]
61. Saby, C.; Rammal, H.; Magnien, K.; Buache, E.; Brassart-Pasco, S.; Van-Gulick, L.; Jeannesson, P.; Maquoi, E.; Morjani, H. Age-Related Modifications of Type I Collagen Impair DDR1-Induced Apoptosis in Non-Invasive Breast Carcinoma Cells. *Cell Adh. Migr.* **2018**, *12*, 335–347. [CrossRef]
62. Maquoi, E.; Assent, D.; Detilleux, J.; Pequeux, C.; Foidart, J.-M.; Noël, A. MT1-MMP Protects Breast Carcinoma Cells against Type I Collagen-Induced Apoptosis. *Oncogene* **2012**, *31*, 480–493. [CrossRef]
63. Tu, H.; Li, J.; Lin, L.; Wang, L. COL11A1 Was Involved in Cell Proliferation, Apoptosis and Migration in Non-Small Cell Lung Cancer Cells. *J. Investig. Surg.* **2021**, *34*, 664–669. [CrossRef] [PubMed]

64. Nyberg, P.; Xie, L.; Sugimoto, H.; Colorado, P.; Sund, M.; Holthaus, K.; Sudhakar, A.; Salo, T.; Kalluri, R. Characterization of the Anti-Angiogenic Properties of Arresten, an A1β1 Integrin-Dependent Collagen-Derived Tumor Suppressor. *Exp. Cell Res.* **2008**, *314*, 3292–3305. [CrossRef] [PubMed]
65. Wu, J.; Jiang, J.; Chen, B.; Wang, K.; Tang, Y.; Liang, X. Plasticity of Cancer Cell Invasion: Patterns and Mechanisms. *Transl. Oncol.* **2021**, *14*, 100899. [CrossRef] [PubMed]
66. Yan, T.; Zhang, A.; Shi, F.; Chang, F.; Mei, J.; Liu, Y.; Zhu, Y. Integrin Avβ3–Associated DAAM1 Is Essential for Collagen-Induced Invadopodia Extension and Cell Haptotaxis in Breast Cancer Cells. *J. Biol. Chem.* **2018**, *293*, 10172–10185. [CrossRef]
67. Artym, V.V.; Swatkoski, S.; Matsumoto, K.; Campbell, C.B.; Petrie, R.J.; Dimitriadis, E.K.; Li, X.; Mueller, S.C.; Bugge, T.H.; Gucek, M.; et al. Dense Fibrillar Collagen Is a Potent Inducer of Invadopodia via a Specific Signaling Network. *J. Cell Biol.* **2015**, *208*, 331–350. [CrossRef]
68. Han, B.; Guan, X.; Ma, M.; Liang, B.; Ren, L.; Liu, Y.; Du, Y.; Jiang, S.-H.; Song, D. Stiffened Tumor Microenvironment Enhances Perineural Invasion in Breast Cancer via Integrin Signaling. *Cell. Oncol.* **2024**, *47*, 867–882. [CrossRef]
69. Lee, C.S.; Siprashvili, Z.; Mah, A.; Bencomo, T.; Elcavage, L.E.; Che, Y.; Shenoy, R.M.; Aasi, S.Z.; Khavari, P.A. Mutant Collagen COL11A1 Enhances Cancerous Invasion. *Oncogene* **2021**, *40*, 6299–6307. [CrossRef]
70. Koorman, T.; Jansen, K.A.; Khalil, A.; Haughton, P.D.; Visser, D.; Rätze, M.A.K.; Haakma, W.E.; Sakalauskaitè, G.; van Diest, P.J.; de Rooij, J.; et al. Spatial Collagen Stiffening Promotes Collective Breast Cancer Cell Invasion by Reinforcing Extracellular Matrix Alignment. *Oncogene* **2022**, *41*, 2458–2469. [CrossRef]
71. Budden, T.; Gaudy-Marqueste, C.; Porter, A.; Kay, E.; Gurung, S.; Earnshaw, C.H.; Roeck, K.; Craig, S.; Traves, V.; Krutmann, J.; et al. Ultraviolet Light-Induced Collagen Degradation Inhibits Melanoma Invasion. *Nat. Commun.* **2021**, *12*, 2742. [CrossRef]
72. Naba, A.; Clauser, K.R.; Lamar, J.M.; Carr, S.A.; Hynes, R.O. Extracellular Matrix Signatures of Human Mammary Carcinoma Identify Novel Metastasis Promoters. *eLife* **2014**, *3*, e01308. [CrossRef]
73. Sahai, E.; Wyckoff, J.; Philippar, U.; Segall, J.E.; Gertler, F.; Condeelis, J. Simultaneous Imaging of GFP, CFP and Collagen in Tumors in Vivousing Multiphoton Microscopy. *BMC Biotechnol.* **2005**, *5*, 14. [CrossRef] [PubMed]
74. Chen, D.; Liu, Z.; Liu, W.; Fu, M.; Jiang, W.; Xu, S.; Wang, G.; Chen, F.; Lu, J.; Chen, H.; et al. Predicting Postoperative Peritoneal Metastasis in Gastric Cancer with Serosal Invasion Using a Collagen Nomogram. *Nat. Commun.* **2021**, *12*, 179. [CrossRef] [PubMed]
75. Deng, J.; Kang, Y.; Cheng, C.-C.; Li, X.; Dai, B.; Katz, M.H.; Men, T.; Kim, M.P.; Koay, E.A.; Huang, H.; et al. DDR1-Induced Neutrophil Extracellular Traps Drive Pancreatic Cancer Metastasis. *JCI Insight* **2021**, *6*, e146133. [CrossRef] [PubMed]
76. Akinjiyan, F.A.; Ibitoye, Z.; Zhao, P.; Shriver, L.P.; Patti, G.J.; Longmore, G.D.; Fuh, K.C. DDR2-Regulated Arginase Activity in Ovarian Cancer-Associated Fibroblasts Promotes Collagen Production and Tumor Progression. *Oncogene* **2024**, *43*, 189–201. [CrossRef]
77. Song, M.; Schnettler, E.; Venkatachalam, A.; Wang, Y.; Feldman, L.; Argenta, P.; Rodriguez-Rodriguez, L.; Ramakrishnan, S. Increased Expression of Collagen Prolyl Hydroxylases in Ovarian Cancer Is Associated with Cancer Growth and Metastasis. *Am. Cancer Res.* **2023**, *13*, 6051.
78. Muz, B.; de la Puente, P.; Azab, F.; Azab, A.K. The Role of Hypoxia in Cancer Progression, Angiogenesis, Metastasis, and Resistance to Therapy. *Hypoxia* **2015**, *3*, 83–92. [CrossRef]
79. Lin, K.; Zhao, Y.; Tang, Y.; Chen, Y.; Lin, M.; He, L. Collagen I-Induced VCAN/ERK Signaling and PARP1/ZEB1-Mediated Metastasis Facilitate OSBPL2 Defect to Promote Colorectal Cancer Progression. *Cell Death Dis.* **2024**, *15*, 85. [CrossRef]
80. Zhang, Y.; Liu, Z.; Yang, X.; Lu, W.; Chen, Y.; Lin, Y.; Wang, J.; Lin, S.; Yun, J.-P. H3K27 Acetylation Activated-COL6A1 Promotes Osteosarcoma Lung Metastasis by Repressing STAT1 and Activating Pulmonary Cancer-Associated Fibroblasts. *Theranostics* **2021**, *11*, 1473–1492. [CrossRef]
81. Edgar, L.T.; Underwood, C.J.; Guilkey, J.E.; Hoying, J.B.; Weiss, J.A. Extracellular Matrix Density Regulates the Rate of Neovessel Growth and Branching in Sprouting Angiogenesis. *PLoS ONE* **2014**, *9*, e85178. [CrossRef]
82. Balcioglu, H.E.; van de Water, B.; Danen, E.H.J. Tumor-Induced Remote ECM Network Orientation Steers Angiogenesis. *Sci. Rep.* **2016**, *6*, 22580. [CrossRef]
83. Chen, M.-C.; Hsu, W.-L.; Hwang, P.-A.; Chou, T.-C. Low Molecular Weight Fucoidan Inhibits Tumor Angiogenesis through Downregulation of HIF-1/VEGF Signaling under Hypoxia. *Mar. Drugs* **2015**, *13*, 4436–4451. [CrossRef] [PubMed]
84. Ahluwalia, A.; Tarnawski, A.S. Critical Role of Hypoxia Sensor-HIF-1α in VEGF Gene Activation. Implications for Angiogenesis and Tissue Injury Healing. *Curr. Med. Chem.* **2012**, *19*, 90–97. [CrossRef] [PubMed]
85. You, L.; Wu, W.; Wang, X.; Fang, L.; Adam, V.; Nepovimova, E.; Wu, Q.; Kuca, K. The Role of Hypoxia-inducible Factor 1 in Tumor Immune Evasion. *Med. Res. Rev.* **2021**, *41*, 1622–1643. [CrossRef] [PubMed]
86. Oudart, J.-B.; Villemin, M.; Brassart, B.; Sellier, C.; Terryn, C.; Dupont-Deshorgue, A.; Monboisse, J.C.; Maquart, F.-X.; Ramont, L.; Brassart-Pasco, S. F4, a Collagen XIX-Derived Peptide, Inhibits Tumor Angiogenesis through Avβ3 and A5β1 Integrin Interaction. *Cell Adh. Migr.* **2021**, *15*, 215–223. [CrossRef] [PubMed]
87. Mundel, T.M.; Kalluri, R. Type IV Collagen-Derived Angiogenesis Inhibitors. *Microvasc. Res.* **2007**, *74*, 85–89. [CrossRef]
88. Ramos, A.; Sadeghi, S.; Tabatabaeian, H. Battling Chemoresistance in Cancer: Root Causes and Strategies to Uproot Them. *Int. J. Mol. Sci.* **2021**, *22*, 9451. [CrossRef]
89. Lin, J.; Zou, B.; Li, H.; Wang, J.; Li, S.; Cao, J.; Xie, D.; Wang, F. Collagen XVII Promotes Dormancy of Colorectal Cancer Cells by Activating MTORC2 Signaling. *Cell Signal.* **2024**, *120*, 111234. [CrossRef]

90. Saatci, O.; Kaymak, A.; Raza, U.; Ersan, P.G.; Akbulut, O.; Banister, C.E.; Sikirzhytski, V.; Tokat, U.M.; Aykut, G.; Ansari, S.A.; et al. Targeting Lysyl Oxidase (LOX) Overcomes Chemotherapy Resistance in Triple Negative Breast Cancer. *Nat. Commun.* **2020**, *11*, 2416. [CrossRef]
91. Sharom, F.J. ABC Multidrug Transporters: Structure, Function and Role in Chemoresistance. *Pharmacogenomics* **2008**, *9*, 105–127. [CrossRef]
92. Baltes, F.; Pfeifer, V.; Silbermann, K.; Caspers, J.; Wantoch von Rekowski, K.; Schlesinger, M.; Bendas, G. B1-Integrin Binding to Collagen Type 1 Transmits Breast Cancer Cells into Chemoresistance by Activating ABC Efflux Transporters. *Biochim. Biophys. Acta—Mol. Cell Res.* **2020**, *1867*, 118663. [CrossRef]
93. Wu, Y.-H.; Huang, Y.-F.; Wu, P.-Y.; Chang, T.-H.; Huang, S.-C.; Chou, C.-Y. The Downregulation of MiR-509-3p Expression by Collagen Type XI Alpha 1-Regulated Hypermethylation Facilitates Cancer Progression and Chemoresistance via the DNA Methyltransferase 1/Small Ubiquitin-like Modifier-3 Axis in Ovarian Cancer Cells. *J. Ovarian. Res.* **2023**, *16*, 124. [CrossRef] [PubMed]
94. Collado, J.; Boland, L.; Ahrendsen, J.T.; Miska, J.; Lee-Chang, C. Understanding the Glioblastoma Tumor Microenvironment: Leveraging the Extracellular Matrix to Increase Immunotherapy Efficacy. *Front. Immunol.* **2024**, *15*, 1336476. [CrossRef] [PubMed]
95. Peng, D.H.; Rodriguez, B.L.; Diao, L.; Chen, L.; Wang, J.; Byers, L.A.; Wei, Y.; Chapman, H.A.; Yamauchi, M.; Behrens, C.; et al. Collagen Promotes Anti-PD-1/PD-L1 Resistance in Cancer through LAIR1-Dependent CD8+ T Cell Exhaustion. *Nat. Commun.* **2020**, *11*, 4520. [CrossRef] [PubMed]
96. Rømer, A.M.A.; Thorseth, M.-L.; Madsen, D.H. Immune Modulatory Properties of Collagen in Cancer. *Front. Immunol.* **2021**, *12*, 791453. [CrossRef]
97. Salmon, H.; Franciszkiewicz, K.; Damotte, D.; Dieu-Nosjean, M.-C.; Validire, P.; Trautmann, A.; Mami-Chouaib, F.; Donnadieu, E. Matrix Architecture Defines the Preferential Localization and Migration of T Cells into the Stroma of Human Lung Tumors. *J. Clin. Investig.* **2012**, *122*, 899–910. [CrossRef]
98. Ohno, S.; Tachibana, M.; Fujii, T.; Ueda, S.; Kubota, H.; Nagasue, N. Role of Stromal Collagen in Immunomodulation and Prognosis of Advanced Gastric Carcinoma. *Int. J. Cancer* **2002**, *97*, 770–774. [CrossRef]
99. Kuczek, D.E.; Larsen, A.M.H.; Thorseth, M.-L.; Carretta, M.; Kalvisa, A.; Siersbæk, M.S.; Simões, A.M.C.; Roslind, A.; Engelholm, L.H.; Noessner, E.; et al. Collagen Density Regulates the Activity of Tumor-Infiltrating T Cells. *J. Immunother. Cancer* **2019**, *7*, 68. [CrossRef]
100. Sun, X.; Wu, B.; Chiang, H.-C.; Deng, H.; Zhang, X.; Xiong, W.; Liu, J.; Rozeboom, A.M.; Harris, B.T.; Blommaert, E.; et al. Tumour DDR1 Promotes Collagen Fibre Alignment to Instigate Immune Exclusion. *Nature* **2021**, *599*, 673–678. [CrossRef]
101. Liu, J.; Chiang, H.-C.; Xiong, W.; Laurent, V.; Griffiths, S.C.; Dülfer, J.; Deng, H.; Sun, X.; Yin, Y.W.; Li, W.; et al. A Highly Selective Humanized DDR1 MAb Reverses Immune Exclusion by Disrupting Collagen Fiber Alignment in Breast Cancer. *J. Immunother. Cancer* **2023**, *11*, e006720. [CrossRef]
102. Tripathi, S.; Najem, H.; Dussold, C.; Pacheco, S.; Miska, J.; McCortney, K.; Steffens, A.; Walshon, J.; Winkowski, D.; Cloney, M.; et al. Cancer-Associated Fibroblast–Secreted Collagen Is Associated with Immune Inhibitor Receptor LAIR1 in Gliomas. *J. Clin. Investig.* **2024**, *134*, e176613. [CrossRef]
103. Rodriguez, B.L.; Huang, J.; Gibson, L.; Fradette, J.J.; Chen, H.-I.H.; Koyano, K.; Cortez, C.; Li, B.; Ho, C.; Ashique, A.M.; et al. Antitumor Activity of a Novel LAIR1 Antagonist in Combination with Anti-PD1 to Treat Collagen-Rich Solid Tumors. *Mol. Cancer Ther.* **2024**, *23*, 1144–1158. [CrossRef] [PubMed]
104. Xie, J.; Gui, X.; Deng, M.; Chen, H.; Chen, Y.; Liu, X.; Ku, Z.; Tan, L.; Huang, R.; He, Y.; et al. Blocking LAIR1 Signaling in Immune Cells Inhibits Tumor Development. *Front. Immunol.* **2022**, *13*, 996026. [CrossRef] [PubMed]
105. Vijver, S.V.; Singh, A.; Mommers-Elshof, E.T.A.M.; Meeldijk, J.; Copeland, R.; Boon, L.; Langermann, S.; Flies, D.; Meyaard, L.; Ramos, M.I.P. Collagen Fragments Produced in Cancer Mediate T Cell Suppression Through Leukocyte-Associated Immunoglobulin-Like Receptor 1. *Front. Immunol.* **2021**, *12*, 733561. [CrossRef] [PubMed]
106. Nicolas-Boluda, A.; Vaquero, J.; Vimeux, L.; Guilbert, T.; Barrin, S.; Kantari-Mimoun, C.; Ponzo, M.; Renault, G.; Deptula, P.; Pogoda, K.; et al. Tumor Stiffening Reversion Through Collagen Crosslinking Inhibition Improves T Cell Migration and Anti-PD-1 Treatment. *eLife* **2021**, *10*, e58688. [CrossRef]
107. Trackman, P.C. Lysyl Oxidase Isoforms and Potential Therapeutic Opportunities for Fibrosis and Cancer. *Expert Opin. Ther. Targets* **2016**, *20*, 935–945. [CrossRef]
108. Li, Z.; Mo, F.; Guo, K.; Ren, S.; Wang, Y.; Chen, Y.; Schwartz, P.B.; Richmond, N.; Liu, F.; Ronnekleiv-Kelly, S.M.; et al. Nanodrug-Bacteria Conjugates-Mediated Oncogenic Collagen Depletion Enhances Immune Checkpoint Blockade Therapy against Pancreatic Cancer. *Med* **2024**, *5*, 348–367.e7. [CrossRef]
109. Fukuda, Y.; Kim, S.-H.; Bustos, M.A.; Cho, S.-N.; Roszik, J.; Burks, J.K.; Kim, H.; Hoon, D.S.B.; Grimm, E.A.; Ekmekcioglu, S. Inhibition of Microsomal Prostaglandin E2 Synthase Reduces Collagen Deposition in Melanoma Tumors and May Improve Immunotherapy Efficacy by Reducing T-Cell Exhaustion. *Cancer Res. Commun.* **2023**, *3*, 1397–1408. [CrossRef]
110. Zhang, X.; Liu, J.; Yang, X.; Jiao, W.; Shen, C.; Zhao, X.; Wang, Y. High Expression of COL6A1 Predicts Poor Prognosis and Response to Immunotherapy in Bladder Cancer. *Cell Cycle* **2023**, *22*, 610–618. [CrossRef]
111. Chen, Y.; Yang, S.; Tavormina, J.; Tampe, D.; Zeisberg, M.; Wang, H.; Mahadevan, K.K.; Wu, C.-J.; Sugimoto, H.; Chang, C.-C.; et al. Oncogenic Collagen I Homotrimers from Cancer Cells Bind to A3β1 Integrin and Impact Tumor Microbiome and Immunity to Promote Pancreatic Cancer. *Cancer Cell* **2022**, *40*, 818–834.e9. [CrossRef]

112. Saad, E.E.; Michel, R.; Borahay, M.A. Immunosuppressive Tumor Microenvironment and Uterine Fibroids: Role in Collagen Synthesis. *Cytokine Growth Factor Rev.* **2024**, *75*, 93–100. [CrossRef]
113. Saad, E.E.; Michel, R.; Borahay, M.A. Senescence-Associated Secretory Phenotype (SASP) and Uterine Fibroids: Association with PD-L1 Activation and Collagen Deposition. *Ageing Res. Rev.* **2024**, *97*, 102314. [CrossRef] [PubMed]
114. Tohme, S.; Yazdani, H.O.; Al-Khafaji, A.B.; Chidi, A.P.; Loughran, P.; Mowen, K.; Wang, Y.; Simmons, R.L.; Huang, H.; Tsung, A. Neutrophil Extracellular Traps Promote the Development and Progression of Liver Metastases after Surgical Stress. *Cancer Res.* **2016**, *76*, 1367–1380. [CrossRef] [PubMed]
115. Sica, A.; Mantovani, A. Macrophage Plasticity and Polarization: In Vivo Veritas. *J. Clin. Investig.* **2012**, *122*, 787–795. [CrossRef] [PubMed]
116. Yao, R.-R.; Li, J.-H.; Zhang, R.; Chen, R.-X.; Wang, Y.-H. M2-Polarized Tumor-Associated Macrophages Facilitated Migration and Epithelial-Mesenchymal Transition of HCC Cells via the TLR4/STAT3 Signaling Pathway. *World. J. Surg. Oncol.* **2018**, *16*, 9. [CrossRef]
117. Santoni, M.; Massari, F.; Amantini, C.; Nabissi, M.; Maines, F.; Burattini, L.; Berardi, R.; Santoni, G.; Montironi, R.; Tortora, G.; et al. Emerging Role of Tumor-Associated Macrophages as Therapeutic Targets in Patients with Metastatic Renal Cell Carcinoma. *Cancer Immunol. Immunother.* **2013**, *62*, 1757–1768. [CrossRef]
118. Qiu, S.; Deng, L.; Liao, X.; Nie, L.; Qi, F.; Jin, K.; Tu, X.; Zheng, X.; Li, J.; Liu, L.; et al. Tumor-associated Macrophages Promote Bladder Tumor Growth through PI3K/AKT Signal Induced by Collagen. *Cancer Sci.* **2019**, *110*, 2110–2118. [CrossRef]
119. Di, X.; Gao, X.; Peng, L.; Ai, J.; Jin, X.; Qi, S.; Li, H.; Wang, K.; Luo, D. Cellular Mechanotransduction in Health and Diseases: From Molecular Mechanism to Therapeutic Targets. *Signal. Transduct. Target Ther.* **2023**, *8*, 282. [CrossRef]
120. Humphrey, J.D.; Dufresne, E.R.; Schwartz, M.A. Mechanotransduction and Extracellular Matrix Homeostasis. *Nat. Rev. Mol. Cell Biol.* **2014**, *15*, 802–812. [CrossRef]
121. Martino, F.; Perestrelo, A.R.; Vinarský, V.; Pagliari, S.; Forte, G. Cellular Mechanotransduction: From Tension to Function. *Front. Physiol.* **2018**, *9*, 824. [CrossRef]
122. Haller, S.J.; Dudley, A.T. Extracellular Mechanotransduction. *J. Gen. Physiol.* **2022**, *154*, e202113026. [CrossRef]
123. Mousavizadeh, R.; Hojabrpour, P.; Eltit, F.; McDonald, P.C.; Dedhar, S.; McCormack, R.G.; Duronio, V.; Jafarnejad, S.M.; Scott, A. B1 Integrin, ILK and MTOR Regulate Collagen Synthesis in Mechanically Loaded Tendon Cells. *Sci. Rep.* **2020**, *10*, 12644. [CrossRef] [PubMed]
124. Romani, P.; Valcarcel-Jimenez, L.; Frezza, C.; Dupont, S. Crosstalk between Mechanotransduction and Metabolism. *Nat. Rev. Mol. Cell. Biol.* **2021**, *22*, 22–38. [CrossRef] [PubMed]
125. Xin, Y.; Li, K.; Huang, M.; Liang, C.; Siemann, D.; Wu, L.; Tan, Y.; Tang, X. Biophysics in Tumor Growth and Progression: From Single Mechano-Sensitive Molecules to Mechanomedicine. *Oncogene* **2023**, *42*, 3457–3490. [CrossRef] [PubMed]
126. Yang, B.; Lieu, Z.Z.; Wolfenson, H.; Hameed, F.M.; Bershadsky, A.D.; Sheetz, M.P. Mechanosensing Controlled Directly by Tyrosine Kinases. *Nano Lett.* **2016**, *16*, 5951–5961. [CrossRef]
127. Fattet, L.; Jung, H.-Y.; Matsumoto, M.W.; Aubol, B.E.; Kumar, A.; Adams, J.A.; Chen, A.C.; Sah, R.L.; Engler, A.J.; Pasquale, E.B.; et al. Matrix Rigidity Controls Epithelial-Mesenchymal Plasticity and Tumor Metastasis via a Mechanoresponsive EPHA2/LYN Complex. *Dev. Cell* **2020**, *54*, 302–316.e7. [CrossRef]
128. Khalil, A.A.; Smits, D.; Haughton, P.D.; Koorman, T.; Jansen, K.A.; Verhagen, M.P.; van der Net, M.; van Zwieten, K.; Enserink, L.; Jansen, L.; et al. A YAP-Centered Mechanotransduction Loop Drives Collective Breast Cancer Cell Invasion. *Nat. Commun.* **2024**, *15*, 4866. [CrossRef]
129. Wu, T.; Xiong, S.; Chen, M.; Tam, B.T.; Chen, W.; Dong, K.; Ma, Z.; Wang, Z.; Ouyang, G. Matrix Stiffening Facilitates the Collective Invasion of Breast Cancer through the Periostin-Integrin Mechanotransduction Pathway. *Matrix Biol.* **2023**, *121*, 22–40. [CrossRef]
130. Shiu, J.-Y.; Aires, L.; Lin, Z.; Vogel, V. Nanopillar Force Measurements Reveal Actin-Cap-Mediated YAP Mechanotransduction. *Nat. Cell Biol.* **2018**, *20*, 262–271. [CrossRef]
131. Elosegui-Artola, A.; Andreu, I.; Beedle, A.E.M.; Lezamiz, A.; Uroz, M.; Kosmalska, A.J.; Oria, R.; Kechagia, J.Z.; Rico-Lastres, P.; Le Roux, A.-L.; et al. Force Triggers YAP Nuclear Entry by Regulating Transport across Nuclear Pores. *Cell* **2017**, *171*, 1397–1410.e14. [CrossRef]
132. Lee, J.Y.; Chang, J.K.; Dominguez, A.A.; Lee, H.; Nam, S.; Chang, J.; Varma, S.; Qi, L.S.; West, R.B.; Chaudhuri, O. YAP-Independent Mechanotransduction Drives Breast Cancer Progression. *Nat. Commun.* **2019**, *10*, 1848. [CrossRef]
133. Miyahara, Y.; Takano, S.; Sogawa, K.; Tomizawa, S.; Furukawa, K.; Takayashiki, T.; Kuboki, S.; Ohtsuka, M. Prosaposin, Tumor-secreted Protein, Promotes Pancreatic Cancer Progression by Decreasing Tumor-infiltrating Lymphocytes. *Cancer Sci.* **2022**, *113*, 2548–2559. [CrossRef] [PubMed]
134. Wu, Y.; Sun, L.; Zou, W.; Xu, J.; Liu, H.; Wang, W.; Yun, X.; Gu, J. Prosaposin, a Regulator of Estrogen Receptor Alpha, Promotes Breast Cancer Growth. *Cancer Sci.* **2012**, *103*, 1820–1825. [CrossRef] [PubMed]
135. Jiang, Y.; Zhou, J.; Luo, P.; Gao, H.; Ma, Y.; Chen, Y.-S.; Li, L.; Zou, D.; Zhang, Y.; Jing, Z. Prosaposin Promotes the Proliferation and Tumorigenesis of Glioma through Toll-like Receptor 4 (TLR4)-Mediated NF-KB Signaling Pathway. *EBioMedicine* **2018**, *37*, 78–90. [CrossRef] [PubMed]
136. Ishihara, S.; Inman, D.R.; Li, W.-J.; Ponik, S.M.; Keely, P.J. Mechano-Signal Transduction in Mesenchymal Stem Cells Induces Prosaposin Secretion to Drive the Proliferation of Breast Cancer Cells. *Cancer Res.* **2017**, *77*, 6179–6189. [CrossRef] [PubMed]

137. Nasser, M.; Wu, Y.; Danaoui, Y.; Ghosh, G. Engineering Microenvironments towards Harnessing Pro-Angiogenic Potential of Mesenchymal Stem Cells. *Mater. Sci. Eng. C* **2019**, *102*, 75–84. [CrossRef]
138. Dong, Y.; Xie, X.; Wang, Z.; Hu, C.; Zheng, Q.; Wang, Y.; Chen, R.; Xue, T.; Chen, J.; Gao, D.; et al. Increasing Matrix Stiffness Upregulates Vascular Endothelial Growth Factor Expression in Hepatocellular Carcinoma Cells Mediated by Integrin B1. *Biochem. Biophys. Res. Commun.* **2014**, *444*, 427–432. [CrossRef]
139. Thorlacius-Ussing, J.; Jensen, C.; Nissen, N.I.; Cox, T.R.; Kalluri, R.; Karsdal, M.; Willumsen, N. The Collagen Landscape in Cancer: Profiling Collagens in Tumors and in Circulation Reveals Novel Markers of Cancer-associated Fibroblast Subtypes. *J. Pathol.* **2024**, *262*, 22–36. [CrossRef]
140. Ricard-Blum, S. The Collagen Family. *Cold Spring Harb. Perspect. Biol.* **2011**, *3*, a004978. [CrossRef]
141. van der Rest, M.; Dublet, B.; Champliaud, M.F. Fibril-Associated Collagens. *Biomaterials* **1990**, *11*, 28–31.
142. Song, K.; Yu, Z.; Zu, X.; Li, G.; Hu, Z.; Xue, Y. Collagen Remodeling along Cancer Progression Providing a Novel Opportunity for Cancer Diagnosis and Treatment. *Int. J. Mol. Sci.* **2022**, *23*, 10509. [CrossRef]
143. Zhang, J.; Liu, J.; Zhang, H.; Wang, J.; Hua, H.; Jiang, Y. The Role of Network-forming Collagens in Cancer Progression. *Int. J. Cancer* **2022**, *151*, 833–842. [CrossRef] [PubMed]
144. Hanley, C.J.; Noble, F.; Ward, M.; Bullock, M.; Drifka, C.; Mellone, M.; Manousopoulou, A.; Johnston, H.E.; Hayden, A.; Thirdborough, S.; et al. A Subset of Myofibroblastic Cancer-Associated Fibroblasts Regulate Collagen Fiber Elongation, Which Is Prognostic in Multiple Cancers. *Oncotarget* **2016**, *7*, 6159–6174. [CrossRef] [PubMed]
145. Stylianopoulos, T.; Diop-Frimpong, B.; Munn, L.L.; Jain, R.K. Diffusion Anisotropy in Collagen Gels and Tumors: The Effect of Fiber Network Orientation. *Biophys. J.* **2010**, *99*, 3119–3128. [CrossRef] [PubMed]
146. Brisson, B.K.; Mauldin, E.A.; Lei, W.; Vogel, L.K.; Power, A.M.; Lo, A.; Dopkin, D.; Khanna, C.; Wells, R.G.; Puré, E.; et al. Type III Collagen Directs Stromal Organization and Limits Metastasis in a Murine Model of Breast Cancer. *Am. J. Pathol.* **2015**, *185*, 1471–1486. [CrossRef] [PubMed]
147. Li, A.; Zhou, T.; Guo, L.; Si, J. Collagen Type I Regulates β-Catenin Tyrosine Phosphorylation and Nuclear Translocation to Promote Migration and Proliferation of Gastric Carcinoma Cells. *Oncol. Rep.* **2010**, *23*, 1247–1255. [CrossRef]
148. Mendonsa, A.M.; Na, T.-Y.; Gumbiner, B.M. E-Cadherin in Contact Inhibition and Cancer. *Oncogene* **2018**, *37*, 4769–4780. [CrossRef]
149. Su, H.; Karin, M. Multifaceted Collagen-DDR1 Signaling in Cancer. *Trends Cell Biol.* **2024**, *34*, 406–415. [CrossRef]
150. Kothiwale, S.; Borza, C.M.; Lowe, E.W.; Pozzi, A.; Meiler, J. Discoidin Domain Receptor 1 (DDR1) Kinase as Target for Structure-Based Drug Discovery. *Drug Discov. Today* **2015**, *20*, 255–261. [CrossRef]
151. Su, H.; Yang, F.; Fu, R.; Trinh, B.; Sun, N.; Liu, J.; Kumar, A.; Baglieri, J.; Siruno, J.; Le, M.; et al. Collagenolysis-Dependent DDR1 Signalling Dictates Pancreatic Cancer Outcome. *Nature* **2022**, *610*, 366–372. [CrossRef]
152. Chen, T.; You, Y.; Jiang, H.; Wang, Z.Z. Epithelial–Mesenchymal Transition (EMT): A Biological Process in the Development, Stem Cell Differentiation, and Tumorigenesis. *J. Cell Physiol.* **2017**, *232*, 3261–3272. [CrossRef]
153. Medici, D.; Nawshad, A. Type I Collagen Promotes Epithelial–Mesenchymal Transition through ILK-Dependent Activation of NF-KB and LEF-1. *Matrix Biol.* **2010**, *29*, 161–165. [CrossRef] [PubMed]
154. Hsu, K.-S.; Dunleavey, J.M.; Szot, C.; Yang, L.; Hilton, M.B.; Morris, K.; Seaman, S.; Feng, Y.; Lutz, E.M.; Koogle, R.; et al. Cancer Cell Survival Depends on Collagen Uptake into Tumor-Associated Stroma. *Nat. Commun.* **2022**, *13*, 7078. [CrossRef] [PubMed]
155. Bhattacharjee, S.; Hamberger, F.; Ravichandra, A.; Miller, M.; Nair, A.; Affo, S.; Filliol, A.; Chin, L.; Savage, T.M.; Yin, D.; et al. Tumor Restriction by Type I Collagen Opposes Tumor-Promoting Effects of Cancer-Associated Fibroblasts. *J. Clin. Investig.* **2021**, *131*, e146987. [CrossRef] [PubMed]
156. Brisson, B.K.; Stewart, D.C.; Burgwin, C.; Chenoweth, D.; Wells, R.G.; Adams, S.L.; Volk, S.W. Cysteine-Rich Domain of Type III Collagen N-Propeptide Inhibits Fibroblast Activation by Attenuating TGFβ Signaling. *Matrix Biol.* **2022**, *109*, 19–33. [CrossRef]
157. Ramirez, M.; Rajaram, S.; Steininger, R.J.; Osipchuk, D.; Roth, M.A.; Morinishi, L.S.; Evans, L.; Ji, W.; Hsu, C.-H.; Thurley, K.; et al. Diverse Drug-Resistance Mechanisms Can Emerge from Drug-Tolerant Cancer Persister Cells. *Nat. Commun.* **2016**, *7*, 10690. [CrossRef]
158. Liu, X.; Li, H.; Wang, T.; Yang, T.; Yang, X.; Guo, K.; Hu, L.; Ming, J. Recombinant Humanized Collagen Type III with High Antitumor Activity Inhibits Breast Cancer Cells Autophagy, Proliferation, and Migration through DDR1. *Int. J. Biol. Macromol.* **2023**, *243*, 125130. [CrossRef]
159. Yun, C.W.; Lee, S.H. The Roles of Autophagy in Cancer. *Int. J. Mol. Sci.* **2018**, *19*, 3466. [CrossRef]
160. Guo, X.; Bu, X.; Yuan, L.; Ji, L. Collagen Type V Alpha 2 Promotes the Development of Gastric Cancer via M2 Macrophage Polarization. *Chin. J. Physiol.* **2023**, *66*, 93. [CrossRef]
161. Lee, B.Y.; Timpson, P.; Horvath, L.G.; Daly, R.J. FAK Signaling in Human Cancer as a Target for Therapeutics. *Pharmacol. Ther.* **2015**, *146*, 132–149. [CrossRef]
162. Jin, Y.; Song, X.; Sun, X.; Ding, Y. Up-Regulation of Collagen Type V Alpha 2 (*COL5A2*) Promotes Malignant Phenotypes in Gastric Cancer Cell via Inducing Epithelial–Mesenchymal Transition (EMT). *Open Med.* **2023**, *18*, 20220593. [CrossRef]
163. Arolt, C.; Meyer, M.; Hoffmann, F.; Wagener-Ryczek, S.; Schwarz, D.; Nachtsheim, L.; Beutner, D.; Odenthal, M.; Guntinas-Lichius, O.; Buettner, R.; et al. Expression Profiling of Extracellular Matrix Genes Reveals Global and Entity-Specific Characteristics in Adenoid Cystic, Mucoepidermoid and Salivary Duct Carcinomas. *Cancers* **2020**, *12*, 2466. [CrossRef] [PubMed]
164. Ellsworth, R.E.; Seebach, J.; Field, L.A.; Heckman, C.; Kane, J.; Hooke, J.A.; Love, B.; Shriver, C.D. A Gene Expression Signature That Defines Breast Cancer Metastases. *Clin. Exp. Metastasis* **2009**, *26*, 205–213. [CrossRef] [PubMed]

165. Galván, J.A.; García-Martínez, J.; Vázquez-Villa, F.; García-Ocaña, M.; García-Pravia, C.; Menéndez-Rodríguez, P.; González-del Rey, C.; Barneo-Serra, L.; de los Toyos, J.R. Validation of COL11A1/Procollagen 11A1 Expression in TGF-B1-Activated Immortalised Human Mesenchymal Cells and in Stromal Cells of Human Colon Adenocarcinoma. *BMC Cancer* **2014**, *14*, 867. [CrossRef] [PubMed]
166. Chattopadhyay, I.; Singh, A.; Phukan, R.; Purkayastha, J.; Kataki, A.; Mahanta, J.; Saxena, S.; Kapur, S. Genome-Wide Analysis of Chromosomal Alterations in Patients with Esophageal Squamous Cell Carcinoma Exposed to Tobacco and Betel Quid from High-Risk Area in India. *Mutat. Res. Genet. Toxicol. Environ. Mutagen.* **2010**, *696*, 130–138. [CrossRef]
167. Hao, S.; Lv, J.; Yang, Q.; Wang, A.; Li, Z.; Guo, Y.; Zhang, G. Identification of Key Genes and Circular RNAs in Human Gastric Cancer. *Med. Sci. Monit.* **2019**, *25*, 2488–2504. [CrossRef]
168. Nizri, E.; Bar-David, S.; Aizic, A.; Sternbach, N.; Lahat, G.; Wolf, I.; Klausner, J. Desmoplasia in Lymph Node Metastasis of Pancreatic Adenocarcinoma Reveals Activation of Cancer-Associated Fibroblasts Pattern and T-Helper 2 Immune Cell Infiltration. *Pancreas* **2019**, *48*, 367–373. [CrossRef]
169. Nallanthighal, S.; Rada, M.; Heiserman, J.P.; Cha, J.; Sage, J.; Zhou, B.; Yang, W.; Hu, Y.; Korgaonkar, C.; Hanos, C.T.; et al. Inhibition of Collagen XI Alpha 1-Induced Fatty Acid Oxidation Triggers Apoptotic Cell Death in Cisplatin-Resistant Ovarian Cancer. *Cell Death Dis.* **2020**, *11*, 258. [CrossRef]
170. Vázquez-Villa, F.; García-Ocaña, M.; Galván, J.A.; García-Martínez, J.; García-Pravia, C.; Menéndez-Rodríguez, P.; Rey, C.G.; Barneo-Serra, L.; de los Toyos, J.R. COL11A1/(pro)Collagen 11A1 Expression Is a Remarkable Biomarker of Human Invasive Carcinoma-Associated Stromal Cells and Carcinoma Progression. *Tumor Biol.* **2015**, *36*, 2213–2222. [CrossRef]
171. Jia, D.; Liu, Z.; Deng, N.; Tan, T.Z.; Huang, R.Y.-J.; Taylor-Harding, B.; Cheon, D.-J.; Lawrenson, K.; Wiedemeyer, W.R.; Walts, A.E.; et al. A COL11A1-Correlated Pan-Cancer Gene Signature of Activated Fibroblasts for the Prioritization of Therapeutic Targets. *Cancer Lett.* **2016**, *382*, 203–214. [CrossRef]
172. Wu, Y.-H.; Chou, C.-Y. Collagen XI Alpha 1 Chain, a Novel Therapeutic Target for Cancer Treatment. *Front. Oncol.* **2022**, *12*, 925165. [CrossRef]
173. Rada, M.; Nallanthighal, S.; Cha, J.; Ryan, K.; Sage, J.; Eldred, C.; Ullo, M.; Orsulic, S.; Cheon, D.-J. Inhibitor of Apoptosis Proteins (IAPs) Mediate Collagen Type XI Alpha 1-Driven Cisplatin Resistance in Ovarian Cancer. *Oncogene* **2018**, *37*, 4809–4820. [CrossRef] [PubMed]
174. Wu, Y.-H.; Chang, T.-H.; Huang, Y.-F.; Chen, C.-C.; Chou, C.-Y. COL11A1 Confers Chemoresistance on Ovarian Cancer Cells through the Activation of Akt/c/EBPβ Pathway and PDK1 Stabilization. *Oncotarget* **2015**, *6*, 23748–23763. [CrossRef] [PubMed]
175. La, T.; Liu, G.Z.; Farrelly, M.; Cole, N.; Feng, Y.C.; Zhang, Y.Y.; Sherwin, S.K.; Yari, H.; Tabatabaee, H.; Yan, X.G.; et al. A P53-Responsive MiRNA Network Promotes Cancer Cell Quiescence. *Cancer Res.* **2018**, *78*, 6666–6679. [CrossRef] [PubMed]
176. Zvackova, I.; Matalova, E.; Lesot, H. Regulators of Collagen Fibrillogenesis during Molar Development in the Mouse. *Front. Physiol.* **2017**, *8*, 554. [CrossRef] [PubMed]
177. Vizzini, A.; Pergolizzi, M.; Vazzana, M.; Salerno, G.; Di Sano, C.; Macaluso, P.; Arizza, V.; Parrinello, D.; Cammarata, M.; Parrinello, N. FACIT Collagen (1α-Chain) Is Expressed by Hemocytes and Epidermis during the Inflammatory Response of the Ascidian Ciona Intestinalis. *Dev. Comp. Immunol.* **2008**, *32*, 682–692. [CrossRef]
178. Coulson-Thomas, V.J.; Coulson-Thomas, Y.M.; Gesteira, T.F.; de Paula, C.A.A.; Mader, A.M.; Waisberg, J.; Pinhal, M.A.; Friedl, A.; Toma, L.; Nader, H.B. Colorectal Cancer Desmoplastic Reaction Up-Regulates Collagen Synthesis and Restricts Cancer Cell Invasion. *Cell Tissue Res.* **2011**, *346*, 223–236. [CrossRef]
179. Chivu-Economescu, M.; Necula, L.G.; Matei, L.; Dragu, D.; Bleotu, C.; Sorop, A.; Herlea, V.; Dima, S.; Popescu, I.; Diaconu, C.C. Collagen Family and Other Matrix Remodeling Proteins Identified by Bioinformatics Analysis as Hub Genes Involved in Gastric Cancer Progression and Prognosis. *Int. J. Mol. Sci.* **2022**, *23*, 3214. [CrossRef]
180. Papanicolaou, M.; Parker, A.L.; Yam, M.; Filipe, E.C.; Wu, S.Z.; Chitty, J.L.; Wyllie, K.; Tran, E.; Mok, E.; Nadalini, A.; et al. Temporal Profiling of the Breast Tumour Microenvironment Reveals Collagen XII as a Driver of Metastasis. *Nat. Commun.* **2022**, *13*, 4587. [CrossRef]
181. Yan, Y.; Liang, Q.; Liu, Y.; Zhou, S.; Xu, Z. COL12A1 as a Prognostic Biomarker Links Immunotherapy Response in Breast Cancer. *Endocr. Relat. Cancer* **2023**, *30*, e230012. [CrossRef]
182. Wu, Y.; Xu, Y. Integrated Bioinformatics Analysis of Expression and Gene Regulation Network of COL12A1 in Colorectal Cancer. *Cancer Med.* **2020**, *9*, 4743–4755. [CrossRef]
183. Yao, W.; Yao, Y.; He, W.; Zhao, C.; Liu, D.; Wang, G.; Wang, Z. PABPC1 Promotes Cell Proliferation and Metastasis in Pancreatic Adenocarcinoma by Regulating COL12A1 Expression. *Immun. Inflamm. Dis.* **2023**, *11*, e919. [CrossRef] [PubMed]
184. Jensen, C.; Nielsen, S.H.; Mortensen, J.H.; Kjeldsen, J.; Klinge, L.G.; Krag, A.; Harling, H.; Jørgensen, L.N.; Karsdal, M.A.; Willumsen, N. Serum Type XVI Collagen Is Associated with Colorectal Cancer and Ulcerative Colitis Indicating a Pathological Role in Gastrointestinal Disorders. *Cancer Med.* **2018**, *7*, 4619–4626. [CrossRef] [PubMed]
185. Ratzinger, S.; Grässel, S.; Dowejko, A.; Reichert, T.E.; Bauer, R.J. Induction of Type XVI Collagen Expression Facilitates Proliferation of Oral Cancer Cells. *Matrix Biol.* **2011**, *30*, 118–125. [CrossRef] [PubMed]
186. Bauer, R.; Ratzinger, S.; Wales, L.; Bosserhoff, A.; Senner, V.; Grifka, J.; Grässel, S. Inhibition of Collagen XVI Expression Reduces Glioma Cell Invasiveness. *Cell. Physiol. Biochem.* **2011**, *27*, 217–226. [CrossRef] [PubMed]
187. Pach, E.; Kümper, M.; Fromme, J.E.; Zamek, J.; Metzen, F.; Koch, M.; Mauch, C.; Zigrino, P. Extracellular Matrix Remodeling by Fibroblast-MMP14 Regulates Melanoma Growth. *Int. J. Mol. Sci.* **2021**, *22*, 12276. [CrossRef]

188. Oudart, J.-B.; Doué, M.; Vautrin, A.; Brassart, B.; Sellier, C.; Dupont-Deshorgue, A.; Monboisse, J.-C.; Maquart, F.-X.; Brassart-Pasco, S.; Ramont, L. The Anti-Tumor NC1 Domain of Collagen XIX Inhibits the FAK/PI3K/Akt/MTOR Signaling Pathway through Avβ3 Integrin Interaction. *Oncotarget* **2016**, *7*, 1516–1528. [CrossRef]
189. Thorlacius-Ussing, J.; Jensen, C.; Madsen, E.A.; Nissen, N.I.; Manon-Jensen, T.; Chen, I.M.; Johansen, J.S.; Diab, H.M.H.; Jørgensen, L.N.; Karsdal, M.A.; et al. Type XX Collagen Is Elevated in Circulation of Patients with Solid Tumors. *Int. J. Mol. Sci.* **2022**, *23*, 4144. [CrossRef]
190. Qin, L.H.; Zhu, X.J.; Zhang, L.Y.; Chen, J.Q.; Jin, G.Y.; Xiang, L.J. Identification of Hub Genes and Pathways in the Development of Gastric Cancer by Gene Co-expression Network Analysis. *J. Biol. Regul. Homeost. Agents.* **2021**, *35*, 35–44. [CrossRef]
191. Knupp, C.; Squire, J.M. *Molecular Packing in Network-Forming Collagens*; Elsevier: Amsterdam, the Netherlands, 2005; pp. 375–403.
192. Egeblad, M.; Rasch, M.G.; Weaver, V.M. Dynamic Interplay between the Collagen Scaffold and Tumor Evolution. *Curr. Opin. Cell Biol.* **2010**, *22*, 697–706. [CrossRef]
193. Liang, Y.; Lv, Z.; Huang, G.; Qin, J.; Li, H.; Nong, F.; Wen, B. Prognostic Significance of Abnormal Matrix Collagen Remodeling in Colorectal Cancer Based on Histologic and Bioinformatics Analysis. *Oncol. Rep.* **2020**, *44*, 1671–1685. [CrossRef]
194. Friedl, P.; Alexander, S. Cancer Invasion and the Microenvironment: Plasticity and Reciprocity. *Cell* **2011**, *147*, 992–1009. [CrossRef] [PubMed]
195. Torzilli, P.A.; Bourne, J.W.; Cigler, T.; Vincent, C.T. A New Paradigm for Mechanobiological Mechanisms in Tumor Metastasis. *Semin. Cancer Biol.* **2012**, *22*, 385–395. [CrossRef] [PubMed]
196. Levental, K.R.; Yu, H.; Kass, L.; Lakins, J.N.; Egeblad, M.; Erler, J.T.; Fong, S.F.T.; Csiszar, K.; Giaccia, A.; Weninger, W.; et al. Matrix Crosslinking Forces Tumor Progression by Enhancing Integrin Signaling. *Cell* **2009**, *139*, 891–906. [CrossRef] [PubMed]
197. Pöschl, E.; Schlötzer-Schrehardt, U.; Brachvogel, B.; Saito, K.; Ninomiya, Y.; Mayer, U. Collagen IV Is Essential for Basement Membrane Stability but Dispensable for Initiation of Its Assembly during Early Development. *Development* **2004**, *131*, 1619–1628. [CrossRef] [PubMed]
198. Bignon, M.; Pichol-Thievend, C.; Hardouin, J.; Malbouyres, M.; Bréchot, N.; Nasciutti, L.; Barret, A.; Teillon, J.; Guillon, E.; Etienne, E.; et al. Lysyl Oxidase-like Protein-2 Regulates Sprouting Angiogenesis and Type IV Collagen Assembly in the Endothelial Basement Membrane. *Blood* **2011**, *118*, 3979–3989. [CrossRef]
199. Večurkovská, I.; Stupák, M.; Kaťuchová, J.; Roškovičová, V.; Mašlanková, J. Comparative Analysis of Matrix Metalloproteinases by Zymography in Patients With Colorectal Carcinoma. *Physiol. Res.* **2023**, *72*, S593–S596. [CrossRef]
200. Kalluri, R. Basement Membranes: Structure, Assembly and Role in Tumour Angiogenesis. *Nat. Rev. Cancer* **2003**, *3*, 422–433. [CrossRef]
201. Chamani, R.; Saberi, O.; Fathinejad, F. An Arresten-Derived Anti-Angiogenic Peptide Triggers Apoptotic Cell Death in Endothelial Cells. *Mol. Biol. Rep.* **2024**, *51*, 513. [CrossRef]
202. Chamani, R.; Taleqani, M.H.; Imanpour, A.; Khatami, M. New Insights into Short Peptides Derived from the Collagen NC1 A1, A2, and A3 (IV) Domains: An Experimental and MD Simulations Study. *Biochim. Biophys. Acta—Proteins Proteom.* **2022**, *1870*, 140769. [CrossRef]
203. Vautrin-Glabik, A.; Devy, J.; Bour, C.; Baud, S.; Choulier, L.; Hoarau, A.; Dupont-Deshorgue, A.; Sellier, C.; Brassart, B.; Oudart, J.-B.; et al. Angiogenesis Inhibition by a Short 13 Amino Acid Peptide Sequence of Tetrastatin, the A4(IV) NC1 Domain of Collagen IV. *Front. Cell Dev. Biol.* **2020**, *8*, 775. [CrossRef]
204. Aikio, M.; Alahuhta, I.; Nurmenniemi, S.; Suojanen, J.; Palovuori, R.; Teppo, S.; Sorsa, T.; López-Otín, C.; Pihlajaniemi, T.; Salo, T.; et al. Arresten, a Collagen-Derived Angiogenesis Inhibitor, Suppresses Invasion of Squamous Cell Carcinoma. *PLoS ONE* **2012**, *7*, e51044. [CrossRef] [PubMed]
205. Brassart-Pasco, S.; Brézillon, S.; Brassart, B.; Ramont, L.; Oudart, J.-B.; Monboisse, J.C. Tumor Microenvironment: Extracellular Matrix Alterations Influence Tumor Progression. *Front. Oncol.* **2020**, *10*, 397. [CrossRef] [PubMed]
206. Assadian, S.; El-Assaad, W.; Wang, X.Q.D.; Gannon, P.O.; Barrès, V.; Latour, M.; Mes-Masson, A.-M.; Saad, F.; Sado, Y.; Dostie, J.; et al. P53 Inhibits Angiogenesis by Inducing the Production of Arresten. *Cancer Res.* **2012**, *72*, 1270–1279. [CrossRef] [PubMed]
207. Kamphaus, G.D.; Colorado, P.C.; Panka, D.J.; Hopfer, H.; Ramchandran, R.; Torre, A.; Maeshima, Y.; Mier, J.W.; Sukhatme, V.P.; Kalluri, R. Canstatin, a Novel Matrix-Derived Inhibitor of Angiogenesis and Tumor Growth. *J. Biol. Chem.* **2000**, *275*, 1209–1215. [CrossRef]
208. Panka, D.J.; Mier, J.W. Canstatin Inhibits Akt Activation and Induces Fas-Dependent Apoptosis in Endothelial Cells. *J. Biol. Chem.* **2003**, *278*, 37632–37636. [CrossRef] [PubMed]
209. Pei, J.; Li, P.; Gao, Y.H.; Tian, B.G.; Wang, D.Y.; Zheng, Y.; Liu, L.Y.; Zhang, Z.Y.; Huang, S.S.; Wen, M.; et al. Type IV Collagen-Derived Angiogenesis Inhibitor: Canstatin Low Expressing in Brain-Invasive Meningiomas Using Liquid Chromatography–Mass Spectrometry (LC-MS/MS). *J. Neurooncol.* **2023**, *161*, 415–423. [CrossRef] [PubMed]
210. Zhu, L.; Guo, Z.; Zhang, J.; Yang, Y.; Liu, C.; Zhang, L.; Gu, Z.; Li, Y.; Ding, Z.; Shi, G. Recombinant Human Arresten and Canstatin Inhibit Angiogenic Behaviors of HUVECs via Inhibiting the PI3K/Akt Signaling Pathway. *Int. J. Mol. Sci.* **2022**, *23*, 8995. [CrossRef]
211. Guo, J.; Ma, X.; Liu, D.; Wang, F.; Xia, J.; Zhang, B.; Zhao, P.; Zhong, F.; Chen, L.; Long, Q.; et al. A Distinct Subset of Urothelial Cells with Enhanced EMT Features Promotes Chemotherapy Resistance and Cancer Recurrence by Increasing COL4A1-ITGB1 Mediated Angiogenesis. *Drug Resist. Updates* **2024**, *76*, 101116. [CrossRef]

212. Wu, Y.; Liu, X.; Zhu, Y.; Qiao, Y.; Gao, Y.; Chen, J.; Ge, G. Type IV Collagen α 5 Chain Promotes Luminal Breast Cancer Progression through c-Myc-Driven Glycolysis. *J. Mol. Cell Biol.* **2023**, *14*, mjac068. [CrossRef]
213. Jansson, M.; Lindberg, J.; Rask, G.; Svensson, J.; Billing, O.; Nazemroaya, A.; Berglund, A.; Wärnberg, F.; Sund, M. Prognostic Value of Stromal Type IV Collagen Expression in Small Invasive Breast Cancers. *Front. Mol. Biosci.* **2022**, *9*, 904526. [CrossRef]
214. Xia, Y.; Jiang, H.; Chen, J.; Xu, F.; Zhang, G.; Zhang, D. Low Dose Taxol Ameliorated Renal Fibrosis in Mice with Diabetic Kidney Disease by Downregulation of HIPK2. *Life Sci.* **2023**, *320*, 121540. [CrossRef] [PubMed]
215. Sato, F.; Sagara, A.; Tajima, K.; Miura, S.; Inaba, K.; Ando, Y.; Oku, T.; Murakami, T.; Kato, Y.; Yumoto, T. COL8A1 Facilitates the Growth of Triple-Negative Breast Cancer via FAK/Src Activation. *Breast Cancer Res. Treat.* **2022**, *194*, 243–256. [CrossRef] [PubMed]
216. Bruckner-Tuderman, L.; Höpfner, B.; Hammami-Hauasli, N. Biology of Anchoring Fibrils: Lessons from Dystrophic Epidermolysis Bullosa. *Matrix Biol.* **1999**, *18*, 43–54. [CrossRef] [PubMed]
217. Chen, S.; Wei, Y.; Liu, H.; Gong, Y.; Zhou, Y.; Yang, H.; Tang, L. Analysis of Collagen Type X Alpha 1 (COL10A1) Expression and Prognostic Significance in Gastric Cancer Based on Bioinformatics. *Bioengineered* **2021**, *12*, 127–137. [CrossRef]
218. Huang, H.; Li, T.; Ye, G.; Zhao, L.; Zhang, Z.; Mo, D.; Wang, Y.; Zhang, C.; Deng, H.; Li, G.; et al. High Expression of COL10A1 Is Associated with Poor Prognosis in Colorectal Cancer. *Onco. Targets Ther.* **2018**, *11*, 1571–1581. [CrossRef]
219. Wang, C.; Wang, J.; Chen, S.; Li, K.; Wan, S.; Yang, L. COL10A1 as a Prognostic Biomarker in Association with Immune Infiltration in Prostate Cancer. *Curr. Cancer Drug Targets* **2024**, *24*, 340–353. [CrossRef]
220. Xu, S.; Liu, D.; Qin, Z.; Liang, Z.; Xie, H.; Yi, B.; Wang, K.; Lin, G.; Liu, R.; Yang, K.; et al. Experimental Validation and Pan-Cancer Analysis Identified COL10A1 as a Novel Oncogene and Potential Therapeutic Target in Prostate Cancer. *Aging* **2023**, *15*, 15134–15160. [CrossRef]
221. Liang, Y.; Xia, W.; Zhang, T.; Chen, B.; Wang, H.; Song, X.; Zhang, Z.; Xu, L.; Dong, G.; Jiang, F. Upregulated Collagen COL10A1 Remodels the Extracellular Matrix and Promotes Malignant Progression in Lung Adenocarcinoma. *Front. Oncol.* **2020**, *10*, 573534. [CrossRef]
222. Bruns, R.R. Beaded Filaments and Long-Spacing Fibrils: Relation to Type VI Collagen. *J. Ultrastruct. Res.* **1984**, *89*, 136–145. [CrossRef]
223. Gara, S.K.; Grumati, P.; Urciuolo, A.; Bonaldo, P.; Kobbe, B.; Koch, M.; Paulsson, M.; Wagener, R. Three Novel Collagen VI Chains with High Homology to the A3 Chain. *J. Biol. Chem.* **2008**, *283*, 10658–10670. [CrossRef]
224. Li, X.; Li, Z.; Gu, S.; Zhao, X. A Pan-Cancer Analysis of Collagen VI Family on Prognosis, Tumor Microenvironment, and Its Potential Therapeutic Effect. *BMC Bioinform.* **2022**, *23*, 390. [CrossRef] [PubMed]
225. Wishart, A.L.; Conner, S.J.; Guarin, J.R.; Fatherree, J.P.; Peng, Y.; McGinn, R.A.; Crews, R.; Naber, S.P.; Hunter, M.; Greenberg, A.S.; et al. Decellularized Extracellular Matrix Scaffolds Identify Full-Length Collagen VI as a Driver of Breast Cancer Cell Invasion in Obesity and Metastasis. *Sci. Adv.* **2020**, *6*, eabc3175. [CrossRef] [PubMed]
226. Kim, K.; Byun, Y.J.; Zheng, C.-M.; Moon, S.; Jo, S.J.; Kang, H.W.; Kim, W.T.; Choi, Y.H.; Moon, S.-K.; Kim, W.-J.; et al. *COL6A1* Expression as a Potential Prognostic Biomarker for Risk Stratification of T1 High Grade Bladder Cancer: Unveiling the Aggressive Nature of a Distinct Non-Muscle Invasive Subtype. *Investig. Clin. Urol.* **2024**, *65*, 94. [CrossRef] [PubMed]
227. Cescon, M.; Rampazzo, E.; Bresolin, S.; Da Ros, F.; Manfreda, L.; Cani, A.; Della Puppa, A.; Braghetta, P.; Bonaldo, P.; Persano, L. Collagen VI Sustains Cell Stemness and Chemotherapy Resistance in Glioblastoma. *Cell. Mol. Life Sci.* **2023**, *80*, 233. [CrossRef]
228. Papalazarou, V.; Drew, J.; Juin, A.; Spence, H.J.; Whitelaw, J.; Nixon, C.; Salmeron-Sanchez, M.; Machesky, L.M. Collagen VI Expression Is Negatively Mechanosensitive in Pancreatic Cancer Cells and Supports the Metastatic Niche. *J. Cell Sci.* **2022**, *135*, jcs259978. [CrossRef]
229. Liu, Y.; Murazzi, I.; Fuller, A.M.; Pan, H.; Irizarry-Negron, V.M.; Devine, A.; Katti, R.; Skuli, N.; Ciotti, G.E.; Pak, K.; et al. Sarcoma Cells Secrete Hypoxia-Modified Collagen VI to Weaken the Lung Endothelial Barrier and Promote Metastasis. *Cancer Res.* **2024**, *84*, 977–993. [CrossRef]
230. Luo, Y.; Ye, Y.; Zhang, Y.; Chen, L.; Qu, X.; Yi, N.; Ran, J.; Chen, Y. New Insights into COL26A1 in Thyroid Carcinoma: Prognostic Prediction, Functional Characterization, Immunological Drug Target and CeRNA Network. *Transl. Cancer Res.* **2023**, *12*, 3384–3408. [CrossRef]
231. Reese-Petersen, A.L.; Willumsen, N.; Palau, P.; Nunez, J.; Sun, S.; Jensen, T.M.; Kamall, B.; Karsdal, M.A.; Genovese, F. Evaluation of a Novel Biomarker of Type XXVIII Collagen Formation, PRO-C28, in Samples from Cancer and Heart Failure with Preserved Ejection Fraction Patients. *J. Pharm. Biomed. Anal.* **2021**, *204*, 114272. [CrossRef]
232. Sakai, L.Y.; Keene, D.R.; Morris, N.P.; Burgeson, R.E. Type VII Collagen Is a Major Structural Component of Anchoring Fibrils. *J. Cell Biol.* **1986**, *103*, 1577–1586. [CrossRef]
233. Gelse, K. Collagens—Structure, Function, and Biosynthesis. *Adv. Drug Deliv. Rev.* **2003**, *55*, 1531–1546. [CrossRef]
234. Oh, S.E.; Oh, M.Y.; An, J.Y.; Lee, J.H.; Sohn, T.S.; Bae, J.M.; Choi, M.-G.; Kim, K.-M. Prognostic Value of Highly Expressed Type VII Collagen (COL7A1) in Patients With Gastric Cancer. *Pathol. Oncol. Res.* **2021**, *27*, 1609860. [CrossRef] [PubMed]
235. You, W.-K.; Bonaldo, P.; Stallcup, W.B. Collagen VI Ablation Retards Brain Tumor Progression Due to Deficits in Assembly of the Vascular Basal Lamina. *Am. J. Pathol.* **2012**, *180*, 1145–1158. [CrossRef] [PubMed]
236. Poomsawat, S.; Kariya, A.; Nimmanon, T.; Kosanwat, T.; Juengsomjit, R.; Sirima, S. Diagnostic Potential of Type VII Collagen during Oral Carcinogenesis. *J. Appl. Oral. Sci.* **2023**, *31*, e20220486. [CrossRef] [PubMed]

237. Franzke, C.-W.; Bruckner, P.; Bruckner-Tuderman, L. Collagenous Transmembrane Proteins: Recent Insights into Biology and Pathology. *J. Biol. Chem.* **2005**, *280*, 4005–4008. [CrossRef]
238. Jones, V.A.; Patel, P.M.; Gibson, F.T.; Cordova, A.; Amber, K.T. The Role of Collagen XVII in Cancer: Squamous Cell Carcinoma and Beyond. *Front. Oncol.* **2020**, *10*, 352. [CrossRef]
239. Krenacs, T.; Kiszner, G.; Stelkovics, E.; Balla, P.; Teleki, I.; Nemeth, I.; Varga, E.; Korom, I.; Barbai, T.; Plotar, V.; et al. Collagen XVII Is Expressed in Malignant but Not in Benign Melanocytic Tumors and It Can Mediate Antibody Induced Melanoma Apoptosis. *Histochem. Cell Biol.* **2012**, *138*, 653–667. [CrossRef]
240. Kashiwagi, R.; Funayama, R.; Aoki, S.; Matsui, A.; Klein, S.; Sato, Y.; Suzuki, T.; Murakami, K.; Inoue, K.; Iseki, M.; et al. Collagen XVII Regulates Tumor Growth in Pancreatic Cancer through Interaction with the Tumor Microenvironment. *Cancer Sci.* **2023**, *114*, 4286–4298. [CrossRef]
241. Tong, D.; Tanaka, M.; Eguchi, H.; Okazaki, Y.; Muramatsu, M.; Arai, T. COL17A1 Germline Variant p.Ser1029Ala and Mucosal Malignant Melanoma: An Autopsy Study. *Mol. Clin. Oncol.* **2021**, *16*, 32. [CrossRef]
242. Lothong, M.; Sakares, W.; Rojsitthisak, P.; Tanikawa, C.; Matsuda, K.; Yodsurang, V. Collagen XVII Inhibits Breast Cancer Cell Proliferation and Growth through Deactivation of the AKT/MTOR Signaling Pathway. *PLoS ONE* **2021**, *16*, e0255179. [CrossRef]
243. Ohta, Y.; Fujii, M.; Takahashi, S.; Takano, A.; Nanki, K.; Matano, M.; Hanyu, H.; Saito, M.; Shimokawa, M.; Nishikori, S.; et al. Cell–Matrix Interface Regulates Dormancy in Human Colon Cancer Stem Cells. *Nature* **2022**, *608*, 784–794. [CrossRef]
244. Crespo-Bravo, M.; Thorlacius-Ussing, J.; Nissen, N.I.; Pedersen, R.S.; Boisen, M.K.; Liljefors, M.; Johansen, A.Z.; Johansen, J.S.; Karsdal, M.A.; Willumsen, N. Levels of Type XVII Collagen (BP180) Ectodomain Are Elevated in Circulation from Patients with Multiple Cancer Types and Is Prognostic for Patients with Metastatic Colorectal Cancer. *BMC Cancer* **2023**, *23*, 949. [CrossRef] [PubMed]
245. Zhang, H.; Fredericks, T.; Xiong, G.; Qi, Y.; Rychahou, P.G.; Li, J.-D.; Pihlajaniemi, T.; Xu, W.; Xu, R. Membrane Associated Collagen XIII Promotes Cancer Metastasis and Enhances Anoikis Resistance. *Breast Cancer Res.* **2018**, *20*, 116. [CrossRef] [PubMed]
246. Dai, Y.; Zhang, X.; Ou, Y.; Zou, L.; Zhang, D.; Yang, Q.; Qin, Y.; Du, X.; Li, W.; Yuan, Z.; et al. Anoikis Resistance–Protagonists of Breast Cancer Cells Survive and Metastasize after ECM Detachment. *Cell Commun. Signal.* **2023**, *21*, 190. [CrossRef] [PubMed]
247. Chen, Y.; Huang, W.; Ouyang, J.; Wang, J.; Xie, Z. Identification of Anoikis-Related Subgroups and Prognosis Model in Liver Hepatocellular Carcinoma. *Int. J. Mol. Sci.* **2023**, *24*, 2862. [CrossRef]
248. Xu, F.; Chang, K.; Ma, J.; Qu, Y.; Xie, H.; Dai, B.; Gan, H.; Zhang, H.; Shi, G.; Zhu, Y.; et al. The Oncogenic Role of COL23A1 in Clear Cell Renal Cell Carcinoma. *Sci. Rep.* **2017**, *7*, 9846. [CrossRef]
249. Keller, C.R.; Ruud, K.F.; Martinez, S.R.; Li, W. Identification of the Collagen Types Essential for Mammalian Breast Acinar Structures. *Gels* **2022**, *8*, 837. [CrossRef]
250. Oh, S.P.; Kamagata, Y.; Muragaki, Y.; Timmons, S.; Ooshima, A.; Olsen, B.R. Isolation and Sequencing of CDNAs for Proteins with Multiple Domains of Gly-Xaa-Yaa Repeats Identify a Distinct Family of Collagenous Proteins. *Proc. Natl. Acad. Sci. USA* **1994**, *91*, 4229–4233. [CrossRef]
251. Lakshmanachetty, S.; Koster, M.I. Emerging Roles for Collagen XV and XVIII in Cancer Progression. *Exp. Dermatol.* **2016**, *25*, 346–347. [CrossRef]
252. Mutolo, M.J.; Morris, K.J.; Leir, S.-H.; Caffrey, T.C.; Lewandowska, M.A.; Hollingsworth, M.A.; Harris, A. Tumor Suppression by Collagen XV Is Independent of the Restin Domain. *Matrix Biol.* **2012**, *31*, 285–289. [CrossRef]
253. Wang, S.; Zhou, M.; Xia, Y. COL15A1 Interacts with P4HB to Regulate the Growth and Malignancy of HepG2.2.15 Cells. *Biochem. Biophys. Res. Commun.* **2023**, *681*, 20–28. [CrossRef]
254. Yao, T.; Hu, W.; Chen, J.; Shen, L.; Yu, Y.; Tang, Z.; Zang, G.; Zhang, Y.; Chen, X. Collagen XV Mediated the Epithelial-Mesenchymal Transition to Inhibit Hepatocellular Carcinoma Metastasis. *J. Gastrointest. Oncol.* **2022**, *13*, 2472–2484. [CrossRef] [PubMed]
255. Liu, Y.; Wang, J.; Shou, Y.; Xu, W.; Huang, Z.; Xu, J.; Chen, K.; Liu, J.; Liu, D.; Liang, H.; et al. Restoring the Epigenetically Silenced LncRNA COL18A1-AS1 Represses CcRCC Progression by Lipid Browning via MiR-1286/KLF12 Axis. *Cell Death Dis.* **2022**, *13*, 578. [CrossRef] [PubMed]
256. Devarajan, R.; Izzi, V.; Peltoketo, H.; Rask, G.; Kauppila, S.; Väisänen, M.-R.; Ruotsalainen, H.; Martínez-Nieto, G.; Karppinen, S.-M.; Väisänen, T.; et al. Targeting Collagen XVIII Improves the Efficiency of ErbB Inhibitors in Breast Cancer Models. *J. Clin. Investig.* **2023**, *133*, e159181. [CrossRef] [PubMed]
257. Yan, B.; Liu, L.; Zhao, L.; Hinz, U.; Luo, Y.; An, X.; Gladkich, J.; de la Torre, C.; Huang, Z.; Schrapel, D.; et al. Tumor and Stroma COL8A1 Secretion Induces Autocrine and Paracrine Progression Signaling in Pancreatic Ductal Adenocarcinoma. *Matrix Biol.* **2022**, *114*, 84–107. [CrossRef] [PubMed]
258. Vaday, G.G.; Lider, O. Extracellular Matrix Moieties, Cytokines, and Enzymes: Dynamic Effects on Immune Cell Behavior and Inflammation. *J. Leukoc. Biol.* **2000**, *67*, 149–159. [CrossRef]
259. Shi, R.; Zhang, Z.; Zhu, A.; Xiong, X.; Zhang, J.; Xu, J.; Sy, M.; Li, C. Targeting Type I Collagen for Cancer Treatment. *Int. J. Cancer* **2022**, *151*, 665–683. [CrossRef]
260. Huang, H.-Y.; Chen, L.-Q.; Sun, W.; Du, H.-H.; Dong, S.; Ahmed, A.M.Q.; Cao, D.; Cui, J.-H.; Zhang, Y.; Cao, Q.-R. Collagenase IV and Clusterin-Modified Polycaprolactone-Polyethylene Glycol Nanoparticles for Penetrating Dense Tumor Tissues. *Theranostics* **2021**, *11*, 906–924. [CrossRef]

261. Wang, J.; Wu, Q.; Wang, Y.; Xiang, L.; Feng, J.; Zhou, Z.; Fu, Q.; Zhang, L. Collagenase-Loaded PH-Sensitive Nanocarriers Efficiently Remodeled Tumor Stroma Matrixes and Improved the Enrichment of Nanomedicines. *Nanoscale* **2021**, *13*, 9402–9414. [CrossRef]
262. García-Olmo, D.; Villarejo Campos, P.; Barambio, J.; Gomez-Heras, S.G.; Vega-Clemente, L.; Olmedillas-Lopez, S.; Guadalajara, H.; Garcia-Arranz, M. Intraperitoneal Collagenase as a Novel Therapeutic Approach in an Experimental Model of Colorectal Peritoneal Carcinomatosis. *Sci. Rep.* **2021**, *11*, 503. [CrossRef]

The FEBS Journal

FEBS PRESS science publishing by scientists

Enhancing therapeutic efficacy through degradation of endogenous extracellular matrix in primary breast tumor spheroids

Alessandra Lo Cicero[1], Simona Campora[1,2], Gabriele Lo Buglio[1,3], Paolo Cinà[4], Margot Lo Pinto[5], Simone Dario Scilabra[5] and Giulio Ghersi[1,4]

1 Department of Biological, Chemical and Pharmaceutical Sciences and Technologies (STEBICEF), University of Palermo, Italy
2 Department of Biomedical Engineering Bioscience Center of the University of Cincinnati, OH, USA
3 Department of Pharmacy, University of Copenhagen, Denmark
4 Abiel Srl, Palermo, Italy
5 Proteomics Group of Ri.MED Foundation, Research Department IRCCS ISMETT (Istituto Mediterraneo per i Trapianti e Terapie ad Alta Specializzazione), Palermo, Italy

Keywords
breast cancer; collagen; collagenase; drug response; extracellular matrix; spheroids

Correspondence
G. Ghersi and A. Lo Cicero, Department of Biological, Chemical and Pharmaceutical Sciences and Technologies (STEBICEF), University of Palermo, Viale delle Scienze, Ed. 16, Palermo 90128, Italy
Tel: +3909123897409
E-mail: giulio.ghersi@unipa.it; alessandra.locicero@unipa.it

(Received 18 July 2024, revised 8 November 2024, accepted 10 March 2025)

doi:10.1111/febs.70069

Solid tumors have a complex extracellular matrix (ECM) that significantly affects tumor behavior and response to therapy. Understanding the ECM's role is crucial for advancing cancer research and treatment. This study established an *in vitro* model using primary cells isolated from a rat breast tumor to generate three-dimensional spheroids. Monolayer cells and spheroid cultures exhibited different protein expression patterns, with primary tumor spheroids presenting an increased level of ECM-related proteins and a more complex extracellular environment. Furthermore, spheroids produce endogenous collagen type I matrix, which is the main component of the tumoral ECM. This matrix is arranged predominantly around the 3D structure, mimicking the conditions of solid tumors. Treatments with recombinant collagenases class II (acting on the linear collagen region) and class I (acting on the 3D-helix region) completely degrade collagen within the spheroid structure. Collagenase pretreatment enhances the accessibility of the anticancer drug doxorubicin to penetrate the core of spheroids and sensitize them to doxorubicin-induced cytotoxicity. Our findings highlight the importance of overcoming drug resistance in breast cancer by targeting the ECM and proposing a novel strategy for improving therapeutic outcomes in solid tumors. By employing a three-dimensional spheroid model, with an endogenous ECM, we can offer more relevant insights into tumor biology and treatment responses.

Introduction

Cancer is a leading cause of death worldwide, with nearly 20 million new cases diagnosed and 10 million deaths reported in 2022 (World Health Organization), and the mortality rate is increasing every year. Solid tumors, which account for approximately 90% of adult human cancers, are characterized by their unique tumor microenvironment (TME). Over the last decades, to understand the complexity of solid tumor biology, research has focused more on the TME, a complex network that consists of tumor vasculature, associated connective tissues, infiltrating immune cells, and the extracellular matrix (ECM) [1–3]. The ECM, a

Abbreviations
CAF, cancer-associated fibroblasts; DMBA, 7,12-dimethylbenz(a)anthracene; ECM, Extracellular matrix; MMP, matrix metalloproteinase; PCTM, primary cells from the tumor mass; TME, tumor microenvironment.

dynamic structure undergoing continuous remodeling through synthesis and degradation mechanisms, plays a crucial role in various cellular signaling cascades involved in the promotion of tumor growth, invasion, and migration [4–8]. The ECM contains several fibrillar proteins, such as collagen, fibronectin, elastin, and laminin, mainly produced by cancer-associated fibroblasts (CAF) [9]. Collagens are the primary components of the ECM, providing structural support to tissues and influencing cellular behavior through biochemical and mechanical mechanisms. Various types and isoforms of collagens are overexpressed in tumors and their organization and density can significantly impact tumor progression. For instance, collagen remodeling and crosslinking can enhance tumor stiffness, which is associated with increased tumor invasiveness and has a key role in drug resistance, acting as a physical barrier to therapeutic agents [10,11]. Moreover, collagen can influence cellular signaling pathways that regulate the proliferation, survival, and migration of cancer cells.

Breast cancer, the most common cancer type among women, causes approximately half a million deaths annually worldwide (World Health Organization). The ECM is increasingly recognized as a significant regulator in breast cancer [12–14], exhibiting high levels of collagens organized in variable compositions indicative of different clinical outcomes [15–18]. For instance, in breast cancer tissues, collagen type I, the most abundant collagen type in the human body and the primary component of the interstitial ECM, is significantly upregulated contributing to increased tissue stiffness and promoting tumor cell invasion and metastasis. Type III, involved in the early stages of breast cancer, and type XII collagen are also significantly overexpressed [19] and often correlated with poor outcomes [20].

The nature and composition of the ECM are hard to replicate *in vitro*, especially when working in a monolayer system. Three-dimensional (3D) spheroids are cell aggregates that form complex networks of cell–cell contacts, features absent in traditional cell monolayers, thus better mimicking the *in vivo* system [21,22]. Several studies have been conducted on 3D tumor culture systems, such as multicellular tumor spheroids [23,24], on cell lines and primary cells that do not present an endogenous matrix and are cultured with coating techniques with ECM-derived components [25,26]. Due to their *in vivo*-like composition, 3D spheroids serve as models for evaluating anticancer drug effectiveness and understanding the tumor mass's intrinsic properties [27]. Breast cancer cell lines have been successfully used to generate spheroids as promising models for medical application and drug discovery [28–30].

Thus, to develop a reliable model of a 3D spheroid with an endogenous ECM, we isolated primary cells from rat breast cancer to generate spheroids. Spheroids present an organized ECM, rich in collagen. By using recombinant collagenases to completely degrade the native collagen of the ECM in the 3D model, we demonstrated that ECM degradation can enhance drug efficacy by improving penetration and chemotherapeutic effects.

Results

Cell isolation from tumor mass and primary breast tumor spheroid formation

To investigate the ECM in primary tumor spheroids, a breast tumor was induced in an immunocompetent female Wistar rat via intraperitoneal injection of a well-established chemical carcinogen, 7,12-dimethylbenz(a)anthracene (DMBA) (Fig. 1A) [31].

After 6 months, a tumor mass visible in the abdominal submammary region was excised and treated with recombinant collagenases and thermolysin to dissociate the tissue and isolate primary cells. The isolated primary cells from the tumor mass (PCTM) exhibited heterogeneous morphological characteristics, indicative of the diverse cellular composition of the tumor microenvironment (Fig. 1B). This heterogeneity was confirmed through collagen type I staining, which identified cells synthesizing collagen type I, the major ECM component (Fig. 1C,D).

To better mimic the tumor condition and functions, modulated by cell–cell and cell–ECM interactions, the isolated PCTM were seeded under low-attachment conditions, promoting the formation of three-dimensional (3D) spheroids. After 6 days in culture, the cells formed spheroids with a homogeneous morphology and consistent size, ranging from 400 to 450 μm in diameter (Fig. 1E,F).

Proteomic analysis revealed an organized extracellular matrix in 3D primary breast tumor spheroids

3D spheroids and two-dimensional (2D) primary cells were analyzed through high-resolution proteomics to identify differential protein abundance in 2D and 3D systems, focusing on proteins involved in ECM organization. The analysis identified 6572 proteins in PCTM spheroids and 6573 proteins in cells grown in 2D, while 6486 proteins were common to both spheroids and 2D

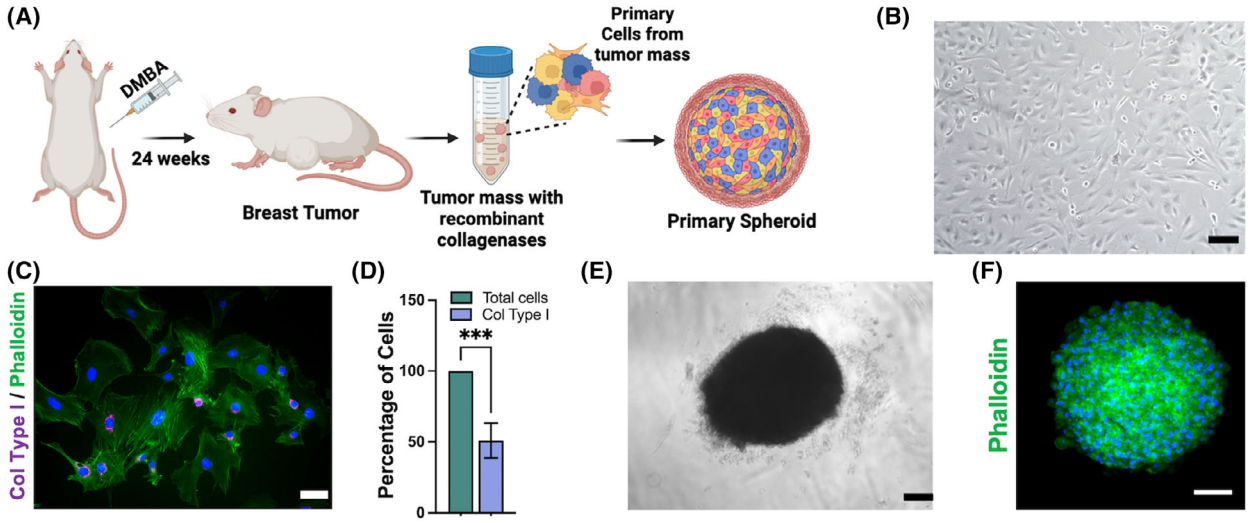

Fig. 1. Cell isolation from tumor mass and primary breast tumor spheroid formation. (A) Schematic representation describing the induction of breast cancer with DMBA and tissue digestion to isolate cells and generate spheroids. (B) Primary cells isolated from the tumor mass (PCTM). (C) Widefield microscopy analysis of PCTM stained with phalloidin-FITC (green), antibody anti-collagen type I (magenta), and DAPI (blue) (D) and collagen type I-positive cells. Scale bar: 15 μm. (E) 3D-spheroid (F) and confocal microscopy analysis of the spheroids stained with phalloidin-FITC (green) and DAPI (blue). Scale bar: 100 μm. Data are mean ± SD. Statistical analysis (*t*-test) was performed ($n = 3$) (***$P < 0.001$).

cells (Fig. 2A, Table S1). Among these common proteins, 1128 proteins were more abundant in the 3D spheroids, whereas 816 proteins were less abundant compared to the 2D cell culture (Table S1). This differential expression highlights the distinct proteomic landscapes of 2D and 3D systems, reflecting their different microenvironments and cellular interactions. To further explore the distinctive organization of the ECM, we focused on changes in ECM proteins (according to the UniProt Gene Ontology Cellular Component 0031012). This analysis identified 128 ECM-related proteins, with 12 proteins significantly decreased in PCTM spheroids (Fig. 2B, Table 1 and Table S2). Conversely, 45 proteins were significantly augmented in primary tumor spheroids (Fig. 2B, Table 2 and Table S2). The increased levels of these proteins in 3D spheroids indicate enhanced ECM remodeling and a more complex extracellular environment, which is more representative of tumor conditions. Notably, the expression of matrix metalloproteinases (MMPs), such as MMP2, MMP19, MMP1b, MMP14, and MMP3, increased in the 3D system, suggesting enhanced ECM remodeling (Fig. 2C). Interestingly, MMP9 and MMP13 were exclusively present in spheroids, pointing to unique proteolytic activities in the 3D context (Fig. 2D). These findings are significant as MMPs play crucial roles in tumor invasion and metastasis. Additionally, various types of collagens, such as Col5a2, Col4a1, Col18a1, Col5a1, Col8a1, Col4a2, Col16a1, and Col5a1, were identified in both 2D and 3D systems. However, these collagens were upregulated in 3D spheroids (Fig. 2E), indicating a more extensive and structurally complex ECM in the 3D model.

Primary breast tumor spheroids produce an endogenous extracellular matrix, which is completely degraded with recombinant collagenases

Since proteomic analysis revealed a different collagen expression between 2D and 3D systems, collagen type I, the most abundant collagen in tumoral ECM, was further investigated by confocal microscopy to evaluate the organization and distribution within and around the spheroids.

Immunostaining highlighted the capability of primary spheroids to produce an endogenous ECM, rich in collagen, which is mainly arranged around the 3D structure, simulating *in vitro* the tumor microenvironment conditions in solid tumors (Fig. 3A). To evaluate the effectiveness of collagenases in digesting collagen expressed in primary tumor spheroids, experiments were conducted by incubating spheroids with either ultrapure recombinant COLH (collagenase class II, acting on the linear collagen region) or COLH in combination with COLG (collagenase class I, acting on the

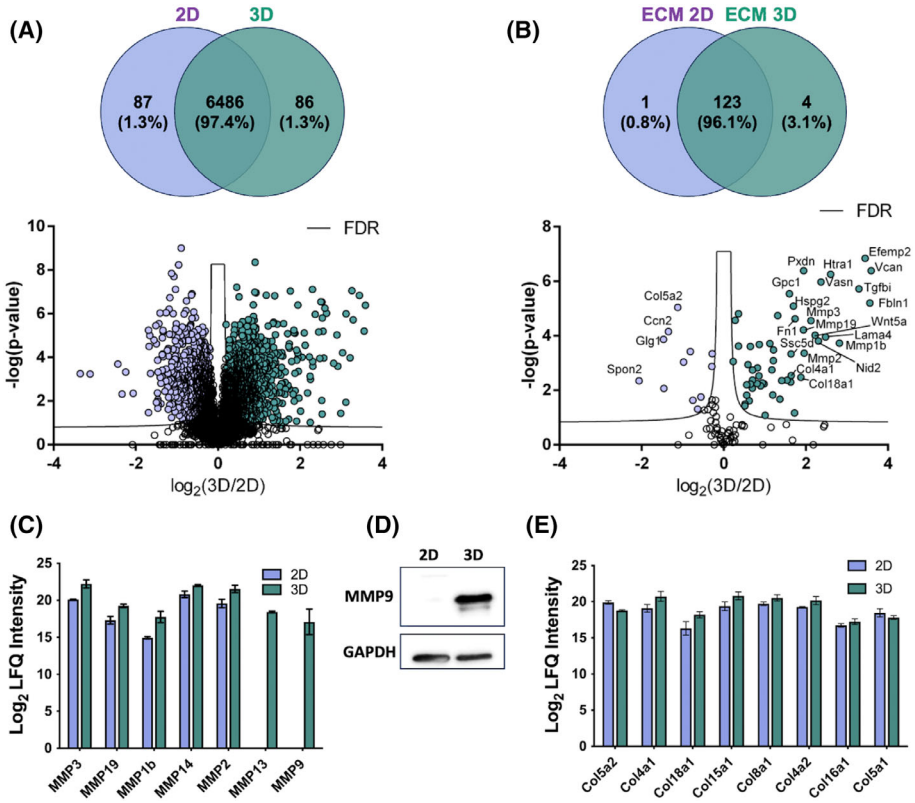

Fig. 2. Proteomic analysis revealed an organized extracellular matrix in 3D primary breast tumor spheroids. (A) Venn diagram and Volcano plot for the proteins identified in five biological samples of the 2D cell culture and 3D spheroids; volcano plot showing the −log10 of *P*-values versus the log2 of protein ratio for all proteins identified in the lysates of cells in 2D cell culture and 3D spheroids ($n = 5$). Blue: proteins of 3D spheroids; red: proteins of 2D cells. (B) Venn diagram and Volcano plot for the ECM proteins identified in five biological samples of the 2D cell culture and 3D spheroids; volcano plot showing the −log10 of *P*-values versus the log2 of protein ratio for ECM proteins identified in the lysates of cells in 2D cell culture versus 3D spheroids ($n = 5$). Blue: proteins of 3D spheroids; red: proteins of 2D cells. (C) LFQ (label-free quantification) intensity of the most significant MMPs (Matrix Metalloproteinases) differently expressed in 2D and 3D cultures ($n = 5$). (D) Western blot analysis of total cell lysates (15 μg) from 2D cell cultures (2D) and 3D spheroids (3D), using anti-MMP9 antibody. (E) LFQ intensity of the most significant types of collagen present in 2D and 3D cultures ($n = 5$). Data are mean ± SD.

3D-helix region) (Fig. 3B). Confocal microscopy observation revealed a reduction in type I collagen in spheroids incubated with COLH alone. However, complete digestion of type I collagen was observed when COLH was combined with COLG, demonstrating the synergistic effect of these enzymes in degrading collagen within the spheroid structure (Fig. 3C). The complete digestion indicates the effective breakdown of the collagen matrix, essential for subsequent experimental manipulations and assessing the impact of ECM degradation on drug delivery.

Collagenase treatment improves doxorubicin uptake and cytotoxicity effects in primary breast tumor spheroids

To investigate the impact of ECM degradation on the accessibility into a 3D model of the commonly used anticancer drug doxorubicin, uptake assays were carried out on PCTM spheroids. Spheroids were incubated with doxorubicin after 6 days of formation, and the drug's uptake was monitored over time. A significant increase in the doxorubicin signal was evident both in the entire spheroids (Fig. 4A) and their central slice (Fig. 4B) in a time-dependent manner. Maximum intensity was observed at 24 h of incubation, whereas in PCTM 2D cell culture, maximum doxorubicin uptake and nuclear translocation were detectable after only 2 h (Fig. S1). This slower uptake in spheroids highlights the barrier effect of the ECM on drug penetration. Furthermore, analysis of the core of the spheroids underlined that doxorubicin uptake increased significantly over time relative to the total intensity, suggesting that the drug initially accumulates in the outer layer of the spheroids and then penetrates towards the core by 24 h (Fig. 4B). Based on the optimized concentration of recombinant collagenases

Table 1. List of the 12 most highly reduced ECM proteins in 3D spheroids compared to 2D cell cultures. Protein name: name of ECM proteins reduced in primary tumor spheroids. Protein ID: UniProt accession number of the protein. Gene name: UniProt gene name associated with each protein. *P-value*: *P*-value calculated after a Student *t*-test of five biological replicates. Ratio: ratio between the mean of LFQ values of primary tumor spheroids and tumor cells in 2D cultures ($n = 5$).

Protein name	Protein ID	Gene name	*P*-value	Ratio
Spondin-2	Q9WV75	Spon2	4.46E-03	0.23873
Golgi apparatus protein 1	Q62638	Glg1	1.34E-04	0.36147
Laminin subunit gamma 2	F1LRH4	Lamc2	8.48E-03	0.36393
CCN family member 2	Q9R1E9	Ccn2	7.02E-05	0.39299
Collagen type V alpha 2 chain	F1LQ00	Col5a2	9.06E-06	0.45915
Integrin subunit alpha 6	G3V667	Itga6	9.18E-04	0.50645
Tissue factor	P42533	F3	3.78E-04	0.56778
Lumican	P51886	Lum	2.32E-02	0.59290
Collagen alpha-1(V) chain	Q9JI03	Col5a1	4.91E-02	0.64259
Extracellular superoxide dismutase [Cu-Zn]	Q08420	Sod3	1.76E-02	0.67894
Prolyl 3-hydroxylase 1	Q9R1J8	P3h1	1.32E-03	0.81622
Metalloproteinase inhibitor 1	P30120	Timp1	4.52E-04	0.82295

Table 2. List of the 23 most highly increased ECM proteins increased in 3D spheroids compared to 2D cell cultures. Protein name: name of ECM proteins increased in primary tumor spheroids with a 3D/2D ratio above 2.82 (which is 1.5 in a log2 scale). Protein ID: UniProt accession number of the protein. Gene name: UniProt gene name associated with each protein. *P-value*: *P*-value calculated after a Student *t*-test of five biological replicates. Ratio: ratio between the mean of LFQ values of primary tumor spheroids and tumor cells in 2D cultures ($n = 5$).

Protein name	Protein ID	Gene name	p-value	Ratio
Versican core protein	Q9ERB4	Vcan	4.06E-07	12 040
Fibulin-1	A0A0G2JY81	Fbln1	6.23E-06	11 779
EGF containing fibulin extracellular matrix protein 2	A0A8I5Y8F2	Efemp2	1.44E-07	10 869
Transforming growth factor, beta induced	D4A8G5	Tgfbi	1.88E-06	9794
Matrix metallopeptidase 1b (interstitial collagenase)	D3ZRZ2	Mmp1b	1.86E-04	7042
Serine protease HTRA1	Q9QZK5	Htra1	5.55E-07	6081
Laminin subunit alpha 4	F1LTF8	Lama4	1.10E-04	5574
Vasorin	D3ZAE6	Vasn	1.06E-06	5158
Nidogen-2	B5DFC9	Nid2	1.55E-04	4942
Protein Wnt-5a	Q9QXQ7; B1WBR9	Wnt5a	9.47E-05	4673
Stromelysin-1	P03957	Mmp3	2.79E-05	4357
72 kDa type IV collagenase	P33436	Mmp2	4.31E-04	3884
Peroxidasin	A0A0G2JWB6	Pxdn	4.05E-07	3845
Matrix metallopeptidase 19	C0M4B0	Mmp19	6.11E-05	3836
Collagen type XVIII alpha 1 chain	A0A8I6GLR1	Col18a1	3.36E-03	3677
Fibronectin	P04937	Fn1	2.37E-05	3326
Fibulin-5	Q9WVH8	Fbln5	6.73E-02	3298
Heparan sulfate proteoglycan 2	A0A8I6ASH2	Hspg2	8.15E-06	3236
Collagen type IV alpha 1 chain	F1MA59; A0A8I5ZZ86	Col4a1	2.88E-03	3121
Scavenger receptor cysteine rich family member with 5 domains	D3ZPK4	Ssc5d	4.60E-04	3117
Apolipoprotein E	P02650	Apoe	4.94E-03	3092
Glypican-1	P35053	Gpc1	2.87E-06	3025
Glia-derived nexin	P07092	Serpine2	4.30E-03	2909

(COLG and COLH), PCTM spheroids were predigested with collagenases before doxorubicin treatments (Fig. 4C). At 24-h post-treatments, these spheroids displayed a 38% increase in doxorubicin uptake signal in the total intensity (Fig. 4A) and a 26% increase in the central slice (Fig. 4B), compared to spheroids treated with doxorubicin alone. This enhanced uptake post-collagenase treatment underscores the significance of ECM degradation in improving drug penetration and efficacy within 3D tumor models.

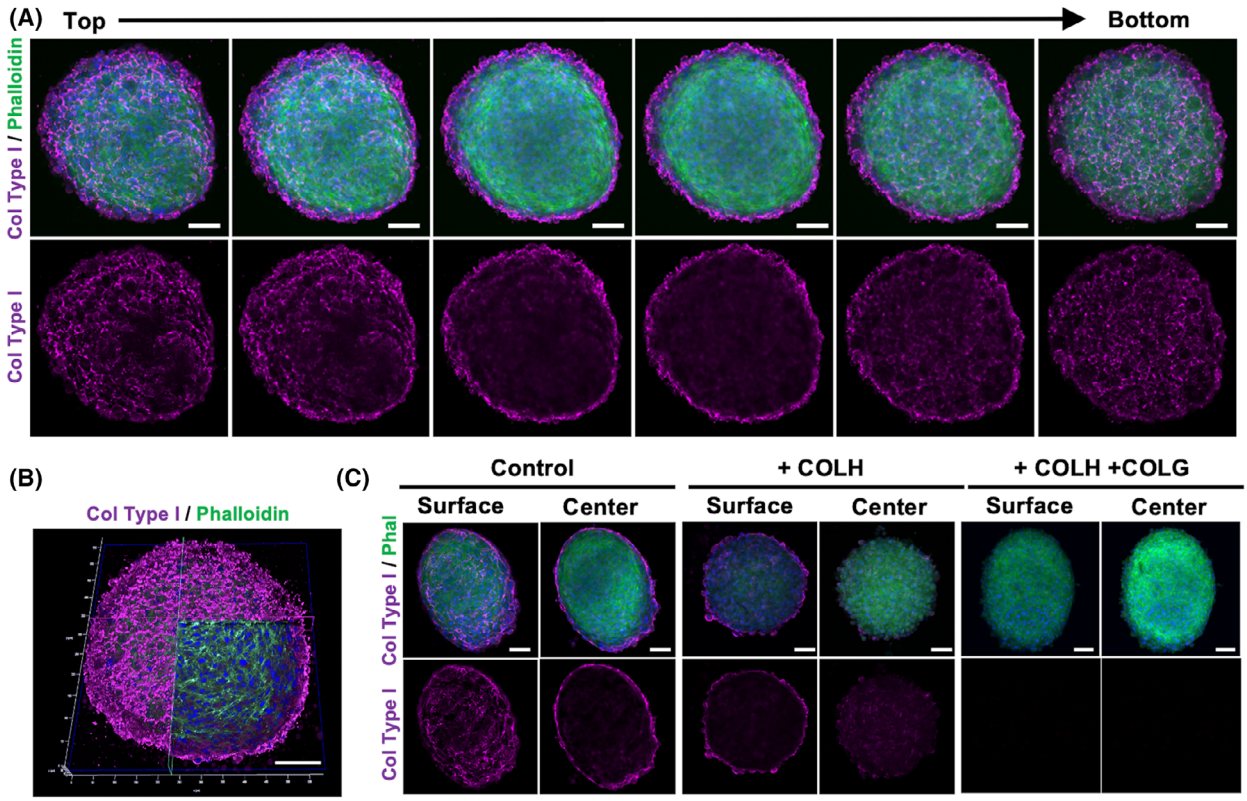

Fig. 3. Primary breast tumor spheroids produce an endogenous extracellular matrix, which is completely degraded with recombinant collagenases. (A) Confocal microscope stacks from top to bottom of primary tumor spheroids, stained with phalloidin-FITC (green), antibody anti-collagen type I (magenta), and DAPI (blue). (B) A section at the confocal microscope. Scale bar: 100 μm. (C) Primary tumor spheroids untreated (control), treated by recombinant collagenase COLH (+COLH) for 1 h 15 min, and treated by recombinant collagenases COLG and COLH (+COLH/COLG) for 1 h 15 min. After the enzymatic treatment, spheroids were stained with phalloidin-FITC (Phal) (green), antibody anti-collagen type I (magenta), and DAPI (blue) and analyzed with confocal imaging, showing the surface (left) and the center (right) of spheroids. Scale bar: 100 μm. Experiments have been conducted three times, '$n = 3$'.

To evaluate the impact of collagen degradation on the cytotoxic effects of doxorubicin in PCTM spheroids, they were first digested with collagenases, followed by treatment with doxorubicin for 24 h (Fig. 4D). After the treatment, the total area of spheroids, including areas of dead cells, was analyzed. Interestingly, spheroids treated with collagenases alone did not exhibit a significant change in size compared to the untreated control, indicating that collagenase treatment by itself did not induce notable cytotoxic effects. In contrast, treatment with doxorubicin alone resulted in a 75% increase in the size of spheroids. When the spheroids' collagen matrix was predigested with collagenases before doxorubicin treatments, the drug's effects were significantly enhanced. This combination led to a 34% increase in doxorubicin efficacy compared to spheroids treated with doxorubicin alone (Fig. 4E).

The role of collagenases in enhancing drug efficacy was further investigated by analyzing the doxorubicin cytotoxicity effect in PCTM spheroids over time, with and without prior collagenase treatment. After 8 h of treatments, no significant cytotoxic effects were observed, indicating that short-term exposure was insufficient to induce noticeable cell death. However, after 16 h, cytotoxic effects became more evident, although there was no significant difference between the two conditions at this stage. By 24 h, the collagenase treatments induced a slow decrease in cell viability, probably due to the release of collagen's peptides with inhibitory effects on cell proliferation. However, the cytotoxic effects of doxorubicin were more pronounced. Spheroids that had been pretreated with collagenases showed a 50% decrease in cell viability compared to those treated directly with doxorubicin (Fig. 4F). These findings reinforce the observation that ECM degradation enhances drug efficacy, as previously indicated by the increased drug uptake and changes in the spheroid area.

Discussion

Tumorigenesis is a complex and dynamic process in which the ECM plays a leading role. In solid tumors, a stiff ECM and its remodeling are involved in different mechanisms in tumor progression, metastasis, immune escape [32], and in resistance to established cancer therapies [6,8,33].

Therefore, novel antitumor approaches should target cancer cells and dysregulated tumor ECM, especially fibrillar collagens that are the most altered in tumor ECM [34,35].

The increasing focus on the tumor microenvironment presents a new challenge to obtain 3D reliable *in vitro* models for preclinical drug studies, which mimic an ECM similar to the tumor mass [36,37]. In this context, many studies have reported the generation of 3D spheroid models using various cell lines [38,39]. Furthermore, the involvement of primary cells, as proposed, can improve the reliability of the system. For this purpose, PCTM spheroids were generated using cells isolated from a chemically induced tumor mass in Wistar rats. PCTMs are a mixture of heterogeneous primary cells that self-assembled to form uniform, round, compacted spheroids of consistent size (400–450 μm), with minimal variability in size and shape. Additionally, they are able to produce a well-organized, endogenous collagen matrix with a capsule-like structure, limiting the accessibility of drugs, as observed in solid tumors. Consequently, it is unnecessary to add additional ECM, as embedding them in a collagen gel, as is commonly reported [39,40]. The proteomic analysis comparing cells grown in 2D to those in the 3D system revealed differences in protein expression and an enhanced ECM organization in the 3D system. Notably, tumor spheroids showed increased expression of proteins associated with solid tumor progression, such as versican and MMPs. In cancer, versican, a member of the proteoglycan family, impacts proliferation, survival, invasion, metastasis, and inflammation [41,42]. MMP9 and MMP13 were specifically expressed in the 3D system and are well known for their involvement in ECM regulation, promoting cell proliferation and extravasation [43–46]. Different types of collagens were also upregulated and this upregulation could influence cell behavior, signaling pathways, and drug response, making 3D spheroids a more relevant model for studying tumor biology and testing therapeutic interventions. Collagen plays a complex role in tumors, depending on the tumor origin, and different collagen types are closely associated with cancer progression and poor prognosis [18,47,48]. Therefore, collagen is considered a potential target for cancer treatment, and breaking it down could facilitate the penetration of chemotherapeutic agents. While collagenases are already used clinically for debridement in wounds and ulcers, their use in cancer treatments has not been validated yet [10,49]. In this study, the digestion of spheroids' collagen was optimized using recombinant collagenases by combining two classes of these enzymes: Class I and Class II. Class I (COLG) recognizes the native collagen, acting on the 3D-helix region, while Class II (COLH) has a higher activity against the linear collagen region [50]. The use of ultrapure recombinant collagenases significantly limits the side effects associated with proteases present in extracted collagenases, which can partially damage spheroids and cause the cells' escape from the spheroid structure. For the first time, this collagen digestion method enables the complete removal of the collagen matrix without altering the spheroid shape. This aspect is fundamental for *in vitro* models, as it allows for the selective study of collagen's role in drug response and the metabolic pathways of cells within a solid tumor mass.

The combination of COLG and COLH on primary tumor spheroids exhibits synergistic activity, resulting in efficient collagen digestion. Furthermore, to investigate the role of ECM on drugs' effects, the time-dependent penetration of doxorubicin into the spheroid core was analyzed. The data emphasize the need for prolonged drug exposure in 3D cultures to achieve effective treatment, contrasting with the rapid uptake observed in 2D cultures. Moreover, the collagenase digestion experiments demonstrated that effective ECM degradation facilitates deeper penetration of therapeutic agents like doxorubicin, which is otherwise hindered by the dense ECM network. The enzymatic treatments enhanced the cytotoxicity effects of doxorubicin, suggesting potential therapeutic strategies that combine ECM degradation with chemotherapy to improve treatment outcomes.

These findings highlighted a novel model of primary tumor spheroids with an endogenous ECM, providing a more physiologically relevant platform for studying tumor biology and evaluating potential treatments. Moreover, this study provides critical insights into the role of the ECM in tumor spheroid models and its impact on drug delivery. Collagenase's proteolytic activity could improve not only the permeability of tumors to chemotherapeutic agents but also potentially facilitate the infiltration of immune cells into the mass. It is well established that the number of T cells found within a tumor as well as their ability to migrate and reach cancer cells is fundamental for an effective

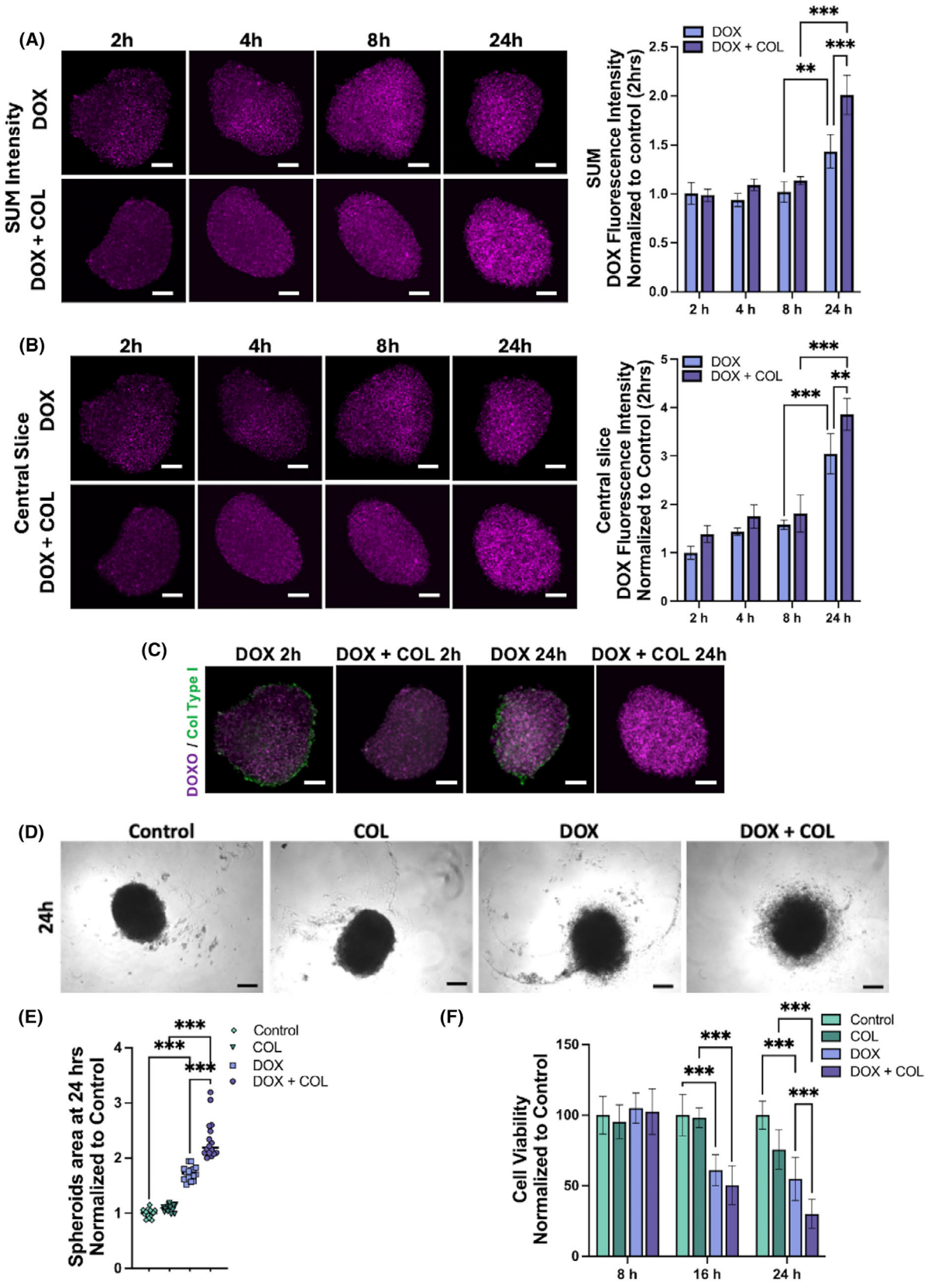

Fig. 4. Collagenase treatment improves doxorubicin uptake and cytotoxicity effects in primary breast tumor spheroids. (A) Confocal analysis (stacks sum intensity) of 20 μM doxorubicin uptake in control (DOX) spheroid and collagenase-treated (DOX + COL) at different time points (2, 4, 8, 24 h). Quantification of the fluorescence Sum intensities was analyzed and normalized to control. (B) Confocal analysis (central stack intensity) of 20 μM doxorubicin uptake in control spheroid and collagenase-treated at different time points (2, 4, 8, 24 h). Quantification of the central stack fluorescence intensities was analyzed and normalized to control. Magenta: DOX autofluorescence. Scale bar: 100 μm. Statistical analysis (two-way ANOVA) was performed ($n = 3$). (C) Confocal analysis (stacks sum intensity) of 20 μM doxorubicin uptake in control (DOX) spheroid and collagenase-treated (DOX + COL) at different time points (2 and 24 h). Magenta: DOX autofluorescence, Green: anti-collagen type I. Scale bar: 100 μm. (D) Representative pictures of control primary tumor spheroid (Control), treated with collagenases (COL), treated with doxorubicin 20 μM (DOX) and with collagenases + doxorubicin 20 μM (DOX + COL) at 24 h (scale bar: 10 μm). (E) Quantification of primary tumor spheroids area at 24 h, including dead cells, normalized to the area at T0 (not shown in this figure). Statistical analysis (one-way ANOVA) was performed ($n = 3$). (F) Cell viability assay of primary tumor spheroid, treated with collagenases (COL), treated with doxorubicin 20 μM (DOX) and with collagenases + doxorubicin 20 μM (DOX + COL) at different times (8, 16, 24 h). Scale bar: 100 μm. Data are mean ± SD. Statistical analysis (two-way ANOVA) was performed ($n = 3$) (**$P < 0.01$, ***$P < 0.001$).

antitumoral response. However, the increased stiffness of ECM produced by tumors can directly regulate T-cell migration [51], acting as a physical barrier and consequently impairing the infiltration of immune cells in the tumor mass [8,52,53].

In addition, recombinant collagenases could be a viable strategy to improve the delivery and efficacy of chemotherapeutic agents in solid tumors, potentially overcoming one of the significant obstacles in cancer treatment. Further research and *in vivo* studies are necessary to validate these findings and determine the safety, optimal dosing, and long-term benefits of using collagenases in combination with chemotherapeutic agents in cancer therapy.

Materials and methods

Rat model

All animal experiments were approved by the University of Palermo. Authorization number 523/2022-PR, issued according to art. 31 del D.lgs. 26/2014 Istituto Superiore di Sanità, Italy. The animals were housed 2 per cage (with EPA filter; controlled temperature 23 °C ± 0.5 °C; controlled humidity 50% ± 5%). The dark/light cycle was set at 12 h (7 a.m. to 7 p.m. light; 7 p.m. to 7 a.m. dark). Access to food at libitum.

Female Wistar rats were obtained from ENVIGO RMS SRL. At 55 days of age, a single dose of 50 mg·kg^{-1} 7,12 dimethylbenz(a)anthracene (DMBA) resuspended in corn oil was intraperitoneally injected [31]. After 6 months, an evident breast tumor mass was individuated.

The rat with a visible tumor mass was sedated with 2% isoflurane, sacrificed, and the tumor excised. A portion of the tumor was processed to isolate cells.

Primary cells

Primary cells were isolated from DMBA-induced tumors in female Wistar rats. The growth media used was Dulbecco's modified Eagle's medium (DMEM, Sigma-Aldrich, Milano, Italy) high glucose (HG-DMEM), which was supplemented with 10% fetal bovine serum (FBS), 100 U·mL^{-1} penicillin, 100 mg·mL^{-1} streptomycin (Euroclone, Celbar, Pero, Italy), and 2 mM L-Glutamine (Euroclone, Celbar). The cells were then incubated at 37 °C, in an incubator at 5% CO_2. Cell culture media was replenished every 3 days.

Primary cancer cell isolation

Primary cells were isolated from DMBA-induced tumors in female Wistar rats. The animal was sedated with 2% isoflurane, sacrificed and the tumor mass was explanted, washed in 70% ethanol, and put in Dulbecco's modified Eagle's medium (DMEM, Sigma-Aldrich, Milano, Italy) high glucose (HG-DMEM) added with 300 U·mL^{-1} penicillin, 300 U·mL^{-1}, streptomycin (Euroclone, Celbar). After dissection in small parts with a scalpel, the tissue was incubated with the digestion buffer, containing ultrapure recombinant collagenases class I (Col G 106.4 U·g^{-1}) and class II (Col H 453.2 U·g^{-1}) (Abiel) and Thermolysin (Promega, Madison, Wisconsin, US) 266.4 μg·g^{-1}. The digestion was performed at 30 °C for 2 h in agitation and then stopped with HG-DMEM containing 10% (v/v) fetal bovine serum (FBS, Euroclone, Celbar). The sample was washed three times with DMEM and centrifuged at 500 ***g*** for 5 min to isolate cells. The pellet was resuspended in DMEM/F12 medium added with 300 units·mL^{-1} penicillin G 300 mg·mL^{-1}, streptomycin (Euroclone, Celbar), 2 mM L-Glutamine (Euroclone, Celbar) and 10% (v/v) FBS and seeded on 50 μg·mL^{-1} (in 0.02 N acetic acid) collagen-coated dishes and cultivated at 37 °C, in a humidified atmosphere of 5% CO_2 in sterile conditions [54].

Cells and spheroid culture

Primary isolated cells were cultured in DMEM high glucose plus 1% penicillin/streptomycin, 1% L-Glutamine, and 10% FBS for 15 passages. Cells were maintained at 37 °C in a humidified atmosphere with 5% CO_2. To form spheroids, primary cancer cells were seeded into a 96-multiwell

low-attachment plate coated with agarose, at 1×10^4 cells per well, in complete DMEM, at 37 °C and 5% CO_2 and were let grow for 6 days.

Proteomic-based characterization: protein extraction and sample preparation

Cells from two-dimensional and three-dimensional cultures were lysed in STET (10 mM Tris/HCl, 1 mM EDTA, 100 mM NaCl, and 5% Triton X-100 (v/v)) with a protease inhibitor cocktail (Roche, Basel, Switzerland) and centrifuged (14,000 x ***g***, 5 min) to eliminate cell membranes. Proteins extracted were quantified with a colorimetric 660 nm micro BCA assay. A protein amount of 30 µg per sample was subjected to filter-aided sample preparation (FASP—with 10 kDa Vivacon 500 spin filter columns from Sartorius, Gottinga, Germany), as previously described [55]. Samples were then reduced and denatured with dithiothreitol (DTT) (Sigma-Aldrich) in 200 µL of UA buffer (8 M Urea in 0.1 M Tris/HCl, pH 8.5) and alkylated with 50 mM iodoacetamide (IAA) (Sigma-Aldrich). After reduction and alkylation, samples were washed three times with UB buffer (8 M Urea in 0.1 Tris/HCl, pH 8.0) and sequentially digested with LysC (1 : 50 enzyme to protein ratio from Promega) and trypsin (1 : 100 enzyme to protein ratio, Promega). Then, peptides were eluted from filter columns by centrifugation (14 000 ***g***; 60 min) and acidified with 20 µL of 8% formic acid (FA). Generated peptides were desalted by stop-and-go extraction (STAGE) on reverse phase C18 and eluted in 40 µL of 60% acetonitrile in 0.1% formic acid [56]. The volume was reduced in a SpeedVac (Thermo Fisher Scientific, Waltham, Massachusetts, US), and the peptides were resuspended in 20 µL of 0.1% formic acid. The peptide concentration was measured with NanoDrop 2000 (Thermo Scientific).

uHPLC–MS/MS and data analysis

As previously described [57] for each sample, 1 µg peptides were separated through a nanoLC system (Vanquish Neo UHPLC, Thermo Scientific) equipped with an Acclaim PEPMap C18 column (25 cm × 75 µm ID, Thermo Scientific) in a 130 min binary gradient of water and acetonitrile containing 0.1% FA. Separated peptides were injected into an Exploris 480 mass spectrometer (Thermo Fischer Scientific) for tandem mass spectrometry analysis. Proteins were identified and quantified with label-free quantification (LFQ) by using data-independent acquisition (DIA). DIA was performed using an MS1 full scan (400–1200 m/z) followed by 60 sequential DIA windows with an overlap of 1 m/z and window placement optimization option enabled. Full scans were acquired with 120 000 resolution, AGC of 3×10^6, and a maximum injection time of 50 ms. Afterward, 60 isolation windows were scanned with a resolution of 30 000, an AGC of 8×10^5 and maximum injection time was set as auto to achieve the optimal cycle time. Collision-induced dissociation fragmentation was induced with 30% of the normalized HCD. The data were analyzed by the software DIA-NN (version 1.8.1) by using a predicted library generated from *in silico* digested Rattus norvegicus (rat) UniProt reference database (proteome ID UP000002494) involving cuts at K* and R*, two missed cleavages allowed, minimal peptide length set a 6. The false discovery rate for peptide and protein identification was set at 0.01%. Label-free quantification (LFQ) was used for protein quantification. The LFQ values were log2 transformed, and a two-sided Student's *t*-test was used to evaluate proteins statistically significantly regulated between two-dimensional and three-dimensional culture ($n = 5$). The mass spectrometry proteomics data have been deposited to the ProteomeXchange Consortium via the PRIDE partner repository with the dataset identifier PXD061082.

Western blot analysis

Cells (2D and 3D) were lysed on ice in RIPA buffer (20 mM Tris, 150 mM NaCl, 0.1% Triton X-100, 1 mM EDTA, pH 7.2) with a protease inhibitor cocktail. Lysates were incubated in a sample buffer under reducing conditions and fractionated with Sodium dodecyl sulfate–polyacrylamide gel electrophoresis (SDS/PAGE) 10% and transferred to nitrocellulose membranes (Amersham). The membranes were blocked in PBS/Tween 0.1% (PBS/T) with 5% non-fat dried milk, incubated with the MMP-9 (Abcam, Cambridge, UK, ab38906) primary antibody diluted 1 : 1000 in PBS/T, washed four times in blocking solution, and incubated with HRP-conjugated secondary antibodies (Sigma) followed by washing in PBS/T.

The membrane was exposed to Super Signal West Femto Maximum Sensitivity substrate (Thermo Scientific), and protein expression was detected by CHEMIDOC XRS (Bio-Rad, Hercules, CA, USA).

Immunofluorescence staining and imaging

Cells were fixed in 3.7% formaldehyde (1 h for spheroids, 15 min for 2D cells, at room temperature) before permeabilization in PBS supplemented with 0.1% Triton X-100 (5 min, room temperature, only for the 2D cells). They were then blocked for 1 h at room temperature using PBS with 1% BSA (Sigma-Aldrich, St. Louis, MO, USA). The primary antibody used was Rabbit anti-collagen type I (1 : 20, 234167, Millipore, Burlington, Massachusetts, US), which was incubated overnight at 4 °C in a blocking buffer. Cells were stained with the species-specific fluorophore-conjugated secondary antibody (Invitrogen, Waltham, Massachusetts, US) (2 h for spheroids, 1 h for 2D cells, at room temperature), actin cytoskeleton was labeled with phalloidin-FITC (1 : 500 in PBS) for 30 min

at room temperature, and nuclei were visualized with DAPI (1 : 20 000 in PBS). Coverslips were mounted in a mounting medium and examined on the confocal microscope (Olympus FV10i and Stellaris 5, Leica, Wetzlar, Germany). Z-stack imaging was carried out using a Fluoview FV10i confocal laser scanning microscope system (Olympus, Tokyo, Japan) at a magnification of 20× with a step size of 10 μm. All stacks were obtained at the same intensity setting between groups. IMAGEJ software (NIH, US) was used to analyze stacks of images.

Collagenase treatment of spheroids

Spheroids were grown for 6 days, as described, washed two times in PBS, and then incubated with recombinant collagenases (Abiel srl) (20 $U \cdot mL^{-1}$ COLG and 80 $U \cdot mL^{-1}$ COLH) in DMEM without FBS for 1 h 15 min at 37 °C. After incubation, they were washed two times with DMEM with FBS to block collagenase activity.

Doxorubicin uptake study by confocal microscopy

To assess the uptake of doxorubicin, spheroids untreated and treated with recombinant collagenases were incubated with 20 μM doxorubicin for 2, 4, 8, or 24 h. Spheroids were then processed for immunocytochemistry, as previously described. IMAGEJ software was used to analyze stacks of images.

Spheroids' area analysis

Spheroids, untreated or treated with collagenases, were incubated with 20 μM doxorubicin for 24 h at 37 °C. After treatment, spheroids' areas were analyzed, including areas of dead cells. The analysis was performed with IMAGEJ.

Cell viability assay

Spheroids, untreated or treated with collagenases, were incubated with 20 μM doxorubicin for 8, 16, and 24 h at 37 °C. After treatment, spheroids were washed three times with PBS, resuspended in 50 μL of DMEM and an equal volume of CellTiter-Glo® 3D Reagent (Promega) following the Manufacturer's protocol. Briefly, 100 mL medium was replaced with 100 mL CellTiter-Glo 3D reagent on the indicated day after growth/treatment. The plates were shaken for 5 min at 240 ***g***, incubated for 25 min at room temperature, and the luminescent signal was recorded using a luminometer (SinergyHT, BioTek, Winooski, VT, USA).

Statistical analysis

Statistical analyses were performed using GRAPHPAD PRISM software (version 8.4.3) (Boston, MA, US). One-way ANOVA with Tukey's *post hoc* test and two-way ANOVA were used. The results are displayed as Mean ± SD, with significance at a level of P-value < 0.05. Three to five replicates were analyzed for each experimental group. The experiments were performed three times.

Acknowledgements

We acknowledge the Italian Ministry of University and Research (MUR) for the PON project on Research and Innovation 2014–2020 (Azione IV.4—Contratti di ricerca su tematiche dell'Innovazione—B75F21002190001). This work has received funding from the European Union—NextGenerationEU through the Italian Ministry of University and Research under PNRR—MUR, PNRR-M4C2, ECS_00000022-SiciliAn MicronanOTecH Research And Innovation CEnter "SAMOTHRACE"—CUP: B73C22000810001. The views and opinions expressed are those of the authors only and do not necessarily reflect those of the European Union or the European Commission. Neither the European Union nor the European Commission can be held responsible for them. We acknowledge ATeN Center–University of Palermo for the confocal microscope and the animal facility. Open access publishing facilitated by Universita degli Studi di Palermo, as part of the Wiley - CRUI-CARE agreement.

Conflict of interest

The authors declare no conflict of interest.

Author contributions

ALC, SC, and GG designed the experiments. ALC, SC, and GLB performed the experiments. PC produced the recombinant collagenases. MLP and SDS performed the proteomic analysis. SC and GLB helped with data analysis. ALC analyzed data and wrote the manuscript. All authors reviewed and edited the manuscript and approved the final version of the manuscript.

Peer review

The peer review history for this article is available at https://www.webofscience.com/api/gateway/wos/peer-review/10.1111/febs.70069.

Data availability statement

The data that support the findings of this study are available in the main text and the Supporting

Information of this article. The mass spectrometry proteomics data have been deposited to the ProteomeXchange Consortium via the PRIDE partner repository with the dataset identifier PXD061082.

References

1 Brassart-Pasco S, Brézillon S, Brassart B, Ramont L, Oudart JB & Monboisse JC (2020) Tumor microenvironment: extracellular matrix alterations influence tumor progression. *Front Oncol* **10**, 397.

2 Henke E, Nandigama R & Ergün S (2020) Extracellular matrix in the tumor microenvironment and its impact on cancer therapy. *Front Mol Biosci* **6**, 470149.

3 Goenka A, Khan F, Verma B, Sinha P, Dmello CC, Jogalekar MP, Gangadaran P & Ahn BC (2023) Tumor microenvironment signaling and therapeutics in cancer progression. *Cancer Commun* **43**, 525–561.

4 Du W, Xia X, Hu F & Yu J (2023) Extracellular matrix remodeling in the tumor immunity. *Front Immunol* **14**, 1340634.

5 Eble JA & Niland S (2019) The extracellular matrix in tumor progression and metastasis. *Clin Exp Metastasis* **36**, 171–198.

6 Bonnans C, Chou J & Werb Z (2014) Remodelling the extracellular matrix in development and disease. *Nat Rev Mol Cell Biol* **15**, 786–801.

7 Walker C, Mojares E & Del Río Hernández A (2018) Role of extracellular matrix in development and cancer progression. *Int J Mol Sci* **19**, 3028. doi: 10.3390/ijms19103028

8 Winkler J, Abisoye-Ogunniyan A, Metcalf KJ & Werb Z (2020) Concepts of extracellular matrix remodelling in tumour progression and metastasis. *Nat Commun* **11**, 5120.

9 Liao Z, Tan ZW, Zhu P & Tan NS (2019) Cancer-associated fibroblasts in tumor microenvironment – accomplices in tumor malignancy. *Cell Immunol* **343**, 103729.

10 Shi R, Zhang Z, Zhu A, Xiong X, Zhang J, Xu J, Sy MS & Li C (2022) Targeting type I collagen for cancer treatment. *Int J Cancer* **151**, 665–683.

11 Safaei S, Sajed R, Shariftabrizi A, Dorafshan S, Saeednejad Zanjani L, Dehghan Manshadi M, Madjd Z & Ghods R (2023) Tumor matrix stiffness provides fertile soil for cancer stem cells. *Cancer Cell Int* **23**, 143.

12 Insua-Rodríguez J & Oskarsson T (2016) The extracellular matrix in breast cancer. *Adv Drug Deliv Rev* **97**, 41–55.

13 Lochter A & Bissell MJ (1995) Involvement of extracellular matrix constituents in breast cancer. *Semin Cancer Biol* **6**, 165–173.

14 Nazemi M, Yanes B, Martinez ML, Walker HJ, Pham K, Collins MO, Bard F & Rainero E (2024) The extracellular matrix supports breast cancer cell growth under amino acid starvation by promoting tyrosine catabolism. *PLoS Biol* **22**, e3002406.

15 Bergamaschi A, Tagliabue E, Sørlie T, Naume B, Triulzi T, Orlandi R, Russnes HG, Nesland JM, Tammi R, Auvinen P *et al.* (2008) Extracellular matrix signature identifies breast cancer subgroups with different clinical outcome. *J Pathol* **214**, 357–367.

16 Casey T, Bond J, Tighe S, Hunter T, Lintault L, Patel O, Eneman J, Crocker A, White J, Tessitore J *et al.* (2009) Molecular signatures suggest a major role for stromal cells in development of invasive breast cancer. *Breast Cancer Res Treat* **114**, 47–62.

17 Acerbi I, Cassereau L, Dean I, Shi Q, Au A, Park C, Chen YY, Liphardt J, Hwang ES & Weaver VM (2015) Human breast cancer invasion and aggression correlates with ECM stiffening and immune cell infiltration. *Integr Biol* **7**, 1120–1134.

18 Badaoui M, Mimsy-Julienne C, Saby C, Van Gulick L, Peretti M, Jeannesson P, Morjani H, Ouadid-Ahidouch H, Badaoui M, Mimsy-Julienne C *et al.* (2018) Collagen type 1 promotes survival of human breast cancer cells by overexpressing Kv10.1 potassium and Orai1 calcium channels through DDR1-dependent pathway. *Oncotarget* **9**, 24653–24671.

19 Kim SH, Lee HY, Jung SP, Kim S, Lee JE, Nam SJ & Bae JW (2014) Role of secreted type I collagen derived from stromal cells in two breast cancer cell lines. *Oncol Lett* **8**, 507–512.

20 Li X, Jin Y & Xue J (2024) Unveiling Collagen's role in breast cancer: insights into expression patterns, functions and clinical implications. *Int J Gen Med* **17**, 1773–1787.

21 Calpe B & Kovacs WJ (2020) High-throughput screening in multicellular spheroids for target discovery in the tumor microenvironment. *Expert Opin Drug Discovery* **15**, 955–967.

22 Rodrigues DB, Reis RL & Pirraco RP (2024) Modelling the complex nature of the tumor microenvironment: 3D tumor spheroids as an evolving tool. *J Biomed Sci* **31**, 13.

23 Ishiguro T, Ohata H, Sato A, Yamawaki K, Enomoto T & Okamoto K (2017) Tumor-derived spheroids: relevance to cancer stem cells and clinical applications. *Cancer Sci* **108**, 283–289.

24 Rodrigues T, Kundu B, Silva-Correia J, Kundu SC, Oliveira JM, Reis RL & Correlo VM (2018) Emerging tumor spheroids technologies for 3D in vitro cancer modeling. *Pharmacol Ther* **184**, 201–211.

25 Goncalves IG & Aznar JMG (2021) Extracellular matrix density regulates the formation of tumour spheroids through cell migration. *PLoS Comput Biol* **17**, e1008764.

26 Tao F, Sayo K, Sugimoto K, Aoki S & Kojima N (2020) Development of a tunable method to generate

various three-dimensional microstructures by replenishing macromolecules such as extracellular matrix components and polysaccharides. *Sci Rep* **10**, 6567.
27 Vakhshiteh F, Bagheri Z, Soleimani M, Ahvaraki A, Pournemat P, Alavi SE & Madjd Z (2023) Heterotypic tumor spheroids: a platform for nanomedicine evaluation. *J Nanobiotechnology* **21**, 249.
28 Gilazieva Z, Ponomarev A, Rutland C, Rizvanov A & Solovyeva V (2020) Promising applications of tumor spheroids and organoids for personalized medicine. *Cancers (Basel)* **12**, 2727.
29 Froehlich K, Haeger JD, Heger J, Pastuschek J, Photini SM, Yan Y, Lupp A, Pfarrer C, Mrowka R, Schleußner E *et al.* (2016) Generation of multicellular breast cancer tumor spheroids: comparison of different protocols. *J Mammary Gland Biol Neoplasia* **21**, 89–98.
30 Yakavets I, Francois A, Benoit A, Merlin JL, Bezdetnaya L & Vogin G (2020) Advanced co-culture 3D breast cancer model for investigation of fibrosis induced by external stimuli: optimization study. *Sci Rep* **10**, 21273.
31 Heffelfinger SC, Gear RB, Taylor K, Miller MA, Schneider J, LaDow K & Warshawsky D (2000) DMBA-induced mammary pathologies are angiogenic in vivo and in vitro. *Lab Invest* **80**, 485–492.
32 Rømer AMA, Thorseth ML & Madsen DH (2021) Immune modulatory properties of collagen in cancer. *Front Immunol* **12**, 791453.
33 Cox TR (2021) The matrix in cancer. *Nat Rev Cancer* **21**, 217–238.
34 Fuller AM & Eisinger-Mathason TSK (2022) Context matters: response heterogeneity to collagen-targeting approaches in desmoplastic cancers. *Cancers (Basel)* **14**, 3132.
35 Nissen NI, Karsdal M & Willumsen N (2019) Collagens and cancer associated fibroblasts in the reactive stroma and its relation to cancer biology. *J Exp Clin Cancer Res* **38**, 115.
36 Abe-Fukasawa N, Watanabe R, Gen Y, Nishino T & Itasaki N (2021) A liquid culture cancer spheroid model reveals low PI3K/Akt pathway activity and low adhesiveness to the extracellular matrix. *FEBS J* **288**, 5650–5667.
37 Kyriakopoulou K, Koutsakis C, Piperigkou Z & Karamanos NK (2023) Recreating the extracellular matrix: novel 3D cell culture platforms in cancer research. *FEBS J* **290**, 5238–5247.
38 Cortini M, Macchi F, Reggiani F, Vitale E, Lipreri MV, Perut F, Ciarrocchi A, Baldini N & Avnet S (2023) Endogenous extracellular matrix regulates the response of osteosarcoma 3D spheroids to doxorubicin. *Cancers (Basel)* **15**, 1221.
39 Calori IR, Alves SR, Bi H & Tedesco AC (2022) Type-I collagen/collagenase modulates the 3D structure and behavior of glioblastoma spheroid models. *ACS Appl Bio Mater* **5**, 723–733.
40 Druzhkova I, Nikonova E, Ignatova N, Koryakina I, Zyuzin M, Mozherov A, Kozlov D, Krylov D, Kuznetsova D, Lisitsa U *et al.* (2022) Effect of collagen matrix on doxorubicin distribution and cancer Cells' response to treatment in 3D tumor model. *Cancers (Basel)* **14**, 5487.
41 Hirani P, Gauthier V, Allen CE, Wight TN & Pearce OMT (2021) Targeting Versican as a potential immunotherapeutic strategy in the treatment of cancer. *Front Oncol* **11**, 712807.
42 Kischel P, Waltregny D, Dumont B, Turtoi A, Greffe Y, Kirsch S, De Pauw E & Castronovo V (2010) Versican overexpression in human breast cancer lesions: known and new isoforms for stromal tumor targeting. *Int J Cancer* **126**, 640–650.
43 Li S, Pritchard DM & Yu LG (2022) Regulation and function of matrix Metalloproteinase-13 in cancer progression and metastasis. *Cancers (Basel)* **14**, 3263.
44 Mendonsa AM, VanSaun MN, Ustione A, Piston DW, Fingleton BM & Gorden DL (2015) Host and tumor derived MMP13 regulate extravasation and establishment of colorectal metastases in the liver. *Mol Cancer* **14**, 1–12.
45 Huang H (2018) Matrix Metalloproteinase-9 (MMP-9) as a cancer biomarker and MMP-9 biosensors: recent advances. *Sensors (Basel)* **18**, 3249.
46 Joseph C, Alsaleem M, Orah N, Narasimha PL, Miligy IM, Kurozumi S, Ellis IO, Mongan NP, Green AR & Rakha EA (2020) Elevated MMP9 expression in breast cancer is a predictor of shorter patient survival. *Breast Cancer Res Treat* **182**, 267–282.
47 Li X, Sun X, Kan C, Chen B, Qu N, Hou N, Liu Y & Han F (2022) COL1A1: a novel oncogenic gene and therapeutic target in malignancies. *Pathol Res Pract* **236**, 154013.
48 Li A, Zhou T, Guo L & Si J (2010) Collagen type I regulates β-catenin tyrosine phosphorylation and nuclear translocation to promote migration and proliferation of gastric carcinoma cells. *Oncol Rep* **23**, 1247–1255.
49 Dolor A & Szoka FC (2018) Digesting a path forward: the utility of collagenase tumor treatment for improved drug delivery. *Mol Pharm* **15**, 2069–2083.
50 Breite AG, McCarthy RC & Dwulet FE (2011) Characterization and functional assessment of clostridium histolyticum class I (C1) collagenases and the synergistic degradation of native collagen in enzyme mixtures containing class II (C2) collagenase. *Transplant Proc* **43**, 3171–3175.
51 Huang J-Y, Cheng Y-J, Lin Y-P, Lin H-C, Su C-C, Juliano R & Yang B-C (2010) Extracellular matrix of glioblastoma inhibits polarization and transmigration of T cells: the role of tenascin-C in immune suppression. *J Immunol* **185**, 1450–1459.

52 Mai Z, Lin Y, Lin P, Zhao X & Cui L (2024) Modulating extracellular matrix stiffness: a strategic approach to boost cancer immunotherapy. *Cell Death Dis* **15**, 1–16.
53 Nicolas-Boluda A, Vaquero J, Vimeux L, Guilbert T, Barrin S, Kantari-Mimoun C, Ponzo M, Renault G, Deptula P, Pogoda K *et al.* (2021) Tumor stiffening reversion through collagen crosslinking inhibition improves t cell migration and anti-pd-1 treatment. *Elife* **10**, e58688.
54 Salamone M, Saladino S, Pampalone M, Campora S & Ghersi G (2014) Tissue Dissociation and Primary Cells Isolation Using Recombinant Collagenases Class I and II. Chemical Engineering Transactions 38.
55 Wiśniewski JR, Zougman A, Nagaraj N & Mann M (2009) Universal sample preparation method for proteome analysis. *Nat Methods* **6**, 359–362.
56 Rappsilber J, Ishihama Y & Mann M (2003) Stop and go extraction tips for matrix-assisted laser desorption/ionization, nanoelectrospray, and LC/MS sample pretreatment in proteomics. *Anal Chem* **75**, 663–670.
57 Rabienezhad Ganji N, Urzì O, Tinnirello V, Costanzo E, Polito G, Palumbo Piccionello A, Manno M, Raccosta S, Gallo A, Lo Pinto M *et al.* (2024) Proof-of-concept study on the use of tangerine-derived nanovesicles as siRNA delivery vehicles toward colorectal cancer cell line SW480. *Int J Mol Sci* **25**, 546.

Supporting information

Additional supporting information may be found online in the Supporting Information section at the end of the article.

Fig. S1. Doxorubicin uptake analysis in PTCM.

Table S1. List of identified proteins common to both spheroids and 2D cells.

Table S2. List of identified ECM-related proteins in spheroids and 2D cells.

Cancer Cell International

RESEARCH

Open Access

A vascularized three-dimensional model integrating primary breast tumor cells and microvascular fragments: mimicking the tumor microenvironment involved in chemoresistance

Alessandra Lo Cicero[1*], Francesco La Monica[1], Gabriele Lo Buglio[1,2], Simona Campora[1], Federico Gangemi[1], Paolo Cinà[3], Monica Salamone[4], Margot Lo Pinto[5], Simone Dario Scilabra[5] and Giulio Ghersi[1,3*]

Abstract

Background Tumorigenesis is a complex and dynamic process in which the tumor microenvironment (TME) plays a central role. In solid tumors, the TME contributes to key mechanisms of tumor progression, including metastasis, immune evasion, and resistance to therapies. One major challenge in preclinical cancer research is the development of reliable three-dimensional (3D) in vitro models, which more accurately replicate the in vivo tumor architecture and microenvironmental conditions, such as hypoxia and extracellular matrix (ECM) organization. However, reproducing functional vascular networks and neo-angiogenesis within these models remains a key challenge.

Methods In this study, an advanced 3D tumor model, referred to as angiotumoroids, was developed by co-culturing primary murine breast tumor cells (PTCs) with species-specific adipose-derived microvascular fragments (MVFs). Angiotumoroids were characterized using scanning electron microscopy and immunostaining, and angiogenesis was evaluated through collagen gel sprouting assays. High-resolution proteomic profiling was conducted, focusing on signatures associated with angiogenesis, extracellular matrix (ECM) composition, and tissue remodeling. Additionally, the response and internalization to anticancer drug treatments were evaluated.

Results MVFs are successfully integrated in angiotumoroids, resulting in the formation of vasculature-like structures and demonstrating robust structural organization with dynamic modulation of matrix metalloproteinase 9. Formation of neovasculature was visualized through sprouting and branching, driven by both direct PTC–MVF interactions and PTC-conditioned media, highlighting the roles of juxtacrine and paracrine signaling. Proteomic profiling revealed distinct expression patterns associated with angiogenesis, ECM components (including collagen types I and IV), and active ECM remodeling with elevated MMP expression. Additionally, angiotumoroids showed increased expression

*Correspondence:
Alessandra Lo Cicero
alessandra.locicero@unipa.it
Giulio Ghersi
giulio.ghersi@unipa.it

Full list of author information is available at the end of the article

of ATP-binding cassette (ABC) transporters, particularly ABCB1 (P-glycoprotein), suggesting potential mechanisms of drug efflux. Functionally, angiotumoroids demonstrated reduced sensitivity to doxorubicin compared to PTC spheroids, maintaining structural integrity and higher cell viability post-treatment. Time-course analysis revealed preferential doxorubicin accumulation in MVF-enriched regions, as confirmed by colocalization with CD31, indicating a spatially regulated distribution of the drug mediated by the vascular compartment.

Conclusions Collectively, these findings establish angiotumoroids as a robust and physiologically relevant in vitro model for studying tumor vascularization, ECM dynamics, and therapeutic response. This platform holds significant promise for predictive cancer research and preclinical drug screening, bridging the gap between traditional in vitro systems and in vivo models.

Keywords Angiogenesis, Spheroids, Microvascular fragments, Tumor microenvironment, 3D tumor model

Background

Solid tumor microenvironment (TME) plays a key role in cancer development, providing a supportive niche for tumor initiation, growth, and expansion. It surrounds tumor cells, supplies essential nutrients and oxygen, modulates tumor cell behavior, establishes an immunosuppressive environment to evade the immune system, and acts as a barrier to effective drug delivery [1, 2]. The TME consists of cellular components, such as cancer-associated fibroblasts (CAFs), infiltrating immune cells, endothelial cells, and pericytes from blood vessels, as well as non-cellular components, including the extracellular matrix (ECM) and signaling molecules [3]. Rapid tumor cell proliferation depletes nutrients and oxygen in the early stages of tumor growth, creating a hypoxic environment that inhibits further tumor expansion [4]. In response to hypoxia, the "angiogenic switch" is triggered, reinitiating tumor growth by promoting new vessel formation [5, 6]. This process is mediated by hypoxia-inducible factors (HIFs), which are produced under low oxygen conditions and drive tumor progression and angiogenesis by activating pro-angiogenic genes, such as vascular endothelial growth factor (VEGF), platelet-derived growth factor (PDGF), and matrix metalloproteinases (MMP-2 and MMP-9). The interplay of these molecules leads to sprouting angiogenesis, by specialized endothelial cells known as tip cells, which guide the formation of new vessels from pre-existing blood vessels [5] through MMP-mediated degradation and ECM protein synthesis, establishing stiffness and adhesion gradients [5, 7].

Vascularized regions within solid tumors significantly impact drug uptake and, consequently, the efficacy of chemotherapeutic treatments [8]. The effective delivery of anticancer agents throughout solid tumors is primarily determined by the structural and functional properties of the tumor vasculature, as well as the physicochemical characteristics of the extracellular matrix (ECM), which govern drug transport within the target tissue. Additionally, drug transport through the extravascular compartment occurs via diffusion or convection, with penetration depth often limited by rapid intracellular uptake of the drug by tumor cells near microvascular structures [9].

To gain deeper insights into TME's role and its interactions with cancer cells, significant efforts are being directed toward developing advanced three-dimensional (3D) models that emulate the TME complexity [2]. In recent decades, 3D cell cultures, such as spheroids and organoids, have been developed to enable cells to grow and interact within an environment that closely mimics the solid tumors' morphology and behavior [10]. Spheroids and organoids act as a bridge between monolayer cell cultures and in vivo models, offering a more accurate representation of the complex cellular interactions and gradients present in solid tumors [11]. Moreover, some tumor spheroids from primary cells have demonstrated the ability to produce a capsule-like endogenous ECM, which effectively replicates the solid tumor microenvironment [12]. Furthermore, as the diameter of the spheroid increases, the outer layers receive nutrients and oxygen, while the inner core suffers from hypoxia, modulating gene expression, such as the activation of HIFs [13]. Among the various types of spheroids, multicellular tumor spheroids (MCTS), composed of different cytotypes, most effectively mimic in vivo tumor gene expression, signaling, and cellular heterogeneity [14]. MCTSs have been developed using numerous tumor cells, including those from breast [11], lung [15], ovarian [16, 17], liver [18], bladder [19], or prostate cancers [20]. To replicate the TME, and particularly the tumoral angiogenesis, Human Umbilical Vein Endothelial Cells (HUVECs) were incorporated into MCTS, alongside various tumor cell lines, resulting in capillary-like structures [21–23].

While HUVECs form vessel-like structures that closely resemble the in vivo biological arrangement, it is challenging to fully replicate the entire microvascular network, which consists of capillaries, venules, arteries, and accessory cells. A promising solution to this limitation is the involvement of Microvascular Fragments (MVFs), which comprise intact vessel fragments, including capillaries, arteries, and veins. They retain the essential endothelial framework and are associated with accessory

cells, such as pericytes, mesenchymal stem cells, progenitor cells, and macrophages [24, 25]. Microvascular fragments can be isolated from adipose tissue [26], a readily available and abundant source that allows for a straightforward isolation procedure. When cultured, MVFs secrete growth factors like VEGF and FGF, promoting rapid microvessel growth and the formation of functional microvascular networks capable of connecting with host tissue upon implantation [25, 27, 28]. For the first time, Nalbach and colleagues created MVF-derived spheroids that demonstrated angiogenic activity and in vivo vascularization capacity, suggesting their potential as vascularization units for future tissue engineering applications [29]. Subsequently, MVFs have been used to create adipose spheroids that demonstrated the ability to sprout and form a new vascular network [30], as well as to reconstruct subcutaneous adipose tissue when transplanted into in vivo localized scleroderma patients, where they fostered an anti-fibrotic and pro-adipogenic microenvironment that aided the regeneration of scleroderma lesions [31]. Moreover, MVFs have been combined with osteoblasts to generate spheroids, which, in this context, exhibited sprouting and inosculation capabilities when implanted into an in vivo murine model [32].

In this study, a novel 3D spheroid model named "angiotumoroids" was generated, combining primary murine breast tumor cells with species-specific MVFs extracted from adipose tissue. They exhibit endothelial integration, enhanced MMP9, vessel sprouting, and altered doxorubicin uptake with reduced cytotoxicity. These features make angiotumoroids a physiologically relevant "in vitro" platform for studying tumor–vascular interactions, angiogenesis, drug response, and therapeutic resistance in cancer research.

Methods

Rat model

All animal experiments were approved by the University of Palermo. Authorization n° 523/2022-PR, issued according to art. 31 del D.lgs. 26/2014 Istituto Superiore di Sanità, Italy. Female Wistar rats were obtained from ENVIGO RMS SRL.

Microvascular fragments (MVFs) isolation

MVFs were isolated from female Wistar rat visceral adipose tissue [33]. The animal was sedated with 2% Isoflurane, sacrificed and the adipose tissue from abdominal region was explanted and put in Dulbecco's Modified Eagle's Medium high glucose (HG-DMEM, Sigma-Aldrich, Milano, Italy) added of penicillin 15.000 U/ml, streptomycin 300 µg/ml, and amphotericin B 0.75 µg/ml (Sigma-Aldrich, USA). The adipose tissue was washed 3 times in Phosphate Buffered Saline (PBS) w/o Ca^{2+} and Mg^{2+}, then dissected into small parts with a scalpel. Furthermore, the tissue was incubated with the digestion buffer, containing ultrapure recombinant collagenases class II (Col H 300 U/gr) (Abiel srl) and Thermolysin (Promega) 10 µg/ml. The digestion was performed at 30 °C for 30 min under agitation. After 30 min, the tissue was mixed and digested for further 20 min at 30 °C. The digestion was then stopped with HG-DMEM containing 10% (v/v) fetal bovine serum (FBS, Euroclone, Celbar, Pero (MI) Italy). The sample was washed three times with HG-DMEM and centrifuged at 700 g for 10 min to isolate MVFs from the adipose tissue. The MVFs pellet was resuspended in HG-DMEM added of penicillin 15.000 U/ml, streptomycin 300 µg/ml, and amphotericin B 0.75 µg/ml, 2 mM L-Glutamine (Euroclone, Celbar, Pero (MI) Italy) and 10% (v/v) FBS, and filtered through a mesh (300 µm). The resulting MVFs were counted in a Burker's chamber.

Primary tumor cells (PTCs) and MVFs 3D co-culture

PTCs isolated from a breast tumor mass [12] were cultured in HG-DMEM plus 1% penicillin/streptomycin, 1% L-Glutamine and 10% FBS (complete HG-DMEM). Cells were maintained at 37 °C in a humidified atmosphere with 5% CO_2. To form angiotumoroids, PTCs from passages 15 to 19 and isolated MVFs were co-cultured in a 96-well low attachment plate in complete HG-DMEM, at 37 °C and 5% CO_2, and were allowed to grow for 5 days. Three co-culture formulations were obtained using the same PTCs density (3×10^3 cells) co-cultured with 60, 125, or 250 MVFs. Moreover, spheroids constituted only of MVFs (500 MVFs per spheroid) or only of PTCs (3×10^3 PTCs per spheroid) were formed and used as controls. The size and shape of angiotumoroids were investigated by optical microscopy and analyzed through ImageJ software.

Spheroids fixation and Preparation for scanning electron microscopy (SEM) imaging

Spheroids were washed with complete PBS (3 times for 3 min) and fixed with 4% Glutheraldeyde in PBS for one hour at 4 °C. Samples were then washed in complete PBS (2 times for 3 min) and dehydrated with an increasing ethanol solution at room temperature (30%, 70%, 90%, and 100% in PBS, each wash for 5 min). After dehydration, 3D cultures were resuspended in hexamethyldisilazane (HMDS, Sigma-Aldrich, 379212) for 10 min for critical point drying. The stubs were covered with carbon tape onto which the samples were dried at room temperature. Then, the stubs were put into the sputter coater device (Quorum SC7620) to coat the samples with platinum for 15 s. The images were acquired in a high vacuum in Secondary Emission (SE) mode using SEM EVO 10 and analyzed using SmartSEM Touch software.

Immunofluorescence staining and imaging of spheroids and spheroids in collagen gels

Spheroids were fixed in 3,7% formaldehyde for one hour at room temperature before permeabilization in PBS supplemented with 0.1% triton X-100 (ON at 4 °C). They were then blocked for one hour at room temperature using PBS with 1% BSA (Sigma-Aldrich, A7906). The primary antibody used were Rabbit anti-CD31 (1:50, ab222783, Abcam), Rabbit anti-Collagen Type I (1:20, 234167, Millipore), Rabbit anti-Collagen Type IV (1:100, ab6586, abcam) and Mouse anti-ABCB1 (1:100, MA5-13854, Invitrogen), which were incubated overnight at 4 °C in a blocking buffer. Spheroids were stained with the species-specific fluorophore-conjugated secondary antibody (Invitrogen) for four hours at room temperature. The Actin cytoskeleton was labeled with phalloidin-FITC (1:500 in PBS, Sigma-Aldrich, P5282) for 30 min at room temperature, while nuclei were labeled with DAPI (1:20.000 in PBS, Sigma-Aldrich, D9542). Coverslips were mounted in a mounting medium, and 3D cultures were analyzed by confocal microscope (Olympus FV10i). Z-stack imaging was carried out using a Fluoview FV10i confocal laser scanning microscope system (Olympus) at a magnification of 20x with a step size of 10 µm. All stacks were obtained at the same intensity setting between groups. ImageJ software was used to analyze stacks of images.

Western blot analysis

Cells from 3D cultures were lysed in RIPA buffer (20 mM Tris, 150 mM NaCl, 0.1% Triton X-100, 1 mM EDTA, pH 7.2) with a protease inhibitor cocktail. Lysates were incubated in a sample buffer under reducing conditions and fractionated with Sodium dodecyl sulphate–polyacrylamide gel electrophoresis (SDS–PAGE) 10% and transferred to nitrocellulose membranes (Amersham). The membranes were blocked in PBS/Tween 0.1% (PBS/T) with 5% non-fat dried milk, incubated with the primary antibody Rabbit anti-CD31 (1:1000, ab222783, abcam) or Rabbit anti-ABCB1(1:500, A808889, antibodies) diluted in PBS/T, washed four times in blocking solution and incubated with HRP-conjugated secondary antibodies (Sigma) followed by washing in PBS/T. The membrane was exposed to Super Signal West Femto Maximum Sensitivity substrate (Thermo Scientific), and protein expression was detected by ChemiDoc XRS (Biorad, Hercules, CA, USA).

Gelatin zymography assay

15 µg of total proteins from 3D Cell lysates (as previously described) were analyzed by gelatin zymography in 10% acrylamide gels, containing 0.09% gelatin (SIGMA Aldrich, USA). Gel was washed for 10 min in 2.5% Triton X-100 at room temperature and incubated overnight at 37℃ in activation buffer (50 mM Tris-HCl, 2 mM $CaCl_2$, NaN3 0.02%, Triton X100 1,5%). Gel was stained for 1 h with Coomassie Brilliant Blue R-250 (0.2% Coomassie Brilliant Blue R-250, 40% methanol, 10% acetic acid in H_2O) and destained in H_2O. White bands were quantified using ImageJ software.

Collagen gel for embedding of MVFs and angiotumorids and sprouting analysis

The isolated MVFs, angiotumoroids and control spheroids were embedded in a collagen gel composed of 35,3% Buffer solution (PBS 2X, 100 mM HEPES, pH 7.4), 35,3% type I collagen from rat tail (3 mg/ml), and 29,4% of complete HG-DMEM [34]. The isolated MVFs (iMVFs) were grown in collagen gel for 1 week, while angiotumoids and control spheroids (MVF and PCT) were embedded for 2 days. The number of sprouts was quantified by analyzing optical microscopy images with ImageJ software.

Treatments with conditioned media from PTCs and sprouting analysis after treatment

The MVF spheroids were embedded in collagen gel and treated with a PTC-conditioned medium recovered from 30.000 PTC cells grown in 2D monolayer condition. As a control, MVF spheroids were embedded in collagen gel and grown in complete HG-DMEM. On day 1 and day 2, the number of sprouts was quantified by analyzing optical microscopy images with ImageJ software.

Proteomic-based characterization: protein extraction and sample Preparation

Angiotumoroids, PTC and MVFs spheroids were lysed in STET (10 mM Tris-HCl, 1 mM EDTA, 100 mM NaCl, and 5% Triton X-100 (v/v)) with protease inhibitor cocktail (Roche) and centrifuged (14.000 rpm, 5 min) to eliminate cells membranes. Proteins extracted were quantified with colorimetric 660 nm microBCA assay. A protein amount of 30 µg per sample was subjected to filter-aided sample preparation (FASP - with 10 kDa Vivacon 500 spin filter columns from Sartorius), as previously described [35]. Samples were then reduced and denatured with dithiothreitol (DTT) (Sigma-Aldrich) in 200 µl of UA buffer (8 M Urea in 0.1 M Tris/HCl, pH 8.5) and alkylated with 50 mM iodoacetamide (IAA) (Sigma-Aldrich). After reduction and alkylation, samples were washed three times with UB buffer (8 M Urea in 0.1 Tris/HCl, pH 8.0) and sequentially digested with LysC (1:50 enzyme to protein ratio from Promega) and trypsin (1:100 enzyme to protein ratio, Promega). Then, peptides were eluted from filter columns by centrifugation (14,000 x g; 60 min) and acidified with 20 µl of 8% formic acid (FA). Generated peptides were desalted by stop-and-go extraction (STAGE) on reverse phase C18 and eluted in 40 µl of 60% acetonitrile in 0.1% formic acid [36]. The volume was

reduced in a SpeedVac (Thermo Fisher Scientific) and the peptides were resuspended in 20 µl of 0.1% formic acid. The peptide concentration was measured with Nanodrop 2000 (Thermo Scientific).

uHPLC-MS/MS and data analysis

As previously described [37] for each sample 1 µg peptides were separated through a nanoLC system (Vanquish Neo UHPLC, Thermo Scientific) equipped with an Acclaim PEPMap C18 column (25 cm × 75 µm ID, Thermo Scientific) in a 110 min binary gradient of water and acetonitrile containing 0.1% FA. Separated peptides were injected into an Exploris 480 mass spectrometer (Thermo Fischer Scientific) for tandem mass spectrometry analysis. Proteins were identified and quantified with label-free quantification (LFQ), by using data-independent acquisition (DIA). DIA was performed using an MS1 full scan (380 m/z to 980 m/z) followed by 49 sequential DIA windows with an overlap of 1 m/z and window placement optimization option enabled. Full scans were acquired with 120,000 resolution, AGC of 3×106, and a maximum injection time of 50 ms. Afterward, 49 isolation windows were scanned with a resolution of 30,000, an AGC of 8×105 and maximum injection time was set as auto to achieve the optimal cycle time. Collision-induced dissociation fragmentation was induced with 28% of the normalized HCD. The data were analyzed by the software DIA-NN (version 2.0.2) by using a predicted library generated from in silico digested Rattus norvegicus (rat) Uniprot reference database (proteome ID UP000002494) involving cuts at K* and R*, two missed cleavage allowed, minimal peptide length set a 6. The false discovery rate for peptide and protein identification was set at 0.01%. Label-free quantification (LFQ) was used for protein quantification. The LFQ values were log2 transformed and a two-sided Student's t-test was used to evaluate proteins statistically significantly regulated between two-dimensional and three-dimensional culture ($n = 4$). The mass spectrometry proteomics data have been deposited to the ProteomeXchange Consortium via the PRIDE partner repository with the dataset identifier PXD067876.

Doxorubicin uptake study by confocal microscopy

To assess the uptake of Doxorubicin, angiotumoroids with 125 MVFs and PTC spheroids were incubated with 10µM Doxorubicin for 30 min, 1 h, 2 h, or 4 h. Spheroids were then processed for immunocytochemistry, as previously described, and analyzed with Fluoview FV10i confocal laser scanning microscope system (Olympus). ImageJ software was used to analyze stacks of images.

Cell viability assay

Angiotumoroids with 125 MVFs and PTC spheroids were incubated with 10 µM Doxorubicin for 24 h at 37 °C in a humidified atmosphere with 5% CO_2. After treatment, spheroids were washed three times with PBS, resuspended in 100 µl of DMEM and an equal volume of CellTiter-Glo® 3D Reagent (Promega) following the Manufacturer's protocol. Briefly, 100 µL medium was replaced with 100 µL CellTiter-Glo 3D reagent on the indicated day after growth/treatment. The plates were shaken for 5 min at 240 rpm, and incubated for 25 min at room temperature, and the luminescent signal was recorded using a luminometer (SinergyHT, BioTek, Winooski, VT, USA).

Statistical analysis

The results are presented as the mean ± standard deviation (SD). Statistical comparisons were made using one-way ANOVA and 2-way ANOVA. Statistical tests were performed with GraphPad Prism. A p-value < 0.05 was considered statistically significant.

Results

Adipose-derived microvascular fragment isolation and 3D co-culture with primary tumor cells

Microvascular Fragments (MVFs) were isolated from visceral adipose tissue of female Wistar rats (Fig. 1A). The tissue was digested using a blend of ultrapure recombinant collagenase (COLH - Class II) and thermolysin as reported in the materials and methods section, yielding approximately 20.000 MVFs per gram of adipose tissue. MVFs ranged in length from 50 µm to 300 µm, with an average lumen diameter of 18 µm. They displayed small lateral branches and retained traces of blood within their lumen (Fig. 1B). Scanning Electron Microscopy (SEM) analysis (Fig. 1C) revealed the tubular structure of isolated MVFs and the presence of erythrocytes in vessels, while adipocytes were absent, indicating the efficiency of the isolation protocol in removing adipose tissue. Isolated MVFs were embedded in a type I collagen gel and maintained for seven days to assess their viability. After 3 days, isolated MVFs showed vessel sprouting and branching, which progressively increased in number and network complexity over time (Fig. 1D). Furthermore, after seven days, some lateral branches derived from different fragments were fused, mimicking in vitro the angiogenic process that typically occurs in vivo.

To develop a reliable and reproducible in vitro tumor model with a well-organized and natural TME, primary tumor cells (PTC) from a rat breast tumor mass were combined with MVFs. The PTCs and the MVFs were seeded in low-attachment conditions to develop three-dimensional (3D) in vitro structures named "angiotumoroids". Angiotumoroids were generated by varying the number of MVFs in culture (60, 125, or 250 MVFs), while

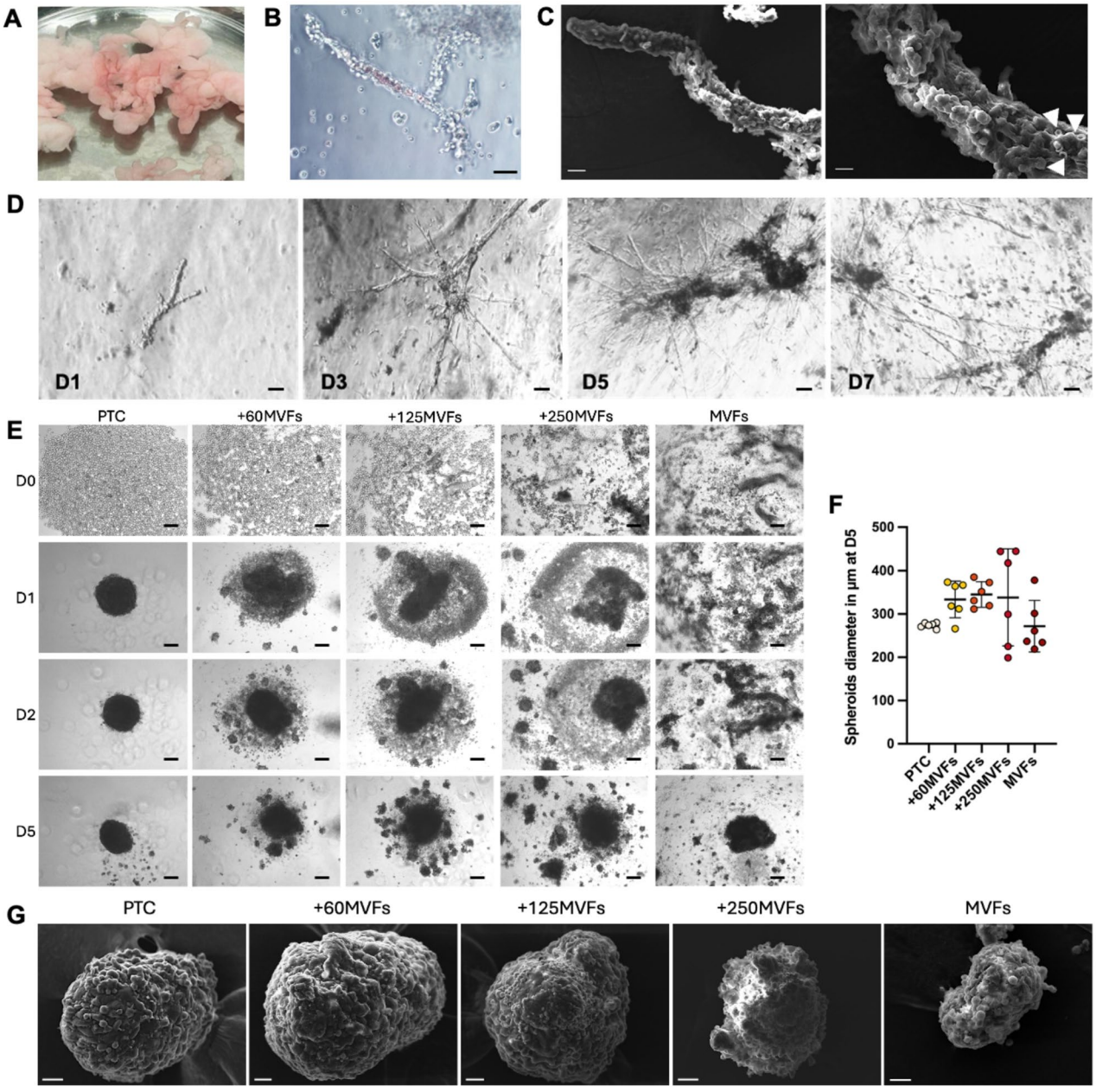

Fig. 1 Adipose-derived microvascular fragment isolation and 3D co-culture with primary tumor cells. (**A**) Rat visceral adipose tissue. (**B**) MVFs analysis through optical microscopy and (**C**) Scanning Electron microscopy (SEM), Scale bar: 20 µm and 10 µm, respectively. White arrows indicate the erythrocytes. (**D**) Isolated MVFs included in type I collagen gel at days 1 (D1), 3 (D3), 5 (D5), and 7 (D7). Scale bar: 10 µm. (**E**) Optical microscope analysis of primary tumor cell spheroids (PTC), angiotumoroids with 60 (+60MVFs), 125 (+125MVFs), or (+250MVFs) 250 MVFs and MVF spheroids at days 0 (D0), day 1 (D1), day 2 (D2), and day 5 (D5). Scale bar: 100 µm. (**F**) Spheroid diameter analysis on day 5. Six spheroids were analyzed for each condition. Data are mean ± SD. (**G**) SEM analysis of spheroid on day 5. Scale bar: 30 µm

maintaining the number of PTC constant (3×10^3 cells/well) per condition. Additionally, spheroids consisting of only MVFs, or PTCs were formed as controls.

Optical microscopy analyses were performed to investigate spheroid structure and size evolution from 0 to 5 days post-seeding (Fig. 1E). PTC spheroids were formed one day after seeding, exhibiting a compact and well-defined structure that was maintained over time. All angiotumoroid formulations (+60, +125, and +250 MVFs) were also formed by day 1 and showed increased compaction in a time-dependent manner, while MVF spheroids spent five days organizing themselves, suggesting a significant role for PTCs in driving the process of formation of spheroidal structures.

As expected, angiotumoroids presented a larger diameter compared to the controls. However, at 5 days

post-seeding, those with 250 MVFs were less homogeneous in size compared to the other conditions, with diameters ranging from 200 µm to 445 µm (Fig. 1F). This variability is probably due to an excess of MVFs compared to PTCs, leading to the formation of "satellite" structures that partially sequester the PTCs. Therefore, to better investigate component integration and morphology, both angiotumoroids and controls were analyzed by SEM at day 5 (Fig. 1G). PTC spheroids, along with those containing 60 and 125 MVFs, and with MVF-only spheroids, exhibited a similar morphology, with a compact ovoid structure and rounded cells on the surface. In contrast, spheroids with 250 MVFs had a distinct morphology, characterized by cells on the surface not perfectly integrated, suggesting a lack of structural compactness.

Integration of microvascular fragments into Angiotumoroids correlates with increased MMP9 expression

To evaluate the presence and distribution of MVFs within the 3D structures, both angiotumoroids and controls were analyzed for the expression of the endothelial vascular marker CD31 (Fig. 2A). At day 5, CD31 was uniformly distributed in both MVF and angiotumoroid, while no signal in the PTC spheroids was detected.

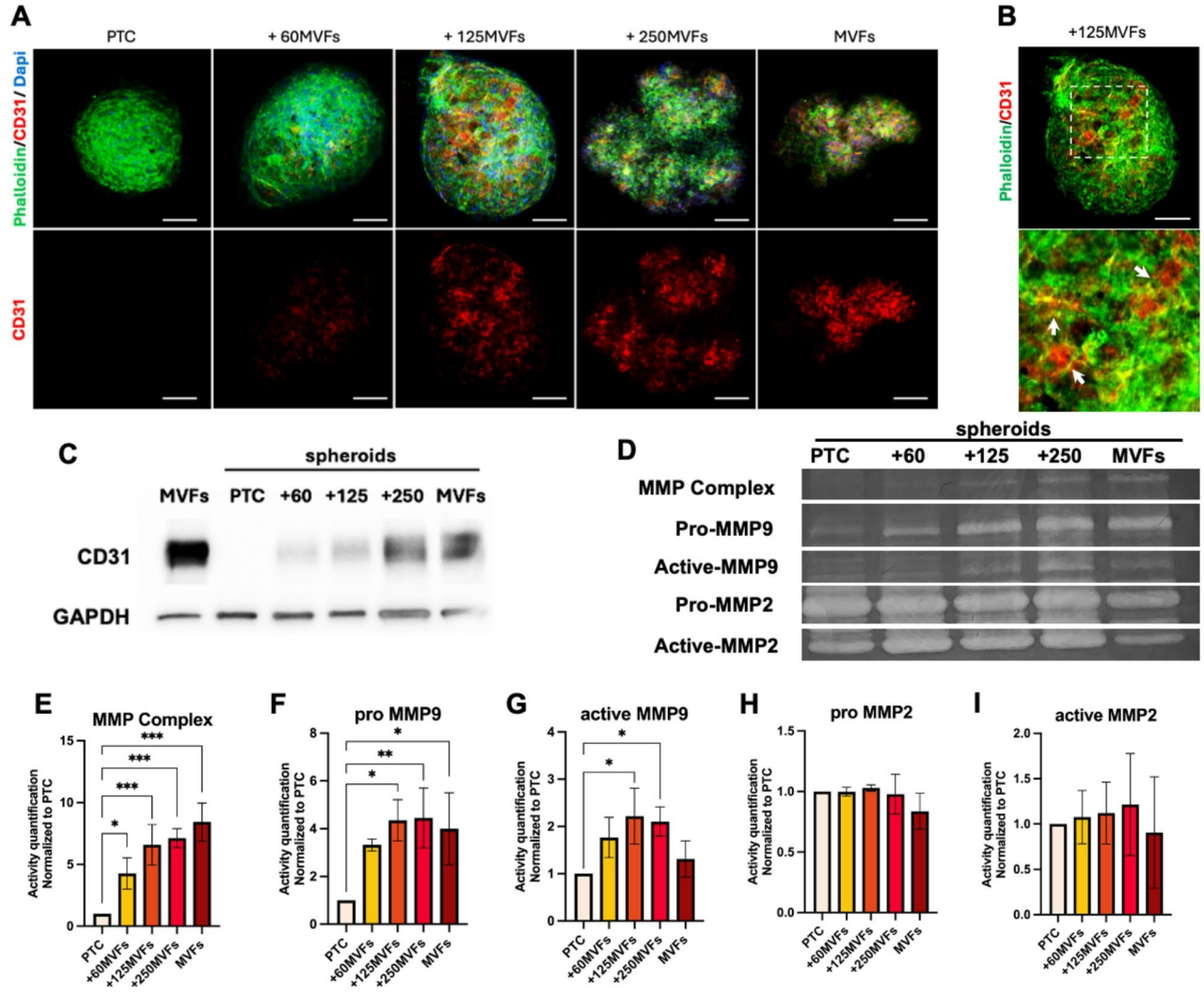

Fig. 2 Integration of microvascular fragments into angiotumoroids correlates with increased MMP9 expression. (**A**) Confocal microscope of primary tumor cell spheroids (PTC), angiotumoroids with 60 (+60MVFs), 125 (+125MVFs), or 250 (+250MVFs) MVFs, and spheroids of MVFs, stained with phalloidin-FITC (green), anti-CD31 antibody (red), and DAPI (blue) at day 5. Scale bar: 100 µm. (**B**) Central section at the confocal microscope of angiotumoroids with 125 MVFs, stained with phalloidin-FITC (green), and anti-CD31 antibody (red). Arrows point to vasculature, CD31 positive. (**C**) Western blot analysis for CD31 and (**D**) Zymography assay of protein extract from PTC spheroids, angiotumoroids with 60 (+60MVFs), 125 (+125MVFs), or 250 (+250MVFs) MVFs, and MVFs spheroids. (**E-I**) Quantification of the gelatinolytic activity of the samples. The matrix metalloproteases (MMPs) analyzed were: MMP complex (**E**); pro-MMP9 (**F**); active MMP9 (**G**); pro-MMP2 (**H**); active MMP2 (**I**). Data are mean ± SD. Statistical analysis (one-way ANOVA) was performed ($n = 3$) (*$p < 0.05$; **$p < 0.01$)

Notably, angiotumoroids exhibited a gradual increase in CD31 expression throughout the structure, directly correlated to the number of MVFs seeded per spheroid.

Furthermore, MVFs successfully integrated into the angiotumoroids, forming vasculature-like structures (Fig. 2B). These data were also confirmed by western

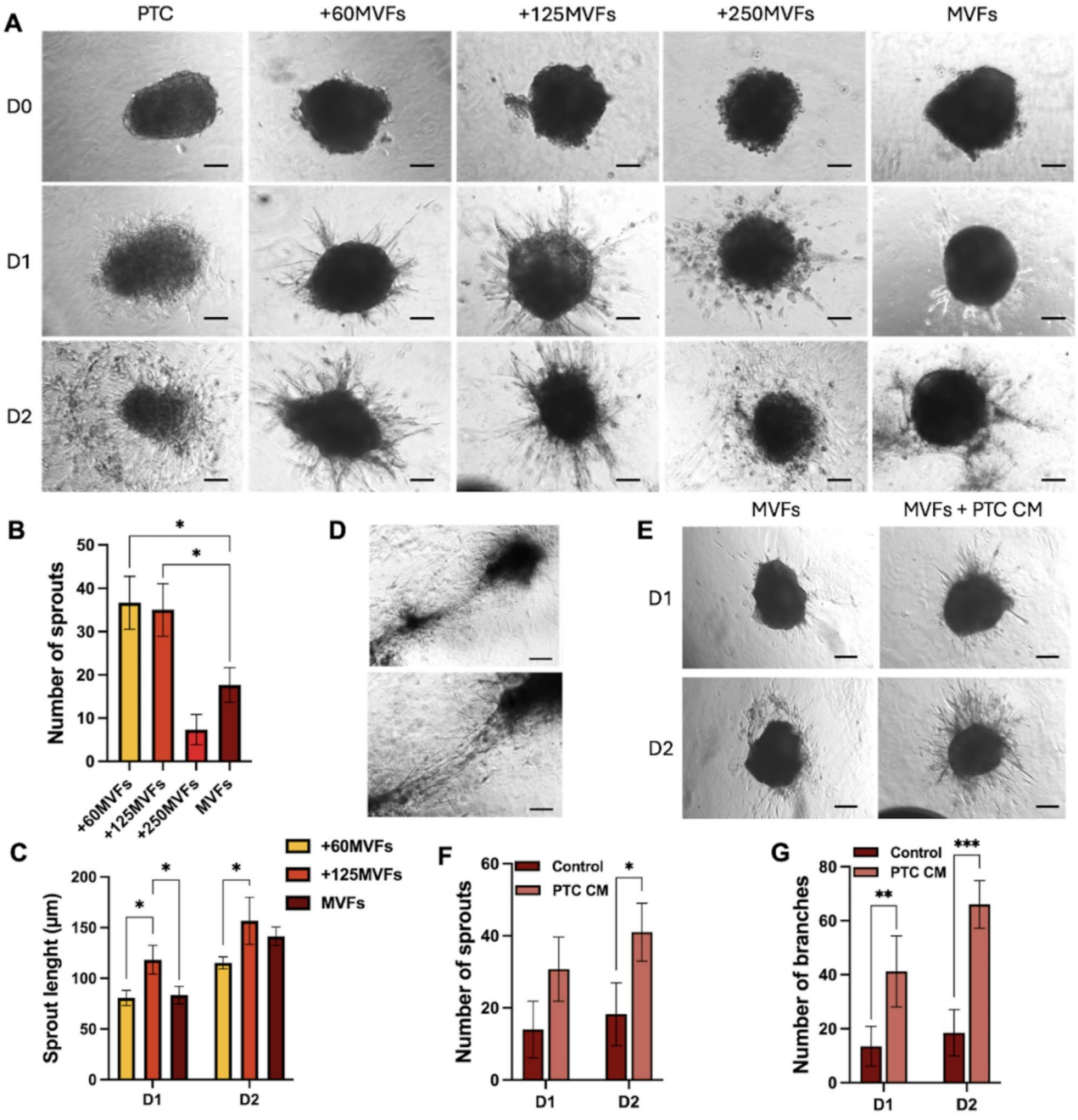

Fig. 3 Angiotumoroids sprouting in collagen gel and the influence of PTCs in neoangiogenesis. (**A**) Primary tumor cell spheroids (PTC), angiotumoroids with 60 (+60MVFs), 125 (+125MVFs) or 250 (+250MVFs) MVFs and spheroids of MVFs in collagen gel at day 0 (D0), day 1(D1) and day 2 (D2). Scale bar: 100 µm. (**B**) Quantification of the number of sprouts at D2 and (**C**) length of sprouts at D1 and D2. Data are mean ± SD. Statistical analysis (2-way ANOVA) was performed ($n = 3$) (*$p < 0.05$). (**D**) Angiotumoroids with 125 MVFs (+125 MVFs) interconnected in collagen gel. Scale bar: 50 µm and 25 µm for the magnification, respectively. (**E**) MVF spheroids incubated in collagen gel with control DMEM (MVFs) or with PTC conditioned medium (MVFs + PTC CM) at day 1 (D1) and day 2 (D2). Scale bar: 100 µm. (**F**) Quantification of the number of sprouts (**G**) and branches at D1 and D2 in MVFs spheroids incubated in collagen gel with control DMEM (Control) or with primary tumor cells conditioned medium (PTC CM). Data are mean ± SD. Statistical analysis (2-way ANOVA) was performed ($n = 3$) (*$p < 0.05$; **$p < 0.01$; ***$p < 0.001$)

blot assay, in which it is evident that the CD31 signal increased in a MVF density-dependent manner (Fig. 3C).

Since matrix metalloproteinases (MMPs), particularly MMP9, are directly involved in tumor angiogenesis, zymography assays were carried out on the total proteins isolated from angiotumoroids and control spheroids (Fig. 2D). MMP expression patterns were compared to those of PTC spheroids (Fig. 2D). The MMP complex activity was proportionally augmented in angiotumoroids as the number of MVFs increased, while it was significantly less in PTC spheroids (Fig. 2E). The catalytic activity, induced by the zymography process, of pro-MMP9 was significantly enhanced in angiotumoroids with 125 and 250 MVFs and MVF spheroids compared to the PTC spheroids, which exhibited three times lower activity (Fig. 2F). Interestingly, the enzymatic activity of active-MMP9 was notably higher in angiotumoroids with 125 and 250 MVFs compared to PTC spheroids, an increase not observed in the MVFs spheroids (Fig. 2G), suggesting a potential effect due to a crosstalk between PTC/MVFs co-culture. Additionally, MMP2 activity analysis revealed no significant differences in the pro- and active forms between angiotumoroids and MVFs or PTC spheroids (Fig. 2H-I). Taken together, these data suggest that different amounts of MVFs combined with primary tumor cells may modulate the MMPs' activity differently, especially MMP9.

Angiotumoroids sprouting in collagen gel and the influence of PTCs in neoangiogenesis

To investigate the neo-angiogenic process in angiotumoroids, they were embedded in 3D collagen gel. Vessel sprouting was evaluated through optical microscopy up to 2 days post-embedding (Fig. 3A). As expected, the PTC spheroids exhibited a loss of compactness and integrity over time, given by cell migration into the gel, with no vessel formation observed. Angiotumoroids with 60 and 125 MVFs and MVF spheroids showed visible sproutings on the first day after embedding, which increased the following day (day 2). Interestingly, angiotumoroids with 60 and 125 MVFs presented a higher number of newly formed vessels and branching than MVF spheroids (Fig. 3B), suggesting an effect on the crosstalk between tumor cells and MVFs. Moreover, angiotumoroids with 125 MVFs generated longer sprouts than those with 60 MVFs, reaching lengths at day 2 comparable to those observed in MVFs spheroids (Fig. 3C). In contrast, angiotumoroids with 250 MVFs exhibited rounded cells surrounding the spheroids on the same embedding day, suggesting reduced compactness relative to other conditions. Therefore, by the first day, only a few new vessels had sprouted, with single cells migrating outward, and no increase in sprout number was observed on day two compared to day one.

Although both 125 MVFs and 250 MVFs presented high active MMP9 levels, these data showed that only 125 MVFs can sprout and branch after embedding in collagen gel. By contrast, 60 MVFs spread in a 3D gel despite showing a slightly lower expression of active MMP-9. Furthermore, when two 125 MVF angiotumoroids were cultured within the same collagen gel, interconnection between them was observed after 2 days, with new vessel formation extending to connect with sprouts from neighboring spheroids (Fig. 3D).

To determine whether the pro-angiogenic effects of PTCs on vessel sprouting were due to direct contact interactions or the release of soluble factors, MVF spheroids were embedded in collagen gels and treated with a PTC-conditioned medium (Fig. 3E). Optical microscopy images were acquired up to two days post-treatment. After 24 h, sprouts in spheroids treated with the conditioned medium increased by 2.2-fold compared to MVF control spheroids. Notably, after 48 h, this difference became statistically significant (Fig. 3F). Additionally, the analysis of vessel branching revealed increased ramification of the sprouts in MVF spheroids treated with conditioned media (Fig. 3G). These data confirm the direct involvement of PTCs in modulating the angiogenic process in angiotumoroids, highlighting the role of soluble factors released by PTCs in promoting neoangiogenesis.

Proteomic profiling reveals vascular-specific tumor microenvironment remodeling and ABCB1 upregulation in Angiotumoroids

Angiotumoroids with 125 MVFs emerged as the most robust and reliable vascularized tumor models, based on their structural integrity, capacity to modulate MMP9 activity, and ability to promote new vessel sprouting and branching. To further characterize these models, high-resolution proteomic analysis was performed on angiotumoroids, PTC spheroids, and MVF spheroids, with a particular focus on proteins involved in angiogenesis, ECM composition, and remodeling. The analysis identified 5629 total proteins (of which 27 proteins are involved in angiogenesis, 60 in ECM composition and remodeling – according to Perseus software). (Supplementary Table 1). Principal Component analysis (PCA) demonstrated that the proteomic profiling of angiotumoroids was clearly separated from that of MVF spheroids and of PTC spheroids (Fig. 4A). We used label-free quantification to evaluate the relative abundance of proteins in angiotumoroids compared to PTC and MVF spheroids. Label-free quantification was used to evaluate the relative abundance of proteins in angiotumoroids compared to PTC and MVF spheroids. 5093 proteins were found in angiotumoroids and PTC spheroids, of which 1587 significantly altered between the two samples (Fig. 4B). 773 proteins were significantly more abundant

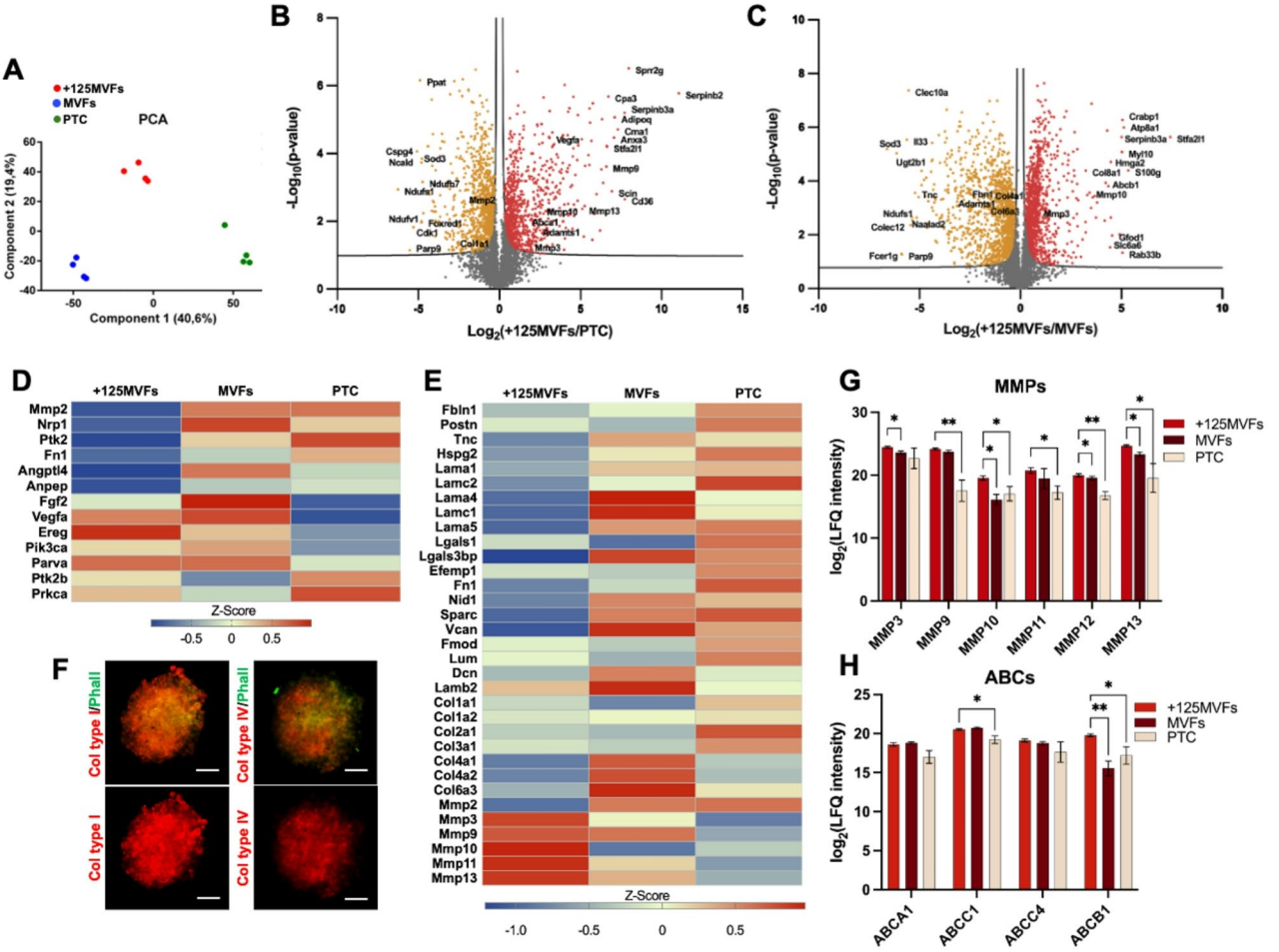

Fig. 4 (**A**) Principal Component analysis (PCA) of 125 MVFs (+125MVFs), MVFs spheroids, and primary tumor cell spheroids (PTC). (**B**) Volcano plot for the proteins identified in four biological samples of angiotumoroids with 125 MVFs (+125MVFs) and MVFs spheroids. (**C**) Volcano plot for the proteins identified in four biological samples of +125MVFs and PTC spheroids. (**D**) Heatmap generated based on protein z-scores in +125MVFs, MVFs spheroids and primary tumor cell spheroids (PTC) involved in angiogenesis (**E**) and ECM composition and remodelling. (**F**) Confocal microscope of primary tumor cell spheroids (PTC), and angiotumoroids with 125 MVFs (+125MVFs) stained with phalloidin-FITC (green), antibody anti-Collagen Type I (red) or Collagen Type IV (red) at day 5 post seeding. Scale bar: 100 µm. (**G**) LFQ (label-free quantification) intensity of the most significant MMPs (Matrix Metalloproteinases) (**H**) and ABC transporters differentially expressed in angiotumoroids with 125 MVFs (+125MVFs), spheroids of MVFs and primary tumor cell spheroids (PTC) ($n=4$)

in angiotumoroids than in PTC spheroids, including MMP9, in line with previous results, and other proteases involved in ECM turnover, such as MMP13, MMP10, and A disintegrin and metalloproteinase with thrombospondin motifs 1 (ADAMTS1). Furthermore, among increased proteins, there were proteins involved in metabolic processes such as the platelet glycoprotein 4 (CD36), Adiponectin d (Adipoq) and the vascular endothelial growth factors A (VegfA). 814 proteins were less abundant in the angiotumoroids compared to the PTC spheroids. Among these, a group of proteins located in the inner membrane of the mitochondrion and involved in cellular respiration were the most altered (including NDUFS1, NDUFV1, NDUFV2, NDUFB7, FOXRED1, etc.), as also proteins of the ECM such as Chondroitin Sulfate Proteoglycan 4 (CSPG4) and Collagen type I (Col1a1).

When angiotumoroids were compared with MVF spheroids, the relative abundance of 2342 proteins was significantly altered (Fig. 4C). 1070 proteins increased in angiotumoroids, including stefin A2-like 1 (Stfa2l1), Protein S100-G (S100g) and some protein transporters, including the phospholipid-transporting ATPase (Atp8a1), sodium- and chloride-dependent taurine transporter (Slc6a6), and two subunits of the Sodium: Potassium-Exchanging ATPase Complex (Fxyd2 and Atp1b1). Notably, several ECM remodeling proteins were more abundant, such as MMP3, MMP10. In contrast, 1272 proteins were decreased in angiotumoroids compared to MVFs spheroids, including several ECM-related proteins such as the extracellular superoxide dismutase [Cu-Zn] (SOD3), collectin-12 (COLEC12), tenascin-C (Tnc), and fibrillin-1 (Fbn1).

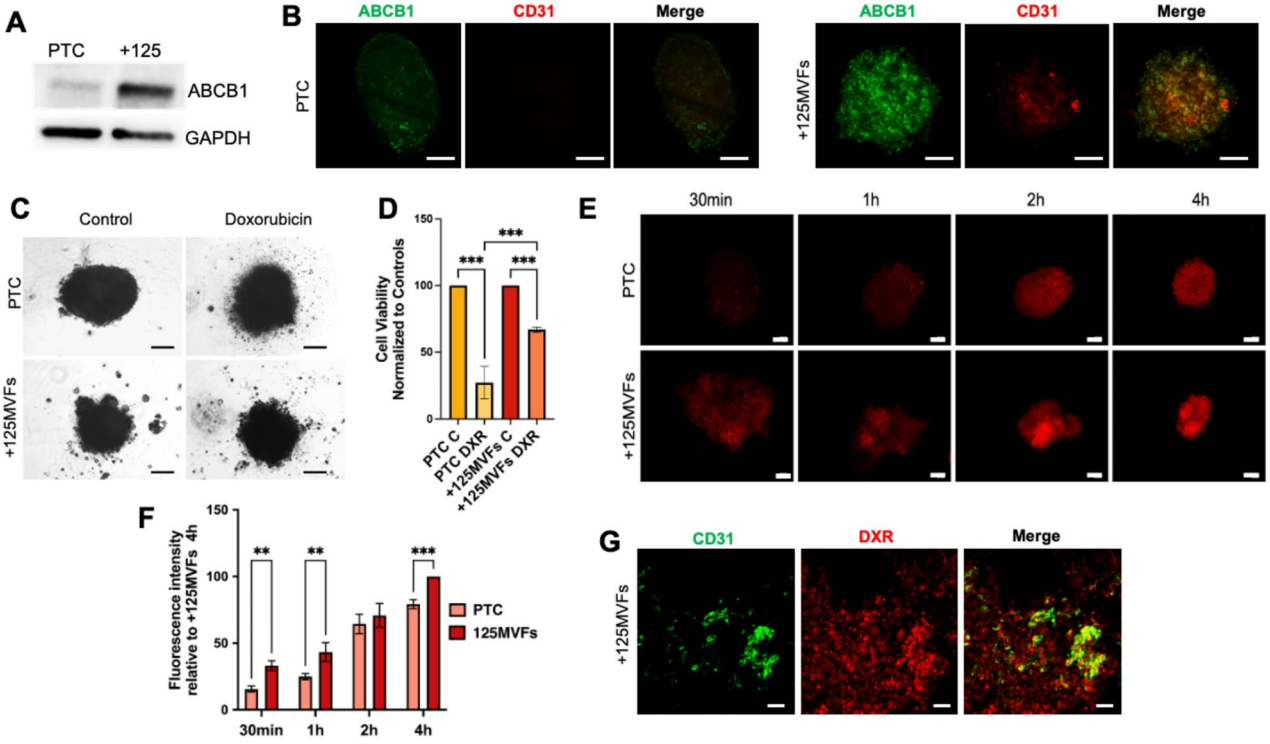

Fig. 5 ABCB1 expression and drug sequestration in angiotumoroids. (**A**) Western blot analysis for ABCB1 in Primary tumor cell spheroids (PTC) and angiotumoroids with 125 MVFs (+125MVFs). (**B**) Confocal microscope of primary tumor cell spheroids (PTC), angiotumoroids with 125 (+125MVFs) MVFs stained with anti-ABCB1 antibody (green) and anti-CD31 antibody (red) at day 5. Scale bar: 100 µm. (**C**) Primary tumor cell spheroids (PTC) and angiotumoroids with 125 MVFs (+125MVFs) after 24 h of treatment with 10 µM doxorubicin. Scale bar 100 µm. (**D**) Cell viability assay of primary tumor cell spheroids (PTC) and angiotumoroids with 125 MVFs (+125MVFs) after 24 h of treatment with 10 µM doxorubicin (DXR). PTC C and +125MVFs C are the controls (not treated spheroids). Data are mean ± SD. Statistical analysis (2-way ANOVA) was performed ($n = 3$) (***$p < 0.001$). (**E**) Fluorescence analysis of 10 µM doxorubicin uptake in primary tumor cell spheroids (PTC) and angiotumoroids with 125 MVFs (+125MVFs) at different time points (30 min, 1 h, 2 h, 4 h). Scale bar: 30 µm. Red: doxorubicin autofluorescence. (**F**) Quantification of the fluorescence intensities was analyzed and normalized to +125MVFs at 4 h. Data are mean ± SD. Statistical analysis (2-way ANOVA) was performed ($n = 3$) (**$p < 0.01$). (**G**) Angiotumoroids with 125 MVFs stained with anti-CD31 antibody (green) and doxorubicin (DXR) (red). Scale bar: 200 µm

Relative quantification of angiogenesis-related proteins, based on UniProt Gene Ontology annotations, revealed marked differences among the models. Specifically, six angiogenic proteins, including neuropilin-1 (NRP1) and MMP2, were significantly decreased in angiotumoroids. In contrast, five proteins were significantly upregulated compared to PTC spheroids, such as VEGFA and Epiregulin (EREG), highlighting a tumor cell-mediated proangiogenic profile. When compared to MVF spheroids, only two proteins, protein kinase C alpha (referred to as PRKCA by gene name) and Protein Tyrosine Kinase 2 Beta (PTK2B), were significantly augmented (Fig. 4D). These proteomic differences suggest that angiotumoroids represent a distinct biological model with features that diverge from both PTC and MVF controls. Notably, angiotumoroids not only contain MVFs with angiogenic sprouting potential but also exhibit altered ECM composition and remodeling, as revealed by proteomics analysis (Fig. 4E). Remarkably, ECM components such as Collagen Type I and Collagen Type IV remained abundant in the vascularized tumor model (Fig. 4F), supporting the presence of a structurally rich ECM. In parallel, a more complex ECM remodeling scenario was indicated by increased levels of several MMPs, including MMP3, MMP9, MMP10, MMP11, and MMP13 (Fig. 4G), underscoring the critical roles these enzymes play in promoting tumor angiogenesis and matrix degradation.

Furthermore, proteomic analysis identified altered expression of several ATP-binding cassette (ABC) transporters, with ABCB1 (P-glycoprotein) being significantly more abundant in angiotumoroids compared to both PTC and MVF controls (Fig. 4H). Given ABCB1's well-established role in drug efflux and chemoresistance [38], its elevated expression suggests that angiotumoroids may also serve as a relevant platform for studying drug distribution and resistance mechanisms within a vascularized TME.

ABCB1 expression and drug sequestration in Angiotumoroids

To investigate the expression and distribution of ABCB1 in angiotumoroids containing 125MVFs, western blot

analysis was performed, confirming a significant upregulation of ABCB1 protein compared to PTC spheroids (Fig. 5A). Consistently, immunofluorescence staining revealed minimal ABCB1 expression in PTC spheroids, whereas in angiotumoroids, ABCB1 was clearly localized to both endothelial and tumor cell compartments, indicating a broader functional role within the vascularized TME (Fig. 5B).

To assess drug accessibility and cytotoxic response in this model, angiotumoroids were treated with doxorubicin five days post-formation, and viability was assessed 24 h after drug exposure. Compared to PTC spheroids, which exhibited widespread cell death, angiotumoroids maintained a more compact structure (Fig. 5C). Quantitative analysis revealed a significantly higher survival rate in angiotumoroids (60%) compared to PTC spheroids (23%) (Fig. 5D), indicating that doxorubicin may be partially retained or sequestered within the angiotumoroid structure, potentially limiting its cytotoxic penetration and efficacy.

To further explore the role of MVFs on drug distribution, doxorubicin uptake was monitored over time (30 min, 1 h, 2 h, and 4 h) by measuring doxorubicin autofluorescence in angiotumoroids and PTC spheroids (used as controls; Fig. 5E). Both models exhibited a time-dependent increase in fluorescence intensity, indicating progressive intracellular drug accumulation. However, angiotumoroids displayed a markedly stronger fluorescent signal already after 30 min of incubation (Fig. 5F), suggesting facilitated drug uptake or compartmentalization in specific regions. Importantly, fluorescence in angiotumoroids was predominantly localized to MVF-rich regions, as confirmed by colocalization with the endothelial marker CD31 (Fig. 5G). This spatial distribution suggests that the vascular components within the angiotumoroids may play an active role in modulating drug distribution and local transport dynamics, contributing to a more physiologically relevant tumor microenvironment.

Discussion

Solid tumors are characterized by a highly complex microenvironment composed of tumor vasculature, connective tissue, infiltrating immune cells, and the tumor extracellular matrix (TEM) [39]. Given the intricate nature of tumor biology and the limitations of traditional two-dimensional culture models, three-dimensional (3D) tumor spheroids have emerged as a more relevant model for cancer research in vitro, making them invaluable for investigating cancer characteristics, progression, drug responses, and therapeutic resistance. 3D models can mimic solid tumor structures, developing features like a hypoxic core [13] and an ECM [12] that partially recreates the tumor microenvironment (TME). However, the TME extends beyond the extracellular matrix, encompassing various associated cells, including cancer-associated fibroblasts and tumor-associated macrophages, as well as a functional vascular network. Angiogenesis is essential for tumor growth and metastasis, making its accurate replication in 3D models a key step toward achieving in vivo conditions. While many studies have incorporated endothelial cells (e.g., HUVECs) into tumor spheroids [23, 40], the resulting vascular networks often remain underdeveloped. To address these limitations, this study aimed to develop a novel model incorporating murine adipose-derived microvascular fragments (MVFs) alongside primary murine breast cancer cells (PTCs). MVFs are intact fragments of blood vessels comprising a mixture of capillaries, veins, and arteries. They retain all the defining features of fully formed blood vessels, including accessory cells, such as pericytes [26]. In research, MVFs have been widely used to establish functional vascular networks within collagen matrices. They have demonstrated the ability to integrate with the host's circulatory system following transplantation, ensuring graft survival by facilitating the delivery of oxygen and nutrients, and removing metabolic toxic products [27]. Isolated MVFs have been employed to generate 3D spheroids, either alone or in combination with other cell types such as adipocytes or osteoblasts [32]. Furthermore, human MVFs have been used to model tumor angiogenesis by placing them adjacent to colorectal cancer spheroids [41]. Based on the unique capabilities of MVFs, this study explores their use as a tool to more accurately mimic the TME. To achieve this goal, an essential initial step was the development of a well-defined and reproducible protocol for isolating MVFs from the visceral adipose tissue of Wistar rats. Structural analysis by scanning electron microscopy (SEM) confirmed the complete removal of surrounding adipose tissue and revealed a clean vascular morphology. The MVFs not only preserved their structural integrity but also exhibited sprouting and branching activity.

To develop a more physiologically relevant in vitro tumor model, PTCs isolated from rat mammary tumors were combined with MVFs to form 3D models referred to as "angiotumoroids". By varying the number of MVFs included in the model (60, 125, or 250) while maintaining a constant number of PTCs, we aimed to explore the impact of the vascular system on the structural organization and potential functionality of these models. The addition of MVFs significantly affected the angiotumoroids' structural development over time. Constructs with the highest MVF number (250) exhibited increased size variability and a less compact morphology, indicating that an excessive vascular load might hinder the self-organizing ability of tumor cells. SEM analyses revealed notable differences in structural integrity. Angiotumoroids with intermediate MVF content showed a cohesive

and well-organized architecture, characterized by closely packed cell populations and integrated microvascular elements. Conversely, angiotumoroids with 250 MVFs revealed surface cells that were not fully incorporated into the structure; probably, due to the excess of satellite microvessels that sequester part of the PTCs, preventing the formation of angiotumoroids with a compact structure. Interestingly, angiotumoroids required approximately five days to compact, and this temporal delay is in contrast with PTC spheroids, which became compact earlier and displayed a more uniform structure from the initial stages. This suggests that while MVFs enrich the biological relevance of the model, their inclusion also adds complexity, impacting the kinetics of tissue-like organization. Overall, these findings indicate a need to balance the use of vascular components to improve the physiological relevance while preserving the structural integrity essential for reliable analysis. The angiotumoroids, particularly those composed of an intermediate MVF density, provide a valuable tool for exploring tumor–vasculature interactions and developing more predictive systems in therapeutic approaches.

The integration of the MVFs into 3D angiotumoroid models leads to a progressive formation of vascular-like structures, indicated by CD31 positivity [42]. The increase in CD31 expression with a higher number of MVF, evidenced through both immunofluorescence and western blot analyses, confirms successful integration of endothelial structures and the potential formation of a vascular-like network within the angiotumoroids. In these models, MVFs and tumor cells crosstalk modulate proteolytic activities, especially those involved in angiogenesis. MMPs, particularly MMP9, are essential for ECM remodeling and angiogenesis [43, 44]. MMP9 activity, specifically its active form, was markedly elevated in PTC co-cultured with 125 and 250 MVFs, suggesting that vessels-tumor cell interactions are essential for full enzymatic activation. In contrast, MMP2 activity remained relatively constant across conditions, indicating a constitutive expression pattern by tumor cells that is not modulated by endothelial interaction. However, these findings highlight the importance of cellular crosstalk in shaping the tumor microenvironment and reinforce the angiotumoroids as a robust model for investigating tumor angiogenesis and matrix remodeling.

Neo-vasculature formation is critical for solid tumor progression, and embedding angiotumoroids in a collagen matrix provided a dynamic in vitro model to evaluate angiogenic potential under various MVF densities. While PTC spheroids showed no signs of neovascularization with a progressive loss of structural integrity due to peripheral cell migration, angiotumoroids with 60 and 125 MVFs displayed an enhanced and time-dependent endothelial sprouting response. This vascularization is more than observed in MVF spheroids. Notably, angiotumoroids containing 125 MVFs not only exhibited a higher expression of MMP9 but also the most robust and branched sprouting. The synergistic interaction between MVFs and PTCs was confirmed by treating MVF spheroids with PTC-conditioned medium, which significantly boosted both sprout formation and branching complexity over time, making one assume a possible communication mediated through both juxtacrine and paracrine signaling pathways. These findings identify the 125 MVF angiotumoroid condition as the potentially more physiologically representative model for in vitro angiogenesis, capable of recapturing some aspects of tumor-driven vascular remodeling.

Importantly, proteomic profiling of angiotumoroids revealed a unique expression signature in angiogenesis-related proteins compared to PTC spheroids, such as an increase in VEGFA, a key driver for neovascularization [45], and ECM remodeling factors, which aligns with the observed vascular development and matrix reorganization. This molecular profile mirrors the dynamic nature of in vivo tumor progression, where ECM degradation facilitates angiogenesis, tumor invasion, and metastasis [46]. The detection of collagen types I and IV further supports the presence of a structured ECM, which not only supports tumor cell growth but also modulates drug penetration and immune cell infiltration [39]. Notably, the angiotumoroids exhibited upregulation of ATP-binding cassette (ABC) transporters, particularly ABCB1 (P-glycoprotein), a key mediator of drug efflux associated with multidrug resistance in cancer [47, 48]. Elevated ABCB1 expression within angiotumoroids suggests the presence of localized drug resistance mechanisms, likely driven by active efflux in vascularized compartments. These findings underscore the potential of angiotumoroids not only to model tumor architecture and vascularization but also to reflect clinically relevant resistance pathways that are often absent in conventional in vitro systems.

Moreover, consistent with in vivo observations, vascularized regions within solid tumors affect drug uptake and chemotherapeutic efficacy [8, 9, 49]. MVFs within the angiotumoroid model significantly alter the distribution and efficacy of chemotherapeutic agents as doxorubicin, as evidenced by its different uptake and cytotoxicity. Uptake assays revealed enhanced and spatially localized drug accumulation in angiotumoroids compared to PTC spheroids. This preferential drug deposition suggests that specific regions potentially act as barriers for soluble drugs, as doxorubicin. Despite the increased drug retention, angiotumoroids exhibited reduced cytotoxicity relative to PTC spheroids after 24-hour exposure, supporting the hypothesis that in angiotumoroids, drug availability to tumor cells is modulated through sequestration mechanisms, ultimately decreasing therapeutic efficacy

as demonstrated by a substantial recovery of tumor cell viability over time.

These findings strongly support the use of angiotumoroids as a versatile in vitro model for studying solid tumors, particularly for investigating tumor angiogenesis and tumor–vasculature crosstalk, and evaluating the delivery of anti-tumor drugs, especially for compounds designed to overcome physiological barriers in the TME. This platform is compatible with high-throughput screening, as approximately 30,000 MVFs can be obtained from just 10 g of adipose tissue, enabling the production of around 250 angiotumoroids. Additionally, various standardized cryopreservation methods allow MVFs to be preserved efficiently, supporting large-scale collection and extended storage for future studies [50].

The angiotumoroid model, although initially established using rat-derived microvascular fragments (MVFs) and tumor cells, provides a versatile framework that could be adapted to human systems. The combination of primary tumor cells obtained from patient biopsies with MVFs isolated from human adipose tissue via liposuction appears technically feasible and represents a promising approach for generating patient-specific vascularized tumor constructs. Ideally, obtaining both PTCs and MVFs from the same patient would be optimal, further supporting the development of personalized therapeutic approaches. However, interspecies differences in extracellular matrix composition, angiogenic signaling pathways, and immune microenvironmental factors may significantly influence the behavior and organization of the co-culture. It will therefore be essential to systematically investigate these species-specific differences to ensure the reliable adaptation and reproducibility of the model in human settings. Furthermore, the current in vitro configuration lacks active perfusion, limiting the physiological relevance of vascular function and metabolic exchange. Future integration of the angiotumoroid platform within microfluidic tumor-on-chip systems could provide controlled perfusion and dynamic nutrient flow, thereby improving vascular functionality, better recapitulating in vivo hemodynamic conditions, and ultimately enhancing the translational potential of this model for personalized oncology research.

Supplementary Information

The online version contains supplementary material available at https://doi.org/10.1186/s12935-025-04154-6.

Supplementary Material 1

Acknowledgements
We are grateful to Flaviana Falci from the Antonio D'Amore group (Ri.MED Foundation) for their help with SEM analysis. We acknowledge ATeN Center–University of Palermo for the confocal microscope and the animal facility.

Author contributions
ALC, FLM, and GLB designed the study. ALC, FLM, GLB, and FG performed the experiments. PC produced the recombinant collagenases. MLP and SDS performed the proteomic analysis. SC and GLB helped with data analysis. ALC analyzed data. ALC, FLM, and GLB wrote the manuscript. GG directed the study. All authors reviewed and edited the manuscript and approved the final version of the manuscript.

Funding
This work has received funding from the European Union—NextGenerationEU through the Italian Ministry of University and Research under PNRR— MUR, PNRR-M4C2, ECS_00000022-SiciliAn MicronanOTecH Research And Innovation CEnter "SAMOTHRACE"—CUP: B73C22000810001. The views and opinions expressed are those of the authors only and do not necessarily reflect those of the European Union or the European Commission. Neither the European Union nor the European Commission can be held responsible for them.

Data availability
The datasets used and/or analysed during the current study are available from the corresponding author on reasonable request.

Declarations

Ethics approval and consent to participate
Not applicable.

Consent for publication
All participants had properly consented.

Competing interests
The authors declare no competing interests.

Author details
[1]Department of Biological, Chemical and Pharmaceutical Sciences and Technologies (STEBICEF), University of Palermo, Viale delle Scienze, Ed. 16–90128, Palermo, Italy
[2]Department of Pharmacy, University of Copenhagen, Copenhagen, Denmark
[3]Abiel srl, Palermo, Italy
[4]Institute for Biomedical Research and Innovation, National Research Council (IRIB-CNR), Palermo, Italy
[5]Proteomics Group of Ri.MED Foundation, Research Department IRCCS ISMETT (Istituto Mediterraneo per i Trapianti e Terapie ad Alta Specializzazione), Palermo, Italy

Received: 15 September 2025 / Accepted: 25 December 2025
Published online: 08 January 2026

References

1. Giussani M, Triulzi T, Sozzi G, Tagliabue E. Tumor extracellular matrix remodeling: new perspectives as a circulating tool in the diagnosis and prognosis of solid tumors. Cells. 2019;8:81. https://doi.org/10.3390/cells8020081.
2. Tiwari A, Trivedi R, Lin S-Y. Tumor microenvironment: barrier or opportunity towards effective cancer therapy. J Biomed Sci. 2022;29:83. https://doi.org/10.1186/s12929-022-00866-3.
3. Biray Avci C, Goker Bagca B, Nikanfar M, Takanlou LS, Takanlou MS, Nourazarian A. Tumor microenvironment and cancer metastasis: molecular mechanisms and therapeutic implications. Front Pharmacol. 2024. https://doi.org/10.3389/fphar.2024.1442888.
4. Jiang X, Wang J, Deng X, Xiong F, Zhang S, Gong Z, et al. The role of microenvironment in tumor angiogenesis. Journal of Experimental & Clinical Cancer Research. 2020;39:204. https://doi.org/10.1186/s13046-020-01709-5.
5. Lugano R, Ramachandran M, Dimberg A. Tumor angiogenesis: causes, consequences, challenges and opportunities. Cell Mol Life Sci. 2020;77:1745–70. https://doi.org/10.1007/s00018-019-03351-7.
6. Al-Ostoot FH, Salah S, Khamees HA, Khanum SA. Tumor angiogenesis: current challenges and therapeutic opportunities. Cancer Treat Res Commun. 2021;28:100422. https://doi.org/10.1016/j.ctarc.2021.100422.

7. Kretschmer M, Rüdiger D, Zahler S. Mechanical aspects of angiogenesis. Cancers (Basel). 2021;13:4987. https://doi.org/10.3390/cancers13194987.
8. Dewhirst MW, Secomb TW. Transport of drugs from blood vessels to tumour tissue. Nat Rev Cancer. 2017;17:738. https://doi.org/10.1038/NRC.2017.93.
9. Primeau AJ, Rendon A, Hedley D, Lilge L, Tannock IF. The distribution of the anticancer drug doxorubicin in relation to blood vessels in solid tumors. Clin Cancer Res. 2005;11:8782–8. https://doi.org/10.1158/1078-0432.CCR-05-1664.
10. Urzì O, Gasparro R, Costanzo E, De Luca A, Giavaresi G, Fontana S, et al. Three-dimensional cell cultures: the bridge between in vitro and in vivo models. Int J Mol Sci. 2023;24:12046. https://doi.org/10.3390/ijms241512046.
11. Froehlich K, Haeger J-D, Heger J, Pastuschek J, Photini SM, Yan Y, Lupp A, Pfarrer C, Mrowka R, Schleußner E, et al. Generation of multicellular breast cancer tumor spheroids: comparison of different protocols. J Mammary Gland Biol Neoplasia. 2016;21:89–98. https://doi.org/10.1007/s10911-016-9359-2.
12. Lo Cicero A, Campora S, Lo Buglio G, Ciná P, Lo Pinto M, Scilabra SD, Ghersi G. Enhancing therapeutic efficacy through degradation of endogenous extracellular matrix in primary breast tumor spheroids. FEBS J. 2025. https://doi.org/10.1111/febs.70069.
13. Aggarwal V, Miranda O, Johnston PA, Sant S. Three dimensional engineered models to study hypoxia biology in breast cancer. Cancer Lett. 2020;490:124. https://doi.org/10.1016/J.CANLET.2020.05.030.
14. Close DA, Johnston PA. Detection and impact of hypoxic regions in multicellular tumor spheroid cultures formed by head and neck squamous cell carcinoma cells lines. SLAS Discov. 2022;27:39–54. https://doi.org/10.1016/J.SLASD.2021.10.008.
15. Arora L, Kalia M, Roy S, Pal D. Assessment of mitochondrial health in cancer-associated fibroblasts isolated from 3D multicellular lung tumor spheroids. J Vis Exp. 2022. https://doi.org/10.3791/64315-v.
16. Parashar D, Geethadevi A, Mittal S, McAlarnen L, George J, Kadamberi I, et al. Patient-derived ovarian cancer spheroids rely on PI3K-AKT signaling addiction for cancer stemness and chemoresistance. Cancers (Basel). 2022;14:958. https://doi.org/10.3390/cancers14040958.
17. Yang Y, Li S, Sun Y, Zhang D, Zhao Z, Liu L. Reversing platinum resistance in ovarian cancer multicellular spheroids by targeting Bcl-2. Onco Targets Ther. 2019;12:897–906. https://doi.org/10.2147/OTT.S187015
18. Song Y, Kim J-S, Kim S-H, Park YK, Yu E, Kim K-H, et al. Patient-derived multicellular tumor spheroids towards optimized treatment for patients with hepatocellular carcinoma. Journal of Experimental & Clinical Cancer Research. 2018;37:109. https://doi.org/10.1186/s13046-018-0752-0.
19. Yoshida T, Sopko NA, Kates M, Liu X, Joice G, McConkey DJ, et al. Three-dimensional organoid culture reveals involvement of Wnt/β-Catenin pathway in proliferation of bladder cancer cells. Oncotarget. 2018;9:11060–70. https://doi.org/10.18632/oncotarget.24308.
20. Gottfried E, Rogenhofer S, Waibel H, Kunz-Schughart LA, Reichle A, Wehrstein M, Peuker A, Peter K, Hartmannsgruber G, Andreesen R, et al. Pioglitazone modulates tumor cell metabolism and proliferation in multicellular tumor spheroids. Cancer Chemother Pharmacol. 2011;67:117–26. https://doi.org/10.1007/s00280-010-1294-0.
21. Hawinkels LJAC, Zuidwijk K, Verspaget HW, de Jonge-Muller ESM, Duijn Wvan, Ferreira V, et al. VEGF release by MMP-9 mediated heparan sulphate cleavage induces colorectal cancer angiogenesis. Eur J Cancer. 2008;44:1904–13. https://doi.org/10.1016/j.ejca.2008.06.031.
22. Heo DN, Hospodiuk M, Ozbolat IT. Synergistic interplay between human MSCs and HUVECs in 3D spheroids laden in collagen/fibrin hydrogels for bone tissue engineering. Acta Biomater. 2019;95:348–56. https://doi.org/10.1016/j.actbio.2019.02.046.
23. Shoval H, Karsch-Bluman A, Brill-Karniely Y, Stern T, Zamir G, Hubert A, et al. Tumor cells and their crosstalk with endothelial cells in 3D spheroids. Scientific Reports 2017 7:1. 2017;7:1–11. https://doi.org/10.1038/s41598-017-10699-y.
24. Strobel HA, Moss SM, Hoying JB. Isolated fragments of intact microvessels: tissue vascularization, modeling, and therapeutics. Microcirculation. 2024. https://doi.org/10.1111/micc.12852.
25. Laschke MW, Menger MD. Adipose tissue-derived microvascular fragments: natural vascularization units for regenerative medicine. Trends Biotechnol. 2015;33:442–8. https://doi.org/10.1016/j.tibtech.2015.06.001.
26. Laschke MW, Später T, Menger MD. Microvascular fragments: more than just natural vascularization units. Trends Biotechnol. 2021;39:24–33. https://doi.org/10.1016/j.tibtech.2020.06.001.
27. Shepherd BR, Chen HYS, Smith CM, Gruionu G, Williams SK, Hoying JB. Rapid perfusion and network remodeling in a microvascular construct after implantation. Arterioscler Thromb Vasc Biol. 2004;24:898–904. https://doi.org/10.1161/01.ATV.0000124103.86943.1e.
28. Hoying JB, Boswell CA, Williams SK. Angiogenic potential of microvessel fragments established in three-dimensional collagen gels. In Vitro Cell Dev Biol Anim. 1996;32:409–19. https://doi.org/10.1007/BF02723003.
29. Nalbach L, Müller D, Wrublewsky S, Metzger W, Menger MD, Laschke MW, et al. Microvascular fragment spheroids: three-dimensional vascularization units for tissue engineering and regeneration. J Tissue Eng. 2021. https://doi.org/10.1177/20417314211035593.
30. Strobel HA, Gerton T, Hoying JB. Vascularized adipocyte organoid model using isolated human microvessel fragments. Biofabrication. 2021;13:035022. https://doi.org/10.1088/1758-5090/abe187.
31. Quan Y, Zhang Y, Li J, Lu F, Cai J. Transplantation of in vitro prefabricated adipose organoids attenuates skin fibrosis by restoring subcutaneous fat and inducing dermal adipogenesis. FASEB J. 2023. https://doi.org/10.1096/fj.202202117R.
32. Wrublewsky S, Schultz J, Ammo T, Bickelmann C, Metzger W, Später T, et al. Biofabrication of prevascularized spheroids for bone tissue engineering by fusion of microvascular fragments with osteoblasts. Front Bioeng Biotechnol. 2024. https://doi.org/10.3389/fbioe.2024.1436519.
33. Salamone M, Rigogliuso S, Nicosia A, Campora S, Bruno CM, Ghersi G. 3D collagen hydrogel promotes in vitro Langerhans islets vascularization through Ad-MVFs angiogenic activity. Biomedicines. 2021;9:739. https://doi.org/10.3390/biomedicines9070739.
34. Burkel, B.; Morris, B.A.; Ponik, S.M.; Riching, K.M.; Eliceiri, K.W.; Keely, P.J.Preparation of 3D Collagen Gels and Microchannels for the Study of 3D Interactions*In Vivo Journal of Visualized Experiments* 2016, doi:10.3791/53989.
35. Wiśniewski JR, Zougman A, Nagaraj N, Mann M. Universal sample preparation method for proteome analysis. Nat Methods. 2009;6:359–62. https://doi.org/10.1038/NMETH.1322.
36. Rappsilber J, Ishihama Y, Mann M. Stop and go extraction tips for matrix-assisted laser desorption/ionization, nanoelectrospray, and LC/MS sample pretreatment in proteomics. Anal Chem. 2003;75:663–70. https://doi.org/10.1021/AC026117I.
37. Rabienezhad Ganji N, Urzì O, Tinnirello V, Costanzo E, Polito G, Palumbo Piccionello A, Manno M, Raccosta S, Gallo A, Lo Pinto M, et al. Proof-of-Concept study on the use of Tangerine-Derived nanovesicles as SiRNA delivery vehicles toward colorectal cancer cell line SW480. Int J Mol Sci. 2024;25:546. https://doi.org/10.3390/IJMS25010546/S1.
38. Robey RW, Pluchino KM, Hall MD, Fojo AT, Bates SE, Gottesman MM. Revisiting the Role of ABC Transporters in Multidrug-Resistant Cancer. *Nature Reviews Cancer 2018 18:7* 2018, *18*, 452–464, doi:https://doi.org/10.1038/s41568-018-0005-8.
39. Lo Buglio G, Lo Cicero A, Campora S, Ghersi G. The multifaced role of collagen in cancer development and progression. Int J Mol Sci. 2024;25(24):13523. https://doi.org/10.3390/ijms252413523.
40. Ascheid D, Baumann M, Pinnecker J, Friedrich M, Szi-Marton D, Medved C, Bundalo M, Ortmann V, Öztürk A, Nandigama R et al. A Vascularized Breast Cancer Spheroid Platform for the Ranked Evaluation of Tumor Microenvironment-Targeted Drugs by Light Sheet Fluorescence Microscopy. *Nature Communications 2024 15:1* 2024, *15*, 1–23, doi:https://doi.org/10.1038/s41467-024-48010-z.
41. Moss SM, Gerton T, Strobel HA, Hoying JB. Isolated human adipose microvessels retain native microvessel structure and recapitulate sprouting angiogenesis. Angiogenesis. 2025;28:1–13. https://doi.org/10.1007/S10456-025-09972-W/FIGURES/4.
42. Lertkiatmongkol P, Liao D, Mei H, Hu Y, Newman PJ. Endothelial functions of PECAM-1 (CD31). Curr Opin Hematol. 2016;23:253. https://doi.org/10.1097/MOH.0000000000000239.
43. Quintero-Fabián S, Arreola R, Becerril-Villanueva E, Torres-Romero JC, Arana-Argáez V, Lara-Riegos J, et al. Role of matrix metalloproteinases in angiogenesis and cancer. Front Oncol. 2019;9:1370. https://doi.org/10.3389/FONC.2019.01370.
44. Bergers G, Brekken R, McMahon G, Vu TH, Itoh T, Tamaki K, et al. Matrix metalloproteinase-9 triggers the angiogenic switch during carcinogenesis. Nat Cell Biol. 2000;2:737–44. https://doi.org/10.1038/35036374.
45. Lee C, Kim MJ, Kumar A, Lee HW, Yang Y, Kim Y. Vascular Endothelial Growth Factor Signaling in Health and Disease: From Molecular Mechanisms to Therapeutic Perspectives. *Signal Transduction and Targeted Therapy 2025 10:1* 2025, *10*, 1–40. https://doi.org/10.1038/s41392-025-02249-0
46. Zhang M, Zhang B. Extracellular Matrix Stiffness: Mechanisms in Tumor Progression and Therapeutic Potential in Cancer. *Experimental Hematology &*

Oncology 2025 14:1 2025, *14*, 1–34. https://doi.org/10.1186/S40164-025-00647-2
47. Duvivier L, Gerard L, Diaz A, Gillet JP. Linking ABC transporters to the hallmarks of cancer. Trends Cancer. 2024;10:124–34. https://doi.org/10.1016/J.TRECAN.2023.09.013/ASSET/03262B91-2C4C-4B34-A3C8-2F98046823D9/MAIN.ASSETS/GR1.JPG.
48. Morimoto M, Maishi N, Hida K. Acquisition of drug resistance in endothelial cells by Tumor-Derived extracellular vesicles and cancer progression. Cancer Drug Resist. 2024;7. https://doi.org/10.20517/CDR.2023.121.
49. Trédan O, Galmarini CM, Patel K, Tannock IF. Drug resistance and the solid tumor microenvironment. JNCI J Natl Cancer Inst. 2007;99:1441–54. https://doi.org/10.1093/JNCI/DJM135.
50. Laschke MW, Karschnia P, Scheuer C, Heß A, Metzger W, Menger MD. Effects of cryopreservation on adipose tissue-derived microvascular fragments. J Tissue Eng Regen Med. 2018;12:1020–30. https://doi.org/10.1002/TERM.2591.

Publisher's note